

Mechanical Activation of Hematite Using Different Grinding Methods with Special Focus on Structural Changes and Reactivity

Parviz Pourghahramani

Luleå University of Technology
Department of Chemical Engineering and Geosciences
Division of Mineral Processing

2007:08 | ISSN: 1402-1544 | ISRN: LTU-DT -- 07/8 -- SE

Mechanical Activation of Hematite Using Different Grinding Methods with Special Focus on Structural Changes and Reactivity

Parviz Pourghahramani
Luleå University of Technology
Department of Chemical Engineering and Geosciences
Division of Mineral Processing

Abstract

The mechanical treatment of solids is one of the most common and widely used operations which man has been concerned from the very beginning of the history of civilization. Nowadays, mechanical activation has a wide range of application potentials. Mechanical activation processes are used to modify the properties of materials, to enhance the reactivity of materials and to produce advanced materials and to separate composite materials into its constituents. When materials are subjected to intensive grinding, the structure and microstructure characters of material change widely. These structural changes determine the reactivity of materials and/or minerals and may play an important role in subsequent processes.

The objective of this study is to investigate the influence of the grinding techniques on the microstructure and structural changes of natural hematite. The influences of the five grinding methods with various grinding variables have been investigated: (1) three types of loose media mills in dry mode, (2) interparticle comminution in a confined piston-die press and (3) a stirred media mill in wet mode. A variety of microstructural characterization methods based on X-ray diffraction line profile analysis such as Warren-Averbach, Williamson-Hall and Rietveld methods associated with other characterizations methods have been employed in the present study. In addition, the effects of mechanical activation on the thermal reactivity of hematite concentrate have been studied using hydrogen reduction of activated samples.

The results reveal that mechanical activation of hematite causes great changes in geometrical and microstructural characteristics with increased grinding intensity, whatever milling methods were applied. In the case of dry grinding with loose media mills, the results show that the particles show a tendency to form agglomerates during prolonged milling. The expansions of hematite lattice and volume cell were identified. The Williamson-Hall method provides itself to be a technique for a rapid overview of the X-ray line broadening effects and facilitates the understanding of the influence of grinding processes on the material structures. The anisotropic character of line broadening for deformed hematite as a function of grinding variables was revealed. From the Warren-Averbach method, it has been found that the planetary mill products yield the smallest crystallites and the maximum root mean square strain (RMSS) with one exception. The products of the vibratory mill yield approximately lower X-ray amorphization degree with regard to the grinding time and media surface variables. The approximation of the energy contribution to the long-lived defects demonstrated that the amorphization character is the most important energy carrier in the activated hematite, accounting for more than 93% of overall stored energy in hematite. The comparison of the loose media mills based on stress energy revealed that the vibratory mill brings about less distortion in the hematite than other mills for the same level of stress energy. In addition, the variance analysis revealed that the media surface and grinding time significantly influence the five main response variables at 95% confidence level. Multivariate techniques are successfully applied for projection of microstructure characters to identify the salient features underlying the data. Principal component analysis (PCA) makes it possible to predict easily which condition leads to production of similar properties or microstructure characters and opens a new window for prediction of microstructure characteristics based on changes in the grinding variables for further investigations. Partial least square discrimination analysis (PLS-DA) analysis suggested that mills could be differentiated from each other.

From the interparticle comminution investigations, it has been found that the energy absorption is the dominating factor for the size reduction, surface area and induced structural

changes in the particle bed comminution. It was also found that the interparticle breakage causes plastic deformation in the material and subsequently induces changes in the structure of the ground hematite and thus provides evidences for the activation potentiality of this method. The comparison with loose media mill (tumbling) in terms of net grinding energy indicated that the interparticle breakage has high energy transfer efficiency to the particles being ground and subsequently favor in the structural changes for a given energy.

The comparison of the dry tumbling milling with wet stirred media milling showed that the stirred media mill is more effective in producing structural changes compared to the dry operation; although the X-ray amorphous phase content remained unaffected by the grinding environments, but a large difference was observed in the production of BET surface area.

The milling process has been shown to have a pronounced influence on the reduction behavior and kinetic scheme of hematite especially at lower temperature or conversion degrees. Mechanical activation of hematite concentrate lead to the initiation of reduction at lower temperatures. The starting temperature of the reduction was decreased to from 420 about 330°C depending on grinding intensity. Moreover, the pretreatment resulted in improved resolution of overlapping reduction events and the activation energy of the first step of reduction decreased with increasing grinding time. The study showed that the activation energy of the two steps of the reduction depends greatly on the extent of conversion implicating that the reduction processes of hematite to magnetite and magnetite to iron features multi-step characteristics.

To investigate the influence of other milling variables in detail, more investigations are recommended, especially as the experiment design and progress in the knowledge to-day provide possibilities to use advanced methods for characterization and analysis. In our opinion, the investigation of the effects of various defects formed during mechanical activation on the reactivity of the minerals are currently only at the beginning of their developments. Systematic investigations are recommended to explore what defects are formed in the crystal of the substances under various types of mechanical action and how these defects influence the reactivity.

Keywords: *Mechanical activation, Extended milling, Line broadening analysis, Profile fitting, XRD diffraction, Microstructure, Ultrafine grinding, Structure changes, Williamson-Hall method, Warren-Averbach approach, Rietveld method, Reactivity, Iron oxide, Reduction behavior, Multivariate analysis, statistical analysis, Nonisothermal Reduction kinetics, interparticle breakage, Hematite nanoparticles, Wet and Dry millings , Bed grinding, Grinding methods.*

Acknowledgments

The research work presented in this thesis has been carried out at the Division of Mineral Processing, Department of Chemical Engineering and Geosciences at Luleå University of Technology (LTU) under the supervision of Professor Eric Forssberg.

I would like to express my deep gratitude to my supervisor, Professor Eric Forssberg, for providing me an opportunity to conduct this subject, his enormous contribution, invaluable guidance, and unlimited support.

I would like to thank invaluable advices and comments of Professor Claes I Helgesson on thesis and papers.

I am grateful to Dr. Bertil Pålsson for his valuable comments in the grinding processes and permanent support. The administrative support received from Mrs. Siv T. Berhan during this entire duration is also gratefully acknowledged. I would like to appreciate discussions from Dr. Hamid-Reza Manouchehri and Dr. Nourreddine Menad. I am also thankful to Ulf Nordström for his help in the laboratory. I also convey my thanks to all my friends and colleagues at the Department of Chemical Engineering and Geosciences for their kindness. My thanks also extend to the Division of Material Science for allowing me to use the planetary mill. Furthermore, I would like to thank Professor Wolfgang Peukert for his co-operation and for taking some experiments at the laboratory of Friedrich-Alexander University in Germany.

I am sincerely grateful to my country Iran for awarding me the scholarship during four years of my studies.

The financial support for the project by Agricola Research Centre (ARC) is gratefully acknowledged.

I would like to thank my friend Dr. Behzad Ghodrati for his kindness and help at Division of Operation and Maintenance Engineering. My sincere gratitude extends to my friend Farzad Tofighi for his willing help. My thanks also extend to all Iranian friends at Luleå University of Technology, especially to Mohammad-Reza Mofidi, Javad Barabadi, Dr. Abbas Keramati, Alireza Ahmadi, Mohammad-Reza Akhavan, and others for their attentions.

My deepest thanks to my father and mother for all their prayers, care and love they have unselfishly given me. Special thanks go to my wife's parents for their supports. I express my gratitude to my brothers and sisters for their love and kindness.

I am deeply indebted to my loving wife, Leila, for her support, encouragement and patience. Special thanks to my daughters, Mobina and Parnia, who have lost much happiness because of this study.

Once more, I would like to express my gratitude to my wife and my parents by dedicating this thesis to them.

Parviz Pourghahramani

April 2007

Luleå-Sweden

List of Appended Papers

I. Microstructure Characterization of Mechanically Activated Hematite Using XRD Line Broadening

Parviz Pourghahramani & Eric Forssberg

International Journal of Mineral Processing, 79 (2006), 106-119

II. Comparative Study of Microstructural Characteristics and Stored Energy of Mechanically Activated Hematite in Different Grinding Environments

Parviz Pourghahramani & Eric Forssberg

International Journal of Mineral Processing, 79 (2006), 120-139

III. Changes in the Structure of Hematite by Extended Dry Grinding in Relation to Imposed Stress Energy

Parviz Pourghahramani & Eric Forssberg

Submitted for publication in Powder Technology

IV. Statistical Interpreting and Modeling of Microstructural Characteristics of Mechanically Activated Hematite in Different Grinding Environments

Parviz Pourghahramani, Bertil Pålsson & Eric Forssberg

Submitted for publication in International Journal of Mineral Processing

V. The Characterization of Structural Changes in Hematite Ground in a Confined Particle Bed Using Rietveld Analysis

Parviz Pourghahramani & Eric Forssberg

Submitted for publication in International Journal of Mineral Processing

VI. Microstructural Characterization of Hematite during Wet and Dry Millings Using Rietveld and XRD Line Profile Analyses

Parviz Pourghahramani, Erguen Altin, Wolfgang Peukert, & Eric Forssberg

Submitted for publication in Powder Technology

VII. Effects of Mechanical Activation on the Reduction Behavior of Hematite Concentrate

Parviz Pourghahramani & Eric Forssberg

International Journal of Mineral Processing 82 (2007), 96-105

VIII. Reduction Kinetics of Mechanically Activated Hematite Concentrate with Hydrogen Gas Using Non-Isothermal Methods

Parviz Pourghahramani & Eric Forssberg

Thermochimica Acta 454 (2007) 69-77

List of Papers not Appended in the Manuscript

I. Review of Applied Particle Shape Descriptors and Produced Particle Shapes in Grinding Environments. Part I: Particle Shape Descriptors

Parviz Pourghahramani & Eric Forssberg

Mineral Processing & Extractive Metallurgy Review 26,145–166, 2005

II. Review of Applied Particle Shape Descriptors and Produced Particle Shapes in Grinding Environments. Part II: The Influence of Comminution on the Particle Shape

Parviz Pourghahramani & Eric Forssberg

Mineral Processing & Extractive Metallurgy Review 26, 167–186, 2005

III. Mechanical Activation of Hematite in Different Grinding Mills

Parviz Pourghahramani & Eric Forssberg

Accepted for publication in the XII Balkan Mineral Processing Congress in Greece

Contents

Abstract	i
Acknowledgments	iii
List of Appended Papers	v
List of Papers not Appended in the Manuscript	vi
Contents	vii
Nomenclature and Abbreviation	x
1. Introduction	1
1.1. Historical perspective	1
1.2. Background	3
1.2.1. Comminution and mechanical activation	3
1.2.2. Physico-chemical changes of mechanically activated material	4
1.2.3. Relaxation modes in mechanical activation process	5
1.2.4. Mechanical activation, relaxations, energy state and reactivity	6
1.2.5. Energy contribution to the long-lived defect structures	8
1.3. The scope of thesis	9
2. Experimental	11
2.1. Materials	11
2.2. Experimental techniques	11
2.2.1. Milling methods	11
2.2.2. Data collection	12
2.2.3. Analysis of X-ray diffraction data	13
2.2.3.1. The source of line breadth	13
2.2.3.2. The definition of microstructure characteristics	13
2.2.3.3. Profile fitting procedures	15
2.3. Microstructure characterization methods	18
2.3.1. The Williamson–Hall integral breadth method	18
2.3.2. The Stokes deconvolution	18
2.3.3. The Warren-Averbach method	20
2.3.4. Rietveld refinement	21
2.3.5. Resolving the size and strain components by TOPAS	22
2.4. Thermal and kinetics analyses	23
2.5. Data treatments	26
3. Results and discussion	29
3.1. Dry milling with loose media mills	29
3.1.1. Particle size and surface area	29
3.1.2. X-ray diffraction results	30
3.1.3. X-ray amorphization degree	31
3.1.4. Comparison of line breadths	32
3.1.5. Resolving the size and strain components	33
3.1.5.1. Integral breadth method (Williamson-Hall plots)	34

3.1.5.2. The results of Warren-Averbach method	34
3.1.6. The variation of lattice parameters	35
3.1.7. The relationship between stress energy and structure changes	36
3.1.8. Multivariate projection and analysis	39
3.2. Interparticle Breakage	44
3.3. The effects of dry and wet milling on the structural changes	46
3.4. The reduction behaviors and kinetics of activated hematite	50
3.4.1. Reduction behaviors	50
3.4.2. Reduction kinetics	53
4. Conclusions	55
5. Further Research	59
References	61
Appended papers	67

Nomenclature and Abbreviation

A	Peak area
A_L	Fourier coefficients
A_L^D	Distortion components in the Fourier coefficient
A_L^S	The size components in the Fourier coefficient
a_3	The unit of the Fourier length in direction of the diffraction vector
b	Burger's vector
D_S	Surface-weighted crystallite size
D_V	Volume-weighted crystallite size
d	Interplanar spacing
d_{av}	The equivalent spherical particle diameter
$FWHM$	Full width at half-maximum of profile
(hkl)	Miller indices
I	Peak intensity
K	Scherrer constant
L	na_3 , column length orthogonal to diffracting planes
$RMSS$	Root mean square strain
S	Specific surface area
d^*	$2 \sin \theta / \lambda = 1 / d = d^*$, variable in the reciprocal space
β	Integral breadth (In XRD analysis)
β_f	The integral breadth of the physically broadened profile
β_g	The integral breadth of the instrumentally broadened profile
β_h	The integral breadth of the observed broadened profile
β_C	Cauchy components of the total integral breadth (physical)
β_G	Gaussian component of the integral breadth (physical)
β_{SC}	Cauchy component of size
β_{DC}	Cauchy component of strain
β_{SG}	Gaussian component of size
β_{DG}	Gaussian component of strain
β^*	$\beta \cos \theta / \lambda$, integral breadth in the units of $d^* (nm^{-1})$
$\langle \varepsilon_L^2 \rangle$	Mean square strain, orthogonal to diffracting planes, averaged over the distance L
ε	Apparent strain
η	Mixing factor of a Pseudo-Voigt function
θ	Bragg's angle
λ	X-ray wavelength
σ	Density
ΔG	Changes in Gibbs free energy

ΔH	Changes in enthalpy
ΔS	Changes in entropy
ΔH_d	Excess energy of relative lattice distortion (dislocation density)
ΔH_s	Excess energy of specific surface area
ΔH_A	Excess energy relating to the formation of amorphous material
ΔH_p	Excess energy relating to the formation of new phases
M_V	Molar volume
μ_s	Shear modulus
ρ	Dislocation density
σ_s	Specific interfacial energy
C_A	Concentration of amorphous phase
E_A	Molar amorphization energy
L_{vol}	Volume weighted mean column height
e	Maximum lattice strain
\otimes	The convolution process
E_a	Activation energy corresponding to a given conversion degree
T_{exp}	Mean experimental temperature
β	Heating rate in thermal analysis
a	Conversion degree or extent of reaction
\AA	Angstrom unit ($10^{-11}m$)
<i>ANOVA</i>	Analysis of variance
<i>DDTA</i>	Derivative differential thermal analysis
<i>DTA</i>	Differential thermal analysis
<i>DTG</i>	Differential Thermogravimetry
<i>E</i>	Activation energy
<i>FPA</i>	Fundamental parameter approach
<i>LPA</i>	Line profile analysis
<i>PCA</i>	Principal component analysis
<i>PLS</i>	Partial least square analysis
<i>PLS-DA</i>	Partial least square discrimination analysis
<i>R</i>	Gas constant
<i>STA</i>	Simultaneous thermal analysis
<i>T</i>	Temperature
<i>TA</i>	Thermal analysis
<i>TG</i>	Thermogravimetry
<i>XRD</i>	X-ray diffraction

1. Introduction

1.1. Historical perspective

The research area mechanical activation is a subfield of mechanochemistry. Therefore, it is appropriate to review the history of general mechanochemistry.

Mechanochemical processes (MCP) use mechanical energy to activate substances by developing structural changes. However, these are not new processes. Mechanically activated processes date back to the early history of humankind, the use of flints to initiate fires (Welham, 2003; McCormick and Froes, 1998). Following these early uses, the field of mechanochemistry has had a rich history, particularly in Europe which has led to the use of ball mills for processing a wide range of materials ranging from minerals to advanced materials. The majority of the review articles dates to the beginnings of the written history of mechanochemistry to the end of 19th century. They refer to experimental works of Carey Lea or to textbooks of F.W. Ostwald. The theoretical considerations concerning the relationship between chemical and mechanical energy could already be found in the first and second edition of Ostwald's text book from 1887 and 1893. Ostwald (1891 and 1919) introduced the mechanochemistry term and Ostwald ripening (small particles are more reactive). He regarded the mechanochemistry as a part of physical chemistry like thermochemistry, electrochemistry or photochemistry.

The establishment of mechanochemistry as a separate branch of chemistry is usually attributed to Matthew Carey Lea at the end of the 19th century (Heinicke, 1984; Juhász and Opoczky, 1990; Takacs, 2004a), who demonstrated that halides of gold, silver, platinum and mercury decomposed to halogen and metal during fine grinding in a mortar but melt or sublime undecomposed when heated. In these publications, the mechanical energy was for the first time pointed out to initiate chemical reactions and local heating is not the only possible mechanism for initiating chemical reactions by mechanical actions.

Most historical reviews mention the papers of Carey Lea as the first written documents of mechanochemical reactions. However, according to the last findings of Takacs (2000b), the mechanochemical preparation of mercury from cinnabar was described by Theophrastus of Eresus in his book *De Lapidibus (on stones)* published at the end of fourth century B.C. According to the cited work, examples of other mechanochemical reactions documented between 300 B.C. and the end of 1800s are mentioned in *Agricola's de nature Fossilicum*.

In the 1929, Tamman studied the effect of mechanical energy on metal. He concluded that grinding increases the dissolution rate of metal and the accumulation of mechanical energy (5-15%) is responsible for this process. In the 1930, it was primarily Fink and later Bowden and Tabor who investigated the effects of friction and abrasion on the oxidation reactions of metals and their compositions. They formulated the conception of "hot spots" (Steinike and Hennig, 1992), which explained the initiation and development of explosion by local increase of temperature at the contacts between two solids under mechanical action. Later, this theory was expanded to other processes, like oxidation of metals.

According to Huttig (1943), the mechanochemistry includes only the release of lattice bonds without any formation of new substances. The influence of mechanical energy on several reactions and their relations with changes in color was investigated by Peters (1962). The author used the thermodynamic argument to discuss these reactions. Peters added the

transformations caused by mechanical stress of material which are accompanied by chemical reaction to the definition of mechanochemistry category. Gerlach and Gock (1973) used the attrition milling to produce activated chalcopyrite. They stated that the milling greatly increased the dissolution rate of leaching processes.

The first book in the Tribochemistry field was published by Heinicke (1984). Heinicke's definition of mechanochemistry is still widely accepted: *"mechanochemistry is a branch of chemistry which is concerned with chemical and physico-chemical transformation of substances in all states of aggregation produced by the effect of mechanical energy"*.

The term of mechanical activation was defined by Smekal in the 1942. According to this author, mechanical activation is a process in which the reaction ability of a material increases without changing the material. If the activation causes changes in composition and structure, it is a mechanochemical reaction. Butjagin (1984) considers the mechanical activation as an increase in the reaction ability caused by stable changes in the solid structure. He proposed three main effects of mechanical activation on solids including structural disordering, structural relaxation and structural mobility (Baláz, 2000).

Mechanochemistry has become the topic of numerous publications and its significance is gradually increasing. Nowadays it is an integral part of agenda of any international congress on comminution. Many papers have been published in different journals and conferences up to now from different viewpoints in different fields of mechanochemistry subjects. Since the chemical effects of mechanical treatment have been investigated in a large number of systems, the following publications with regard to mechanical treatment recently published in English should be emphasized:

- Mechanical Activation of Minerals (Tkáčová, 1989)
- Mechanical Activation of Minerals by Grinding, Pulverizing and Morphology of Particles (Juhász and Opoczky, 1990)
- Mechanochemistry of Solid Surfaces (Gutman, 1994)
- Mechanochemistry of Materials (Gutman, 1998)
- Extractive Metallurgy of Activated Minerals (Baláz, 2000).
- Soft mechanochemical synthesis (Evgenii Avvakumov et al., 2001)

Terms like mechanical activation, mechanochemical processing (MCP), mechanical alloying (MA) and mechanical milling (MM) reflects the versatility of these techniques and how they have been employed in different fields (and at different scales) ranging from fundamental physics and advanced material science to traditional mineral processing. There are some disagreements among authors regarding the definition of aforementioned terms; however, the most accepted definitions are (Welham, 1996):

- *Mechanical activation: using mechanical energy to enhance a reaction during subsequent processing.*
- *Mechanochemistry: using mechanical energy to induce a reaction whilst the energy is being input to the system.*
- *Mechanical milling, milling of a pure metal or compound that is in a state of thermodynamic equilibrium at the start of milling.*
- *Mechanical alloying: using mechanical energy to cause (mutual?) solid solution (or dispersion) of elements (or compounds) during energy input. The terms refer especially to the formation of alloys from elemental precursors during processing in a ball mill.*

The main application of mechanical activation of minerals is found within the field of extractive metallurgy, where mechanical activation is used as a pre-treatment step prior to leaching and extraction in order to increase the solubility of the minerals in question. In extractive metallurgy, reactivity is measured in terms of dissolution kinetics. It was shown by Zelikman et al. (1975) that mechanical activation of crystalline materials resulted in a decrease in activation energy of dissolution reactions; therefore increasing the rate of leaching. Similar mechanisms are thought to be responsible for increasing the reactivity of activated material in different applications such as the kinetic of adsorption, catalysis and synthesis.

The effect of mechanical activation has been studied on many ore concentrates in order to build up an appropriate technological flow sheet. Concentrates of sulfides of Fe, Cu, Pb, Zn, Ni, Mo, As, Au and Re were tested in order to utilize the advantage of mechanical activation [Gerlach et al., 1973; Pawlek, 1976; Gock, 1977; Aytekin, 1981; Gerlach, 1982; Daiger and Gerlach, 1982; Daiger and Gerlach, 1983; Gock and Asiam, 1988; Kammel et al., 1987; Baláz et al., 1988, 1998, 2000; Kuzeci et al., 1989; Pawlek et al., 1989; Tkáčová et al., 1993; Kušnierová et al., 1993; Amer, 1995, 2002; Kahler et al., 1996; Maurice and Hawk 1998, 1999a, b; Welham, 1997a, b; 2001a, b, c, d; Welham and Llewellyn, 1998; Ficeriová, 2000; Godočiková, 2001; Godocikova et al., 2002a, 2002b; Ficeriová et al., 2002 and Mulak et al., 2002].

The method of mechanical activation has also been used for the concentrates of rutile (Gock and Jacob, 1980), ilmenite (Welham, 1997a, b), wolframite (Amer, 2000), zircon (Welham, 2001f), cassiterite (Amer, 2001), tantalite/columbite (Welham, 2001e) and silicates (Juhász 1974, Puclin et al.1995, Zhang et al. 1997 and Kalinkin et al.2003).

In addition to the application of mechanical activation in mineral processing and extractive metallurgy, mechanical activation is heading for new fields of research such as preparation of alloys, portland and pozzolanic cements, composite materials, nanocrystalline and amorphous substances, intermetallic compounds and smart materials for the 21st century.

1.2. Background

1.2.1. Comminution and mechanical activation

The application of treatments in milling devices may be briefly divided into three main categories: coarse grinding, fine grinding and mechanical activation. The coarse grinding is mainly used in mineral beneficiation and ore dressing to liberate locked minerals. Coarse grinding is rather well explored. It is known that the correlation between the average particle size and intensity or duration of milling may be described satisfactorily. In contrast, the oversimplified idea is invalid for sub-micron grinding range (Boldyrev et al., 1996, Karagedov and Lyakhov, 2003).

In the case of fine grinding, the size reduction takes paces but its explanation requires a more fundamental knowledge of process physics, especially the physics of mechanical energy relaxation (Austin, 1992). The fine grinding is an intermediate between coarse grinding and mechanical activation and its grinding limit is determined by ductile-brittle transition state if the mechanical energy relaxation in grains of a polycrystal has the same nature as in the particles of powder. However, when describing the grinding limit, the material property and mill intensity, which depends on mill construction and mode of operation, should be kept in

mind. For example, if the milling device can not transfer sufficient energy and impacts to powder being ground, so that the particles cannot be ground even if the size of particles are still larger than the ductile-brittle transition (Boldyrev et al., 1996).

The objectives for using mechanical activation are structural changes not size reduction, although the size reduction also takes place. When the mechanical energy relaxation changes from breakage to ductile (tough), the strain increases drastically in the material, from 0.1-0.3% up to 30-100% (McLean, 1965). Consequently, the extreme dislocation flows take place and subsequently moving and interacting dislocations develop other types of defects. In other words, changing the grinding process from breakage to plastic deformation causes structure distortions (Schönert, 1990, Goldberg and Pavlov, 1990). These structural changes determine the reactivity of activated materials (Boldyrev, 1996). The ground material is mechanically activated due to the increase of both the specific surface energy and the elastic strain energy. The activation free energy can be dissipated by different ways of energy transitions. Various relaxation processes can take place such as heating, formation of new surface, aggregation, adsorption, imperfections and chemical reactions. The surface activation can be relaxed as the newly exposed fracture surfaces are becoming active to the extent that agglomeration or adsorption of environmental gaseous species and moisture take place. The bulk activation can be relaxed by fracturing of brittle material or crystallographic lattice rearrangement by polymorphic transformation, mechanical alloying, mechanochemical decomposition or synthesis (of a new chemical compound). The elastic strain energy transforms into elastic energy of lattice defects such as point defects (vacancies), linear defects (dislocations), planar defects (stacking faults or sub-crystallite interfaces) and volumetric defects (structural disordering). The availability of these processes depends largely on the structural nature of the material involved and their kinetics depend much on the dissipation process involved (Lin, 1998). It should be noted that the kinetics of the activation process, or the overall rate of the activation process, depends on kinetics of the grinding process (Boldyrev, 1996).

1.2.2. Physico-chemical changes of mechanically activated material

Grinding may change the physical and chemical properties of the material. Sometimes, the changes can be utilized as an increase of the rate and amount of solubility, decrease of processing time and reaction time, increase of surface reactivity and attaining better catalytic effects, formation of new synthetic materials, improvement of the sinterability and strain stronger products, and production of new alloys and cements. Various processes may take place during mechanical activation of solids depending on the stress conditions. According to the published literature (Baláz, 2000; Lin et al., 1975, Fernandez-Bertran, 1999; Heegn, 1987 and 1979; Tkáčová, 1989) stress, deformation and fracture initiate changes in solids. Their types and volume are a function of material properties and the stress conditions in the milling devices. Generally the following effects may be observed in the activated solid substances:

- *Disintegration and fracturing, formation of new surfaces, enlargement of surface area, surface aggregation and surface oxidation*
- *Material abrasion and material transitions between solid particles*
- *Plastic deformation and disordering of crystal structure (lattice distortions), the formation of various lattice defects such as point lattice, linear defects, electron defects and amorphization; consequently increase of dislocation density, lattice strain and decrease of crystallite size*
- *Phase transformation in polymorphic materials*
- *Emission of photons, electrons and lattice components*

- *Stimulation of lattice oscillations and local heating of solids*
- *Electrostatic charge-discharge processes*
- *Magnetic properties and susceptibility*
- *Chemical reactions, decomposition, ionic changes, oxidation-reduction, complex formation, etc.*

Besides, the secondary effects of interaction between the stressed solids and the ambient medium must be taken into account. This interaction with the environment can be on intentional or not.

1.2.3. Relaxation modes in mechanical activation process

The structural relaxation has important effects on the reactivity of solids. There are two types of disorder and instability in activated material. One of these relates to highly excited, short lived defects with the relaxation time of $10^{-7} - 10^{-3} s$, which cause the activation to attain the highest level (Meyer, 1968). The short lived defects decay as soon as they are generated. The same short time is required for destruction of a solid by fracture. On the other hand, some long-lived defects, having a life length from 10^{-3} to $10^6 s$, are generated due to deep imperfections in the activated solid substances. These are very hot and unstable defects. The relaxation of these defects decrease the activation energy considerably, but they never reach the initial state (free defect-level energy) and consequently a residual activity (residual disorder) remains (Meyer, 1968). The influence of these defects has to be the subject of further mechanical activation studies.

The type of stress relaxation depends on external and internal conditions of stressing, i.e. on the magnitude and direction of forces acting, on the stress rate and frequency of loading and on the material nature. A variety of processes can take place during intensive grinding such as plastic deformation, heat release, fragmentation of particles, chemical reaction and phase transformation. Fig. 1 displays the changes in relaxation modes during mechanical activation.

Under the action of cyclic loading, the mechanism of failure changes with the particle size and the structure of the particles undergoing grinding. The brittle fracture is typical for the initial stage of the grinding process when the particles are larger than the critical size. With increasing grinding time (number of loading cycles), the particle size tends to decrease and previous cracks disappear. Defects are accumulated at the surface due to plastic deformation. By analogy with the well known mechanism of plastic fatigue in metals, it may be assumed that the initiation of micro plastic fatigue takes place in regions with a high concentration of micro plastic strain (Tkáčová, 1989). Depending on the internal and external conditions of stressing, the process can be halted at this stage ($d \leq d_{crit}$) or the cracks can propagate in a multistage energy-intensive process with a partial relaxation, which causes changes in the surface state of the particles formed. Ultimately, if the rate of deformation turns into a high level, the former changes may occur by the time during which the pulse acts is less than the critical time required to generate a crack. When a crack can not be formed in both cases ($d < d_{crit}$, $t < t_{crit}$), an increase of dislocation density and other lattice deformations takes place due to dislocation motion. The complete relaxation of the elastic energy as formation of lattice defects in plastic strain may take hours, days or even years. Elastic energy that remains in the activated material as defects is the source of the excess Gibbs energy and enthalpy.

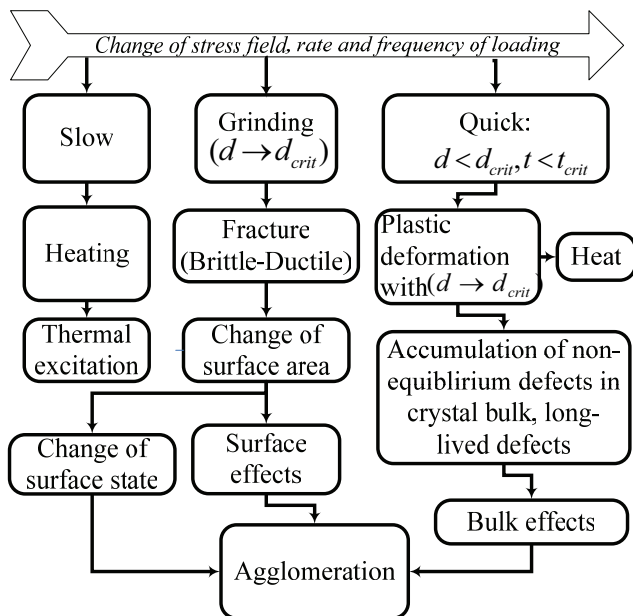


Fig. 1. *Changes in relaxation modes vs. the stress field (Boldyrev, 1986).*

1.2.4. Mechanical activation, relaxations, energy state and reactivity

The partially transferred active mechanical energy is stored in the form of lattice defects. In this way, the solid systems gain an activated state. The disordering process is equivalent to a decrystallization and an entropy increase which is reflected and characterized by an volume increase (decrease of bulk density). The structural disordering implies an increase of both entropy and enthalpy and thus stimulates the crystal properties according to the thermodynamic modifications. Fig. 2 displays the relationship between Gibbs energy and relaxations during mechanical activation processes.

In the case of comminution, only a small fraction (approximately 10%) of the excess enthalpy of the activated product may account for the surface enlarging. The main part of the excess enthalpy and modified properties can mostly be assigned to the development of thermodynamically unstable states of the lattice and not to the reduction of particle size. Since the activated system is unstable, the process of activation is reversible resulting in deactivation, re-crystallization, entropy loss and energy output of system. The reverse process continues to a thermodynamical equilibrium, but never reaches an ideal structure free of defects. As a result, in the course of mechanical activation of minerals, the relaxation processes cannot completely decrease Gibbs free energy and some energy remains in the material in the form of lattice defects. A proper subsequent reaction such as dissolution, can decrease the excess energy level in the reactant (activated material) and produce new components with low energy and stable conditions. In the same way, such reactions can take place during mechanical alloying or synthesis with extended of grinding and some other processes can occur like decomposition or solid solution reactions.

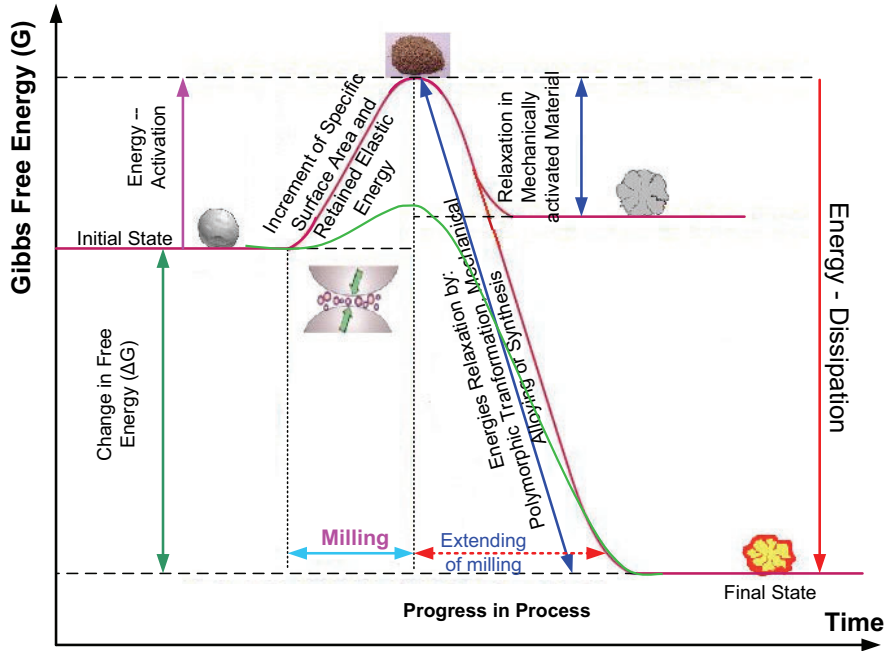


Fig. 2. Relationships between mechanical activation, relaxation and energy state. The red and green lines refer to energy state before and after mechanical treatments.

Reactivity of solids depends on the changes in Gibbs free energy during mechanical activation. Huttig (1943) defined activated solid substances as a thermodynamically and structurally unstable state. According to this author, the activated state of solid substances can be explained in terms of residual Gibbs energy:

$$\Delta G = G_T^* - G_T \quad (1)$$

where G_T^* , G_T and T are the Gibbs free energy of mechanically activated solid, Gibbs free energy of non-activated solid and temperature, respectively. According to the Gibbs-Helmholtz equation, the Gibbs free energy between activated and non-activated solid state depends on changes in the difference in enthalpy (ΔH) and entropy (ΔS).

$$\Delta G = \Delta H - T\Delta S \quad (2)$$

The values of ΔS are very small and negligible if the crystal disordering is low. In contrast, in highly deformed and disordered crystals, the values of ΔS can be significant and will influence the Gibbs free energy. The excess Gibbs free energy or enthalpy in the activated solid substances is due to the two main components: specific surface area and defect structure. In the case of comminution, only a small fraction, approximately 10%, of the excess energy of an activated product may account for the surface area. In contrast, the excess energy component of defect structure contains almost the remaining fraction of excess energy (Tkáčová et al., 1993; Baláž, 2000).

The activation energy for a chemical reaction, E , is a level of the energy barrier that initiates a reaction, i.e. the larger the activation energy, the slower the reaction. To progress a reaction, sufficient Gibbs free energy is necessary to overcome the activation energy. Generally speaking from the thermodynamic viewpoint, what is happening during mechanical activation is an increase of Gibbs free energy and this makes the activated material to reach a high enough potential to overcome the activation energy barrier to initiate a reaction. Zelikman et al. (1975) stated that the breaking of bonds in crystalline minerals causes a decrease in activation energy (ΔE).

1.2.5. Energy contribution to the long-lived defect structures

An important part of an analysis of the grinding process is the calculation of the contribution from the long-lived defects to energy content of activated solid substances. The calculation of the total energy contributing to the activated solid is not satisfactory in most cases. However, the energy contribution for each defect structure to satisfactorily interpret the grinding process is necessary. The energy of macro state is equal to the sum of the energy of the microstates.

$$H = \sum_{i=1}^m c_i H_i \quad (3)$$

where $\sum_{i=1}^m c_i = 1$ the concentration of lattice elements, c_i is their concentration in the i^{th} energy level and H_i is the enthalpy required to transfer a lattice element to the i^{th} state. In the case of fine grinding and mechanical activation, the detection of the mode of the state of lattice atoms and concentration is difficult. It seems that the following variables are the most suitable for characterizing the state of activated solids (Heegn, 1979; Tkáčová, 1989; Tkáčová et al., 1993; Tromans and Meech 2001):

- *Relative lattice distortion as a measure for dislocation density (ΔH_d)*
- *The formation of new phases such as polymorphic transformation (ΔH_p)*
- *The formation of amorphous material (ΔH_A)*
- *Specific surface area as a measure for the grain boundary to the surrounding medium (ΔH_s)*

For the enthalpy increase of the active solid the following equation is valid:

$$\Delta H_T = \Delta H_d + \Delta H_s + \Delta H_A + \Delta H_p \quad (4)$$

Further defects, and especially short-term activated states are also important, but can only be quantified theoretically and experimentally with difficulties. The presented approximation is not intended to take into account these defects. The quantitative estimate of the increase in molar chemical free energy (increase in stored energy) has been theoretically connected to the dislocation density by Tromans and Meech (2001) according to the expression:

$$\Delta H_d = (\rho M_v) \frac{b^2 \mu_s}{4\pi} \ln \left(\frac{2(\rho)^{-1/2}}{b} \right) \quad (5)$$

where M_v, b, μ_s and ρ correspond to the molar volume of mineral, Burger's vector, elastic shear modulus and dislocation density respectively.

The specific surface energy as a measure for the grain boundary to the surrounding medium has been given by the expression (Heegn, 1979 and 1987):

$$\Delta H_s = \sigma_s o_s \quad (6)$$

where σ_s and o_s refer to specific interfacial energy and specific surface respectively.

The energy fraction of newly formed phases (our experiments suggested only amorphization not the formation of other new phases) can be estimated in first approximation by equation (Heegn, 1979 and 1987):

$$\Delta H_A = C_A E_A \quad (7)$$

C_A and E_A denote the concentration of amorphous phase and molar amorphization energy respectively. Amorphization, which is in fact a highly distorted periodicity of lattice elements, is often compared to a quasi-molten state. In order to calculate the contribution of X-ray amorphous regions, the energy coefficients are substituted by molar enthalpies of fusion (Heegn, 1979 and 1987; Tkáčová et al., 1993).

1.3. The scope of thesis

The overall aim of this work is to test analysis techniques for studies of the influence of operational conditions and milling devices on the induction of microstructural characteristics during mechanical activation on hematite concentrate, subsequently, the conversation of energy into activated hematite. In addition, the study was applied on various grinding methods with different structural characterization methods in order to compare the efficiency of the grinding devices in inducing structural changes which are of importance and interest in the course of mechanical activation. Another goal of the project was to investigate the relationship between stress energy (grinding work) and structure changes in hematite treated in the mills instead of investigating of individual variables using stress energy and multivariate analysis. Five grinding methods were used in the study with various grinding variables to explore their effects. For quantitative and qualitative characterizations, three methods have been used; Integral breadth method, Warren-Averbach method and Rietveld analysis of X-ray diffraction (XRD) pattern. In addition, in the case of loose media mills, data were collected according to a statistical design at three levels for mill types and grinding time and two levels for media surface factors respectively. The study has been extended to explore the effects of structural changes on the thermal reactivity of mechanically activated hematite. For measuring the reactivity, a hydrogen reduction reaction using non-isothermal conditions was employed.

2. Experimental

2.1. Materials

The chemical analysis showed that the initial hematite powder contained about 97.91% Fe_2O_3 , 0.73% Al_2O_3 , 0.73% SiO_2 , 0.27% TiO_2 , 0.20% MgO , 0.0218% MnO , and 0.088% P_2O_5 . Other components such as K_2O , CaO , and Na_2O comprise 0.051 %. The X-ray diffraction analysis represented only the hematite diffraction lines. From the size analysis the mean diameter and F_{80} of the starting powder were estimated to around 46 and 80 μm respectively. The XRD diffraction pattern and size distribution of initial sample are given in paper I.

To exclude the instrumental broadening contribution from the samples, a standard reference sample, lanthanum hexaboride powder, LaB_6 with reference number SRM660a, proposed by National Institute of Standard and Technology (NIST) of U.S.A was used. The use of a standard sample allows a true comparison of results presented by different laboratories. The typical particle size distribution as determined by Laser Scattering is displayed in Fig. 3. The size of the crystallites was between 2 and 5 μm range. The XRD patterns and peak positions using CuK_α radiation ($\lambda = 0.15406 \text{ nm}$) is given in paper II.

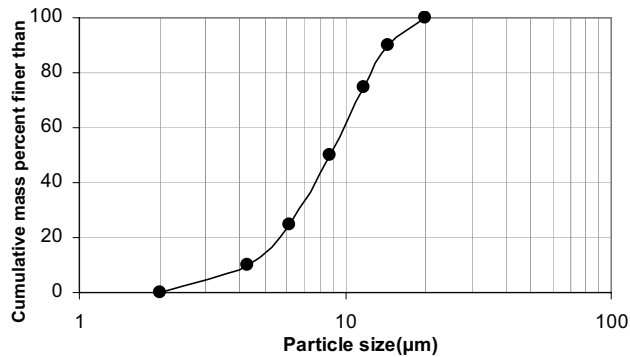


Fig. 3. Particle size distribution of standard sample (LaB_6).

2.2. Experimental techniques

2.2.1. Milling methods

Since the detailed data collection procedures are described in the attached papers, we only give here the main steps. For data collection, a full factorial experiment design with one qualitative and two quantitative factors was constructed. The qualitative factor, grinding mill, was set at three levels: tumbling, vibratory and planetary mills. The quantitative grinding time factor was leveled at 1, 3 and 9 h. The two levels 1 and 4 m^2 per kg of material were chosen for media surface variable. Dry grinding tests were performed according to the design. The martial temperature and specific energy input were recorded after finishing each experiment run. The material temperature was measured by a thermometer instantly after stopping the mill. The detail experimental conditions of milling tests are given in papers II and III.

The interparticle breakage of the fine feed fraction of hematite concentrate was investigated by stressing two particle beds with a pressure between 255 and 1,000 MPa. Grinding tests were carried out in a piston-die press, which consists of a steel die and a piston of 50 mm diameters, which can be fairly considered as a fully confined system. The material was loaded with a high pressure rock testing load frame X-Z-450-enhanced. The experiments were conducted in such a way that the wall friction effects during compression were eliminated. For details information, see paper V.

A stirred media mill which was operated in a re-circulated mode at a fixed flow rate was used for wet grinding. It consists of a 200 mm×90 mm stainless steel cylinder chamber (0.95 l of net grinding chamber volume) and an agitator with six perforated discs installed on a horizontal driven shaft. Furthermore, the mill is equipped with different sensors to measure simultaneously the temperature, the pH value and conductivity as well as zeta potential. The solid content was set at 20%. The pH value of the pulp was adjusted to 3 using commercially available nitric acid (HNO₃). Detail experimental conditions can be found in paper VI.

2.2.2. Data collection

The X-ray diffraction (XRD) patterns were collected using a Siemens D5000 powder diffractometer with Bragg-Brentano geometry equipped with a curved graphite monochromator in the diffracted beam arm and using Cu K α ($\lambda = 0.154 \text{ nm}$) radiation. The XRD patterns of samples were recorded in the range $2\theta = 10 - 90^\circ$, using a step size of 0.02° and a counting time of 5 s per step.

We loaded the recorded XRD patterns into Profile software to calculate the line broadening parameters. This procedure will be discussed in next section. After the extraction of line profile parameters, the physically broadened profile obtained by subtracting the instrumental contribution from using the standard reference sample (*LaB₆*). At the next step, the crystallite and strain components were deconvoluted from the physically broadened profile. To achieve this, three methods were used: Integral breadth (Williamson-Hall), Warren-Averbach and Rietveld methods. All methods are discussed in detail in the coming sections.

The particle size distributions of samples were measured by the method of Laser diffraction (CILAS 1064) in the liquid mode. From the Laser diffraction measurements, the mean particle diameter and granulometric specific surface area were also calculated. The specific surface area of samples was determined by the BET method with the Flow Sorb II 2300 (Micromeritics), from which the equivalent particle diameter was determined, assuming spherical shape of the particles.

The morphological characterization of the samples was performed using a Philips XL 30 scanning electron microscope (SEM) equipped with a LaB₆ emission source running at 20 kV. After drying, the samples were gold coated using gold sputtering prior to SEM investigation.

After the extraction of the microstructure characteristics and their comparison, the energy contributions of the long-lived defects were evaluated with a first approximation by previously proposed expressions based on microstructure characters. Finally, the stress energy (grinding work) has been estimated with regard to the grinding variables.

Simultaneous thermal analyses (STA) were conducted using a NETZSCH STA 409C instrument at heating rates of 10, 15 and 20 °C min⁻¹ to 850 °C. The high temperature furnace

was heated by graphite heating elements, which were protected by injection of inert argon gas. The furnace temperature was controlled by a tungsten thermocouple. The heating was performed under highly pure hydrogen as reduction gas with a rate of flow of 100 ml min⁻¹. The mass of samples was almost 95 mg.

2.2.3. Analysis of X-ray diffraction data

X-ray diffraction analysis is used as the main tool for characterization. In the following sections, some of the most important features of the analyses are described.

2.2.3.1. The source of line breadth

The broadening of diffraction peaks arises mainly due to three factors; instrumental effects, crystallite size and lattice strain. The instrumental effects are due to: (1) imperfect focusing, (2) unresolved α_1 and α_2 peaks or including the limited widths of the α_1 and α_2 in cases where they are resolved, (3) wavelength dispersion, (4) flat sample effect and (5) detector resolution. Therefore, the ideal peak shape (with negligible width) becomes broadened due to instrumental effects (Fig. 4). In addition to the instrumental effects, the broadening is due to small crystallite and lattice strain introduced. Dislocations, vacancies, interstitials, substitutionals, and similar defects are the causes of strain broadening. If a crystal is broken into smaller incoherently diffracting domains by dislocation arrays (small-angle boundaries), stacking faults, twins, or other extended imperfections, then crystallite size broadening occurs. To precisely extract the microstructure characteristics, the instrumental effect must be subtracted from the XRD diffractions and the microstrain and crystallite size contributions must also be separated from each other.

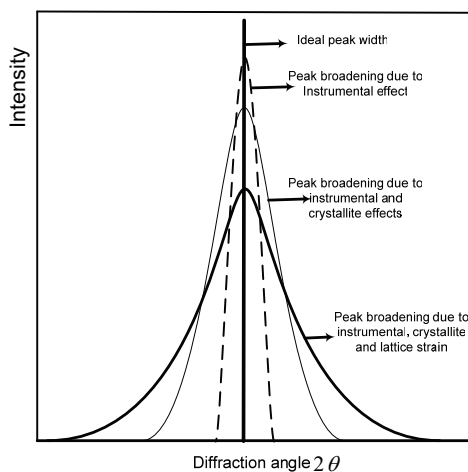


Fig. 4. *The broadening of X-ray diffraction peaks; the different sources of broadening are shown (not drawn to scale). The decrease of the line intensity implies the formation of an amorphous phase.*

2.2.3.2. The definition of microstructure characteristics

Unfortunately, there is an enormous confusion in literature concerning the definition of particle size, crystal size, crystallite size, and domain size.

A particle may consist of one or more crystals ("primary grains"). The different crystals may be separated by large angle boundaries as well as amorphous or crystalline interfaces. It is worth mentioning that the particle size itself can not be detected and measured by the XRD diffraction method (Fig. 5a). Similarly, the size of crystal is not accessible by XRD diffraction. The size of a crystal is, in general, equal to or less than the particle size (Fig. 5b). Each crystal may consist of one or more crystallites and the size of a crystallite is in general equal to or less than the crystal size. The crystallite size can be determined by means of powder diffraction, but not directly (Fig. 5b).

Each crystallite may consist of one or more coherently reflecting domains. A crystallite is broken into two domains as a result of stacking fault twinning ABCBA (Fig. 5d). For a reflection (hkl) represented by the diffraction vector a there are two domains, but only one crystallite. In contrast to this, for a reflection (hkl) represented by the diffraction vector b there may exist two domains and two crystallites.

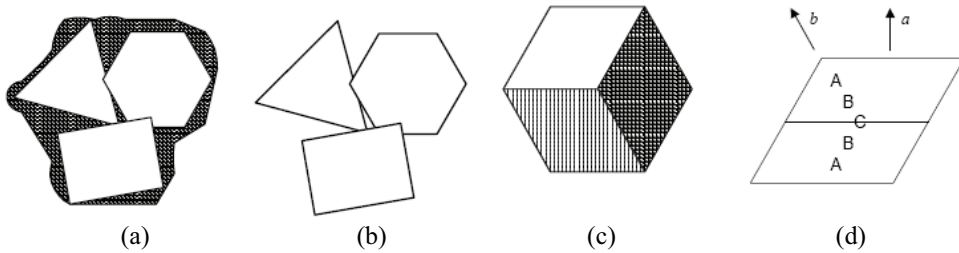


Fig. 5. Schematic representation of (a) particle or grain size, (b) crystal size, (c) crystallite size, and (d) domain size (Bruker Axs, 2003).

The crystallite size is a quantity which can not be directly measured. Actually measurable quantities are so-called column heights, as illustrated in Fig. 6. As the scattering power of a column is dependent on its volume, it makes sense to use volume weighted mean column heights (L_{Vol}). For example, only for a cube and only for (h00) reflections, the column height L_{Vol} is identical with the edge-length (L_0) of the cube (crystallite size for (h00)) as shown in Fig. 6a. For any other (hkl) a column height distribution will be observed with a mean less than the crystallite size. This is illustrated in Fig. 6b for a sphere, where for any given (hkl), a column height distribution is observed. For any given (hkl), L_{Vol} will not be identical with the diameter of the sphere, but can be derived from the known crystallite shape: $L_0 = 4L_{Vol}/3$. From this follows that any crystallite size term has to be used tentatively. With powder diffraction, only column heights can be determined. To obtain the true crystallite size, the true mean shape of the crystallites must be known in order to derive and apply a correction to the column height of each (hkl).

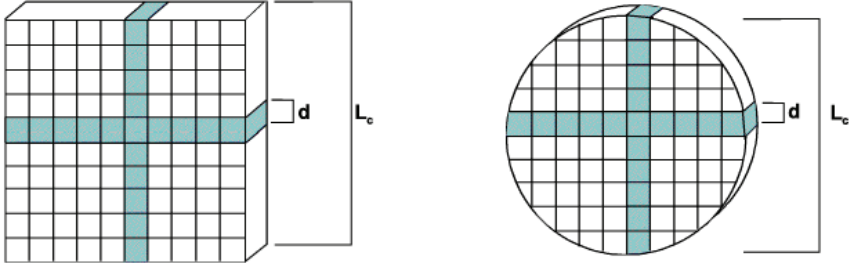


Fig. 6. Schematic representation of a square and a circular cross-section of a crystallite built up of columns perpendicular to the lattice planes (Haberkorn, 1999 cited in Bruker Axs, 2003). d : d -spacing; L_0 : Edge length and sphere diameter respectively.

Strain (e_0) (Fig. 7) is calculated by considering two extreme values of the lattice spacing d , namely $d + \Delta d$ and $d - \Delta d$, with $e_0 = \Delta d / d$. By equating the full width at half of maximum (FWHM) and/or β with the angular range corresponding to $d + \Delta d$ and $d - \Delta d$, and by assuming that Bragg's law holds over this range (implying that parts of the specimen with spacings $d + \Delta d$ and $d - \Delta d$ diffract independently, i.e. incoherently), it follows that:

$$\beta = 4e_0 \tan \theta \quad (8)$$

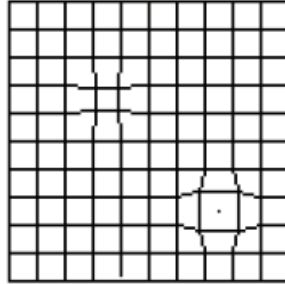


Fig. 7. Schematic representation of lattice strain (Haberkorn, 1999 cited in Bruker Axs, 2003).

2.2.3.3. Profile fitting procedures

In order to characterize the microstructure in terms of defect parameters such as crystallite (domain) sizes and microstrain and to obtain high precise and accurate line position, intensities, widths, and shapes from diffraction spectra, the Profile software was used. The procedures of profile fitting are summarized in Fig. 8. More information can be found in paper I.

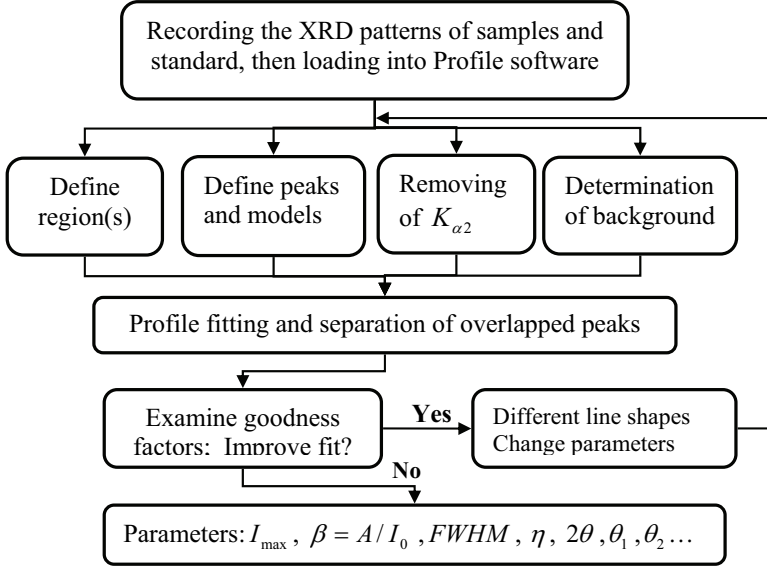


Fig. 8. The summary of profile fitting procedures.

It was experimentally verified that the Pseudo-Voigt line shape has a high correspondence to the XRD patterns which is an approximation form of Voigt line shape and consists of a linear form of Gaussian and Lorentzian line shape functions, as follow (Young et al., 1982):

$$I_p(x) = I_p \{ \eta C(x) + (1 - \eta) G(x) \} \quad (9)$$

where $C(x) = (1 + x^2)^{-1}$ and $G(x) = \exp[-(\ln 2)x^2]$, with $x = (2\theta - 2\theta_0) / FWHM$, η is Cauchy constant (mixing factor) and $2\theta_0$ is the position of the peak maximum. Fig. 9 shows schematically Cauchy and Gaussian line profile shapes where the tails decay rapidly for a Gaussian profile and slowly for a Lorentzian (Cauchy) profile. The Pseudo-Voigt occupies the intermediate situation of both functions.

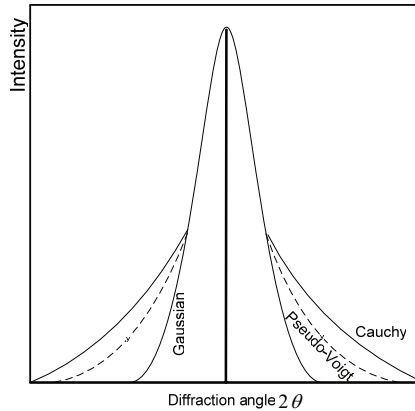


Fig. 9. Comparison of Cauchy, Gaussian and Pseudo-Voigt line profiles (not drawn to scale).

The integral breadth of the Pseudo-Voigt function is given by:

$$\beta = \frac{FWHM}{2} \left[(1-\eta)(\pi / \ln 2)^{1/2} + \eta\pi \right] \quad \text{or} \quad \beta = \eta\beta_L + (1-\eta)\beta_G \quad (10)$$

where β_L and β_G is Cauchy and Gaussian broadening components contributing to the profile.

Several fitting criteria for the profile shape function to the actual profile were considered and examined. Their definitions are (Siemens AG, 1996a)

$$\text{Reliability factor: } R = 100 \times \sqrt{\frac{\sum w(I_o - I_c)^2}{\sum wI_o^2}} \quad (11)$$

$$\text{Or, a weighted reliability factor: } RW = 100 \times \frac{\sum \sqrt{w} |I_o - I_c|}{\sum \sqrt{w} I_o} \quad (12)$$

$$\text{And theoretical reliability: } TR = 100 \times \sqrt{\frac{\sum wI_o}{\sum wI_o^2}} \quad (13)$$

where w is the weighting factor, I_c corresponds to the calculated intensity and I_o to the observed intensity. In the profile fitting process, each of the above mentioned factors were refined to a value of <5% for all the studied samples. Fig. 10 exemplifies the Pseudo-Voigt line shapes which are fitted to XRD diffraction patterns of hematite concentrate ground in the vibratory mill for one hour with media surface of $1 \text{ m}^2 / \text{kg}$. More information regarding profile fitting and modeling of standard sample characters can be found in paper I.

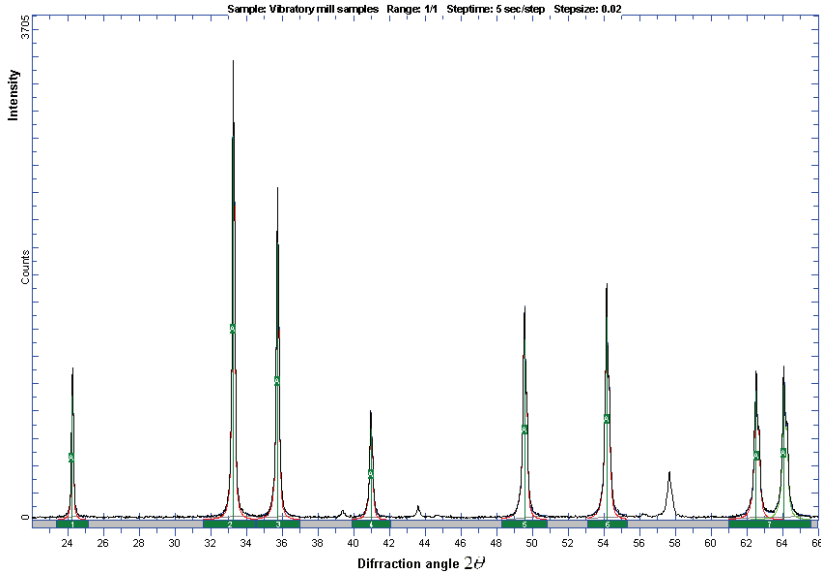


Fig. 10. Pseudo- Voigt line shape fitted to XRD pattern of hematite activated in the vibratory mill with low media surface for 1 hour.

2.3. Microstructure characterization methods

The X-ray diffraction line profile analysis (LPA) is a powerful tool to characterize the behavior of a material powder obtained under high-energy ball milling and prolonged grinding conditions. The causes of the line broadening are numerous. Generally, any lattice imperfection will cause additional diffraction line broadening. Analysis and deconvolution of the peak broadening can give important information regarding microstructural characteristics. To analyze peak broadening, two of the most common parameters are frequently used.

- 1) *The full width at half of maximum intensity (FWHM)*
- 2) *The integral breadth* and defined as $\beta = A/I_0$, A being the peak area and I_0 the height of the observed line profile.

The *FWHM* and β can be related to each other for a specific peak shape. Furthermore, there are several methods to extract the size of coherent diffracting domains from the diffraction peak. The applied methods in our work are described in the following paragraphs.

2.3.1. The Williamson–Hall integral breadth method

Williamson and Hall (1953) assumed that the size and strain profile components have Cauchy shape and proposed a method for deconvoluting size and strain broadening by looking at peak widths as a function of 2θ . The corresponding integral breadths are linearly combined and the integral breadth of the total broadening β_f can be written as (known also as Cauchy-Cauchy or Williamson-Hall plot):

$$\beta_f^* = \frac{\beta_f \cos \theta}{\lambda} = \frac{1}{D_v} + 2\epsilon d^* \quad ; \quad \frac{2 \sin \theta}{\lambda} = \frac{1}{d} = d^* \quad (14)$$

To make a Williamson and Hall plot, a plot of β_f^* (y axis) versus $2d^*$ (x axis) should result in a straight line, and the values for size and strain can then be obtained from the zero intercept and slope of the straight line respectively. Other variants of the Williamson-Hall method exist. That can be applied to a Gaussian profile in a similar way (known as Gaussian-Gaussian approximation). More details are presented in paper I.

2.3.2. The Stokes deconvolution

The Stokes Fourier deconvolution method (Stokes, 1948) followed by Warren-Averbach analysis of the physically broadened line profile is the least biased approach to analysis of the line broadening (Balzar and Ledbetter 1993 and 1995). Because this method analyze the entire shape of several reflections in the pattern (ideally higher order reflection of the same type i.e. (1 0 0), (2 0 0), (3 0 0). In this method, a Fourier series is fitted for each reflection of interest in the test samples and the standard sample. Once those results were obtained, they were used to deconvolute the sample broadening from the instrumental broadening via a Stokes Fourier deconvolution.

A general Fourier series which is periodic in x with a period length a can be represented as:

$$f(x) = \sum_{n=-\infty}^{n=+\infty} \left(A_n \cos 2\pi n \frac{x}{a} + B_n \sin 2\pi n \frac{x}{a} \right) \quad (15)$$

The index n takes all integral values from $-\infty$ to $+\infty$ and for each value of n , there is a cosine coefficient and a sine coefficient.

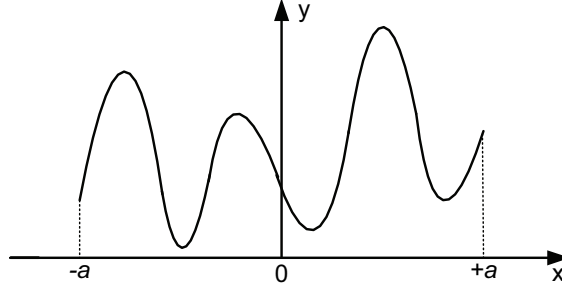


Fig. 11. Representation of the function $y=f(x)$ which is periodic in x with a period a .

The coefficient is made up of a real, $C_r(n)$, and imaginary, $C_i(n)$, part and the following expressions give the coefficients:

$$A_n = C_r(n) = \frac{1}{a} \int_{-a/2}^{a/2} f(x) \cos 2\pi n x/a dx \quad (16)$$

$$B_n = C_i(n) = \frac{1}{a} \int_{-a/2}^{a/2} f(x) \sin 2\pi n x/a dx \quad (17)$$

In the Fourier analysis the line breadth is corrected for instrumental broadening using Stocke's correction (1948).

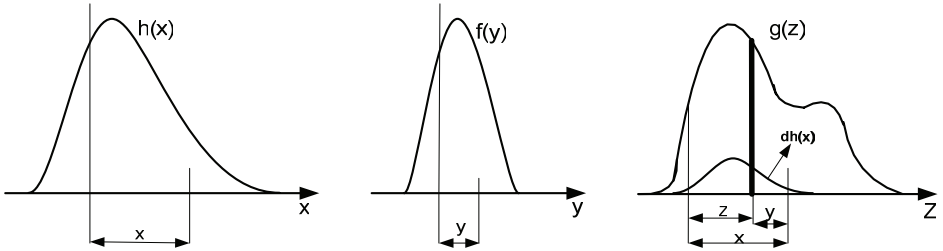


Fig. 12. Three curves which are involved in the correction for instrumental broadening. where $f(y)$, $g(z)$ and $h(x)$ are the curves corresponding to physical, instrumental and measured broadenings respectively (Warren, 1969).

According to Stockes approach, the observed distribution of X-ray intensity across a line is related to the instrumental and specimen broadenings by the following expression:

$$h(x) = \int_{-a}^a f(y)g(x-y)dy \quad ; \quad y = x - z \quad (18)$$

To obtain the structural parameters in a specimen, the physically broadened profile f must be extracted from the observed profile. Knowing $g(z)$ and $h(x)$, the Fourier coefficients of $f(y)$ can be calculated by Fourier analysis. The Fourier components $G(t)$ of the instrumental profiles $g(x)$ are given by:

$$G_r(t) = \frac{1}{a} \int_{-a/2}^{a/2} g(z) \cos(2\pi z t / a) dz \quad (19)$$

$$G_i(t) = \frac{1}{a} \int_{-a/2}^{a/2} g(z) \sin(2\pi z t / a) dz \quad (20)$$

where t is the harmonic number and the profile is divided into a intervals. A similar expression can be written for $h(x)$. Once those are known, the corresponding sine and cosine Fourier coefficients are calculated by:

$$F_r(t) = \frac{H_r(t)G_r(t) + H_i(t)G_i(t)}{G_r^2 + G_i^2} \quad (21)$$

$$F_i(t) = \frac{H_i(t)G_r(t) - H_r(t)G_i(t)}{G_r^2 + G_i^2} \quad (22)$$

The $f(x)$, physically broadened profile, can be calculated from $F_r(t)$ and $F_i(t)$ using the equation:

$$f(x) = \int_0^t F_r(t) \cos(2\pi x t / a) dt + \int_0^t F_i(t) \sin(2\pi x t / a) dt \quad (23)$$

2.3.3. The Warren-Averbach method

Warren and Averbach derived another definition of domain size: the surface weighted average. The Warren-Averbach method was originally developed for plastically deformed materials, but since its introduction it has been found successful applications for many other materials. The method is described extensively by Warren (1969). Each domain is represented by columns of cells along the a_3 direction normal to the diffracting planes (001) (see Fig. 13). All variables are expressed as a function of column length $L = n|a_3|$, which is assumed to be positive and comprising the distance in real space between a pair of cells along direction a_3 . The distances L and a_3 are calculated with a good approximation from the relation:

$$L = n|a_3| ; \quad a_3 = \frac{\lambda}{2(\sin \theta_2 - \sin \theta_1)} \quad (24)$$

L is the Fourier length, n denotes the integer and a_3 is the unit of the Fourier length in the direction of the diffraction vector, g , and the line profile is measured from θ_1 to θ_2 and λ is wavelength of the X-rays.

According to Warren (1969), the distribution of diffracted intensity can be expressed as a Fourier series. The convolution of the size and strain contributions on the profile in reciprocal space corresponds to the product of the Fourier transforms in real space. The expressions for deconvolution of size and strain components are given in paper I.

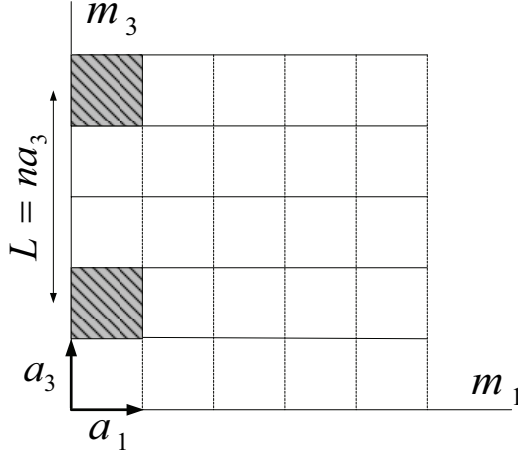


Fig. 13. Representation of the crystal in terms of column of cells along the a_3 direction. a_1 , a_2 and a_3 are the crystal axes. m_1 , m_2 and m_3 are integers such that the cell $m_1m_2m_3$ is the one whose origin is displaced from the crystal origin by $m_1a_1 + m_2a_2 + m_3a_3$ (Warren, 1969).

2.3.4. Rietveld refinement

The Rietveld method is becoming progressively more popular for microstructure characterization of materials. The method is a so-called “full pattern method”. In the Rietveld refinement, all the data points of a powder pattern are fitted to structure models which depend on adjustable parameters. The fitting to the measured XRD pattern was performed by a least square calculation. The calculated curve was based on the crystallographic structure models which also take into account sample and instrumental effect. The parameters of this model were refined simultaneously to achieve the best fit to the data by least square method. By the least square refinement a so-called figure of merit function R is defined, which describes the residual values between calculated and measured data (Young, 1993):

$$R = \sum_i w_i [y_i(ops) - y_i(calc)]^2 \rightarrow \min \quad (25)$$

where R is the residual value of the figure-of-merit function, w_i is $1/y_i$, $y_i(calc)$ denotes the calculated density and $y_i(ops)$ is the measured intensity at the i^{th} step.

The Bragg reflection position of a phase can be defined by the unit cell dimension of the phase. The absorption and polarization corrections, the structure factor, the Lorentz factor, grain size effects and preferred orientation define the intensity of a Bragg reflection for a given phase. It is expressed in the following form (Young, 1993).

$$y_{ci} = S \times \sum_K L_K |F_K|^2 \phi(2\theta_i - 2\theta_K) P_K A + y_{bi} \quad (26)$$

where S corresponds to the scale factor, K the Miller indices, L_K the Lorentz polarization, F_K the structure factor, the reflection profile between $2\theta_i$ and $2\theta_K$, P_K the preferred orientation function, A the absorption factor, and y_{bi} the background intensity at the i^{th} step.

The profile of a Bragg reflection is influenced by the geometry of the XRD instrument and experimental conditions, including the emission profile of the X-ray source and the slit sizes as well as the crystallinity, lattice errors of the investigated structure. The software TOPAS 2.1 from Bruker Axs (2003) was used for refinement in which it is possible to make all needed correction and refinement processes. The software package TOPAS 2.1 uses the fundamental parameter approach (FPA), and is therefore capable of estimating the instrumental influence and unit specific parameters. Cheary and Coelho (1998 and 1992) developed a fundamental model for a Bragg-Brentano-diffractometer, which describes peak broadening as a function of the geometrical settings. For these investigations, a Bragg Brentano model is required which causes the same peak broadening compared to the used measurement system. The software TOPAS 2.1 calculates the Bragg reflection profiles by the convolution of the mathematical functions of the above mentioned parameters (Cheary and Coelho, 1998 and 1992).

$$Y(2\theta) = (W \otimes G_{Ax} \otimes G_{Eq}) \otimes S_i \otimes P_i \otimes U_i + b \quad (27)$$

where $Y, W, G_{Eq}, G_{Ax}, S_i, P_i, U_i$ and b refers to the profile of the Bragg reflection, the emission file of X-ray tube, the instrument convolution in the horizontal plane, the sample convolution, the microstructure effects, any user supplied convolutions and the background respectively. \otimes denotes the convolution process.

In powder diffractometry, the above mathematical functions can be interpreted as the aberration functions of the diffractometer (Wilson, 1963) as well as the various specimen contributions leading to the so-called FPA. More generally, any combination of appropriate mathematical functions may be used in this context. TOPAS can accurately convolute and refine a wide variety of profile shapes both numerically and analytically without the need for explicit analytical convolution.

2.3.5. Resolving the size and strain components by TOPAS

After resolving the Bragg reflection profile, many methods are applied for detection of microstructure components, their separation and calculation. For modelling of microstructure effects, TOPAS is supporting the Double-Voigt Approach (Balzar, 1999), where crystallite size and strain comprise the Lorentzian and Gaussian component convolutions varying in 2θ as a function of $1/\cos\theta$ and $\tan\theta$ respectively. Furthermore, the Double-Voigt approach can be applied with fundamental parameters approach (FPA) and measured instrument functions. It is assumed that both size and strain effects are approximated by Voigt function. According to Balzar (1999), integral breadths of the size and strain components of Cauchy and Gauss parts can be expressed:

$$\beta_C = \beta_{SC} + \beta_{DC} \quad \beta_G^2 = \beta_{SG}^2 + \beta_{DG}^2 \quad (28)$$

where β_C and β_G are the Cauchy and Gauss components of total integral breadths β respectively. The term β_{SC} and β_{DC} are the Cauchy components of size and strain integral breadth, respectively and β_{SG} and β_{DG} are the corresponding Gaussian components. Once the components are calculated, the maximum lattice strain, e , and volume weighted crystallite size, D_V , can be calculated (Balzar et al., 2004).

$$e = \beta_D / 4 \tan \theta \quad D_V = \lambda / \beta_S \cos \theta \quad (29)$$

where β_D and β_S are the integral breadths of a Voigt function comprising the Gaussian and the Lorentzian components respectively. λ is the wave length and θ is diffraction angle.

Several criteria of fit (R factor) for judging the quality of a Rietveld refinement have been proposed. Those criteria show the deviation in accordance with the used model in percent. The most common R factors are the weighted profile R-factor (R_{wp}), the expected R factor (R_{exp}) and goodness of fit ($GOF = R_{wp} / R_{exp}$). Their definitions are (Bruker Axs, 2003):

$$R_{wp} = \sqrt{\frac{\sum w_m (Y_{o,m} - Y_{c,m})^2}{\sum w_m Y_{o,m}^2}}; R_{exp} = \sqrt{\frac{\sum M - P}{\sum w_m Y_{o,m}^2}}; GOF = \sqrt{\frac{\sum w_m (Y_{o,m} - Y_{c,m})^2}{M - P}} \quad (30)$$

where $Y_{o,m}$ and $Y_{c,m}$ are the observed and calculated data respectively at data point m respectively and M is the number of data points and P is the number of parameters. w_m refers to the weighting given to the data point m which is given for counting statistics by $w_m = 1/\sigma(Y_{o,m})^2$, where $\sigma(Y_{o,m})$ is the error in $Y_{o,m}$. An example of whole pattern fitting using Rietveld refinement is shown in Fig. 14. More information regarding the refinement procedure can be found in papers V and VI.

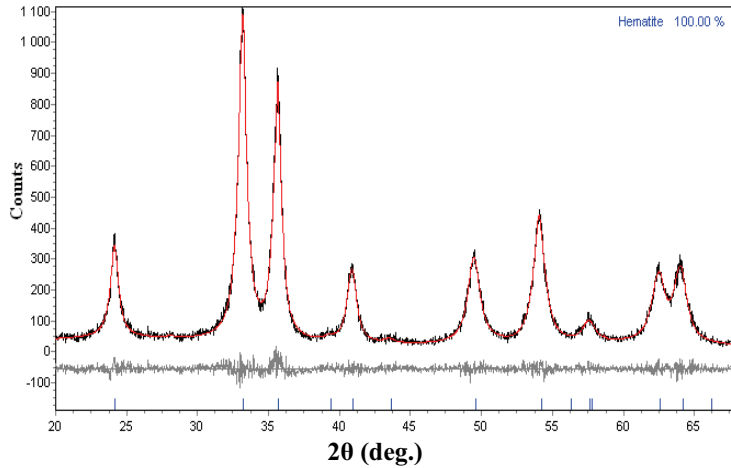


Fig. 14. Whole profile fitting using Rietveld analysis for X-ray powder diffraction patterns of the sample ground in the stirred media mill for 5 hours. The observed and calculated patterns are shown as continuous solid and red lines. The difference between the observed and calculated data is shown as continuous gray line under the diffraction pattern.

2.4. Thermal and kinetics analyses

Thermal analysis techniques were used to obtain insight concerning the effects of mechanical activation on the reactivity of hematite, reduction behaviors and kinetic parameters and their relationship with structural changes during activation.

Thermal analysis (TA) means the analysis of a reaction in a sample, which is related to an imposed temperature alteration. The present study involves TG (Thermogravimetry), DTG (Derivative Thermogravimetry), DTA (Differential Thermal Analysis) and DDTA (Derivative Differential Thermal Analysis). TG represents the weight loss of material during heating as a function of temperature. DTG carries additional information about the reaction steps clearly. DTA gives information regarding exothermic and endothermic processes of the reactions.

DDTA helps to characterize different reaction steps more clearly. Simultaneous thermal analysis (STA) technique combines thermogravimetry with differential thermal analysis or differential scanning calorimetry in one run (Brown, 2001). Thermogravimetric analysis (TGA) techniques have a number of advantages that are relevant to the study of any reaction, in which there is a weight loss or gain; the temperature can be controlled more accurately than by almost any other technique and, this is most important for rate studies. The chosen reaction temperature may be reached very quickly (Opfermann et al., 2002). The thermal analysis can provide a great information on the decomposition, reduction and oxidation, phase changes, and structural changes of substances.

Kinetic studies are to-day one of the most important applications of thermal analysis. Solid state kinetic data are of importance in many technological processes. Several methods have been applied for kinetics studies of solid state reactions. The methods for kinetic analysis can be classified based on experimental conditions selected and the mathematical analysis performed. Experimentally, either isothermal or non-isothermal methods are used. The mathematical approaches employed can be divided into model fitting and iso-conversional (model free) methods.

The earliest kinetic analyses were performed under isothermal conditions. The isothermal methods are based on the initial assumption that a single conversion function and a single set of Arrhenius parameters, A and E , apply over the full range of the conversion degrees. It is always necessary to watch for any indication, such as curved Arrhenius plots, that may indicate that these assumptions are not valid. The main problem in the isothermal kinetic analyses is that a sample needs some time to reach the experimental temperature. On the other hand, the non-isothermal experiments provide information on both $k(T)$ and $f(a)$, but not a separate forms.

In the non-isothermal analysis, two methods of model fitting and model free analysis have been used in the kinetic description. Model fitting methods were among the first and most popular methods for kinetic studies in particular for non-isothermal experiments because model fitting methods need only a single heating rate experiment to evaluate the kinetic triplets. In the model fitting method, the $f(a)$ term is determined by fitting various reaction models to experimental data. The popularity of these methods has been declined in favor of iso-conversional method of model free approaches (Vyazovkin and Wight, 1999; Khawam and Flanagan, 2005a, b). Because in the model fitting analysis, a single pair of Arrhenius parameters results from each application of the model fitting method. The majority of solid state reactions are not simple one step processes, and thus a combination of serial and parallel elementary steps result in an activation energy that changes during the course of reaction. In addition, the model-fitting methods yield high uncertainties of the Arrhenius parameters when applied to non-isothermal data (Vyazovkin and Wight, 1999). The obtained results in non-isothermal experiments can not be meaningfully compared with the triplets evaluated from isothermal experiments. The most important feature of model-free kinetic analysis is based on interpreting the dependence of E on the extent of reaction.

Model free kinetics is based on an isoconversional computational technique that calculates the effective activation energy as a function of the conversion (α) of a chemical reaction. Recently, isoconversional methods have been attracted considerable interests in different courses of science. In these methods, the basic assumption is that the reaction rate for a constant extent of conversion depends only on the temperature (Ozawa, 1965; Vyazovkin and Dollimore, 1996). Therefore, constant E values may be expected in the case of single-state

reaction, while in a multi-step process, E varies with conversion degree due to the variation in the relative contributions of the single steps to the overall reaction rate. In the model free analysis, several methods are used. To use these methods, a series of experiments has to be conducted at different heating rates (Vyazovkin, 1997). It has been known that the dependence of activation energy on the extent of conversion is the source of extra information and helps to identify the kinetic scheme of reaction. It is also worthy noting that the results from isothermal conditions are internally consistent with the results from model-free analyses results.

By using isoconversional methods one does not obtain directly neither the reaction model nor the pre-exponential factor, but the effective activation energy that tends to vary with the extent of conversion. However, Vyazovkin (2006) stated that in the standard kinetic description, the experimentally determined reaction model and the pre-exponential factors are deficient in physical meaning and needed only for the practical purpose of kinetic prediction. However, the model free approach allows kinetic predictions to be accomplished without evaluation of the reaction model and the pre-exponential factor that makes these two practically redundant.

For analysis of the reduction of hematite, nonisothermal experiments were conducted at three heating rates of 10, 15 and 20 C/min. The corresponding extents of conversion were calculated and a combination analysis of the isoconversional and model-fitting approaches were employed in kinetic analysis to obtain the kinetic parameters of the hydrogen reduction of hematite to iron using hydrogen gas. The Coats-Redfern analysis (Coats and Redfern, 1965) of the thermogravimetric data recorded at a single heating rate has been carried out by inserting various functions of $g(a)$ into the following equation that results in a set of Arrhenius parameters determined from the plot $\ln \frac{g(a)}{T^2}$ vs. $\frac{1}{T}$.

$$\ln \frac{g(a)}{T^2} = \ln \left(\frac{AR}{\beta E} \left[1 - \left(\frac{2RT_{\text{exp}}}{E} \right) \right] \right) - \frac{E}{RT} \quad \text{If: } (2RT/E) \ll 1 \Rightarrow \ln \frac{g(a)}{T^2} = \ln \left(\frac{AR}{\beta E} \right) - \frac{E}{RT} \quad (31)$$

where T_{exp} is the mean experimental temperature. A plot of $\ln \frac{g(a)}{T^2}$ vs. $\frac{1}{T}$ gives straight line. The activation energy and pre-exponential factor can be evaluated from the slope and zero intercept of the curves with a single heating rate respectively.

Among the isoconversional methods, the Kissinger-Akahira-Sunose method (KAS) (Kissinger, 1957; Akahira and Sunose, 1971) method has been widely used to estimate activation energy regardless of the rate expressions of reactions as follows:

$$\ln \frac{\beta}{T^2} = \ln \left(\frac{AE}{g(a)R} \right) - \frac{E}{RT} \quad (32)$$

For $\alpha = \text{const.}$, the plot $\ln \frac{\beta}{T^2}$ vs. $\frac{1}{T}$ obtained from curves recorded at several heating rates, should be a straight line whose slope can be used to calculate the activation energy.

The kinetic analysis procedures are summarized in Fig.15. More information concerning the kinetic analysis can be found in paper VIII.

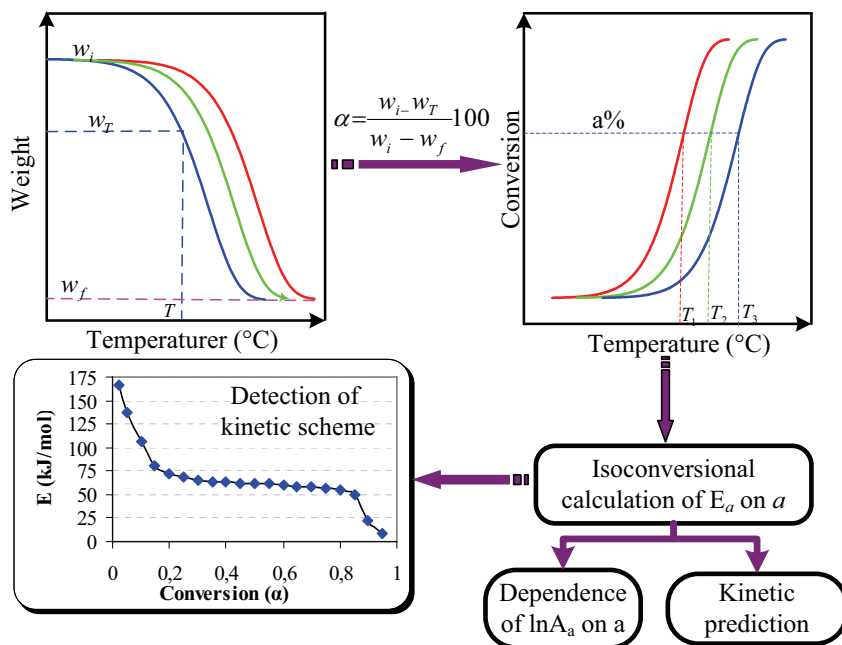


Fig. 15. The procedures of kinetic analysis in nonisothermal condition.

2.5. Data treatments

Profile fitting procedures were performed with the commercial software Profile (Siemens AG, 1996a). This software is used for fitting a line shape to measured XRD patterns in order to extract the line profile parameters. It also allows changing fitting parameters and different line shapes to fit properly line shape for measured XRD diffraction patterns.

The software WIN-CRYSIZE (Siemens AG, 1996b) was applied for extraction of crystallite size, crystallite size distribution, lattice strain data and its distribution from the diffraction peak broadening using the Warren-Averbach theory. WIN-CRYSIZE works with the fitted profiles from both test sample and a standard sample measurement. The lattice expansions were evaluated based on the peak positions which were derived from profile fitting.

For further Microstructural characterizations, we used TOPAS 2.1 software proposed by Bruker Axs GmbH (2003). TOPAS is a graphics based profile analysis program built around a general nonlinear least square fitting system. TOPAS integrates various types of X-ray and neutron diffraction analyses by supporting all profile fit methods currently employed in powder diffractometry:

1. Single line fitting up to whole powder pattern fitting,

2. Whole powder pattern decomposition according to Pawley (1981) and Le Bail et al. (1988), referred to as "Pawley method" and "Le Bail method",
3. Rietveld structure refinement (Rietveld, 1967, 1969)
4. Quantitative Rietveld analysis (Hill and Howard, 1987).

Profile fitting can be categorized as structural and non-structural models; whereas structural models are based on atomic positions, whereas non-structural models take into account the contributions of individual line profiles. The total intensity of the Bragg reflections and their positions are determined by the structural models. The non-structural models and hence the representation of diffraction lines depend on the instrument used as well as on microstructural or other properties of the sample.

We used Unit Cell software which is a free software proposed by Holland and Redfern (1997). It refines cell parameters from powder diffraction data. It uses a non-linear least square method, which allows the refinement to be carried out on the actual observed data (e.g. two-theta in the case of angle-dispersive monochromatic diffraction or energy in the case of energy-dispersive diffraction). Furthermore, the program incorporates regression diagnostics, particularly deletion diagnostics, to aid in the detection of outliers and influential data which could be deleterious to the regressed results.

The Variance analyses of structural changes were performed with a commercial computer program STATGRAPHICS PLUS 5.0 (Manugistics, 1999). With this software, it is easy to calculate the main effects and the interaction effects of the factors investigated which results in a better interpretation of data and the significance level of the effects.

Multivariate analyses were made by commercial SIMCA-P10.0 (Umetrics, 2002) software, which provides a large number of multivariate analyses techniques such as principle component analysis, PLS, PLS –DA analysis, etc.

3. Results and discussion

Through the experiments the particle size reduction, newly formed surface area, the changes in XRD diffraction pattern and broadening of the diffraction lines and microstructural characteristics were measured and estimated. Some important features of the obtained results are given in the following sections. More detailed information can be found in the papers presented in Appendix.

3.1. Dry milling with loose media mills

3.1.1. Particle size and surface area

Three types of mills with loose media, tumbling, vibratory and planetary mills are applied in this part. To increase grinding intensity, grinding time and media surface were extended up to 9 h and 4 m^2 per kg of hematite respectively.

Mechanical activation of hematite is accompanied by disintegration of the particles and increasing of the surface area. The particle size reduction and surface area measurements are summarized in Table 1 in terms of grinding variables.

Table 1. *The characterization of particle size and surface area.*

Grinding variables			Laser diffraction method				BET method	
Mill types	Ms (m^2 / kg)	Time (h)	d_{50} μm	R_{10}^* %	R_1^* %	SG m^2 / g	Surface m^2 / g	Size μm
<i>Tumbling mill</i>	1	1	10.8	61.8	19.3	1.1	1.4	0.81
	1	3	5.9	77.3	34.8	2.1	2.6	0.44
	1	9	4.5	83.9	44.3	2.2	4.6	0.25
	4	1	6.7	77.2	37.0	1.6	4.1	0.28
	4	3	4.1	85.1	47.0	2.4	5.3	0.21
	4	9	5.7	79.9	44.5	2.2	6.8	0.17
<i>Vibratory mill</i>	1	1	6.2	75.4	27.9	1.6	1.9	0.61
	1	3	3.9	86.7	45.6	2.1	3.9	0.29
	1	9	3.4	90.0	54.3	2.6	5.2	0.22
	4	1	5.7	79.8	41.6	2.1	4.4	0.26
	4	3	3.4	88.0	53.0	2.5	7.5	0.15
	4	9	5.6	73.6	42.9	2.1	18.4	0.07
<i>Planetary mill</i>	1	1	8.1	69.7	23.5	1.2	2.1	0.54
	1	3	5.0	84.0	42.2	1.8	3.4	0.34
	1	9	4.8	84.7	42.8	1.9	4.4	0.26
	4	1	4.4	85.8	45.7	2.2	5.1	0.22
	4	3	6.0	78.6	44.4	2.3	8.0	0.14
	4	9	6.7	74.0	38.8	2.0	8.8	0.13
<i>initial</i>	--	--	46.6	19.1	7.8	0.4	0.6	1.9**

R_{10}^* and R_1^* refer to the fraction of particles smaller than 10 and 1 μm respectively.

SG denotes Granulometric surface area; **data is not very precise.

According to table 1, there are two stages in the changes of the measured parameters. Most of the parameters change sharply in the initial stages of milling and continue to change slightly with the progress of milling. In the case of the lower media surface, $M_s = 1 \text{ m}^2$ per kg of material, prolonged grinding in both tumbling and vibratory mills tends to produce finer particles. This indicates that further size reduction in such mills at the given circumstances is possible. The size reduction with lower media surface is completed within three hours of milling in the planetary mill. The use of higher media surface provides a rapid size reduction in the initial stage of milling and a tendency of the particles to agglomerate during prolonged milling, which also could be investigated by granulometric surface area. The agglomeration of particles during extended milling was reported for various minerals by Welham and Llewellyn (1998), Welham (2001), Baláz (2000), and Zhang et al. (1996). Thus, it can be concluded that agglomeration phenomena may be a feature of extended dry milling. Grinding of hematite in lower media surface did not show any evidence of the formation of agglomerates with grinding in tumbling and vibratory mills.

The portion of particles smaller than $10 \text{ }\mu\text{m}$ is characterizing ultrafine grinding (Baláz, 2000). If the fraction of particles smaller $10 \text{ }\mu\text{m}$ is above 50%, the grinding proceeds into the ultrafine grinding region. Clearly, our ground samples have been affected by ultrafine grinding regime. The results concerning the BET surface area show that the specific surface area increases as the milling time and media surface go up. The maximum specific surface area in the milling with vibratory, planetary and tumbling mill amounted to 18.4, 8.8 and $6.8 \text{ m}^2/\text{g}$ respectively. The use of higher media surface produces larger BET surface area whatever milling devices are applied. The vibratory mill produced larger surface area, in particular in prolonged milling probably due to stressing of particles in shear mode and generation of higher temperatures. The comparison of particle size, granulometric surface area and BET surface area results give evidence to the agglomeration of particles in intensive grinding conditions, without decreasing of the BET surface area. This indicates that the pores of the agglomerates remain accessible for the nitrogen gas and probably the grinding process prevails the aggregation of particles. The effect of changing of media surface appears to be more important than the grinding time and mill type variables.

3.1.2. X-ray diffraction results

The XRD patterns of the mechanically-ground hematite show rapid changes during the grinding process (Fig. 16). The milled and unmilled samples are mainly composed of hematite indicating that hematite did not undergo a reaction or phase transformation during mechanical activation. As the milling time and media surface increased, the peaks became weaker and broader, suggesting refinement of the crystallites and increasing the lattice strain within the powder whatever milling methods were used. Both plastic deformation of the structure and disintegration cause broadening of X-ray diffraction lines. The structural disorder due to increasing abundance of X-ray amorphous material is manifested by decreases in the intensity of diffraction lines. Clearly, there are significant changes in the crystalline structure due to the extended milling and increasing of media surface. The peaks become broader and weaker with increasing of the milling intensity. With a first approximation, it was concluded that the planetary mill causes broader and weaker peaks than tumbling and vibratory mills. The alteration in the XRD diffraction patterns for hematite powder caused by milling was reported by many authors (Zdujić et al., 1999; Stewart et al., 2003; Tokumitsu, 1997). It must be emphasized that the literature data diverge to a large extent and there are large differences with respect to, for instance, the characteristics of the starting powder, mill

type, grinding variable and operation conditions and etc. The observed general trend, however, is consistent with each other, although the quantitative comparisons are not reliable.

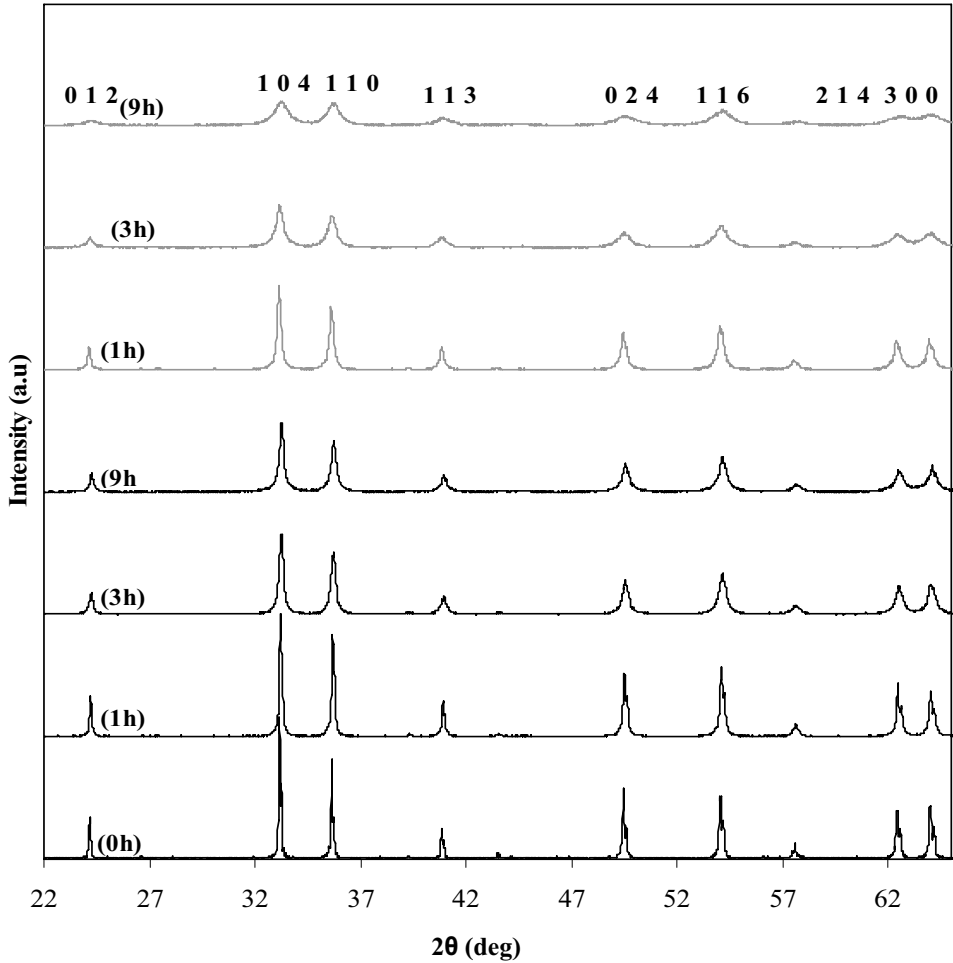


Fig. 16. The X-ray diffraction patterns of activated hematite as functions of the grinding time and media surface for planetary mill. The solid line and grey line refer to X-ray spectra obtained using media surface 1 and 4 m^2 per kg of hematite respectively.

3.1.3. X-ray amorphization degree

For a quantitative comparison, the average relative intensity and X-ray Amorphization degree, which are estimated based on the intensity and background of the eight most intensive reflections with comparing to those of starting sample, are determined from XRD diffraction lines. The influence of the media surface and grinding time are evident from Fig.17. It is obvious that there is a marginal difference between tumbling and vibratory mills. The maximum and minimum fractions of amorphous phase in the case of lower media surface created during grinding in the planetary and vibratory mills, amounts to 72 and 58 % respectively. There are small differences between tumbling and planetary mill products. In the case of higher media surface, with a first approximation, the planetary mill produced more X-

ray amorphous phase: after 9 hours of milling, 85% of the initial hematite was converted into amorphous phase.

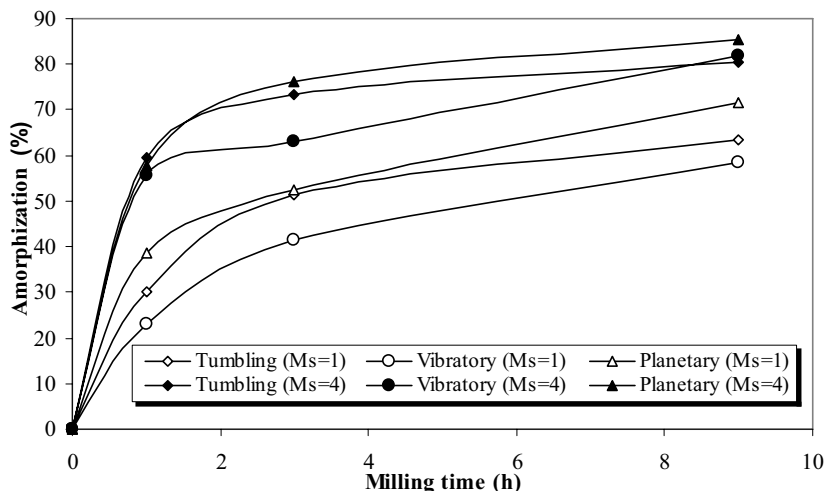


Fig. 17. *The changes in the amorphization degree vs. grinding variables. The average values calculated by taking into account the eight most intensive reflection peaks.*

As mentioned, the planetary mill favors the production of amorphous material whatever media surface levels are used. It should be noted that the amorphization increases sharply in the initial stages of milling and continues to increase steadily. The amorphization degree for activated gibbsite (Kitamura and Senna, 2001) and sulphide minerals (Baláz, 2000) has been investigated vs. grinding time. Our data trend agrees with their findings. The intensive milling seems to drastically alter the symmetry of activated material and subsequently the formation of amorphous phase. Since higher media surface (higher ball to powder weight ratio) imposes higher impact energy to the particles being ground, this leads to the formation of great amorphous phase.

3.1.4. Comparison of line breadths

XRD measurements of hematite powders showed that the XRD lines became substantially broadened after ball milling (Fig. 18). This broadening can be ascribed to crystallite-size reduction and introduction of lattice microstrain as shown in the next sections. According to Fig. 18, the physical broadening was calculated according to Halder Halder-Wagner (1966) approximation. From Fig. 18, it can be observed that the planetary mill causes the maximum broadening of reflection peaks. The broadening for the samples milled with the tumbling and vibratory mills differs marginally, the vibratory mill products shows slightly larger broadening than the products from tumbling mill. These characteristics will be discussed in the next section.

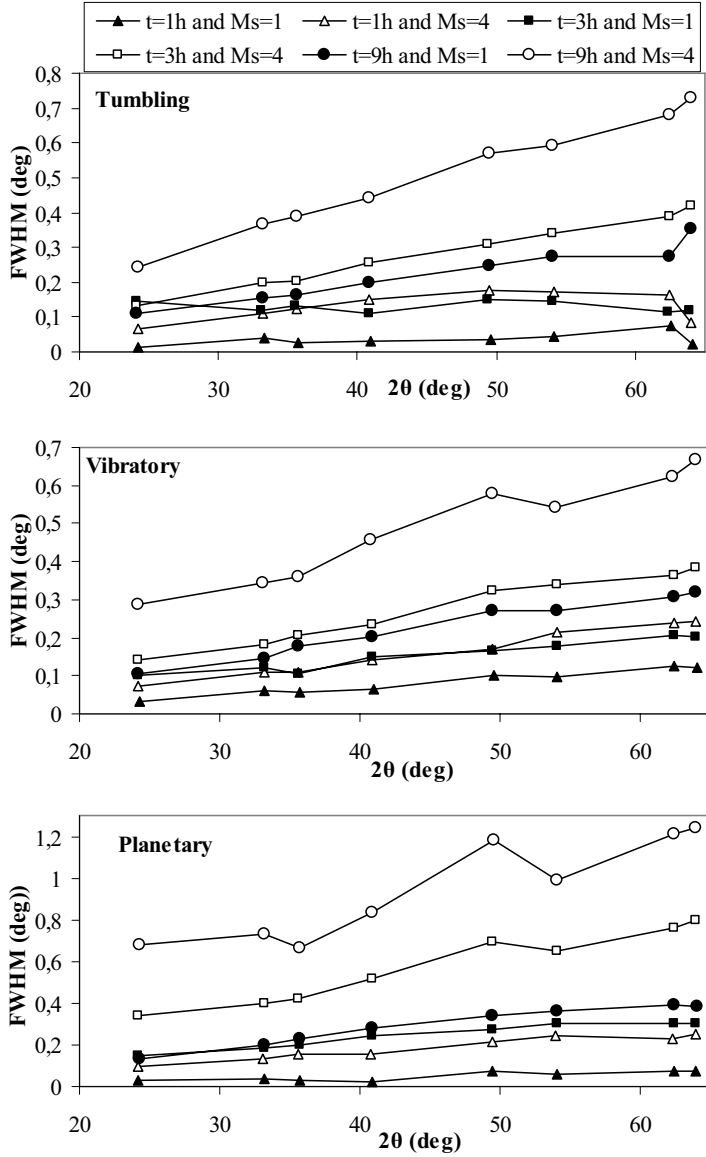


Fig. 18. Change in the physical FWHM for activated samples in different grinding times and media surfaces for three mills.

3.1.5. Resolving the size and strain components

Through the experiments, two methods of the Williamson-Hall plots and Warren-Averbach approach were used to deconvolute the strain and domain size components. Simple qualitative information regarding the nature of the coherently diffracting domain (i.e., morphology, size and strain information) prior to any detailed analysis, may be obtained on the basis of the Williamson-Hall plot. In addition, the Warren-Averbach method based on Fourier analysis,

which can precisely determine microstructure characters (Balzar, 1999), was used for [012] direction to precisely determine microstructure characteristics.

3.1.5.1. Integral breadth method (Williamson-Hall plots)

As discussed in papers I and II, based on the integral breadth method, it is possible to study the anisotropic character of the line broadening for deformed hematite as well as changes in the microstructural characteristics as a function of milling condition. The Williamson-Hall plots suggested that strain and size components simultaneously contribute to the line broadening in the milled samples. It was concluded that there is a difference in the elastic moduli of single crystal hematite existing between (024) and other crystallographic directions. The hematite lattice is 'soft' between the (024) and the other crystallographic directions. The scatter of the β_f^{*2} values indicates that the crystallite shape differs from a spherical form. The Williamson-Hall plots are given in papers I and II.

3.1.5.2. The results of Warren-Averbach method

The variation of crystallite size and root mean square strain (RMSS), $\langle \varepsilon_{L=10nm}^2 \rangle^{1/2}$, in direction [012] as functions of grinding variables are summarized in Table 2. Since the integral breadth method reveals the anisotropy contribution to the line broadening, the Warren-Averbach method is an unbiased method to evaluate the microstructure characters.

Table 2. The microstructural characteristics in [012] direction using the Warren-Averbach method for activated hematite in different environments. D_s and $\langle \varepsilon_{L=10nm}^2 \rangle^{1/2}$ indicate the surface weighted crystallite size and root mean square strain at $L=10$ nm respectively.

Parameters		$Ms = 1m^2 / kg$		$Ms = 4m^2 / kg$	
Mills	Time(h)	$D_s (nm)$	$\langle \varepsilon_{L=10nm}^2 \rangle^{1/2} \times (10^{-3})$	$D_s (nm)$	$\langle \varepsilon_{L=10nm}^2 \rangle^{1/2} (10^{-3})$
Tumbling	1	54.16	0.062	44.4	2.236
	3	42.6	1.52	25.0	2.84
	9	27.3	2.25	17.3	4.44
Vibratory	1	73.5	1.75	36.4	1.84
	3	43.5	2.08	23.7	2.79
	9	29.6	2.58	12.2	3.95
Planetary	1	66.7	1.25	28.1	1.94
	3	20.5	2.03	11.6	4.44
	9	16.5	3.011	5.6	5.32
Initial*	0	199.1	n.d.(0)	--	--

*Calculated using the single peak method.

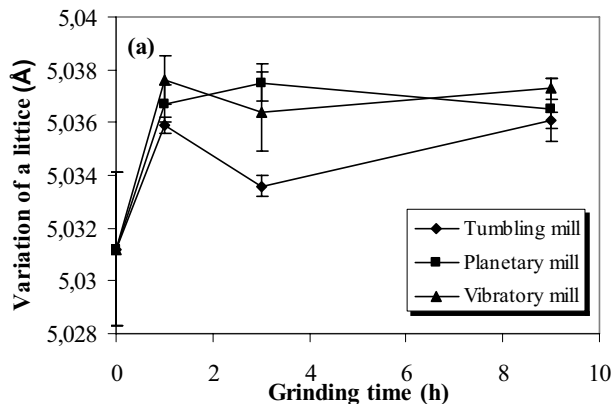
From Table 2, it is clear that the surface weighted crystallite size in direction [012] decreases and the microstrain increases as the milling time and media surface increase. The planetary mill showed a larger reduction of domain size and an increase of microstrain than the vibratory and tumbling mills in the intensive grinding condition. In the earlier stages of milling, the crystallite size declines rapidly to the nanometer range. Obviously, both the refinement rate and the ultimate grain crystallite size depend on the type of mill used, the milling intensity and the overall milling temperature. Variations in the ball media surface have a more important influence on the crystallite refinement: the larger the media surface, the faster is the reduction of grain size. Samples ground in the planetary mill for one hour

with lower media does not follow the general changes in microstructure characters among mills, which probably can be ascribed to the higher powder to ball weight ratio and subsequently hindering of ball motion during the milling process. On the other hand, the results related to the tumbling and vibratory mills products show some slight differences between size and strain components when the media surface changes in milling process. Obviously, grinding of hematite with lower media surface in the vibratory mill resulted in larger crystallite size and higher strain than grinding in tumbling mill. Furthermore, the products of the tumbling mill have slightly larger crystallites and higher strain values than of those for the vibratory mill, when hematite is subjected to grinding with higher media surface. This may be related to the changes in stressing conditions of particles in the milling process, especially in the vibratory mill. Perhaps, when grinding with lower media surface proceeds to higher media surface, the dominant type of stress changes from compressive and impact change to shear and/or attrition. These changes can facilitate the size reduction and breakage in fine and ultrafine range. The results regarding to the strain and crystallite size are in line with observations of Bid et al. (2001) and Sahu et al. (2003). Our results regarding crystallite sizes and strain in direction [012], however, show some differences. This can be related to the initial material characteristics and milling conditions. Bid et al. and Sahu et al. used planetary mills with a high angular velocity.

The Warren-Averbach method also gives some valuable information regarding the crystallite size and strain distribution in terms of crystal length (column length) from which some qualitative results and conclusions about homogeneity, the new phase formation and disordering of material can be drawn. These results are thoroughly discussed in paper II.

3.1.6. The variation of lattice parameters

The calculated lattice parameters and unit volume cell for the activated samples with lower media surface in different milling machines are shown in Fig. 19 as a function of milling time. It can be observed that the unit cell parameters and unit cell volume increased with activation time. This suggests a lattice and volume expansion of hematite during the mechanical activation process. The confidence level of data at 95% is also given in Fig. 19. There are some significant differences among different mill types for the lattice and unit cell volume characteristics as a function of grinding times, but they do not stand with higher media surface. The results concerning to higher media surface level is given in paper II.



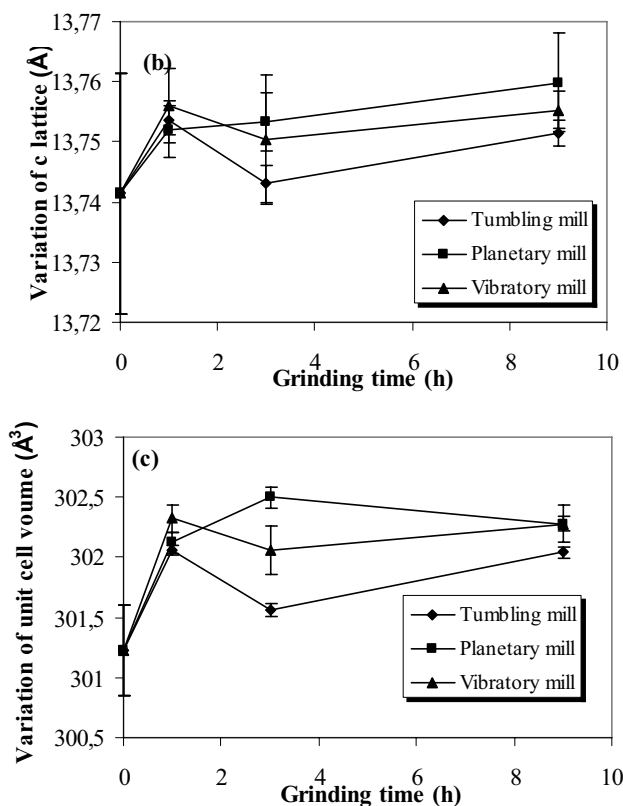


Fig. 19. Variation of lattice parameter and unit cell volume with grinding time in different milling devices using lower media surface level ($Ms=1 \text{ m}^2 / \text{kg}$).

3.1.7. The relationship between stress energy and structure changes

During mechanical activation, mechanical energy is partially transferred to the particles being ground. The stored energy relaxes by forming lattice defects and enlarging the surface area. The energy input energy during milling was recorded by an energy meter. An approximate evaluation of the stress energy has been made on the basis of an analysis of the forces acting in the predominant mode of stress in various grinding mills using the equations proposed by Heegn (1986). It should be kept in mind that these equations are derived on basis of the periodic-impulsive character of the energy transfer during grinding. This approach is only a mental abstraction that describes an idealized case, in which the material being ground is considered to be uniformly distributed throughout the mill and that the spatial conditions of interactions between particles and grinding bodies, as well as between the members of the particulate assembly, do not vary during the course of grinding. The advantage of this simplified approach is that it allows an estimation of the efficiency with which the energy is converted to grinding work. Paper III summarizes the equations used, which take into account the number of impulses and the rate of stress, which can be estimated from the known characteristics of the mill performance.

The amorphous phase content is determined based on the reduction of diffraction intensities and their background. The results are displayed in Fig. 20 for different mills as a function of

the stress energy. The amorphization degree increased to 80, 82 and 86% by grinding in the tumbling, vibratory and planetary mills, respectively, after releasing 5230, 51300 and 15600 kJ/kg of energy. These results indicate that much more energy is needed in the vibratory and planetary mills to produce the same amorphization degree as tumbling mill. The increase of X-ray amorphous phase due to intensive milling was reported for calcite, quartz and magnesite (Heegn, 1986), sulphide minerals (Baláz, 2000). The amorphization is in fact a highly distorted periodicity of lattice elements, and it is often characterized as a short range order in contrast to the long range order of a fully crystalline structure.

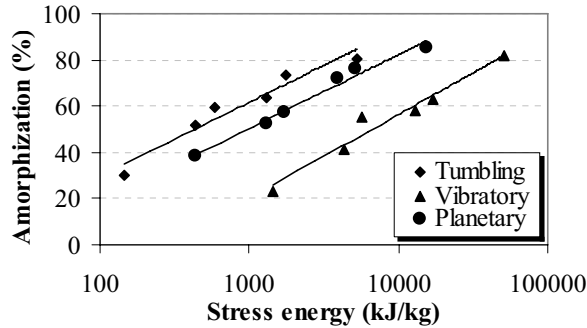


Fig. 20. *The content of X-ray amorphous phase for different milling environments as a function of stress energy.*

The changes in the surface weighted crystallite size and root mean square strain (RMSS) are shown in Fig. 21. With a first approximation, we can draw the conclusion that the largest crystallites for a given stress energy are resulted from the milling in the vibratory mill. With planetary, tumbling and vibratory mills, the hematite crystallites refined maximum up to the values of 5.6, 17.3 and 13.5 nm, respectively, after receiving the stress energy levels to the values of 15600, 5230 and 51300 kJ/kg. Generally, more severe decreases of crystallite sizes can be observed for hematite mechanically activated in the planetary mill regardless of stress energy.

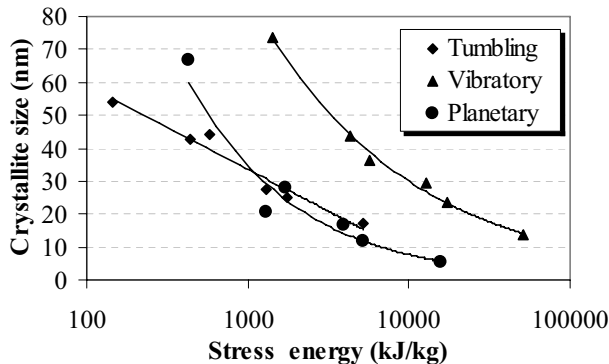


Fig. 21. *The variations of the surface weighted crystallite size in [012] direction with milling in different mills as a function of stress energy.*

The root mean square strain values, $\langle \varepsilon_{L=10nm}^2 \rangle^{1/2}$, for activated hematite in the different mills are displayed in Fig. 22. At lower levels of stress energy, there is only a small difference in the deformation of hematite lattice between the mills, while with growing grinding intensity, the difference becomes large. The distinct difference among mills starts after releasing more than 1700 kJ/kg of energy and the magnitude of differences maintains to increase as the stress energy intensifies. After releasing 5230, 51300 and 15600 kJ/kg in tumbling, vibratory and planetary mills, respectively, the microstrain $\langle \varepsilon_{L=10nm}^2 \rangle^{1/2}$ exceeds 4.4×10^{-3} , 3.9×10^{-3} and 5.3×10^{-3} .

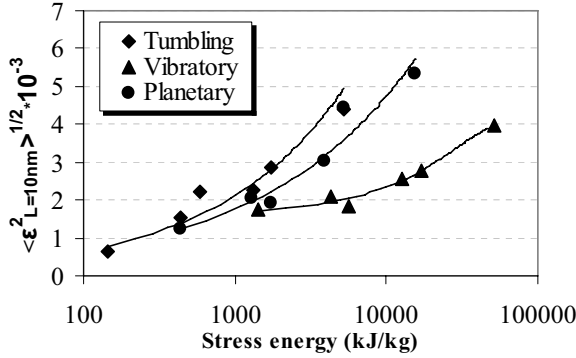


Fig. 22. Variations of the lattice strain values ($\langle \varepsilon_{L=10nm}^2 \rangle^{1/2}$) in different grinding machines vs. stress energy.

For our operation conditions, a comparison of the mills used can be seen in Fig. 23. Higher grinding energies are released in the vibratory mill. The planetary mill is placed in the medium position while the tumbling mill has a low level of grinding energy input. In addition, only a small fraction of energy input affects the particles being ground. This relation is linear. The planetary mill needs a higher energy input than other mills to achieve an identical grinding energy (stress energy). Grinding in the vibratory mill needs the smallest level of energy input to achieve the same stress energy as the tumbling and/or the vibratory mills. This is in accordance with the capacity and scale of the mills.

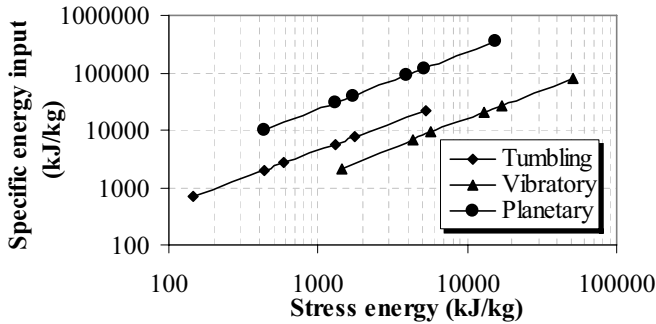


Fig. 23. Stress energy vs. energy input in milling operation conditions.

The stored energy (excess enthalpy) on basis of long-lived defects and stress energy are compared in Fig. 24. An increasing trend for the excess energy and the stress energy can be

observed, i.e., the higher the specific energy, the more excess energy is stored in hematite. According to Fig. 24, a distinguished difference can be observed between the mills. For a given stress energy level, the activated hematite in the tumbling mill contains the maximum excess enthalpy and the vibratory mill has the minimum excess energy. For example, to achieve a excess energy in hematite by mechanical treatment at about 60 kJ/mol, the required stress energies in tumbling, planetary and vibratory are around 1300, 2800, 17000 kJ/kg respectively. It should be pointed out that the X-ray amorphization is the most important energy carrier during mechanical activation (about 93-98% of the total stored energy).

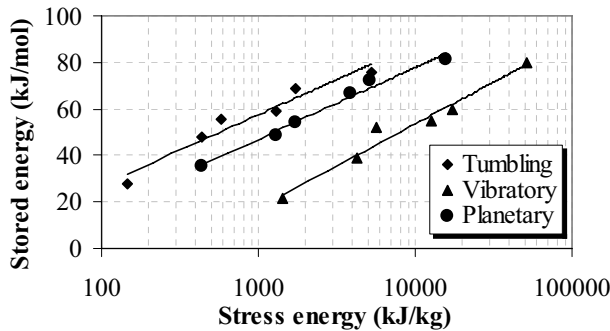


Fig. 24. *The comparison of stress energy and excess energy stored in activated hematite for different mills.*

Although these considerations are based on a very simple model, they will be helpful for a better understanding of the influence of different mills and operating parameters on grinding results and mechanical activation and induction of microstructure characters in the hematite lattice.

3.1.8. Multivariate projection and analysis

To investigate the relationship between grinding variables and structural changes during mechanical activation of hematite concentrate with loose media mills, a statistical analysis was done. The experiments were performed according to a statistical design by varying the grinding time, media surface and mill type. Based on a full factorial design, 18 experiments were conducted. The grinding tests were considered as objects. The microstructure characters and grinding factors were regarded as variables. An overview principle component analysis (PCA) on 27 variables yielded a three component model explaining 89% and predicting 76% of the total variance. An overview PCA analysis score plot (t1/t3) and loading plot (p1/p3) for acquired data are given Fig. 25.

According to the PCA score plot, it is clear that the observations obtained from higher and lower media surfaces are entirely separated from each other in the Y-direction. In addition, a clear trend in each group can be observed. As the intensity of milling (grinding time) increases, the observations shift from the left to the right side of the plot. The observations that contain similar characteristics are projected closely to each other.

From the loading plot (p1/p3), it can be observed that two main groups of variables are fairly correlated in the left and right sides of the X-direction: the variables CH, CA, Bs, Pin in left and the variables IE, SE, Dc, Ds, Dd, IB, SA, SH, A, Ht, Ha, Hs, Hd in the right part of the

plot. The variables within both groups are far from the origin and subsequently have high influence on the model. The variables within each main group are correlated positively as well. Further, two main groups of correlated variables in the left and the right sides of the plot are negatively correlated.

The PCA analyses reveal that the structural distortion reflected on XRD pattern data with increasing the line breadths (integral breadth) and reflection intensity reduction. The energetic excitation of the hematite structure is manifested by an increase in the excess enthalpy content in the ground hematite. The changes in the dislocation density, BET surface area and the formation of the amorphous material are the energy contributions to the excess enthalpy. The strongest correlation between amorphization (A) and excess enthalpy (Ht) indicates that the energy contribution from amorphization to the excess enthalpy (stored energy) is decisive. The comparison of the loading and score plots reveals that the objects concerning low intensity of milling (short milling time and lower media surface) are related to large crystallites, BET size and higher peak intensity. As the milling time increases, objects shift to the right side of the X-direction. The samples Tu11 and Pl94 yield the weakest and strongest structural changes during mechanical activation of hematite respectively.

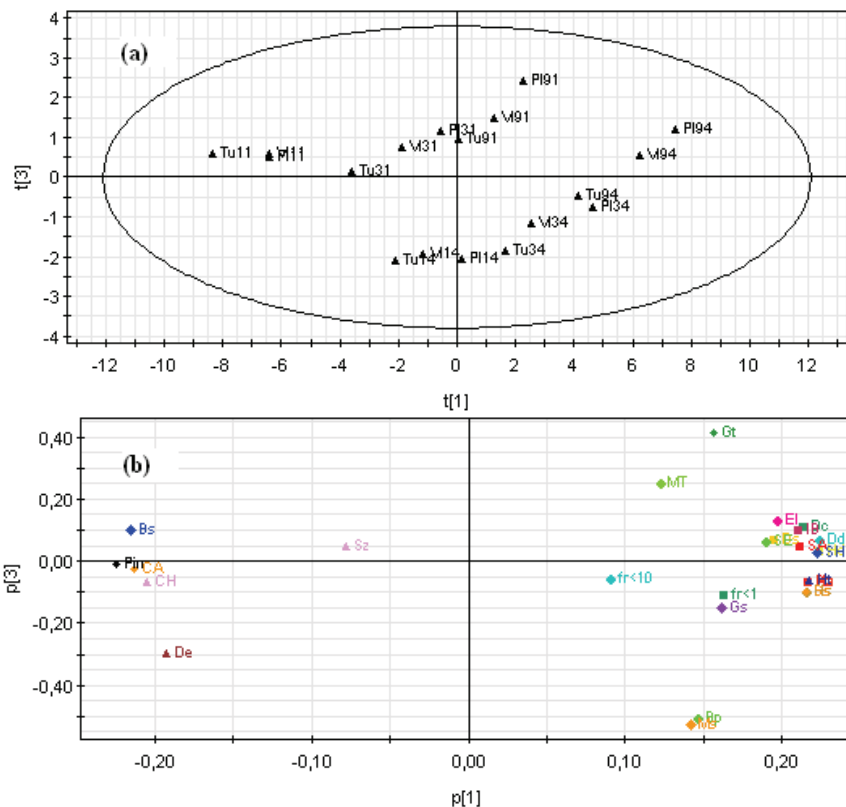


Fig. 25. PCA score plot ($t1/t3$) (a); and loading plots ($p1/p3$) (b) of data set. Terms Pl, Tu and Vi denote planetary, tumbling and vibratory mills respectively. The first and second number after each abbreviation refer to the grinding time level (h) and media surface (m^2 / kg) respectively.

To find out how the observations related to the levels of media surfaces are differentiated, the SIMCA method (soft independent modeling of class analogy) (Wold et al., 1984) was used. PCA analysis on each class indicated that one significant component is necessary to model adequately the class1 and class 2 sample sets, respectively. Fig. 26 shows DModx (class distance) for the class of lower media surface. The displayed critical distance D-Crit corresponds to a 5% level, and defines a 95% tolerance interval. It was found that all observations belonging to lower media surface class are within the critical distance. Moreover, it is clear that higher media surface observations are outside the tolerance interval of lower media surface DModx model, indicating that the observations belonging to lower media surface do not fit the observations of high media surface. Consequently, they are different from each other. The obtained results are in line with the PCA analysis.

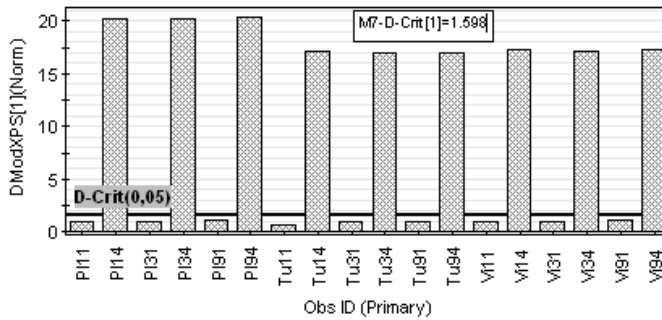


Fig. 26. *DModx plot for low level of media surface ($M_s=1 \text{ m}^2 / \text{kg}$)*

To understand whether further separations in terms of the mills are possible and which variables contribute to the separation, the PLS-DA method (partial least square discrimination analysis) (Sjöström et al., 1989) was used. PLS-DA analysis using SIMCA software yielded a four component model with $R^2X=0.90$, $R^2Y=0.87$ and $Q^2=0.62$. It was found that the components t1 and t2 (t1/t2) displayed separation better than other components. In Fig. 27a, it is evident that the different mills are well separated from each other in the second direction, Y, in a way that the observations of tumbling, planetary and vibratory mills are placed in upper, middle, and lower parts of the plot, respectively. This implies that the three mills might be different from each other based on the data set variables.

The three dummy variables are named by \$DA1 (tumbling mill), \$DA2 (vibratory mill) and \$DA3 (planetary mill) (Fig. 27b). From the projection of the dummy variables, it was concluded that the vibratory mill caused comparatively less structural changes in hematite than the other mills in spite of releasing higher stress energy. The planetary mill introduced relatively higher dislocation defects and generated higher lattice strain. The hematite ground in tumbling and planetary mills had comparatively higher X-ray amorphization degree and subsequently higher excess energy than hematite ground in the vibratory mill. The tumbling mill produced relatively lower specific surface than the others. It was concluded that the products of tumbling mill represented higher defect concentration (amorphization) per unit surface area despite the release of lower stress energy level by the mill.

approximately 55 kJ/kg. If the other X-variables are adjusted to their low and high levels, the transition from initial to steady state needs about 45 and 70 kJ/mol respectively.

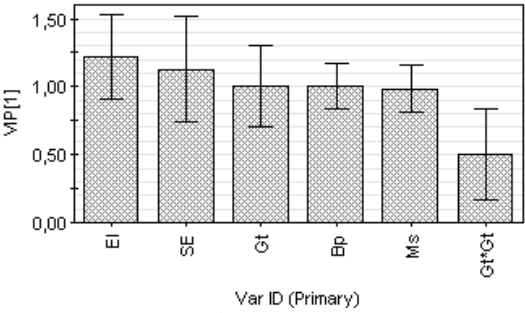


Fig. 28. VIP plot of PLS model on the five main response variables

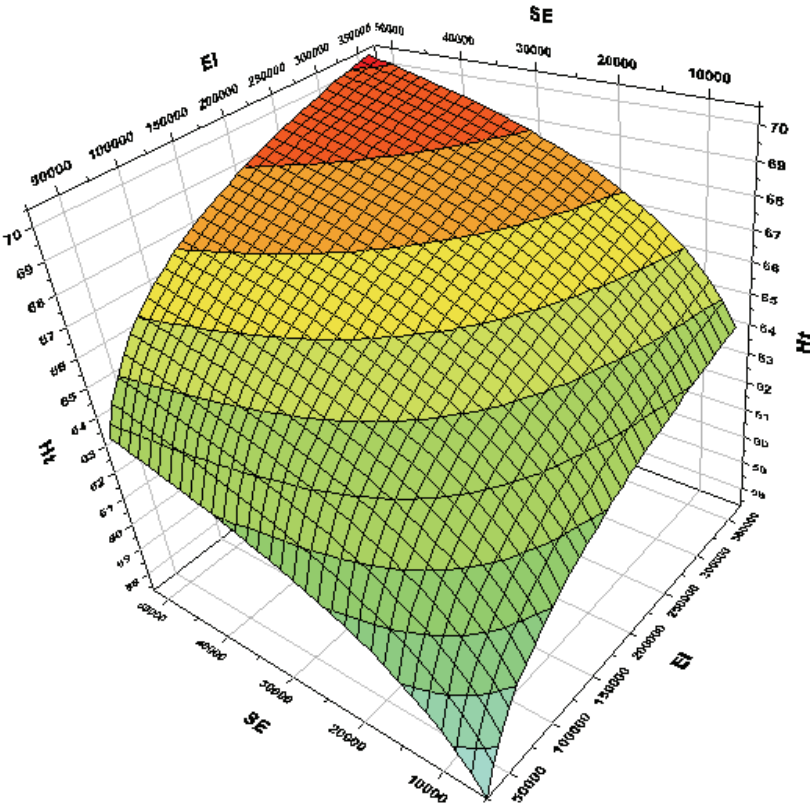


Fig. 29. 3D response surface plot for the stored energy (H_t) in activated material vs. specific energy input (EI) and stress energy (SE). Other X variables adjusted at their center levels.

3.2. Interparticle Breakage

With increasing industrial interest in high pressure roll grinding (HPGR) technology, there is a need for a more detailed understanding of the structural changes with stress field or grinding pressure that exist in the interior of the particle bed. The compressed bed with a piston and die is a typical example of bed comminution, which is called interparticle breakage method. Interparticle breakage occurs when a particle has contact points shared with other surrounding particles. In the bed comminution, the grinding of a large number of particles takes place simultaneously. It was found that the particle bed comminution has a higher energy efficiency, lower metal wear and higher energy transfer to the particles being ground compared to the ball millings (Fuerstenau and Kapur, 1995). Thus, the application potential of the bed comminution for activation of minerals comes into question and, subsequently, the structural changes during comminution in the confined particle bed have yet to be studied. To our knowledge, this study is the first survey on the structural changes during bed comminution.

The interparticle breakage of fine feed fraction of hematite concentrate was investigated by stressing two particle beds with a pressure between 255 and 1,000 MPa. The experiments were conducted in such a way that the wall friction effects during compression were eliminated considering the suggestions by Aziz and Schönert (1980). The effects of interparticle breakage in a confined bed on the structural changes of hematite concentrate were studied using a combination analysis of XRD line broadening, BET and particle size measurements. Structural changes were analyzed XRD line broadening analysis using Rietveld refinement and Warren-Averbach approach. The specific energy consumption (energy absorption) was estimated using loading and de-loading hysteresis curves. The obtained results were compared with the results from the milling in the tumbling mill in terms of net grinding energy.

It was found that the energy absorption by the particle bed varies between 6 and 31 J/g depending on the applied pressures and bed heights. The experiments indicated that energy absorption was a major factor for the interparticle breakage of hematite. In addition, it was revealed that an increasing bed height caused a higher stiffness and hence reduced energy absorption and subsequently declined the surface area, solid content as well as structural changes.

Fig. 30 shows changes in the BET surface area and X-ray amorphous contents for the samples ground in piston-die press as a function of energy absorption. The linear increase of the surface area is evident which agrees with the observations by Schönert and Reichardt (1993) for the comminution of corundum in a confined die-press. The BET surface area increased from $0.73 \text{ m}^2/\text{g}$ in the initial sample to $1.38 \text{ m}^2/\text{g}$ after an energy absorption of 31 J/g. The investigation of XRD patterns revealed slight increases in the line breadths and a reduction of reflection intensity as a function of energy absorption. These behaviors of interparticle breakage are similar to those observed during loose media milling. An evaluation of X-ray amorphous phase content based on the two most intensive reflection peaks (014) and (110) indicated that with increasing absorbed energy in the bed up to 15 J/g, the degree of amorphization increased sharply initially and then continued to change slightly. The maximum X-ray amorphization was calculated at maximum energy absorption, accounting for 31%.

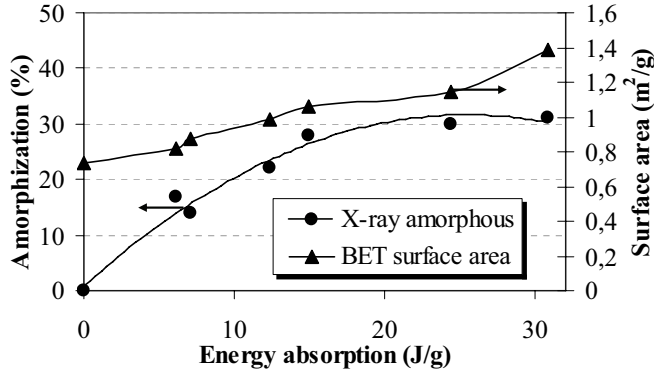


Fig. 30. Changes in the surface area and X-ray amorphization degree of hematite ground in piston-die press as a function of energy absorption.

The variations of crystallite size and lattice strain of hematite with energy absorption by the particle bed were calculated using Warren-Averbach approach and Rietveld analyses. The detailed analyses are given in paper V. It was revealed that the microstructure parameters of strain and crystallite size increases and decreases, respectively, as a function of energy absorption whatever methods are used for calculation. The results from Rietveld analysis are displayed in Fig. 31. The volume and surface weighted crystallite sizes reduced to about 108 and 53 nm, respectively, after releasing 31 J/g specific grinding energy. For the same energy, the root mean square strain (RMSS), $\langle \varepsilon_{L=10nm}^2 \rangle^{1/2}$, and the maximum lattice strain (ε) increased to 9.4×10^{-4} and 4.1×10^{-3} respectively. In addition, the compressive load leads to a slight decrease in the lattice variables and subsequently a slight increase in the density of ground material. A comparison with the results from loose media milling indicates that the stress types influence the lattice parameters differently, the first one (loose media) increases and the latter (bed comminution) decreases the lattice parameters.

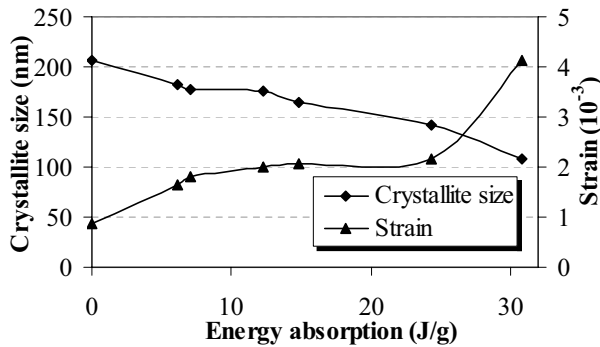


Fig. 31. Variation of volume weighted crystallite size and maximum strain obtained using Rietveld analysis.

The comparison of the results obtained from tumbling the milling and interparticle comminution is discussed in detail in paper V. A comparison of the results with loose media milling (tumbling) gives interesting results and confirms that the interparticle comminution

consumes less energy to achieve an identical structural refinement than tumbling mill. In other words, the interparticle breakage shows higher efficiency in structural changes in analogy with comminution. The obtained results of X-ray amorphization degree and crystallite size is given in Table. 3. It is clear that to achieve a X-ray amorphous phase about 30%, the tumbling milling needs 88 J/g net grinding energy while the particle bed grinding needs only 31 J/g. For the same levels of the energy in the two grinding regimes, the surface weighted crystallite size reaches about 54 nm. Similar results were obtained for other structural characteristics. This can be related to the fact that in the tumbling mill considerable energy losses occur in overcoming friction and wear of media and mill liners when energy is transferred to the particles by the grinding media. Furthermore, many collisions turn out to be largely ineffective because the entrapment of particles in the impact zone is a highly probabilistic hit-and-miss affair. On the other hand, no separate medium is required to transfer energy when a confined bed of particles is loaded under compression. Thus, energy losses are negligible due to interparticle friction (Fuerstenau and Kapur, 1995).

Table 3. Comparison of the X-ray amorphization degree of hematite ground in tumbling mill and confined particle bed.

Interparticle comminution				Tumbling mill			
Energy Absorption (J/g)	A%	Ds (nm)	Strain (10^{-3})	Net grinding energy (J/g)	A%	Ds (nm)	Strain (10^{-3})
0	0	186.2	0.86	0.0	0	199	0.57
6.1	16.9	99.7	1.65	88.5	30	54.16	1.304
7.04	14	77.9	1.82	265.0	51.5	42.6	2.2261
12.3	22	68.8	2.01	358.1	59.45	44.4	2.313
14.88	28	72.4	2.071	752.6	63.56	27.3	2.689
24.4	30	67.3	2.17	1052.0	73.5	25	3.607
30.86	31	53.4	4.14	3074.5	80.319	17.3	7.654

The study reveals the structural changes in confined particle bed comminution. As a result, the occurrence of structural distortions makes it possible use the bed comminution as a method for mechanical activation, although inducing severe structural changes needs higher pressures.

3.3. The effects of dry and wet milling on the structural changes

The effects of extended milling in a stirred media mill and a tumbling mill on the structural changes in hematite concentrate have been examined using a combination of particle size analysis, BET surface area measurement and X-ray diffraction (XRD), thermal (TG and DSC) and FTIR analysis. Rietveld's whole profile fitting based on crystal structure refinement is applied to monitor the microstructural evolution of the hematite phase. Warren-Averbach method of X-ray line profile analysis is also applied for a comparison of the above results. To avoid the agglomeration of particles during milling in the stirred media mill, a hematite suspension was adjusted at pH=3 (Fig. 32) where the highest absolute values for the ξ potential were obtained. Thus the best conditions were provided for electrostatic stabilization of the particles.

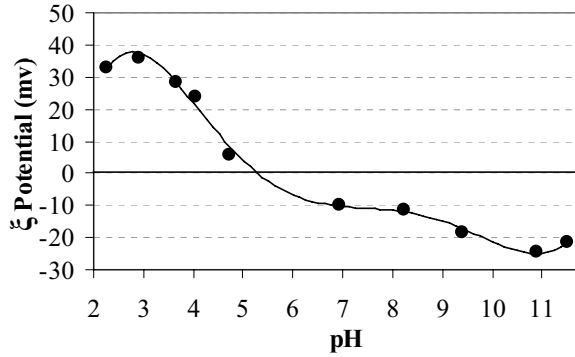


Fig. 32. *pH-dependency of the zeta-potential for hematite suspension.*

The structural changes and the microstructure characterizations characters were investigated using XRD analysis. For analysis of the structural changes based on line broadening, the Warren-Averbach and Rietveld methods were applied. Fig. 33 shows the XRD pattern of the sample ground for 24 hours in the stirred media mill wherein the whole profile fitting was adjusted on XRD pattern to extract microstructure characteristics.

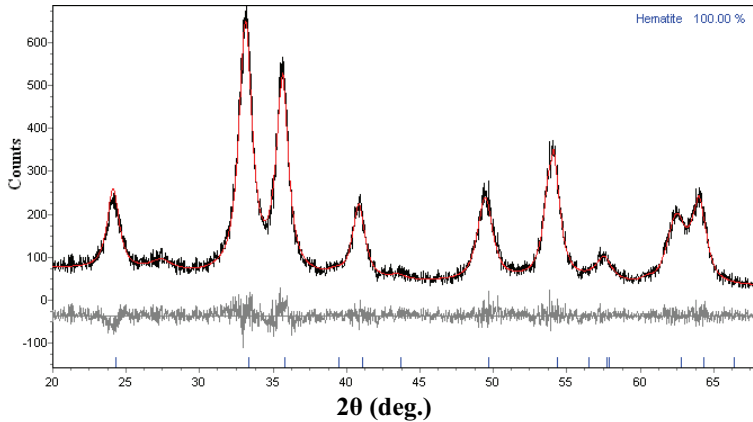


Fig. 33. *Graphical representation of Rietveld analysis for X-ray powder diffraction pattern of the sample milled for 24 h in the stirred media mill. Experimental data and refined simulated patterns are shown as continuous solid and red lines. The difference between experimental data and fitted simulated pattern is shown as a continuous gray line below the diffraction pattern.*

The XRD patterns of the samples ground in the stirred media mill as a function of energy input are given in Fig. 34. The distortion of the structure is reflected in the line broadening, the reduction of peak intensity and the shifting of reflections. The diffraction peaks for mechanically treated samples are lower and broader than of those for the initial samples, mainly due to a disordering process of hematite crystal structure by intensive grinding. The reduction of the diffraction peaks intensities implies the formation of amorphous material. The decrease of the X-ray diffraction intensities is accompanied by a general broadening of the XRD patterns. The increase of the XRD line breadths is due to the plastic deformation and disintegration of hematite. The presence of small, but remarkable, reflection peaks after

intensive grinding in the grinding mills can be taken as a further indication of the high milling resistance and the mechanical strength of the submicron hematite crystallites.

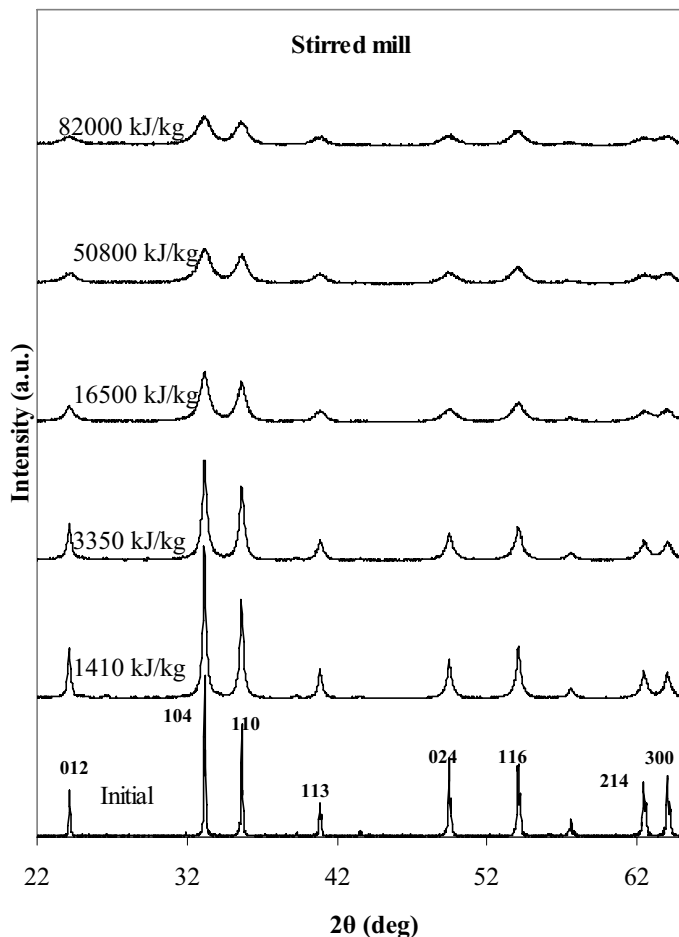


Fig. 34. XRD patterns of the initial and ground samples as a function of energy input in the stirred media mill.

Some important results concerning structural changes are summarized in Table 4 and further detailed information can be found in paper VI. It is found that the BET surface area, the X-ray amorphization phase content, and the XRD line breadths increases with increasing of energy input in the mills. The use of stirred media mill exhibits larger surface areas, more XRD line broadening and subsequently greater structural distortions compared to the tumbling mill for a given energy input, although the X-ray amorphous phase content remains unaffected by the grinding environments. The maximum X-ray amorphization degrees are calculated to about 80 and 95% after releasing of 22400 and 82000 kJ/kg energy in the tumbling and stirred media mills respectively. The maximum specific BET surface areas in the stirred media and tumbling milling increase to about 72.5 and 6.8 m^2 / g after 82000 and 22400 kJ/kg energy consumption respectively. It is worth noting that the BET surface areas in the products of the mills increase sharply in the initial stages of the milling. With the progress of the milling the

production of the BET surface area in the stirred media continues to increase gradually while in the tumbling mill the increase is very small. According to Table 4, it can be concluded that the formation of unit surface area in tumbling is associated slightly with a sharper increase in the amorphization degree. The content of amorphization material per unit surface area with tumbling milling is more than for the stirred media milling. According to Tkáčová (1989), the long-lived defects are being equally distributed throughout the bulk of particles when the material is subjected to grinding in mills bearing higher stress rate such as jet mills and high-speed disintegrator. If the material is subjected to grinding in mills producing lower rate of stress like tumbling and planetary mills, the long-lived defects accumulate preferentially in the near surface layer.

The microstructure results depict the nature of progressive evolution of the microstructure of the milling products vs. grinding energy input. Obviously, the crystallite size shows a decreasing and the strain an increasing trend as a function of energy input whatever mills used. In the earlier stages of milling, the crystallite size decreases rapidly to the nanometer range. As the intensity of milling increases, the ground hematite in stirred media mill yields more smaller crystallites than that of ground in tumbling mill. As a result of the structural refinement during milling, the volume weighted crystallite size in ground hematite are 17.4 and 10.9 nm after consuming 22400 and 82000 kJ/kg in the tumbling and stirred media mills respectively. For the same energy consumption in the mills, in turn, the maximum strain, ϵ , increased to about 7.7×10^{-3} and 12.9×10^{-3} . The results of the two Warren-Averbach and Rietveld are compared and discussed in detail in paper VI.

Table 4. *The summary of microstructure characters obtained using Rietveld analysis and BET surface areas and X-ray amorphous of the samples ground in the mills vs. energy input.*

Mills	Energy Input (kJ/kg)	BET surface (m^2 / g)	X-ray amorphous (%)	$D_v(nm)$	$\epsilon (10^{-3})$
Tumbling	720	1.4	30	61.7	1.30
	1930	2.6	51.5	48.4	2.2
	2670	4.1	59.4	32	2.3
	5450	4.6	63.6	27.9	2.7
	7520	5.3	73.5	26.8	3.6
	22400	6.8	80.3	17.4	7.7
Stirred media	1410	6.2	50.7	26	2.4
	3350	10.2	67.4	19.6	6.7
	16500	26.2	83.4	12.7	11.4
	50800	63.6	92.5	11.9	12.8
	82000	72.5	94.8	10.9	12.9
Initial*	0	0.59	$\cong 0$	106	0.57

The chemical characterization of the surface bonds absorbing specific IR radiation (DRIFTS) is shown in Fig. 35 for the ground samples in the stirred media mill. By comparison of the evolution of the spectra with the energy input it is clear that in the stirred media mill new peaks were observed at around 3600 cm^{-1} which are characteristics of the O-H vibration mode. The peak area of the hydroxyl group is increasing with the milling energy input, indicating that with an increase of the specific surface area, the surface O-H groups is increased. Physical adsorbed water can be excluded due to the pre-treatment of the powders, but the presence of new peaks may suggest the formation of a new phase during wet milling. However, a new phase could not be observed in the diffraction patterns, which is not

surprising since the amount of possible new phases are small compared to the bulk. Further surface sensitive measurements are necessary to conduct to gain a better insight into the mechanochemical changes of hematite during wet milling.

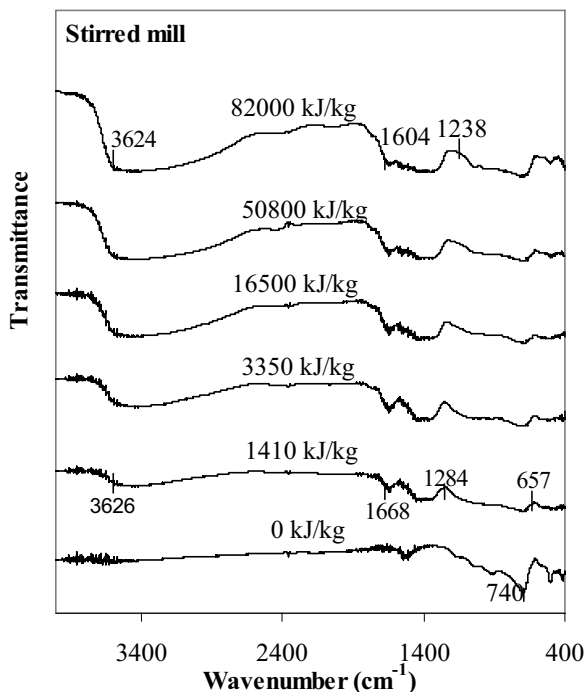


Fig. 35. DRIFTS measurements of ground hematite in stirred media mill as a function of the energy input.

3.4. The reduction behaviors and kinetics of activated hematite

3.4.1. Reduction behaviors

The effect of mechanical activation on the reduction behavior of a hematite concentrate has been examined using simultaneous thermal analysis (STA). Fig. 36 shows the thermal analysis curves for the initial sample. The investigation of DDTA and TG curves gives evidence of sequential reactions. A peak is centered at about 480 °C on the DDTA curve. The DTG curve displays a weight loss between 380 °C and 480 °C that is immediately continued by a second step of weight loss. The XRD pattern of the reduction product of the initial sample heated to 450 °C represented both magnetite and hematite phases. The weight loss was calculated to about 2.87% up to 450 °C, which is still lower than the weight loss value corresponding to the complete conversion of hematite to magnetite (3.33%). The reduction of the initial hematite to 500 °C produces reflection peaks of magnetite and iron phases in the XRD powder pattern. As a result, the reduction proceeds stepwise ($Fe_2O_3 \rightarrow Fe_3O_4 \rightarrow Fe$). However, the DTA peak corresponding to the first step of reduction is absent in the DTA curve. The effect is probably weak and subsequently masked and/or overlapped by the strong endothermic effect of the second step.

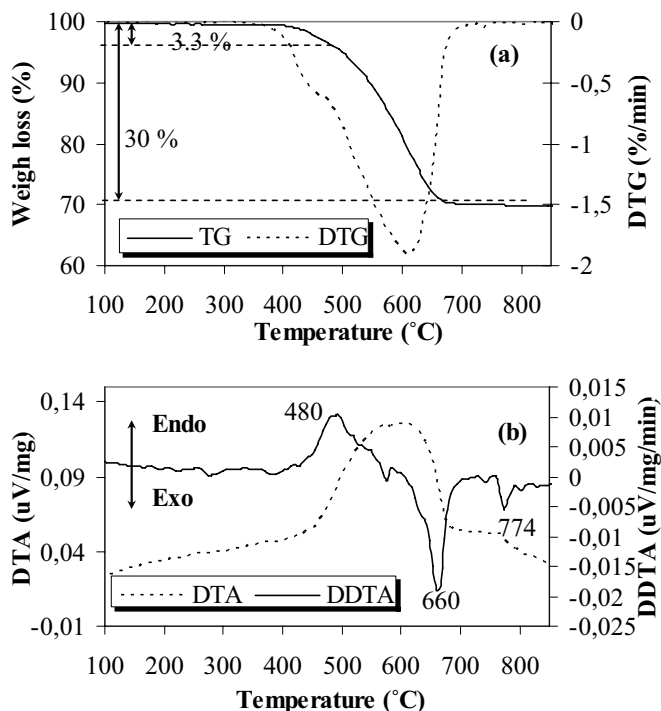


Fig. 36. TG and DTG curves (a) and DTA and DDTA curves (b) for the initial sample.

The thermal analysis curve for the sample ground in the vibratory mill under higher media surface for 9 hours are displayed in Fig. 37. It is clear that a broad and weak exothermic effect appeared at lower temperature. Developing and sharpening of the exoeffect was observed with increasing grinding time and is reported in detail in papers VII and VIII. This is a consequence of the reduction of the energy required to destroy the crystalline structure of hematite. The energy supplied by milling causes structural disorder due to the distortion or breakage of the crystalline network. This was evident from the reduction of the intensities of XRD peaks reported in previous sections. On the other hand, the appearance of the exoeffect may imply an increase of exothermic peak intensity. This can also be explained by the action of mechanical activation. The active mechanical energy partially transferred to the ground particles is stored in the form of lattice defects. In this way, the solid systems reach an activated state and the energy (enthalpy) of ground hematite increases. Thus, the excess energy can be released when the activated material is heated. As a result, the exoeffect peak appears on the DTA curve. The exothermic peak is followed by an important, broad and strong endothermic peak at higher temperature ranges. The maximum characteristic temperature of the endothermic peaks also shifts slightly to a lower temperature with increasing grinding time. This peak is caused by the reduction of magnetite to iron metal. The reduction of magnetite to wüstite, as an intermediate reduction product was not observed, which agrees with previous observations (Munteanu et al., 1997; Sastri, 1982).

According to the TG curves, the reduction of hematite to iron exhibits a two-step weight loss that can be identified from changes in the slope of the curves. The total weight loss for all of the samples is 30%, which corresponds to the complete conversion of hematite to magnetite.

From the investigation of the TG curves, it can be seen that the hydrogen reduction of mechanically activated samples initiates at low temperatures compared with the initial sample. It was found that the beginning temperature (onset) of the reduction decreases from 421 °C in the initial sample to 330 °C in the mechanically activated sample, depending on the grinding intensity. Further, the reduction of hematite to magnetite in the activated samples is more pronounced due to the mechanical activation. At low temperatures, the activated samples give a higher degree of conversion than the initial sample. Besides, intensive grinding resulted in improved resolution of overlapping reduction events (see Figs.36 and 37).

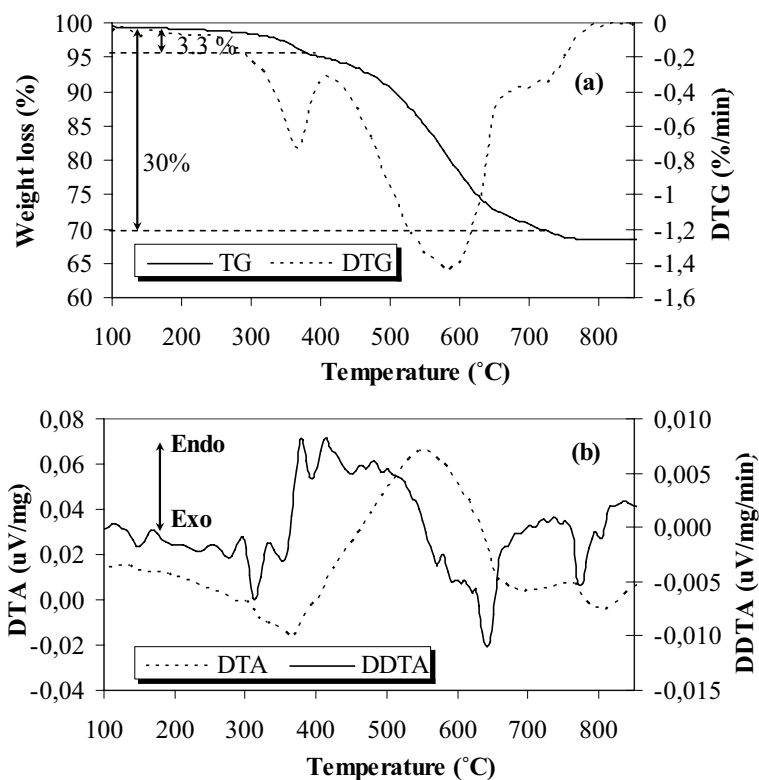


Fig. 37. TG and DTG curves (a) and DTA and DDTA curves (b) for the ground sample in the vibratory mill for 9 hours with higher media surface.

The two weight loss steps are observed as minima in the DTG curves. Interestingly, the first step of weight loss for mechanically activated samples is more pronounced than for non-activated hematite. The mechanical activation resolved two steps of reduction. Moreover, the area of the peak in the second step of reduction decreases concomitantly as the area of the peak in the first weight loss step increases, depending upon grinding variables. Detailed information regarding the effects of grinding variables and the effect of structural changes are given in paper VII.

3.4.2. Reduction kinetics

The reduction kinetics of both non-activated and mechanically activated hematite concentrate in a vibratory mill for different grinding periods have been studied using thermogravimetry (TG). The isoconversional methods of Kissinger-Akahira-Sunose (KAS) (Kissinger, 1957; Akahira and Sunose, 1971) were used to determine the activation energy of the different reactions. The application of the isoconversional methods requires the determination of the absolute temperature at which a fixed extent of reduction is recorded from the TG curves using different heating rates. The experiments were made at three different heating rates of 10, 15 and 20 °C/min. The degree of conversion between 0.02 and 0.95 is investigated. The correlation coefficients for the linear regressions were higher than 0.94. Applying the Kissinger-Akahira-Sunose method, the activation energy for various conversion degrees is calculated. An example of the obtained curves for the activated sample for one hour with higher media surface in the vibratory mill is given in Fig. 38.

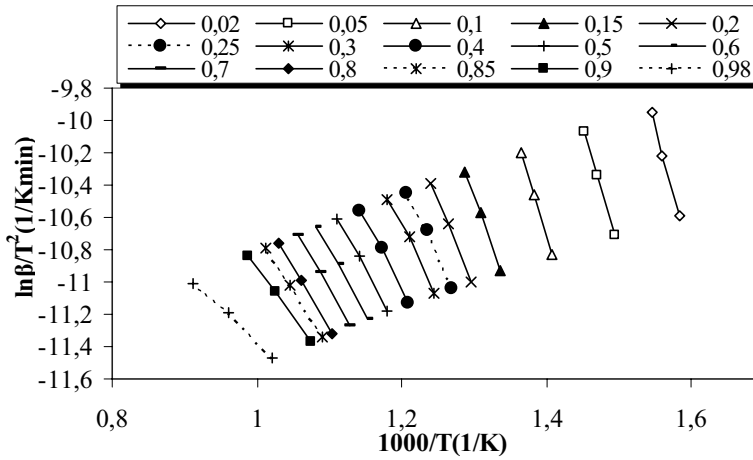


Fig. 38. Isoconversional plots at various conversion degrees for the sample ground within 1 hour using Kissinger-Akahira-Sunose method.

The overall decreasing dependence of the activation energy on α (Table 5) indicates that the overall reaction contains at least two steps. The results corresponding to the initial sample and the mechanically activated samples show that E decreases with increasing grinding time when the extent of conversion (α) is $\alpha \leq 0.11$, corresponding to the reduction of hematite to magnetite. After this range, the activation energy continues to decrease for the initial sample and mechanically activated samples up to three hours. This is opposed to the activation energy for mechanically activated sample within 9 hours in which the activation energy tends to increase slightly and then decreases by $\alpha \leq 0.85$. The activation energy of the initial sample and the ground sample for 1 hour decreases drastically when the conversion degree exceeds 0.85, as opposed with the reduction of the activated samples for more than 1 hour. Since the reduction of the initial sample and activated sample for one hour extends up to 900 °C at higher heating rates, the decrease of the activation energy can probably be due to the phase transition of $\alpha - Fe$ to $\gamma - Fe$ (906 °C).

Table 5. Activation energies obtained using KAS methods as a function of conversion degree for the initial and mechanically activated samples.

α	0 (h)	1 (h)	3 (h)	9 (h)
0.02	166.1	135.3	109.0	102.0
0.05	137.0	123.4	106.0	85.4
0.1	106.0	105.2	98.0	70.0
0.15	81.2	95.2	86.0	73.5
0.2	72.2	84.7	74.0	83.3
0.3	65.3	70.5	62.3	84.1
0.4	62.9	66.3	57.9	76.5
0.5	62.2	62.1	56.2	70.5
0.6	59.9	60.0	54.5	68.7
0.7	57.9	59.2	55.0	67.0
0.8	55.2	57.5	52.0	68.2
0.9	22.3	46.0	50.2	69.0
0.95	9.0	40.9	53.2	72.2
0.98	---	30.0	58.2	79.0

With increasing grinding time, the activation energy at lower conversion extent ($\alpha \leq 0.11$) decreased from the 166-106 kJ mol⁻¹ range in the initial sample to about 102-70 kJ mol⁻¹ in the sample ground for 9 hours. The complexity of the reduction of hematite to magnetite and magnetite to iron was illustrated by the dependence of E on the extent of conversion, α ($0.02 \leq \alpha \leq 0.95$). The values of E decreased sharply with α for $0.02 \leq \alpha \leq 0.11$ range in the initial sample and mechanically activated samples, followed by a slight decrease in the values of E during further reduction by $\alpha \leq 0.85$ in the ground samples up to three hours. A slight increasing dependence of E on α for mechanically activated sample within 9 hours in the second step of reduction was observed due to the finely agglomerated particles during intensive milling and subsequently the formation of a dense layer during the reduction processes. The decreasing trend of activation energy in the two steps of the reduction can be explained in terms of a nucleation and growth of the model of reduction in which the activation energy required during nucleation is higher than that needed in the growth stage (autocatalytic effects). Detailed analyses regarding the kinetic scheme and isokinetic relationship can be found in paper VIII.

4. Conclusions

The thesis is devoted to the development of nontraditional method of preparation of advanced material, exhibiting broad range exploitation. Due to the mechanical activation of materials, a departure from an ideal structure, known as microstructural changes, takes place and the microstructure changes can profoundly influence the physical, mechanical and physico-chemical properties of materials. Microstructural characterizations in the material science by the study of structural imperfections by means of X-ray powder diffraction is known as Line Profile Analysis (LPA) are thus of crucial importance.

The results presented in this thesis show that the techniques developed and used in this study are well suited for the investigations of the influences of grinding parameters on the structure and properties of the milled material as well as on the milling energy values in the mills and absorption energy in the interparticle comminution. It is demonstrated that precise and accurate analyses of the XRD patterns provide reliable results if the profile fitting and the deconvolution of the microstructural characteristics perform carefully which really are a complicated and difficult task. The use of X-ray diffraction line broadening measurements and different methods of line broadening analysis such as Rietveld, Warren-Averbach and Williamson-Hall has been proved to be useful in the analysis of the strain, degree of amorphization, crystallite size and defect structures of milled material. The use of different characterization methods for mechanically activated hematite in different mills provides inclusive understanding of structural changes.

The research presented here shows that the structural changes are reflected on the XRD patterns by: (1) a reduction of reflection intensity due to the formation of amorphous phase, (2) peak broadening due to changes in the crystallite size and lattice strain and (3) peaks position shifts because of changes in the lattice parameters in hematite. Their magnitude depends mainly on the grinding intensity; as the grinding intensity increases, the line broadening increases and the integral intensity decreases. In addition, during milling hematite did not undergo any significant reaction or mechanochemical changes. In addition, the study provides a bridge between the intensity of grinding variables and the concentration of structural changes and subsequently on the reactivity of hematite. Furthermore, the changes in lattice parameters depend on the type of stressing manner. For example, the lattice and unit cell volume of hematite during mechanical activation in loose media mills and bed comminution with compressive load undergo expansion and compaction, respectively, with extending of milling and increasing of pressure. In addition, the positive effects of mechanical treatment on hydrogen reduction of hematite are demonstrated.

Further detailed conclusions from the investigations are:

I. Dry milling with loose media mills

- The size reduction in the planetary mill is completed earlier than with the other mills. During dry grinding, agglomerates are formed rapidly in planetary mill rather than in the other mills, in particular with higher media surface. The vibratory mill produced a larger specific surface area and smaller particles than the other mills, in particular when hematite is subjected to prolonged milling. The maximum surface area reached $18 \text{ m}^2 / \text{g}$ after 9 hours of milling with higher media surface in the vibratory mill. For a

given grinding time and media surface level, tumbling mill produced the smallest specific surface area.

- From the Williamson-Hall plots, it was realized that strain and size contributions exist simultaneously in the milled samples. The Williamson-Hall and Scherrer relations revealed the anisotropic character of line broadening. It was concluded that hematite lattice is 'soft' between the (024) and the other crystallographic directions.
- The use of higher media surface and prolonged grinding lead to higher specific surface area, the amount of X-ray amorphous material, physical broadening, microstrain, dislocation density, and stored energy as well as smaller crystallites whatever milling types and methods were applied.
- The Warren-Averbach method revealed that the products of planetary mill have smaller crystallites and higher microstrain than the products of tumbling and vibratory mills with the exception for the samples activated for 1 hour with low media surface. The final products contain crystallites between 5.6 and 73.5 nm and the lattice strain (RMSS) at $L = 10 \text{ nm}$, $\langle \varepsilon_{L=10nm}^2 \rangle^{1/2}$, varies from 0.06×10^{-3} up to 5.3×10^{-3} depending on the milling performance. The crystallite size and strain distribution for [012] direction suggested a homogeneous activation of hematite concentrate with mainly single crystallite group at high-intensive milling operation and non-homogeneous activation at low intensive milling accompanying at least two main crystallite groups.
- It is also verified that the amorphous material is the most important energy carrier in the activated material. The amorphous material contains between 93 and 98% of the total stored energy (excess enthalpy).
- For a given stress energy, the vibratory mill produces the lowest BET surface area, the minimum reduction of the XRD diffraction intensities and their broadenings, the largest crystallites, the lowest lattice strain and the least defect concentration among the used mills. The activated hematite in the tumbling mill accounted for the highest levels of the excess energy while the activated hematite in vibratory mill contained the minimum excess energy for an identical stress energy. The planetary mill needs a much larger energy input to attain an identical level of stored energy value compared to the other mills.

Statistical analyses revealed some distinguished features in data analysis and facilitate the interpretation of data by considering all variables in the data set simultaneously:

- The ANOVA analyses revealed that two design factors of milling time and media surface have statistically significant effects on the five main response variables at 95% confidence level.
- PCA makes it possible predict which observations leads to production of similar properties or microstructural characteristics.
- The Soft independent modeling (SIMCA) of class analogy indicated that the observations belonging to lower and higher media surfaces are different from each other.
- The PLS-DA analysis suggested that mills could be separated and differentiated from each other at 95% confidence level.

- The investigations of dummy variables show that the tumbling and planetary mills favor the induction of structural changes and subsequently higher reactivity potential irrespective to capacity and specific energy input and stress energy.

II. Interparticle Comminution

- It is found that the interparticle breakage causes plastic deformation in material and subsequently induces changes in the structure of the ground hematite. The trends in the results from the studies of structural changes indicate that further structural refinement will occur at higher energy absorption levels. Therefore, the structural changes in particle bed breakage make it possible to apply this technique for mechanical activation of minerals.
- The experiments indicated that energy absorption was a major factor for the interparticle breakage of hematite. It is demonstrated that the structural changes such as BET surface area, crystallite size, X amorphous phase content and strain can be fairly expressed as functions of the energy absorption. The maximum X-ray amorphization was calculated at maximum energy absorption, accounting for 31%. The volume and surface weighted crystallite sizes were reduced to about 108 and 53 nm, respectively, after releasing 31 J/g energy. For the same energy, the root mean square strain (RMSS), $\langle \varepsilon_{L=10nm}^2 \rangle^{1/2}$, and maximum lattice strain (ε) increased to 9.4×10^{-4} and 4.1×10^{-3} respectively.
- The comparison of the interparticle grinding with tumbling mill indicated that the grinding in tumbling mill needs much more energy to induce the same structural changes as in the particle bed grinding. With respect to grinding energy, it was concluded that the particle bed grinding represents higher efficiency in structural changes than tumbling milling. This can be related to the fact that in the tumbling mill considerable energy losses occur in overcoming friction and the wear of media and mill liners when energy is transferred to particles by the grinding media.

III. The comparison of wet and dry millings

- The study of extended milling in a stirred media mill and a tumbling mill on the structural changes in hematite concentrate revealed that the use of stirred media mill exhibits larger surface areas, smaller particle sizes, more XRD line broadening and subsequently greater structural distortions compared to the tumbling mill for a given energy input; the X-ray amorphous phase content, however, remains unaffected by the grinding environments. Furthermore, the concentration of amorphous phase per unit surface area in the products of the stirred media mill is higher than that in the products of tumbling mill.
- The maximum specific BET surface areas in the stirred media and tumbling millings increased to about 72.5 and 6.8 m^2/g , respectively, after 82000 and 22400 kJ/kg of energy consumption. As a result of the structural refinement during milling, the surface weighted crystallite sizes in ground hematite are 17.3 and 3.6 nm, respectively, after consuming 22400 and 82000 kJ/kg in the tumbling and stirred media mill, corresponding to the volume weighted crystallite size of 17.4 and 10.9 nm. For the same energy

consumption in the mills, in turn, the root mean square strain, $\langle \varepsilon_{L=10nm}^2 \rangle^{1/2}$, increased to about 4.4×10^{-3} and 4.9×10^{-3} .

- Infrared measurements revealed that in the stirred media mill new peaks were observed at around 3600 cm^{-1} which are characteristics of the O-H vibration mode. The peak area of the hydroxyl group increased with the milling energy, indicating that with developing the specific surface area, an increase of the O-H groups takes place. This may be related to slight mechanochemical changes of the hematite during wet milling.

IV. Effects of mechanical activation on the reduction behaviors

- Differential thermal analysis (DTA) and thermogravimetric (TG) analysis revealed that reduction of mechanically activated and initial hematite proceeds stepwise ($\text{Fe}_2\text{O}_3 \rightarrow \text{Fe}_3\text{O}_4 \rightarrow \text{Fe}$). The hydrogen reduction of mechanically activated samples initiates at lower temperatures compared with the initial sample. The beginning temperature (onset) of the reduction decreases from 421°C in the initial sample to around 330°C in the mechanically activated samples (depending on the grinding intensity). At low temperatures, the activated samples give a higher degree of conversion than the initial sample regardless of which milling device is used. Furthermore, intensive grinding resulted in improved resolution of the overlapping reduction events. The studies of the effects of structural changes on the reduction behaviors of the mechanically activated hematite in planetary and vibratory mills revealed that the mill-type effect on the reaction is confined by a stress energy of 4300 kJ/kg . After releasing 4300 kJ/kg energy, planetary milling decreased the onset temperature more than vibratory milling.
- The isoconversional kinetic studies revealed that the mechanical activation has a positive effect on the first step of reduction. The activation energy of the first step of reduction decrease with increasing grinding time. Intensive milling slightly increase the average activation energy of the second reduction step due to the presence of finely agglomerated particles and the intensive sintering of the particles in the higher temperature ranges. In addition, it was found that the activation energies of the two steps of the reduction depend greatly on the extent of conversion, implicating that the reduction of hematite to magnetite and magnetite to iron features a multi-step characteristic. The decreasing trend of the activation energies in two steps of the reductions can be explained in terms of a nucleation and growth of the reduction model. In addition, the dependence of $\ln A_a$ on α was detected and it was found that the $\ln A_a$ shows the same dependence on α as the apparent activation energies. Finally, the prediction of the reduction behavior of the samples, revealed that with increasing temperature, the difference between the samples for achieving a given conversion reduces at identical temperatures.

5. Further Research

- In our opinion, the investigation of the effects of various defects formed during mechanical activation on the reactivity of the minerals are now only at the beginning of their development. Systematic investigations are recommended to explore what defects are formed under various types of mechanical actions in crystals of different minerals and how these defects influence reactivity.
- In addition to the studied defects in this research, other types of defects such as point defects, surface defects, dislocations and their characterizations are also recommended to be explored.
- Further experiments and research have to be conducted to explore the effects of other grinding variables such as amplitude, mill diameter, mill speed, frequency, grinding media density, acceleration, grinding atmosphere and grinding mode (wet and dry) through experimental designs which provide advantages to the conventional methods. More investigations are also necessary to provide an approach to compare different mills and their efficiency in different mills based on stress energy or a proper intensity definition.
- The Warren-Averbach and Rietveld methods along with integral breadth methods are recommended for microstructure characterization. However, when different phases exist, the characterizations using Rietveld refinement method is promising and therefore should be tested further.
- Kinetics of the microstructural evolution is of importance and should be investigated. The kinetic parameters of microstructure evolution may provide enhanced understanding of the milling performance and a comparison of different mills.
- The application potentiality of the interparticle breakage for mechanical activation has been proved in the study. More investigations are recommended to explore the effects of other variables and apparatuses in the bed comminution.
- Reactivity tests based on desired applications for the activated hematite are necessary to find the influence of mechanical activation and microstructure parameters refinement. In addition to the correlation between the reaction kinetics and microstructure characters, the influences of the individual microstructure parameters must be investigated.
- The mechanical activation should be extended to other minerals and concentrates to explore possible structural changes and their effects on the reactivity of activated minerals.
- The number of publications in the mechanochemistry field, speaking in the broadest context, increases rapidly but the transfer of the obtained results from the laboratory to practical application is much less than the total number. The reasons for this phenomenon must be analyzed from different viewpoints and it is necessary to explore actions to be taken.

References

- Akahira, T., and Sunose, T., 1971, J. Res. Report Chiba Inst. Technol. (Sci. Technol.), 16 22.
- Amer, A.M., 2002. Alkaline pressure leaching of mechanically activated Rosetta ilmenite concentrate. *Hydrometallurgy* 67, 125-133.
- Amer, A.M., 2001. Kinetics of acid pressure leaching of mechanically activated cassiterite concentrate. *Erzmetall* 54, 446– 449.
- Amer, A.M., 2000. Investigation of the direct hydrometallurgical processing of mechanically activated low-grade wolframite concentrate. *Hydrometallurgy* 58, 251– 259.
- Amer, A.M., 1995. Investigation of the direct hydrometallurgical processing of mechanically activated complex sulphide ore, Akarem area, Egypt. *Hydrometallurgy* 38, 225– 234.
- Austin, L.G., 1992. Some topics for research on fine grinding. In: Lecture in Harrogate Meeting IFPRI.
- Avvakumov, E., Senna, M., Kosova, N., *Soft mechanochemical synthesis*, Kluwer Academic publishers, New York, 2001.
- Aytekin, Y., 1981. Wet chemical extraction of metals from bulk concentrates of nonferrous ores. *Aufbereitungs-Technik* 22, 62– 71.
- Aziz, A., Schönert, K., 1980, Einzelkommerkleinmng und Gutbetbeanspruchung von Zementklinkerfraktionen. *Zement-Kalk-Clips*, 5, 213-218.
- Baláz, P., 2003. Mechanical activation in hydrometallurgy. *International Journal of Mineral Processing* 72, 341-354
- Baláz, P., *Extractive Metallurgy of Activated minerals*. Elsevier, Amsterdam, 2000
- Baláz, P., Aláčová, A., Achimovičová, M., Ficeriová, J., Godočiková, E., 2005. Mechanochemistry in hydrometallurgy of sulphide minerals. *Hydrometallurgy* 77, 9-17.
- Baláz, P., Ficeriová, J., Boldižárová, E., Háber, E., Jeleň, S., Kammel, R., 2000. Thiosulphate leaching of gold from a mechanochemically pretreated complex sulphide concentrate. In: Massaci, P., (Ed.), *Proc. of the XXI. Int. Miner. Proc. Congress Rome*, Vol. A. Elsevier, Amsterdam, pp. A6-74–A6-81.
- Baláz, P., Huhn, H.J., Tkáčová, K., Heegn, H., 1988. Laugungsverhalten und physikochemische Eigenschaften von in unterschiedlichen mühlen vorbehandelten chalkopyrit. *Erzmetall* 41, 325– 331.
- Baláz, P., Številová, N., Kammel, R., Malmstrom, R., 1998. Extraction of Ni, Cu and Co from mechanically activated pentlandite concentrate. *Metall* 10–11, 620–623.
- Balzar, D., 1999, Voigt-Function Model in Diffraction Line-Broadening Analysis, in *Defect and Microstructure Analysis from Diffraction*, edited by R.L. Snyder, H.J. Bunge, and J. Fiala, International Union of Crystallography Monographs on Crystallography No. 10 (Oxford University Press, New York, 1999), pp. 94-126.
- Balzar, D., Audebrand, N., Daymond, M. R., Fitch, A., Hewat, A., Langford, J. I., Bail, A.Le., Louër, D., Masson, O., McCowan, C. N., Popa, N. C., Stephens, P.W., Toby, B.H., 2004, Size-strain line-broadening analysis of the ceria round-robin sample, *J. Appl.crys.* 37, 911-924.
- Balzar, D., Ledbetter, H., 1995. Accurate Modeling of Size and Strain Broadening in the Rietveld Refinement: the "Double-Voigt" Approach. *Advances in X-ray Analysis* 38, 397-404.
- Balzar, D., Ledbetter, H., 1993. Crystal Structure and Compressibility of 3:2 Mullite. *American Mineralogist* 78, 1192-1196.
- Bid, S., Banerjee, A., Kumar, S., Pradhan, S. K., De, U., Banerjee, D., 2001. Nanophse iron oxides by ball-mill grinding and their Mössbauer characterization. *Journal of Alloys and Compounds* 326, 292-297.
- Boldyrev, V.V., 1986. Mechanochemistry of inorganic solids. *Proc. Indian natn. Sci. Acad.*

52A, 400-417.

- Boldyrev, V.V., Pavlov, S.V., Goldberg, E.L., 1996. Interrelation between fine grinding and mechanical activation. *International Journal of Mineral Processing* 44-45, 181-185.
- Brown, Michael E., *Introduction to Thermal Analysis. Second Edition. Techniques and Applications.* Kluwer Academic Publishers, New York, USA, 2001.
- Cheary, R. W. and Coelho, A. A. 1998, Axial divergence in a conventional X-ray powder diffractometer II. Implementation and comparison with experiment, *J. Appl. Cryst.*, 31, 862-868.
- Cheary, R. W. and Coelho, A. A., 1992, a fundamental parameters approach to X-ray line profile fitting, *J. Appl. crystallogr.*, 25, 109-21.
- Coats, A. W., and Redfern, J. P., 1965, Kinetic parameters [of polymers] from thermogravimetric data. II, *J. Polym. Sci. B: Polym. Lett.* 3, 917-920.
- Daiger, K., Gerlach, J., 1983. Ueber den Katalytischen Effekt der Schwingmahlung auf die Lösungsgeschwindigkeit bei der direkten Laugung sulfidischer Erze des Kupferkiestypus. *Erzmetall* 36, 82-87.
- Daiger, K., Gerlach, J., 1982. On the kinetics of direct leaching of sulphide ores. *Erzmetall* 35, 609-611.
- DIFFRAC^{plus} TOPAS/ TOPAS R/ TOPAS P Version 2.1, Technical Reference, Bruker Axs GmbH, Karlsruhe, 2003 and www.bruker-axs.com.
- Fernandez-Bertan, J., 1999. Mechanochemistry: an overview. *Pure Applied chemistry* 71, 4, 581-586.
- Ficeriová, J., 2000. Possibilities of mechanical activation at intensification of non-cyanide leaching of gold bearing concentrate. PhD thesis, Institute of Geotechnics of Slovak Academy of Sciences, Kosice. In Slovak.
- Ficeriová, J., Baláž, P., Boldižárová, E., Jeleň, S., 2002. Thiosulphate leaching of gold from a mechanically activated Cu Pb Zn concentrate. *Hydrometallurgy* 67, 37-43.
- Fuerstenau, D.W., Kapur, P.C., 1995, Newer energy approach to particle production by comminution, *Powder Technol.* 82, 51-57
- Gerlach, J. K., Gock, E., Ghosh, S.H., 1973. Activation and leaching of chalcopyrite concentrates by diluted H₂SO₄ solutions. In: Evans, D.I., Schoemaker, R.S. (Eds.), *Proc. 2nd Int. Symp. On Hydrometallurgy.* Metall. Soc. AIME, Chicago, pp. 87-94.
- Gerlach, J., 1982. Untersuchungen zur direkten Laugung komplexer sulfidischer Erze. *Metall* 36, 518- 523.
- Gock, E., 1977. The Influence of Solid State Reactions in Vibratory Mill on leachability of Sulphidic Raw Materials. Habilitationsschrift, TU Berlin. In German.
- Gock, E., Asiam, E., 1988. Gewinnung von Edelmetallen aus Kohlenstoffhaltigen Arsenopyritkonzentraten nach mechanischer Aktivierung. In: Tkáčová K. (Ed.), *Proc. Vth Int. Symp. "Theoretical and theoretical Aspects of Comminution and Mechanical Activation"*. Institute of Mining, Slovak Academy of Sciences, Kosice pp. 60- 65.
- Gock, E., Jacob, K.-H., 1980. Direct dissolution of rutile with sulphuric acid. *Erzmetall* 33, 308- 314.
- Godočiková, E., 2001. Chloride leaching of mechanically activated complex CuPbZn concentrate. PhD thesis, Institute of Geotechnics of Slovak Academy of Sciences, Kosice. In Slovak.
- Godočiková, E., Baláž, P., Boldižárová, E., 2002b. Structural and temperature sensitivity of the chloride leaching of copper, lead and zinc from a mechanically activated complex sulphide. *Hydrometallurgy* 65, 83-93
- Goldberg, E.L. and Pavlov, S.V., 1990. Conceptual grinding-activation model. In: *Proceedings of Second World Congress Particle Technology, Society of Powder Technology, Kyoto*, pp. 507-515.

- Gutman, E.M., *Mechanochemistry of Materials*. Cambridge International Science Publishing, Cambridge, 1998.
- Gutman, E.M., *Mechanochemistry of Solid Surfaces*. World Scientific, Singapore, 1994.
- Halder, N.C., Wagner, C.N.J., 1966. Separation of particle size and lattice strain in integral breadth measurements. *Acta Crystallography* 20, 312-313.
- Heegn, H., 1987. Model describing the resistance against structural changes and the hardness of crystalline solids. *Crystal Research Technology* 22, 9, 1193-1203
- Heegn, H., 1986. Concerning some fundamentals of fine grinding. In: Leschonski, K., Editor, 1986. *Proc. 1st World Congress on Particle Technology, Part II. Comminution*, Nürnberger Messe und Ausstellungsgesellschaft, Nürnberg, pp. 63–67.
- Heegn, H., 1979. Effect of fine grinding on structure and energy content of solids, in: *Proc. of 6th POWRECH*, Birmingham, pp. 61-69
- Heinicke, G., "Tribiochemistry". Akademie-Verlag, Berlin, 1984.
- Hill, R.J. and Howard, C. J., 1987, Quantitative phase analysis from neutron powder diffraction data using the Rietveld method. - *J. Appl. Cryst.* 20, pp 467-474.
- Holland, T.J.B., Redfern, S.A.T., 1997. Unit cell refinement from powder diffraction data: the use of regression diagnostics. *Mineralogical Magazine* 61: 65-77.
- Huttig, G.F., 1943. Zwischenzustände bei Reaktionen in Festen Zustand und ihre Bedeutung für die Katalyse. In: *Handbuch der Katalyse IV*, Springer Verlag, Wien, pp. 318-331
- Juhász, A. Z., and Opocki, L., *Mechanical Activation of Minerals by Grinding, Pulverizing and Morphology of Particles*. Ellis Horwood, London, 1990.
- Juhász, A.Z., 1974. Mechanochemical activation of silicate minerals by dry fine grinding. *Aufbereitungs-Technik* 10, 558-562
- Kahler, J., Friedrich, I., Gock, E., 1996. Processing of molybdenite concentrate containing rhenium without exhaust gas generation. *Erzmetall* 49, 415– 425.
- Kalinkin, A.m., Kalinkina, E.V., and Makarov, V.N., 2003. Mechanical activation of natural titanite and its influence on the mineral decomposition. *International Journal of Mineral Processing* 69, 143-155
- Kammel, R., Pawlek, F., Simon, M., Li, X., 1987. Oxidizing leaching of sphalerite under atmospheric pressure. *Metall* 41, 158– 161.
- Karagedov, G.R., Lyakhov, N.Z., 2003. Mechanochemical grinding of inorganic oxides. *Kona* 21, 76-86.
- Khawam, A., and Flanagan, D. R., 2005a, Role of isoconversional methods in varying activation energies of solid-state kinetics I. isothermal kinetic studies, *Thermochim. Acta* 429, 93-102.
- Khawam, A., and Flanagan, D. R., 2005b, Complementary Use of Model-Free and Modelistic Methods in the Analysis of Solid-State Kinetics, *J. Phys. Chem. B* 109, 10073-10080.
- Kissinger, H. E., 1957, Reaction kinetics in differential thermal Analysis, *J. Anal. Chem.* 29, 1702-1706.
- Kitamura, M., Senna, M., 2001. Electroreological properties of mechanically activated gibbsite. *Inorganic Materials* 3, 563-567
- Kušnierová, M., Šepelák, V., Briančin, J., 1993. Effects of biodegradation and mechanical activation on gold recovery by thiourea leaching. *JOM*, December, 54– 56.
- Kuzeci, E., Li, X., Kammel, R., 1989. Untersuchungen zur sauren Laugung von sulfidischem Nickelkonzentrat. *Metall* 43, 434– 439.
- Le Bail, A., Duroy, H. and Fourquet, J. L., 1988, Ab-initio Structure Determination of LiSbWO₆ by X-Ray Powder Diffraction. - *Mat. Res. Bull.* 23, 447-452.
- Lin, I.J., 1998. Implications of fine grinding in mineral processing; mechanochemical approach. *Journal of Thermal Analysis* 52, 453-361.

- Lin, I.J., Nadiv, S., and Grodzian, J.M., 1975. Changes in the state of solids and mechanochemical reactions in prolonged comminution processes. *Materials Science Engineering* 7, 4.
- Lucks, I., Lamparter, P., Mittemeijer, E.J., 2004. An evaluation of methods of diffraction-line broadening analysis applied to ball-milled molybdenum. *Journal of Applied Crystallography* 37, 300-311.
- Manugistics., *Tutorials for Statgraphics Plus for Windows*. Manugistics, Inc., 2115 East Jefferson Street Rockville, Maryland, USA, 1999.
- Maurice, D., Hawk, J.A., 1999a. Ferric chloride leaching of a mechanically activated Pentlandite-chalcopyrite concentrate. *Hydrometallurgy* 52, 289-312.
- Maurice, D., Hawk, J. A., 1999b. Simultaneous autogenous grinding and ferric chloride leaching of chalcopyrite. *Hydrometallurgy* 51, 371-377.
- Maurice, D., Hawk, J. A., 1998. Ferric chloride leaching of a mechanically activated chalcopyrite. *Hydrometallurgy* 49, 103-124
- Mccormick, P.G., and Froes, F.H., 1998. The fundamentals of mechanochemical processing. *Wilson Applied Science and technology abstracts* 50,11, pp-61-65
- McLean, D., *Mechanical Properties of Metals*. Metallurgia, Moscow, 1965.
- Meyer, K., 1968. *Physikalisch-chemische Kristallographie*. VEB Deutscher Verlag Fur Grundstoffindustrie Leipzig, pp 302-320.
- Mulak, W., Baláž, P., Chojnacka, M., 2002. Chemical and morphological changes of millerite by mechanical activation. *International Journal of Mineral Processing* 66, 233–240.
- Munteanu, G., Ilieva, L., Andreeva, D., 1997. Kinetic parameters obtained from TPR data for α -Fe₂O₃ and Au/ α -Fe₂O₃ systems. *Thermochim. Acta* 291, 171-177
- Opfermann, J. R., Kaisersberger, E., Flammersheim, H.J., 2002, Model-free analysis of thermoanalytical data-advantages and limitations, *Thermochim. Acta* **391**, 119-127.
- Ostwald, W., 1919. *Handbuch der Allgemeinen Chemie*. Akademische Verlagsgesellschaft1, Leipzig.
- Ostwald, W., 1891. *Lehrbuch der Allgemeinen Chemie*. Bd.2 Stöchiometrie (Engelmann, Leipzig, 1163 S.
- Ozawa, T., 1965, A New Method of Analyzing Thermogravimetric Data, *Bull. Chem. Soc. Jpn.* 38, 1881-1886.
- Pawlek, F., 1976. The influence of grain size and mineralogical composition on the leachability of copper concentrates. In: Yannopoulos, J.C., Agarwall, J.C. (Eds.), *Proc. Int. Symp. "Extractive Metallurgy of Copper"*, vol. II. Metall. Soc. AIME, Las Vegas, pp. 690– 705.
- Pawlek, F., Kheiri, M.J., Kammel, R., 1989. Optimierung der Feinstmahlung mit einer Rührwerkskugelmühle gezeigt am Beispiel eines Zinkkonzentrates. *Metall* 43, 838–842.
- Pawley, G.S., 1981, Unit-cell refinement from powder diffraction scans. - *J. Appl. Cryst.* 14, 357-361
- Peters, K., 1962, Mechanochemische Reaktionen, in *Proc. I. Europäischen Symp."Zerkleinern"* (Rumpf, H, ed.) Weinheim, Frankfurt. p78-98
- Puclin, T., Kaczmarek, W.A., Ninham, B.W., 1995. Mechanochemical processing of ZrSiO₄. *Materials chemistry and Physics* 40, 73-81
- Rietveld, H.M., 1969, A profile refinement method for nuclear and magnetic structures. *J. Appl. Cryst.*, 2, 65-71.
- Rietveld, H.M., 1967, Line profiles of neutron powder-diffraction peaks for structure refinement. - *Acta Cryst.* 22, 151-152.
- Sahu, P., De, M., Zdujić, M., 2003. Microstructural characterization of the evolved phases

- of ball-milled $\alpha - Fe_2O_3$ powder in air and oxygen atmosphere by Rietveld analysis. *Material Chemistry and Physics* 82, 864-876.
- Sastri, M. V. C., Viswanath, R. P., Viswanathan, B., 1982. Studies on the reduction of iron oxide with hydrogen. *Int. J. Hydrogen energy* 7, 951-955.
- Schönert, K., 1990. Physical and technical aspects of very and micro fine grinding. In: *Proceedings of Second World Congress Particle Technology*, Society of Powder Technology, Kyoto, pp. 257-271.
- Schönert, K., Reichardt, Y., 1993, Interparticle breakage of very fine materials by alternating crosswise stressing with a high pressure. XVIII international mineral processing congress, Sydney, 23-28 May, pp 213-217.
- Siemens AG, 1996a. *Diffac^{plus}*, profile Fitting Manual program
- Siemens AG, 1996b. *WIN-CRYSIZE 3*, Crystallite size and microstrain manual.
- Sjöström, M., Eriksson, L., Hellberg, S., Johansson, J., Skagerberg, B., and Wold, S., Peptide QSARs: PLS Modelling and Design in Principle Properties. In: J. L. Fauchere (ed.) *QSAR-Quantitative Structure-Activity Relationship in Drug Design*. Proc. 7th European Symposium on QSAR, Sept. 1988, Interlaken, Switzerland. Alan R. Liss, Inc., New York, 1989, pp. 131-134.
- Steinike, U., and Hennig, H. P., 1992. Mechanically induced reactivity of solids, *Kona* 10, 15-23
- Stewart, S.J., Borzi, R.A., Cabanillas, E.D., Punte, G., Mercader, R.C., 2003. Effects of milling-induced disorder on the lattice parameters and magnetic properties of hematite. *Journal of Magnetism and Magnetic Material* 260, 447-454.
- Stokes, A. R., 1948. A numerical Fourier –analysis method for the correction of widths and shapes of lines on X-ray powder photographs. *Proc. phys. Soc, London* 61, 382-391.
- Takacs, L., 2004a. M. Carey Lea, the first mechanochemist. *Journal of Material Science* 39, 4987-4993
- Takacs, L., 2004b. *J. Minerals Met. Mater. Soc.* 52, 12 (2000).
- Tkáčová, K., *Mechanical Activation of Minerals*. Elsevier, Amsterdam, 1989.
- Tkáčová, K., Baláž, P., Mišura, B., Vigdergauz, V. E., Canturija. 1993. Selective leaching of zinc from mechanically activated complex Cu–Pb–Zn concentrate. *Hydrometallurgy* 33, 291– 300.
- Tokumitsu, K., 1997. Reduction of metal oxides by mechanical alloying method. *Solid State Ionics* 101-103, 25-31
- Tromans, D., Meech, J.A., 2001. Enhanced dissolution of minerals: stored energy, amorphism and mechanical activation. *Mineral Engineering* 14, 11, 1359-1377
- Umetrics, Tutorial to SIMCA-P, SIMCA-P⁺. *Multivariate Modelling, Data analysis and Design of Experiments group*, Umeå, Sweden, 2002.
- Vyazovkin, S, 1996, A unified approach to kinetic processing of non-isothermal data, *J.int. J. Chem. Kine.* 28, 95-101.
- Vyazovkin, S., 1997, Evaluation of activation energy of thermally stimulated solid-state reactions under arbitrary variation of temperature, *J. Comput. Chem.* 18, 393-402.
- Vyazovkin, S., and Dollimore, D., 1996, Linear and Nonlinear Procedures in Isoconversional Computations of the Activation Energy of Nonisothermal Reactions in Solids *J. Chem. Inf. Comput. Sci.* 36, 42-45.
- Vyazovkin, S., and Wight, C. A., 1999, Model-free and model-fitting approaches to kinetic analysis of isothermal and nonisothermal data, *Thermochim. Acta* 340–341, 53-68
- Vyazovkin. S., 2006, Model-free kinetics; staying free of multiplying entities without necessity, *Journal of thermal analysis and calorimetry*, 83, 1, 45-51
- Warren, B.E., *X-ray diffraction*. Addison-Wesley, New York, 1969.
- Welham, N.J., 2003. Plenary lecture on mechanical activation at the 4th INCOME conference

- in Braunschweig, Germany.
- Welham, N.J., 2001a. Enhanced dissolution of tantalite/columbite following milling. *International Journal of Mineral Processing* 61, 145-154.
- Welham, N.J., 2001b. Effect of extended grinding on the dissolution of a Ta/Nb concentrate. *Canadian Metallurgical Quarterly* 40, 143- 154.
- Welham, N.J., 2001c. Mechanochemical processing of enargite (Cu_3AsS_4). *Hydrometallurgy* 62, 165-173.
- Welham, N.J., 2001d. Mechanochemical processing of gold-bearing sulphides. *Minerals Engineering* 14, 341- 347.
- Welham, N.J., 2001e. Enhanced dissolution of tantalite and columbite following milling. *International Journal of Mineral Processing* 61, 145- 154.
- Welham, N.J., 2001f. Enhancing zircon ($ZrSiO_4$) dissolution by ambient temperature processing. *Proceedings - Australasian Institute of Mining and Metallurgy* 305, 1- 3.
- Welham, N.J., 1997a. The effect of extended milling on minerals. *Canadian Institute of Metallurgy Bulletin* 90, 64- 68.
- Welham, N.J., 1997b. Enhancement of the dissolution of ilmenite ($FeTiO_3$) by extended milling. *Transactions of Institution of Mining and Metallurgy* C106, 141- 144.
- Welham, N.J., Llewellyn, D.J., 1998. Mechanical enhancement of the dissolution of ilmenite. *Mineral Engineering* 11, No 9, 827-841.
- Welham, N.J., 1996. Mechanical activation in mineral processing, in *Proceedings of the 98th Annual General Meeting of the Canadian Institute of Mining, Metallurgy and Petroleum*, Edmonton,
- Williamson, G.K., Hall, W.H., 1953. X- ray line broadening from field aluminium and wolfram. *Acta Metallurgy* 1, 22-31.
- Wilson, A. J. C., *Mathematical Theory of X-ray Powder Diffractometry*, Gordon and Breach, New York. 1963.
- Wold, S., Albano, C., Dunn, W.J., Edlund, U., Esbensen, K., Geladi, P., Hellberg, S., Johansson, E., Lindberg, W., and Sjöström, M., *Multivariate data analysis in chemistry*. In: B.R. Kowalski, Editor, *Chemometrics: Mathematics and Statistics in Chemistry*, 1984, Reidel Publishing company, Dordrecht, Holland, pp.17-95.
- Young, R.A., *Introduction to the Rietveld method.- The Rietveld Method*, edited by R.A. Young, IUCr Book Series, Oxford University Press. 1993.
- Young, R.A., Wiles, D.B., 1982. Profile shape function in Rietveld refinements. *Journal of Applied Crystallography* 15, 430-438.
- Zdujčić, M., Jovalekić, C., Karanović, L.J., Mitrić, M., 1999. The ball milling induced transformation of $\alpha - Fe_2O_3$ powder in air and oxygen atmosphere. *Material Science Engineering A* 262, 204-213.
- Zelikman, A. N., Voldman, G.M., Beljajevskaja, L.V., *Theory of hydrometallurgical processes*. Metallurgija, Moscow, In Russian, 1975.
- Zhang, Q., Kasai, E., Saito, F., 1996. Mechanochemical changes in gypsum when dry ground with hydrated minerals. *Powder Technology* 87, 67-71.
- Zhang, Q., Sugiyama, K., and Saito, F., 1997. Enhancement of acid extraction of magnesium and silicon from serpentine by mechanochemical treatment. *Hydrometallurgy* 45, 323-331.

Appended papers

Paper I

Microstructure Characterization of Mechanically Activated Hematite Using XRD Line Broadening

Parviz Pourghahramani & Eric Forsberg, International Journal of Mineral Processing, 79 (2006), 106-119

Microstructure characterization of mechanically activated hematite using XRD line broadening

Parviz Pourghahramani *, Eric Forssberg

Division of Mineral Processing, Luleå University of Technology, Luleå, Sweden

Received 28 October 2005; received in revised form 2 February 2006; accepted 2 February 2006
Available online 9 March 2006

Abstract

The effect of dry milling in a vibratory mill on the structural changes and microstructural characteristics of hematite using different methods was investigated. We have described the line profile analysis (LPA) to extract the size of coherently diffracting domains and the lattice strain of activated hematite in a vibratory mill. The Warren–Averbach and Williamson–Hall methods were used as the main tools for characterization. The changes in the particle size, surface area and new phase formation of hematite concentrate were also investigated. It was concluded that the breakage and agglomeration of particles take place mainly at lower and higher levels of specific energy input, respectively. The pores in agglomerates remain accessible for the nitrogen gas. Milling of hematite increased specific surface area up to $18.4 \text{ m}^2/\text{g}$. The hematite milled under various levels of specific energy input did not undergo a significant reaction or phase transformation during milling. The Williamson–Hall method confirms its merit for a rapid overview of the line broadening effects and possible understanding of the main causes. The anisotropic character of line broadening for deformed hematite as a function of specific energy input was revealed. Higher level of specific energy input favors the generation of small crystallite size, higher microstrain, BET surface area, amorphization and line breadth. The Warren–Averbach method suggested that the nanocrystalline hematite with grain sizes of 73.5–12.2 nm was formed by mechanical treatment using different milling intensities in the vibratory mill. The root mean square strain (RMSS) at $L = 10 \text{ nm}$ varies between 1.7×10^{-3} and 4.0×10^{-3} depending on the level of energy input. Limits in the applicability of Williamson–Hall method and reliability of the results are discussed in detail.

© 2006 Elsevier B.V. All rights reserved.

Keywords: microstructure; mechanical activation; grinding; line profile analysis; vibratory mill

1. Introduction

Mechanical activation (MA), a narrow field of the Mechanochemistry (MC) applied for the activation of chemical reaction by mechanical energy, has been used in mineral processing to produce finely ground particles,

increased surface area and improved chemical reactivity of milled materials. The process involves prolonged grinding and is reported to cause a variety of processes to take place such as generation of a large new surface, formation of dislocations and point defects in the crystalline structure, phase transformations in polymorphic materials, chemical reactions, decomposition, ionic exchange, and oxidation and reduction reactions.

Mechanical activation increases the free energy of the particulate material systems by addition of both

* Corresponding author. Tel.: +46 920 491313; fax: +46 92097364.
E-mail address: Parviz.Pourghahramani@ltu.se
(P. Pourghahramani).

surface free energy and volumetric elastic strain energy. Therefore, the ground material is activated and gained free energy can be relaxed through different modes of energy transitions (Lin, 1998). Decreasing the particle size during mechanical activation beyond its initial size leads to changes in relaxation from brittle fracture to ductile fracture. These changes are accompanied with rises in strain. As a result, the dislocation flows take place in the particles. Consequently, it leads to the growth of structure distortion. Those structural changes determine the reactivity (Boldyrev et al., 1996). With the development of research in mechanical activation of solids, it has been known that activation increases defect concentration and subsequently the reactivity of the solids (Balaz, 2000; Tkacova, 1989; Zoltan Juhasz, 1998). The characterization of structural changes is important in the course of mechanical activation.

Peak shape analysis, known as line profile analysis (LPA), is used to obtain information from the material structure. X-ray diffraction line profile analysis is an adopted technique, powerful tool and non-destructive method, to characterize the behavior of milled powder under various high-energy ball milling conditions. The X-ray diffraction patterns recorded from an activated material show broadening due to imperfections in the crystal structure. Structural line broadening is usually subdivided into crystallite size and microstrain broadening. Consequently, we can acquire information from microstrain, crystallite size and dislocation generated during intensive-milling condition. The X-ray line broadening analysis has been used widely to characterize the microstructure of materials. However, the use of this technique requires careful experimentation, sample preparation and calculation. Two basic methods of line profile analysis have been used: deconvolution and convolution methods (Balzar, 1999).

A number of attempts have been made to characterize the behavior of mechanically activated sulfide minerals. The influence of mechanical activation on the dissolution and leaching behavior of a large number of sulfide minerals and the principles of extracting of metals from sulfide minerals were studied; the whole process was described by Balaz (2000). Moreover, the chemical and morphological changes of millerite (Mulak et al., 2002) and leaching behavior of pentlandite–chalcopyrite concentrate (Maurice and Hawk, 1999) have been investigated. Extensive studies have been made on the structural changes of hematite especially on the polymorphic transformation of α -Fe₂O₃ to Fe₃O₄ and γ -Fe₂O₃ during mechanochemical treatment of α -Fe₂O₃. Kosmac and Courtney (1992) reported the transformation (reduction) of α -Fe₂O₃ to Fe₃O₄ and subsequently to FeO phase

Table 1

Experimental milling conditions

Parameter	Value
Media filling (%)	70
Milling time (h)	139
Ball to powder weight ratio	16.92:1, 67.68:1
Speed (RPM)	1000
Amplitude (mm)	8
Media apparent density (g/cm ³)	4.875
Amplitude (mm)	8
Temperature of material (°C)	48–105

either in argon or air atmosphere. The complete transformation of α -Fe₂O₃ to Fe₃O₄ by ball milling under vacuum or in argon atmosphere is possible; while in air the transformation is very slow or does not occur (Kaczmarek and Ninham, 1994). It was demonstrated that the transformation of α -Fe₂O₃ to Fe₃O₄ greatly depends on the manner in which milling was performed. Frequent opening of the mill door suppresses the transformation, while closing the door of the mill, the complete transformation of α -Fe₂O₃ to Fe₃O₄ takes place. The oxygen atmosphere delays the transformation process (Zdujic et al., 1998, 1999).

Most of the aforementioned treatments were made in planetary mills or in shaker mills such as SPEX mills on commercial hematite powder, wherein small amounts of commercial hematite powders in the order 10 g were examined. The goal of this work is to study the influence of milling operation conditions in terms of specific energy input on the structural changes of hematite concentrate with large powder weight (1959.4 and 490 g) and line broadening technique, which has not been studied yet. Quantitative and qualitative characterizations of the microstructural features of activated hematite as a function of specific energy input using integral breath methods and Fourier analysis are discussed in detail.

2. Experimental

The dry grinding tests were carried out in a vibratory ball mill with dimensions of $L320 \times \phi 185$ mm. Steel balls with different sizes from 6 to 22.2 mm with total media surface of 1.9594 m² were used as grinding media. Milling experiments were made in air atmosphere under closed milling condition, i.e., the door of mill was kept closed during the milling process periods. The temperature was measured by a thermometer immediately after stopping the mill. The energy consumed by the mill was measured during grinding test by an electrical meter called a Micro VIP (Elcontrol Co. Italy).

The samples were sealed into plastic tubes and kept in a freezer for further measurements. The grinding conditions are summarized in Table 1.

The particle size distribution of samples was measured by the laser diffraction method (CILAS 1064) in the liquid mode. From the laser diffraction measurements, the mean particle diameter and granulometric specific surface area were calculated. The specific surface area of the samples was determined by the BET method with the Flow Sorb II 2300 (Micromeritics Co. Ltd., USA), from which the equivalent particle diameter assuming spherical shape for particles was determined. The density of the starting material was calculated by using a Pycnometer (Micromeritics Co. Ltd., USA).

The X-ray diffraction (XRD) patterns were collected using a Siemens D5000 powder diffractometer with Bragg–Brentano geometry equipped with a curved graphite monochromator in diffracted beam arm and using Cu K α radiation (Siemens, Germany). The XRD patterns of samples were recorded in the range $2\theta = 10^\circ$ – 90° using a step size of 0.02° and a counting time of 5 s per step. Similarly, the X-ray diffraction pattern of the standard sample powder LaB $_6$, a standard proposed by the National Institute of Standards and Technology of USA, was obtained. The standard sample profile was used to remove the instrumental broadening effects from the observed profile broadening.

3. Materials

The chemical analysis showed that initial hematite powder contained about 97.91% Fe $_2$ O $_3$, 0.73% Al $_2$ O $_3$, 0.73% SiO $_2$, 0.26% TiO $_2$, 0.20% MgO, 0.022% MnO, and 0.088% P $_2$ O $_5$. Other components such as K $_2$ O, CaO and Na $_2$ O comprise 0.051%. The X-ray diffraction analysis represented only the hematite diffraction lines. From the size analysis, the mean diameter and F_{80} of the starting powder were estimated around 23 and 80 μ m, respectively. The BET measurements gave a specific surface area of 0.59 m 2 g $^{-1}$. The density of the starting material was calculated about 5240 kg/m 3 .

4. Profile fitting procedure

In order to characterize the microstructure in terms of defect parameters such as crystallite (domain) sizes and microstrain, the parameters of line positions, intensities, widths, and shapes must be obtained from X-ray diffraction spectra. For this purpose, the Profile software (Siemens, 1996) was used. The $K_{\alpha 2}$ component was removed from the recorded XRD patterns with the assumption that $K_{\alpha 2}$ intensity is half of the $K_{\alpha 1}$ intensity.

The background was subtracted from the measured profiles. Each goodness factor was refined to a value of <5% for all used reflections of the studied samples.

For profile analysis, the eight most intensive reflection peaks (012), (104), (110), (113), (024), (116), (214) and (300) were selected. The overlapped peaks were carefully separated by using the Profile software. The profile fitting procedure was performed without smoothing of the XRD patterns to avoid introducing any bias in calculations. For each adjusted line profile, the following parameters were obtained:

- (1) The maximum height of the peak (I_{\max}).
- (2) The integral breadth of line profile, ($\beta = A/I_{\max}$, where A is the peak area).
- (3) The full-width at half of maximum (FWHM).
- (4) The mixing factor (η) of Lorentzian and Gaussian functions.
- (5) The peak position (2θ).

5. Microstructure characterization (theoretical background)

Deviation from the ideal crystallinity such as finite crystallite size, strain (at the atomic level) and extended defects (stacking faults and dislocations) leads to broadening of the diffraction lines. Crystallite size is a measure of the size of coherently diffracting domains and is not generally the same as particle size due to polycrystalline aggregates. Strain is defined as change in length per unit length and is measured as the change in d spacing of a strained sample compared to the unstrained state.

According to Scherrer (1918), the apparent crystallite size can be obtained:

$$D_V = \frac{K\lambda}{\text{FWHM}} \cos\theta \quad (1)$$

where K is a constant close to unity, θ is the Bragg angle of the (h k l) reflection and λ is wavelength of X-rays used. D_V is a volume-weighted quantity. Wilson (1963) used integral breadth β instead of FWHM in Eq. (1).

The dependence of strain ε to line broadening is defined as (Stokes and Wilson, 1944):

$$\varepsilon = \frac{\beta}{4} \cot\theta = \frac{\beta}{4\tan\theta} \quad (2)$$

When the XRD patterns are adjusted to a combination of Cauchy and Gaussian line shapes, the Halder and

Wagner (1966) approximation is better suited for obtaining the physical broadening:

$$\beta_f \cong (\beta_h^2 - \beta_g^2) / \beta_h \quad (3)$$

where terms β_g , β_h and β_f refer to the integral breadths of the instrumental, observed and measured (physical) profiles, respectively.

5.1. The Williamson–Hall integral breadth method

Williamson and Hall (1953) proposed a method for resolving size and strain broadening. Williamson–Hall plots can be applied to a Gaussian profile (Santra et al., 2002).

$$\beta_f^{*2} = \left(\frac{\beta_f \cos \theta}{\lambda} \right)^2 = \frac{1}{D_v^2} + 4\epsilon^2 d^{*2} \quad (4)$$

A plot of β_f^{*2} against $4d^{*2}$ gives a straight line. From the intercept and slope of line crystallite size and strain can be calculated.

5.2. The Warren–Averbach Fourier method

According to Warren (1969), each diffraction domain is represented by columns of cells along the a_3 direction normal to the diffracting planes (00l):

$$L = n|a_3|, \quad a_3 = \frac{\lambda}{2(\sin \theta_2 - \sin \theta_1)} \quad (5)$$

where n denotes the integer and a_3 is the unit of the Fourier length in the direction of the diffraction vector. The line profile is measured from θ_1 to θ_2 .

It has been shown that the cosine Fourier coefficients A_L of the profile are the products of the size coefficients A_L^S and distortion coefficients A_L^D :

$$A_L = A_L^S \cdot A_L^D \Rightarrow \ln A_L = \ln A_L^S + \ln A_L^D \quad (6)$$

$$A_L^D = \exp(-2\pi L^2 d^{*2} \langle \epsilon_L^2 \rangle) \quad (7)$$

$$\begin{aligned} \ln A_L &= \ln A_L^S - 2\pi^2 L^2 d^{*2} \langle \epsilon_L^2 \rangle \Rightarrow \ln A_L \\ &= \ln A_L^S - 2\pi^2 L^2 \langle \epsilon_L^2 \rangle / d^2 \end{aligned} \quad (8)$$

where $\langle \epsilon_L^2 \rangle$ is the mean-squared strain for the correlation distance L and d is the interplanar spacing of the reflecting planes (Balzar, 1999; Santra et al., 2002). The separation of distortion and size coefficients can be made by preparing proper plots according to above-mentioned equations.

6. Results and discussions

6.1. Particle size and surface area

The BET specific surface area and granulometric surface area are compared in Fig. 1. The BET surface area increases during the grinding process. Higher levels of specific energy input favor the production of great surface area. The specific surface area increases up to 31 times after consuming the energy of 22 kWh/kg by the mill. The generation rate of surface area at lower level of energy input is larger than the higher level of energy input. This can be ascribed to the fact that the breakage rate at initial stages of comminution is great and continues to decrease with progress in milling. The granulometric surface area increases rapidly at earlier stages of milling and continues to decrease steadily when energy

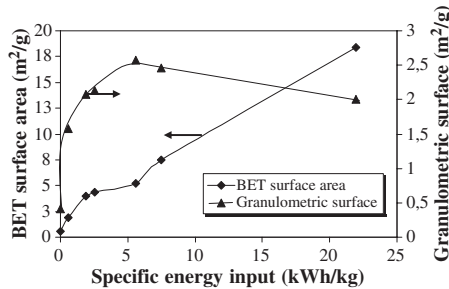


Fig. 1. Change in the BET specific surface area and granulometric surface area with specific energy input. Hereafter 0 kWh/kg refers to the initial sample.

input exceeds 5.5 kWh/kg as opposed to the BET surface area. This addresses the agglomeration of the particles during extend dry grinding.

This is in agreement with observations of Tkacova (1989) for oxide minerals. A similar trend was observed for sulfide minerals (Balaz, 2000) with short grinding times. This addresses the influence of milling conditions and mineral type on the formation of agglomerates and beginning stage of agglomeration. In addition, the agglomeration of particles in most previous studies was manifested by a decrease in the BET surface area. As with hematite, it seems that the agglomerate pores remain accessible for the nitrogen gas.

From the BET measurements, the particle size was determined via surface area by using well known equation:

$$d_{av} = 6/\sigma S \quad (9)$$

where d_{av} is the equivalent spherical particle diameter (μm), σ is the density (g/cm^3) and S is the specific surface area (m^2/g). Fig. 2 shows change in the BET particle size and mean diameter (d_{50}) of the particles in samples. The particles produced in intensive grinding are finer than of those obtained in the initial stages of milling. The mean BET particle size decreases as the specific energy input increases. The particle size decreased remarkably in the initial stage of milling after consuming the energy of 0.6 kWh/kg by the mill. By extending energy input in milling up to 5.5 kWh/kg, the particle size declines very slightly. A small increase in d_{50} (mean diameter) after intensive grinding is an indication of agglomeration which is inevitable in the finest grinding regime. For a given energy input, the mean particle size of hematite obtained from the laser diffraction method are larger than the sphere-equivalent diameter of those determined from the BET specific surface area. This also implies that pore agglomerates of primary particles are produced during intensive milling.

A comparison of particle size, BET surface area and granulometric surface indicates that the particle pores

remain accessible in agglomerates and the nitrogen gas can penetrate the pore space of particles. As a result, the BET method determined higher specific surface area and yielded small particles in contradiction with the particle size measurements from the laser diffraction method. The agglomeration of particles during extended milling was reported for various minerals by Balaz (2000), Welham (2001), Welham and Llewellyn (1998), and Zhang et al. (1996). These results suggest that agglomeration phenomena may be a feature of extended dry milling.

6.2. X-ray diffraction

The starting sample and ground hematite are indexed in a hexagonal (trigonal) symmetry (R-3c space group). The X-ray patterns of the milled samples only show the Bragg reflections of hematite (Fig. 3), suggesting that the starting material did not undergo significant reactions during milling and after milling. The XRD method studies do not show phases below 2 wt.%. This agrees with the observations of Kaczmarek and Ninham (1994) and Stewart et al. (2003). However, our observations disagree with the findings of Kosmac and Courtney (1992) and Zdujic et al. (1998). They reported a transformation of $\alpha\text{-Fe}_2\text{O}_3$ to Fe_3O_4 during ball milling in a planetary mill. In our opinion, the reason for this contradiction is the grinding condition and probably the source of starting material. Zdujic et al. (1998, 1999) made comprehensive studies to discuss the published results of the hematite transformation to Fe_3O_4 and subsequently to FeO . They stated that the transfer of sufficient energy to the particles is necessary to change the stability state of $\alpha\text{-Fe}_2\text{O}_3$ to Fe_3O_4 and subsequently to FeO .

From the XRD patterns, it can be further observed that the resolution of $K_{\alpha 1}$ from $K_{\alpha 2}$ even at high Bragg angles vanished owing to structure symmetry reduction. With increased specific energy input, a continuous broadening of the diffraction peaks and decreased

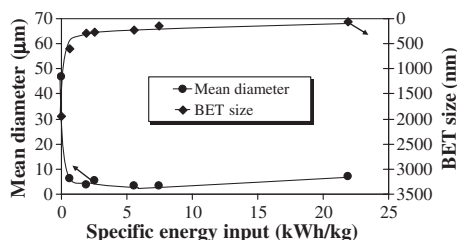


Fig. 2. Effect of specific energy input on the mean particle diameter (d_{50}) and BET particle size.

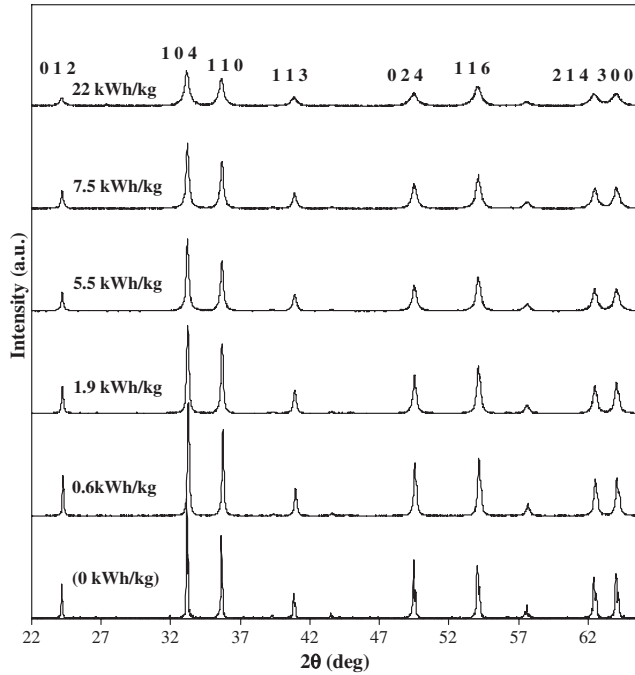


Fig. 3. XRD patterns of activated hematite as a function of specific energy input.

intensity of diffraction peaks were observed. These observations indicate an increase in the degree of lattice disorder and a decrease in the crystallite size; reducing the symmetry of the unit cell until some fraction of the material becomes amorphous. Comparing the XRD patterns indicates that the maximum line broadening and minimum reflection intensity were obtained from the hematite sample ground at a higher level of energy input.

The structural disorder due to increasing the abundance of X-ray amorphous material is manifested by decreases in the integral intensity of diffraction lines.

The fractional amorphization is defined as (Ohlberg and Strickler, 1962):

$$A = 100 - X = 100 - \left(\frac{U_0}{I_0} \times \frac{I_x}{U_x} \times 100 \right) \quad (10)$$

where U_0 and U_x refer to the background of non-activated sample and activated sample while I_0 and I_x are integral intensities of diffraction lines of non-activated sample and activated sample. A and X denote the degree of amorphization and the degree of crystallinity, respectively. The results are shown in Fig. 4. The X-ray

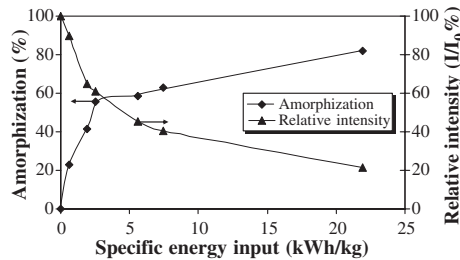


Fig. 4. Change in the X-ray amorphization degree and average relative intensity (I/I_0) of ground hematite with specific energy input.

amorphization degree increased and the reflection intensity decreased rapidly in the earlier stages of milling. The amorphization degree reached almost 80% after consuming the energy of 22 kWh/kg energy by the mill. The curve trend indicates that the long-range ordering of hematite was lost rapidly at the early stages of grinding.

The changes in average integral breadth values $\bar{\beta}$ from the eight most intensive reflection peaks and for (014) reflection in terms of energy input are shown in Fig. 5. As grinding intensity increases, the line breadths increase for both (014) reflection and the eight most intensive reflection peaks, which is in agreement with the observations of Stewart et al. (2003). This suggests that all the hematite lattice faces are distorted.

The lattice parameters were refined in Hexagonal system by regression diagnostics method using Unitcell software (Holland and Redfern, 1997). The regression diagnostics are numbers, calculated during the regression, which supply valuable information on the influence of each observation the least squares result and on the estimated parameters. The initial hematite yields the value of lattice parameters ($a=5.0312$ Å, $c=13.7414$ Å and $V=301.2291$ Å³) displaying very slight variations to the values given in the mineralogy database (Mineral database, 2005) ($a=5.0317$ Å, $c=13.737$ Å and $V=301.20$ Å³). The changes in the lattice parameters a -parameter and c -parameter for samples were calculated and displayed in Fig. 6. Generally, we observed a unit cell expansion and an increase of the lattice parameters in comparison to the starting material. There are not any significant differences in the expansion of lattice parameters among the milled samples at different levels of energy input.

6.3. Microstructure characterizations

For microstructure characterization, two methods are applied: the integral breadth and Warren–Averbach

methods. The results are discussed in the following paragraphs.

6.3.1. The integral breadth method

The integral breadths β_{f} of the physically broadened X-ray diffraction lines were separated into the two components (broadening resulting from small crystallite size and induced lattice strain) by the Williamson–Hall method. The Williamson–Hall plots for milled samples are illustrated in Fig. 7 according to Eq. (4). The plots for the first and second orders of the (012) reflection, [012] direction; and all intensive reflection peaks were made. The correlation coefficients for plots were between 0.90 and 0.96, indicating a strong relationship between β_{f}^2 and d^*^2 .

According to Fig. 7, there is no doubt that mechanical activation results in severe broadening of diffraction lines. A systematic deviation was observed relative to the line connecting the orders of (012) and (024) reflections, all data points lie below it. The differences between all reflections and direction [012] for lower level of energy input are negligible. The deviation increases as the milling intensity goes up. This could be due to difference of the elastic moduli of single crystal hematite existing between (024) and other crystallographic directions (Borner and Eckert, 1997; Vives et al., 2004). The scatter of β_{f}^2 values indicates that the crystallite shape differs from a spherical one. From Fig. 7, it can be observed that the physical broadening of the samples milled with higher grinding intensity is much larger than of the samples milled with less intensive milling. From the curves trend, it is apparent that strain increases with rising the specific energy input level and crystallite size decreases due to much higher impact and stress on the powder particles. Similar trends were observed for iron powder milled in a planetary ball mill with different disk speeds (Vives et al., 2004). Lucks et al. (2004) observed that the broadening of molybdenum

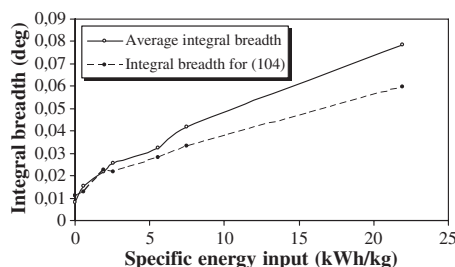


Fig. 5. Change in the physical integral breadth for reflection (104) and average physical integral breadth for the eight most intensive reflection peaks as a function of specific energy input.

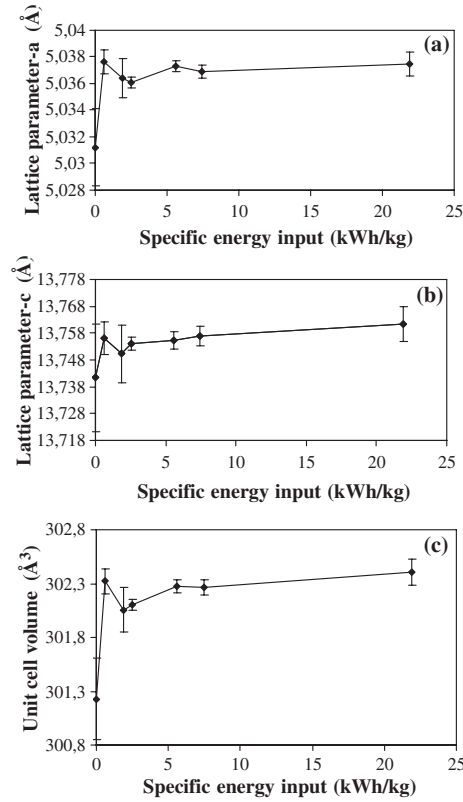


Fig. 6. Variation of lattice parameters of a (a), c (b) and unit cell volume (c) with specific energy input. The confidence level of measurements at 95% is included.

samples milled with an attritor mill is much larger than the broadening of samples milled with a planetary mill. The observed trend agrees with our observations with regard to the intensity of milling conditions. The production of material with specific microstructural

characteristics using the appropriate milling type and conditions seems promising. The Warren–Averbach method shows higher sensitivity in the calculation of crystallite size, i.e., a very small change in line slope causes dramatic changes in the values of the crystallite

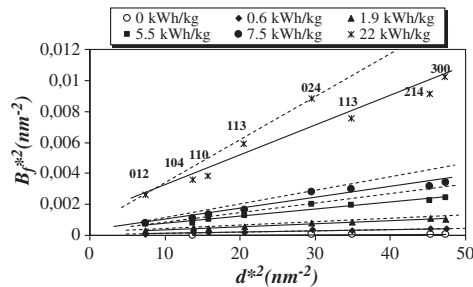


Fig. 7. Williamson–Hall plots for hematite samples milled with different specific energy input. Dashed and solid lines correspond to the first and second order of (012) reflections and to all reflection peaks, respectively.

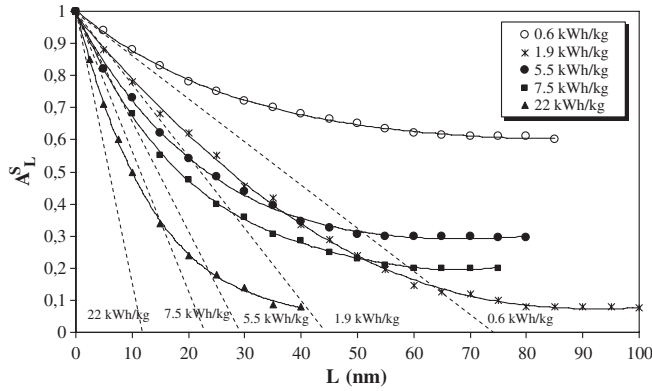


Fig. 8. Change of initial slope of A_L^S for samples milled with different specific energy input.

size. The strain and crystallite size values obtained from the slope and intercept of each straight line are compared with the results of other methods in Section 6.3.3.

6.3.2. The Warren–Averbach analysis

Since the milled samples represented the anisotropy behavior in broadening (according to the Williamson–Hall plot), the precise extraction of the crystallite size and strain for particular direction using the Warren–Averbach analysis is possible. The Warren–Averbach analysis was applied for [012] direction and the results are discussed in the following paragraphs.

6.3.2.1. Crystallite size and strain results. We calculated the A_L^S coefficients as a function of Fourier length

for line profile of milled samples in different levels of specific energy input (Fig. 8). The A_L^S levels off with increasing L whatever specific energy input was applied. From the intercept of the initial slope on the L -axis (dashed line), the surface weighted crystallite size values were extracted. The use of intensive grinding produces small crystallites. This may be related to intensive line defects, which disrupt the particles and consequently result in small crystallites.

The Warren–Averbach analysis also provides the distribution of RMSS (root mean square strain) as a function of Fourier length. A typical plot of $\langle \epsilon_L^2 \rangle$ as a function of L shows a monotonically decreasing curve for increasing L values as shown in Fig. 9. It is obvious that intensive milling leads to higher microstrain in particular at small L . A hematite sample, however,

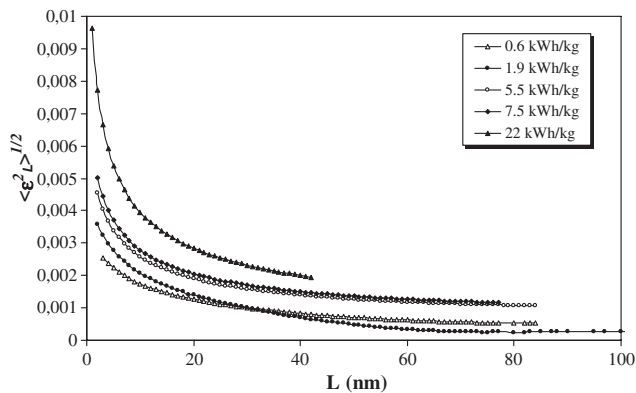


Fig. 9. The RMSS strain obtained using Warren–Averbach method for milled samples with various specific energy input.

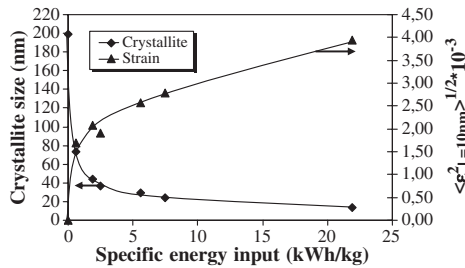


Fig. 10. Variation of surface weighted crystallite size and root mean square strain (RMSS) with specific energy input. The RMSS strain for initial sample assumed to be negligible. The crystallite size for the initial sample is calculated using single peak method.

milled with the specific energy input of 1.9 kWh/kg shows smaller microstrain in higher column length and A_L^S in comparison to that of hematite ground with 0.6 kWh/kg. This may be related to uncertainties in background estimation due to overlapping peaks (measurement accuracy) and/or non-uniform activation. Some uncertainty always exist in all the methods, inasmuch as the task is to determine the tails, which are either hidden or marked by an adjacent overlapping profile or distorted by a non-level background. This may occur when the sample contains an amorphous fraction that can give broad bumps in diffraction pattern which extend over several Bragg reflections. The $\langle \epsilon_L^2 \rangle^{1/2}$ plot as a function of the L contains more information than a single value at an arbitrary L value. The degree of disorder in samples from the observed trend in $\langle \epsilon_L^2 \rangle^{1/2}$ versus L plot can be indicated. The lattice disorder can be attributed to the crystalline distortions. This arises from the fluctuations in the interplanar distances and presence of the dislocations in samples which result in a Gaussian distribution of the microstrain (Dong Lin and Gong Duh, 1997).

The normally quoted values for strains are the local values, i.e., at $L=0$. However, the microstrain at $L=0$, $\langle \epsilon^2 \rangle_{L=0}^{1/2}$ can not be directly determined by using the Warren–Averbach method. The experimental A_L^D functions are often affected by errors, in particular due to the truncation in the Fourier transformation of the diffraction lines (Lucks et al., 2004). Thus, we decided to calculate the strain at $L=10$ nm. The crystallite size and lattice strain are displayed in Fig. 10. The microstrain, $\langle \epsilon_L^2 \rangle^{1/2}$ at $L=10$ nm increases up to 4.0×10^{-3} after consuming the energy of 22 kWh/kg by the mill. The results regarding the strain and crystallite size are in line with observations of Bid et al. (2001) and Sahu et al. (2003); however, our results regarding crystallite sizes and strains in direction [012] are larger and smaller, respectively, than their observations. This can be related

to the initial material characteristics and milling conditions. Bide et al. and Sahu et al. used planetary mills with high angular velocity. This implies that the ability of energy transfer in a vibratory mill, at least in our grinding conditions, is not as high as when using a planetary mill.

6.3.2.2. The crystallite size distribution characteristics. Another advantage in using the Warren–Averbach method rather than any other method to calculate microstructural characteristics is its ability to give information on the distribution of crystallite size (column length). It is known that the relationship between D_V and D_S depends on the distribution of crystallite size. The differences between D_V and D_S increase as the distribution of crystallite size becomes broader.

The crystallite size (column length) distribution characteristics are summarized in Table 2. At the first glance, the maximum relative frequency for ground samples appears at small L and the maximum relative frequency of column length increases as the intensity of milling grows except the ground sample with 1.9 kWh/kg specific energy input. The investigation of the left and right width values (L_{fwhm} and R_{whm}) corresponding to column length distribution indicates that the distribution functions also follow the lognormal distribution form. The lognormal probability distribution of crystallite size during intensive milling conditions was reported by several authors for different materials: zirconia powders (Dong Lin and Gong Duh, 1997), α - Al_2O_3 prepared by combustion technique (Santra et al., 2002), ball-milled molybdenum (Lucks et al., 2004) and milled iron powders (Vives et al., 2004).

Grinding up to 1.9 kWh/kg energy input resulted in two maxima, suggesting two main crystallite size groups exist in the milled samples. This could be related to the fact that the powder distribution around grinding media affected the energy and stress transferring quantity to the particles being ground due to existing coarser particles.

Table 2

Maximum of relative frequency (R.F) of column length and size distribution widths of crystallite size resulting from the Warren–Averbach approach in direction [012]

Specific energy input (kWh/kg)	<i>L</i> (nm)	R.F (%)	Lfwhm (nm)	Rfwhm (nm)	fwhm (nm)
0.6	11.4 (65)	2.1 (1.4)	9.6	22.3	31.9
1.9	42.5 (9)	1.7 (1.3)	41.0	25.5	66.5
2.5	10.1	2.6	8.6	19.2	27.8
5.5	7.3	3.1	6.3	16.3	22.6
7.5	6.2	4.0	5.3	13.5	18.8
22	3.7	6.8	3.2	8.7	11.9

Terms Lfwhm, Rfwhm and fwhm correspond to the width of crystallite length distribution at left and right, respectively. Term fwhm is the overall widths of distributions. The values in parentheses denote the second maxima.

With less intensity of grinding, the coarse particles prevent the media from coming into contact with finer particles. Fragmentation of the coarsest particles results in the establishment of a uniform contact between the grinding media and particles being ground. Having this in mind, the existence of two main crystallite size groups can be either attributed to the new phase formation and/or changes of the materials being ground. However, in our investigation we did not observe any phase transformation or new phase formation according to the XRD patterns. In our opinion, less intensive stressing of powders resulted in a wide range crystallite sizes. According to Table 2, as the intensity of milling increases, the widths of crystallite size distributions (fwhm) decline except the sample ground with 1.9 kWh/kg of energy input. As it is expected, the column length distribution becomes sharper, when hematite is subjected to severe

grinding; therefore, we can conclude that the intensive grinding brings about the homogeneous activation of hematite.

6.3.3. The comparison of results

In order to make a rapid comparison, we used Scherrer equation with a first approximation to calculate the crystallite size and strain values. This also confirmed the extremely anisotropic character of crystallite size and strain, i.e., each reflection peaks yielded different crystallite size and strain values. We compared the average values obtained from Scherrer equation using the eight most intensive reflections (with integral breadth), Williamson–Hall by taking all the diffractions and Warren–Averbach method for the [012] direction in Fig. 11 as a function of specific energy input. The crystallite sizes decrease and strain values increase

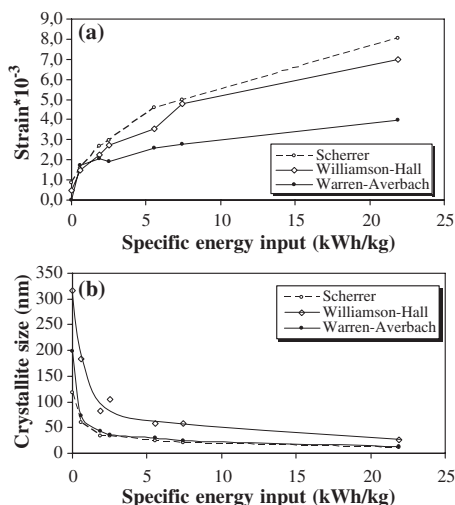


Fig. 11. Variation of crystallite size and strain obtained using different methods with specific energy input.

drastically as the specific energy input grows. Among all of the methods, the Scherrer equation gives the smallest crystallites and the highest values of the strain. The largest crystallites and lowest strain were obtained using Williamson–Hall and Warren–Averbach methods for $L=10$ nm, respectively.

The quantitative analysis of size and strain without considering the underlying assumptions is impossible. The Scherrer equation only addresses the line broadening that is entirely caused by size effect or strain effect. This is not valid in case of mechanical activation. The broadening is subdivided into the two components by Williamson–Hall plots and Warren–Averbach method. It should be noted that the Warren–Averbach method does not necessarily assume a gauss strain distribution or that mean square strain is independent of distance L . However, the Warren–Averbach analysis becomes exact in the case of the Gaussian distribution of ε_L for each L . The strain value ε obtained from the Williamson–Hall plots expresses only the maximum value for the strain (Balzar, 1999). In the case of pure-gauss strain broadening, the RMSS is independent of L and the relationship between $\langle \varepsilon_L^2 \rangle^{1/2}$ and ε , strain resulting from integral method, is given by Balzar (1999), Halder and Wagner (1966), and Keijser et al. (1983) follows as:

$$\langle \varepsilon_0^2 \rangle^{1/2} = \langle \varepsilon_{L=0}^2 \rangle^{1/2} = (2/\pi)^{1/2} \varepsilon \quad (11)$$

However, there is no clear connection between RMSS and ε ; if the strain broadened contains a Cauchy component. A rough estimate was given by Balzar (1999) when the Gauss and Cauchy extremes of the strain broadened Voigt profile exist:

$$0.5 \leq \varepsilon / \langle \varepsilon_L^2 \rangle^{1/2} \leq 2. \quad (12)$$

If D_V and D_S denote the volume weighted parameter and the surface weighted value, respectively, the relationship between D_V and D_S has been given by Balzar (1999) and Lucks et al. (2004):

$$1.31 \leq \frac{D_V}{D_S} \leq 2 \quad \text{for a Voigt size-broadened profile} \quad (13)$$

$$\frac{D_V}{D_S} \geq r \quad \text{otherwise (Alternative methods)} \quad (14)$$

r ranges typically between 1 and 3.

Our findings regarding the strain resulting from the integral breadth are in good agreement with the Warren–Averbach analysis. The crystallite size values obtained from the integral breadths, however, represent a rough correspondence to those obtained from the Warren–Averbach analysis, indicating the sensitivity of crystallite size rather than strain due to Pseudo–Voigt line shape fitting. The obtained results are in line with Santra's (2002) observation. Scardi et al. (2004) stated that the reliability of results in integral breadth methods vanishes for some reasons. For example, the crystallites in polycrystalline material have different sizes and shapes and these affect the width and shapes of all diffraction line profiles. The size distribution and shape for simple polyhedra can be decoupled in principle; but this separation is impossible using the integral breadths. Besides, the line profiles produced by dispersed small crystallites (e.g., according to a Lognormal or Gamma distributions) are non-Voigtian and Eq. (4) is not appropriate. Thus, the integral breadth methods are utilized best when trying to identify trends in the change of microstructure by comparing samples belonging to a series of experiments.

7. Conclusions

The following conclusions based on the experimental results presented in the article can be made:

1. The agglomeration of particles during mechanical activation occurs after consuming the energy of 5.5 kWh/kg by the mill and the agglomerate pores are accessible for the nitrogen gas. Milling of hematite increased surface area up to 18.4 m²/g after energy consumption of 22 kWh/kg.
2. As the specific energy input increased, the line broadening increases and integral intensity decreased. The lattice parameters and unit cell volume of hematite expanded during mechanical activation. The activated hematite did not undergo significant chemical reaction.
3. The Williamson–Hall plots suggested that strain and size contributions in line broadening exist simultaneously in the milled samples and anisotropic character of line broadening is revealed in products. It was pointed out that the hematite lattice is 'soft' between the (024) and the other crystallographic directions.
4. All the methods display the same trend, rapid decrease of the coherently diffracting domain size and increase of the strain state. Williamson–Hall and Scherrer relations have to be employed only in the

first qualitative approximation, more accurate results are obtained using the Warren–Averbach method in direction [012].

- From the Warren–Averbach method the crystallite sizes were estimated between 73.5 and 12.2 nm depending on the intensity of grinding. The root mean square strain (RMSS) for activated samples exceeds 4.0×10^{-3} for the maximum intensity of grinding. Finally, intensive grinding brings about homogeneous activation of hematite.

Nomenclature

A	Peak area
A_L	Fourier coefficients
A_L^D	Distortion components in the Fourier coefficient
A_L^S	The size components in the Fourier coefficient
a_3	The unit of the Fourier length in direction of the diffraction vector
b	Burgers vector
D_S	Surface-weighted crystallite size
D_V	Volume-weighted crystallite size
d	Interplanar spacing
d_{av}	The equivalent spherical particle diameter
FWHM	Full width at half-maximum of profile
$(h\ k\ l)$	Miller indices
I	Intensity
K	Scherrer constant
L	na_3 , column length (distance between two cells in a real space) orthogonal to diffracting planes
RMSS	Root mean square strain
S	Specific surface area
d^*	$2 \sin \theta / \lambda = d^*$, variable in the reciprocal space
β	Integral breadth
β_f	The integral breadth of the physically broadened profile
β_g	The integral breadth of the instrumentally broadened profile
β_h	The integral breadth of the observed broadened profile
β^*	$\beta \cos \theta / \lambda$, integral breadth in the units of d^* (nm^{-1})
$\langle e_L^2 \rangle$	Mean square strain, orthogonal to diffracting planes, averaged over the distance L
ε	Apparent strain
η	Mixing factor of a Pseudo-Voigt function
θ	Bragg angle
λ	X ray wavelength
σ	Density
LPA	Line profile analysis
XRD	X ray diffraction
Å	Angstrom unit (10^{-11} m)

Acknowledgments

The authors would like to thank professor Claes I Helgesson for his valuable comments on this paper.

References

- Balaz, P., 2000. Extractive Metallurgy of Activated Minerals. Elsevier, Amsterdam.
- Balzar, D., 1999. Voigt-function model in diffraction line-broadening analysis. In: Snyder, R.L., H.J. (Eds.), Defect and Microstructure Analysis from Diffraction, pp. 94–126.
- Bid, S., Banerjee, A., Kumar, S., Pradhan, S.K., De, U., Banerjee, D., 2001. Nanophase iron oxides by ball-mill grinding and their Mössbauer characterization. *J. Alloys Compd.* 326, 292–297.
- Boldyrev, V.V., Pavlov, S.V., Goldberg, E.L., 1996. Interrelation between fine grinding and mechanical activation. *Int. J. Miner. Process.* 44–45, 181–185.
- Borner, I., Eckert, J., 1997. Nanostructure formation and steady-state grain size of ball-milled iron powders. *Mater. Sci. Eng., A Struct. Mater.: Prop. Microstruct. Process.* 226–228, 541–545.
- Dong Lin, J., Gong Duh, J., 1997. The use of X-ray line profile analysis to investigate crystallite size and microstrain for zircon powders. *J. Mater. Sci.* 32, 5779–5790.
- Halder, N.C., Wagner, C.N.J., 1966. Separation of particle size and lattice strain in integral breadth measurements. *Acta Crystallogr.* 20, 312–313.
- Holland, T.J.B., Redfern, S.A.T., 1997. Unit cell refinement from powder diffraction data; the use of regression diagnostics. *Mineral. Mag.* 61, 65–77.
- Kaczmarek, W.A., Ninham, B.W., 1994. Preparation of Fe_3O_4 and $\gamma\text{-Fe}_2\text{O}_3$ powders by magnetomechanical activation of hematite. *IEEE Trans. Magn.* 30 (2), 732–734.
- Keijser, TH., DE, H., Mittemeijer, E.J., Rozendaal, C.F., 1983. The determination of crystallite-size and lattice-strain parameters in conjunction with the profile-refinement method for determination of crystal structures. *J. Appl. Crystallogr.* 16, 309–316.
- Kosmac, T., Courtney, T.H., 1992. Milling and mechanical alloying of inorganic nonmetallics. *J. Mater. Res.* 7 (6), 1519–1525.
- Lin, J.I., 1998. Implications of fine grinding in mineral processing; mechanochemical approach. *J. Therm. Anal. Calorim.* 52, 453–461.
- Lucks, I., Lamparter, P., Mittemeijer, E.J., 2004. An evaluation of methods of diffraction-line broadening analysis applied to ball-milled molybdenum. *J. Appl. Crystallogr.* 37, 300–311.
- Maurice, D., Hawk, J.A., 1999. Ferric chloride leaching of a mechanically activated Pentlandite–Chalcopyrite concentrate. *Hydrometallurgy* 52, 289–312.
- Mineral database, 2005. <http://webmineral.com/data/hematite.shtml>.
- Mulak, W., Balaz, P., Chojnacka, M., 2002. Chemical and morphological changes of millerite by mechanical activation. *Int. J. Miner. Process.* 66, 233–240.
- Ohlberg, S.M., Strickler, D.W., 1962. Determination of percent crystallinity of partly devitrified glass by X-ray diffraction. *J. Am. Ceram. Soc.* 45, 170–171.
- Sahu, P., De, M., Zdubic, M., 2003. Microstructural characterization of the evolved phases of ball-milled $\alpha\text{-Fe}_2\text{O}_3$ powder in air and oxygen atmosphere by Rietveld analysis. *Mater. Chem. Phys.* 82, 864–876.
- Santra, K., Chatterjee, P., Sen Gupta, S.P., 2002. Voigt modeling of size–strain analysis: application to $\alpha\text{-Al}_2\text{O}_3$ prepared by combustion technique. *Bull. Mater. Sci.* 25 (3), 251–257.

- Scardi, P., Leoni, M., Delhez, R., 2004. Line broadening analysis using integral breadth methods: a critical review. *J. Appl. Crystallogr.* 37, 381–390.
- Scherrer, P., 1918. Bestimmung der Grösse und der inneren Structure von Kolloidteilchen mittels Röntgenstrahlung. *Nachr. Ges. Wiss. Gött.* 2, 98–100.
- Siemens, A.G., 1996. *Diffac Plus Profile Fitting Manual Program*. 1-1-5-26.
- Stewart, S.J., Borzi, R.A., Cabanillas, E.D., Punte, G., Mercader, R.C., 2003. Effects of milling-induced disorder on the lattice parameters and magnetic properties of hematite. *J. Magn. Magn. Mater.* 260, 447–454.
- Stokes, A.R., Wilson, A.J.C., 1944. The diffraction of X-rays by distorted crystal aggregates — I. *Proc. Phys. Soc. Lond.* 56, 174.
- Tkacova, K., 1989. *Mechanical Activation of Minerals*. Elsevier, Amsterdam.
- Vives, S., Gaffet, E., Meunier, C., 2004. X-ray diffraction line profile analysis of Iron ball milled powders. *Mater. Sci. Eng., A Struct. Mater.: Prop. Microstruct. Process.* 366, 229–238.
- Warren, B.E., 1969. *X-Ray Diffraction*. Addison-Wesley, New York.
- Welham, N.J., 2001. Enhanced dissolution of tantalite/columbite following milling. *Int. J. Miner. Process.* 61, 145–154.
- Welham, N.J., Llewellyn, D.J., 1998. Mechanical enhancement of the dissolution of ilmenite. *Miner. Eng.* 11 (9), 827–841.
- Williamson, G.K., Hall, W.H., 1953. X-ray line broadening from field aluminum and wolfram. *Acta Metall.* 1, 22–31.
- Wilson, A.J.C., 1963. *Mathematical Theory of X-Ray Powder Diffractometry*. Philips Technical Library, Centrex publishing company, Eindhoven, Netherland, pp. 21–53.
- Zdujic, M., Jovalekic, C., Karanovic, L.J., Mitric, M., Poleti, D., Skala, D., 1998. Mechanochemical treatment of α -Fe₂O₃ powder in air and atmosphere. *Mater. Sci. Eng., A Struct. Mater.: Prop. Microstruct. Process.* 245, 109–117.
- Zdujic, M., Jovalekic, C., Karanovic, L.J., Mitric, M., 1999. The ball milling induced transformation of α -Fe₂O₃ powder in air and oxygen atmosphere. *Mater. Sci. Eng., A Struct. Mater.: Prop. Microstruct. Process.* 262, 204–213.
- Zhang, Q., Kasai, E., Saito, F., 1996. Mechanochemical changes in gypsum when dry ground with hydrated minerals. *Powder Technol.* 87, 67–71.
- Zoltan Juhasz, A., 1998. Aspects of mechanochemical activation in terms of comminution theory. *Colloids Surf., A Physicochem. Eng. Asp.* 141, 449–462.

Paper II

Comparative Study of Microstructural Characteristics and Stored Energy of Mechanically Activated Hematite in Different Grinding Environments

Parviz Pourghahramani & Eric Forssberg, International Journal of Mineral Processing, 79 (2006), 120-139

Comparative study of microstructural characteristics and stored energy of mechanically activated hematite in different grinding environments

Parviz Pourghahramani *, Eric Forssberg

Division of Mineral Processing, Luleå University of Technology, Luleå, Sweden

Received 31 October 2005; received in revised form 7 January 2006; accepted 20 January 2006

Available online 24 March 2006

Abstract

Hematite concentrate was mechanically treated using different milling machines and experimental conditions in air atmosphere. The changes in phase constitution, particles size, specific surface area, lattice parameters and X-ray amorphous phase fraction of activated hematite were determined. It was found that the agglomeration of the particles take place during extended milling with accessible pores for Nitrogen gas. The higher media surface brought about the largest specific surface area whatever milling devices used. After 9 h of grinding with higher media surface, the maximum and minimum specific surface area resulted from the grinding in the tumbling and vibratory mills, accounting for 6.83 m²/g and 18.42 m²/g, respectively. For the same grinding condition, tumbling mill produced the lowest X-ray amorphous phase. The maximum X-ray amorphous material estimated around 85% from the grinding in the planetary mill with higher media surface for 9 h of milling.

Structural changes were followed by XRD line broadening analysis (LPA) using the integral breadth method and Warren–Averbach approach. From the Williamson–Hall plots, it was understood that strain and size contributions exist simultaneously in the milled samples. Besides, the physical broadening increases as milling time and media surface increase regardless of milling types. Besides, it was found that hematite crystal is ‘soft’ between (024) and other crystallographic directions.

From the Warren–Averbach approach, it was observed that the higher grinding media surface and prolonged milling favor the generation of small crystallite, higher microstrain, limited crystallite length and subsequently uniform activation of hematite. After 9 h of milling with higher media surface in tumbling, vibratory and planetary mills, the surface weighted crystallite size reached 17.3, 12.2 and 5.6 nm respectively. The maximum lattice strain, $\langle \epsilon_{h=10}^2 \rangle^{1/2}$, in the grinding with tumbling, vibratory and planetary mills was found about 4.44×10^{-3} , 3.95×10^{-3} and 5.23×10^{-3} , respectively. The maximum dislocation density accounted for 46.3×10^{14} m/m³ in the planetary milling with higher media surface after 9 h of milling. The evaluation of energy contributions of structural defects suggested that the energy contribution of the amorphization was dominant and amounted to 92–98% of the overall stored energy in hematite, depending on milling conditions. Finally, for a given stress energy, the products of tumbling mill represent higher reactivity potential.

© 2006 Elsevier B.V. All rights reserved.

Keywords: grinding methods; mechanical activation; line broadening analysis; microstructure; structural changes

DOI of original article: doi:[10.1016/j.minpro.2006.02.001](https://doi.org/10.1016/j.minpro.2006.02.001).

* Corresponding author. Tel.: +46 920 491313; fax: +46 920 97364.

E-mail address: Parviz.Pourghahramani@ltu.se

(P. Pourghahramani).

1. Introduction

The applications of treatment of minerals in milling devices are numerous and can roughly be divided into

three categories: coarse grinding, fine grinding and mechanical activation. The most important goal in coarse grinding is size reduction. In contrast, the objective of mechanical activation is the changes in the structure, tension state and chemical composition and reactivity (Zoltan Juhasz, 1998), although the size reduction takes place primarily by mechanical activation. The fine grinding limit is determined by ductile–brittle transition state (Boldyrev et al., 1996). The direct correlation between size reduction and milling intensity becomes absolutely unreliable and invalid in the case of mechanical activation (Karagedov and Lyakhov, 2003).

The active mechanical energy is partially transferred to the particles, e.g. by the impact of solid particles or by induction of tensile and compressive forces in powder mass. The influence of mechanical energy on solids includes a multitude of elementary physicochemical micro- and macro-processes. The mechanical energy leads to changes of the material structure, to the occurrence of structural defects such as changes of the surface, lattice distortion and conversion of long range order to short range order. Therefore, the free energy or chemical potential gained and the composition can change during the mechanical activation. In this way, the solid systems reach an activated state (Balaz, 2000; Tkacova, 1989).

The activation ability of milling equipment is controlled by the frequency of impacts and the modes of stress influence the nature of structural changes. Generally, it has been established that with shear and pressure stresses structural changes are concentrated at regions near the surface and decrease with increasing distance from the surface. With impact stresses the size of the primary crystallite become smaller in the whole volume and the disturbances start at the corners and borders (Tkacova et al., 1993). Based on a geometrical model for defect distribution, mills were divided into two groups of jet mill and disintegrator and mills with loose media by Bernhardt and Heegn (1978). It was concluded that in the former group, the mechanical energy imparted to individual particles during impact. In contrast, in mills with loose media, the particles are stressed in a material bed.

The influence of the density of milling media on mechanical activation of inorganic oxides was investigated by Karagedov and Lyakhov (2003). Dry grinding was found to be more effective than wet milling in the dissolution of Tantalite despite the generation of large specific surface in wet milling (Welham, 2001). It was reported that the crystallite size decreased exponentially and the strain increased with increasing activation time during the mechanical activation of ilmenite (Welham and Llewellyn, 1998). A comparative study of the

influence of attritor, ball and vibratory mills on the reactivity of Sulfide minerals was carried out by Balaz et al. (1988). $\gamma\text{-Fe}_2\text{O}_3$ samples ground with smaller amplitude in a vibratory mill showed higher reactivity (Senna, 1983).

The aim of the present paper is to investigate the influence of different experimental conditions and activation devices on hematite concentrate. The first part of this paper discusses the mechanical activation of hematite concentrate in different activation mills with various grinding variables. The second part is assigned to the characterization of microstructural characteristics of the activated hematite using integral breadth and Warren–Averbach approach in order to distinguish the influence of different milling devices and experimental conditions on the generation of microstructural characteristics and their contributions to the stored energy.

2. Experimental

The changes brought about by different milling devices during the mechanical activation of hematite concentrate were investigated using three types of ball mills; vibratory, planetary and tumbling mills. The milling was carried out by different sizes of steel media from 6 mm to 22.2 mm. A statistical design for three levels of grinding methods, three levels of milling time (1, 3 and 9 h) and two levels of media surface (1 and 4 m²/kg of hematite) was used. Experiments were performed in dry mode (without any additives) and batch scale grinding. All experiments were performed in air atmosphere. Each experiment was carried out independently and in closed condition. During milling, the temperature of the material was measured by a thermometer immediately after stopping the mill. Obtained powders were sealed into plastic tubes and kept in a freezer for further experiments and measurements. The experimental milling conditions are displayed in Table 1.

The particle size distribution of the samples was measured by Laser diffraction (CILAS 1064) in the liquid mode. The mean particle diameter and granulometric surface area based on particle size distribution were calculated. The specific surface area of the samples was determined by the BET method with the Flow Sorb II 2300 (Micromeritics). Samples were degassed by heating at 220 °C for 90 min immediately prior to measurements.

The X-ray diffraction (XRD) patterns were collected by a Siemens D5000 powder diffractometer with Bragg–Brentano geometry equipped with a curved graphite monochromator in the diffracted beam arm and using Cu K α radiation ($\lambda=0.15406$). The XRD patterns of the samples were recorded in the range

Table 1
Experimental milling conditions and mill types

Milling conditions	Tumbling milling	Vibratory milling	Planetary milling
Specific input energy (kWh/kg)	0.1996–6.221	0.6–21.92	5.286–190.52
Media filling (%)	38.9	70	23.4
Media surface (m ² /kg)	1, 4	1, 4	1, 4
Milling time (h)	1, 3, 9	1, 3, 9	1, 3, 9
Ball to powder weight ratio	16.77:1, 67:1	16.92:1, 67.68:1	19.1:1, 76.34:1
Speed (rpm)	60	1000	100 (axle), 200 (drum)
Amplitude (mm)	—	8	—
Media apparent density (g/cm ³)	4.875	4.875	4.875
Amplitude (mm)	—	8	—
$L \times \phi$ mm	275 × 245	320 × 185	87 × 115
Temperature of material (°C)	24–38	48–105	39–68

$2\theta = 10^\circ$ – 90° , using a step size of 0.02° and a counting time of 5 s/step.

To characterize the microstructural characteristics encountered during the mechanical activation of specimens, the line broadening analysis was applied. The broadening analysis is accompanied with difficulties in the case of overlapped peaks. This can make the line broadening analysis more difficult. Special care was

exercised in the scanning of samples and on the profile fitting procedures. The eight most intensive reflection peaks of the samples were used in the line broadening analysis. The Profile software supplied by Bruker/Socabin was used in the profile fitting procedures and in the extraction of the parameters. An example of profile fitting and separation of overlapped peaks is displayed in Fig. 1. The obtained X-ray diffraction patterns were

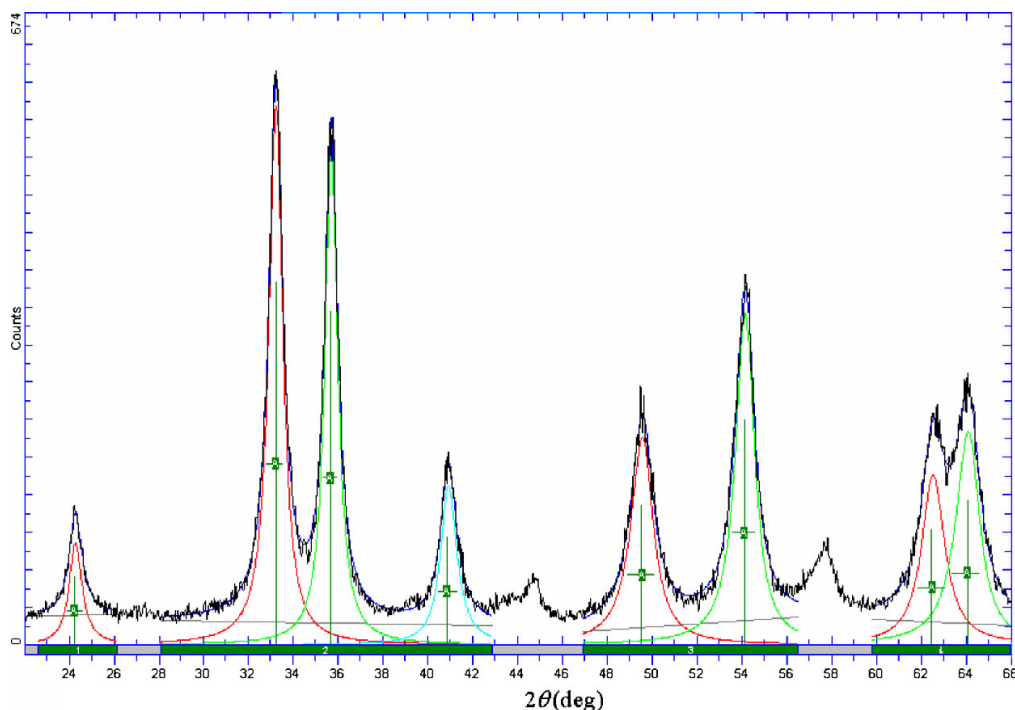
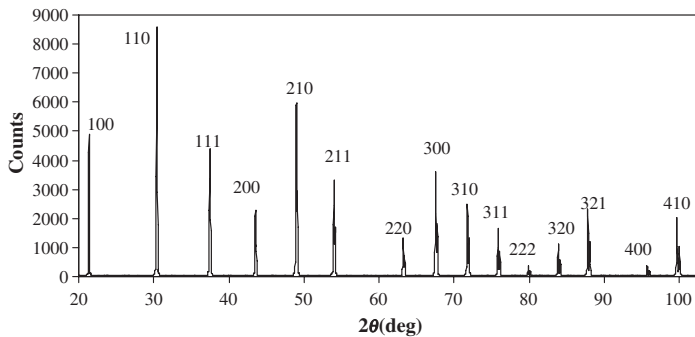


Fig. 1. An example of profile fitting in which the Pseudo-Voigt function is fitted to the Hematite samples ground for 9 h with media surface of 4 m²/kg in a planetary mill.

Fig. 2. Standard LaB₆ (SRM660a) diffraction patterns.

fitted to Pseudo-Voigt line shape function, which is a linear combination of Cauchy and Gaussian functions. For each adjusted line profile, the following parameters were obtained: (1) the maximum intensity of peaks (I_{\max}), (2) the full-width at half of its maximum intensity (FWHM), (3) integral breadth (β), (4) the mixing factor (η), and (5) peak position (2θ).

The same procedure was applied for the standard sample, LaB₆(SRM 660a), proposed by the National Institute of Standards and Technology (NIST) of the U. S.A. to obtain the instrumentally broadened profile. This profile was used to subtract the instrumental contribution from the measured profiles. The standard sample shows very narrow peaks and provides a good approximation from the instrumental effects (Fig. 2). Since the $K\alpha_2$ component in the XRD patterns increases the line broadening and introduces asymmetry into profile, the $K\alpha_2$ component was removed from the XRD patterns of standard and specimens.

The physical broadening due to strain and crystallite size was obtained according to the Halder and Wagner approximation (1966). This gives reasonable approximation when the line profile is adjusted to a combination of Lorentzian and Gaussian functions. To extract the microstructure characters, two conventional methods, integral breadth and Warren–Averbach methods, were used. The profile fitting procedure and principles of the methods were discussed in detail in previous work (Pourghahramani and Forssberg, 2006).

3. Material

The high-purity hematite concentrate containing about 97.91% Fe₂O₃ was supplied by the LKAB (Luossavaara Kiirunavaara Aktiebolag) Company in Sweden. The XRD pattern of hematite concentrate (hereafter referred to as initial hematite) only showed the hematite reflection peaks (Fig. 3). The chemical analysis

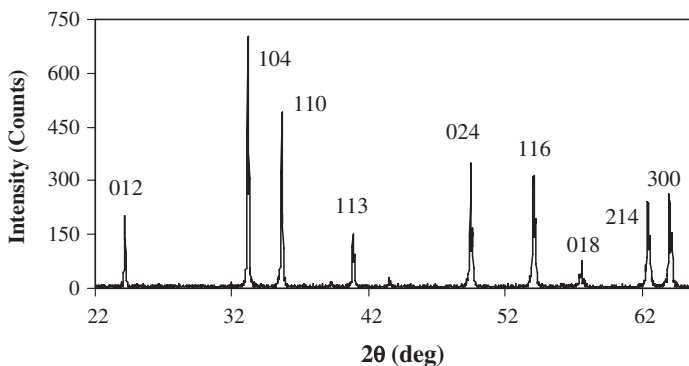


Fig. 3. The XRD patterns of initial Hematite.

Table 2
The chemical analysis of the initial Hematite (%)

Fe ₂ O ₃	Al ₂ O ₃	SiO ₂	TiO ₂	MgO	MnO	P ₂ O ₅	Other elements
97.91	0.73	0.73	0.27	0.20	0.022	0.088	0.051

of initial hematite is also given in Table 2. From the BET measurement the specific surface area was estimated about 0.59 m²/g. The mean diameter, F_{80} and density of starting hematite were calculated to around 23, 80 μ m and 5240 kg/m³, respectively.

4. Results and discussions

4.1. Particle size and surface area

The effects of the milling on the particle size distributions are summarized in Fig. 4. The initial hematite has relatively wide distribution in comparison to the milled samples. The gap differences between the curves imply that the rate of breakage in the earlier stages of milling is higher than the later stages of grinding. As the milling progresses, the breakage rate decreases whatever methods and experimental condition are applied.

However, there are some differences among the particle size distributions resulted in different grinding methods and operational conditions. In the case of the lower media surface, $M_s=1$ m²/kg of material, prolonged grinding in both tumbling and vibratory mills tends to produce finer particles. This indicates that further size reduction in such mills at the given circumstances is possible. In the planetary mill with the same media surface, there were no differences between the particles size distributions obtained from 3 and 9 h of milling, i.e., the further size reduction is impossible. Regarding the higher media surface ($M_s=4$ m²/kg of material), it is evident that the grinding up to 3 h in tumbling and vibratory mills favors the formation of finer particles. The further size reduction is impossible if the milling time exceeds 1 h in planetary mill with large media surface. Further milling in the planetary mill causes the particle size distributions move marginally toward large sizes due to agglomeration phenomena. The planetary milling tends to agglomerate particles sooner than both tumbling and vibratory mills. The higher media surface leads to faster production of finer particles and as a consequence to the agglomeration of particles. The agglomeration could be expected to continue with the extended milling, in particular in vibratory and tumbling mills. The agglomeration of particles were reported previously by many authors for

various minerals (Balaz et al., 1996; Welham, 2001; Welham and Llewellyn, 1998; Zhang et al., 1996) almost in the prolonged milling and intensive milling conditions, suggesting that this may be a feature of extended intensive dry milling.

The specific surface area of the samples after different milling times is illustrated in Fig. 5. The most obvious feature in the figure is that the higher media surface brought about higher specific surface area whatever milling methods were applied. Furthermore, the specific surface area in the initial stages of grinding increases rather sharply and continues to rise gradually except the hematite sample ground in vibratory mill with large media surface, which continues to increase sharply. This may be related to the ability of vibratory milling in size reduction because of applying mainly shear stress on the particles being ground. The maximum specific surface areas in the milling with vibratory, planetary and tumbling mill are 18.42, 8.82 and 6.83 m²/g, respectively.

The granulometric surface areas of the activated samples are compared in Fig. 6. With progress in the milling, the granulometric surface area shows increasing trend in the case of lower media surface. The increasing trend for vibratory mill is clear even up to 9 h of milling and its value exceed 2.58 m²/g, which is the maximum granulometric surface area. It stands only up to 3 h of milling for tumbling and planetary mills and continues to increase very slightly. Regarding the higher media surface level, the granulometric surface increases rather slightly than lower media surface at the initial stages of milling and continues to decrease as grinding time extends. The decreasing trend of the granulometric surface implies the formation of agglomerates among particles without decreasing the specific surface area. The decreasing rate of granulometric surface area indicates that the agglomeration rate in the planetary milling is higher than the other mills.

The decrease of the BET specific surface area during mechanical activation previously was reported for many minerals: gypsum (Zhang et al., 1996), chalcocite (Tkacova and Balaz, 1996), ilmenite (Welham and Llewellyn, 1998), tantalite (Welham, 2001), and feldspar (Cruz Sanchez et al., 2004). But our measurements do not agree with such trends. This is because the magnitude of the BET specific surface area depends on the morphology of the adsorbent, or more precisely on the size of its internal pores and cracks, and on the shape and curvature of the external surface. It seems that the internal surface of aggregates remains accessible to the molecules of nitrogen gas. Thus, the nitrogen gas can penetrate the pores in agglomerated particles and

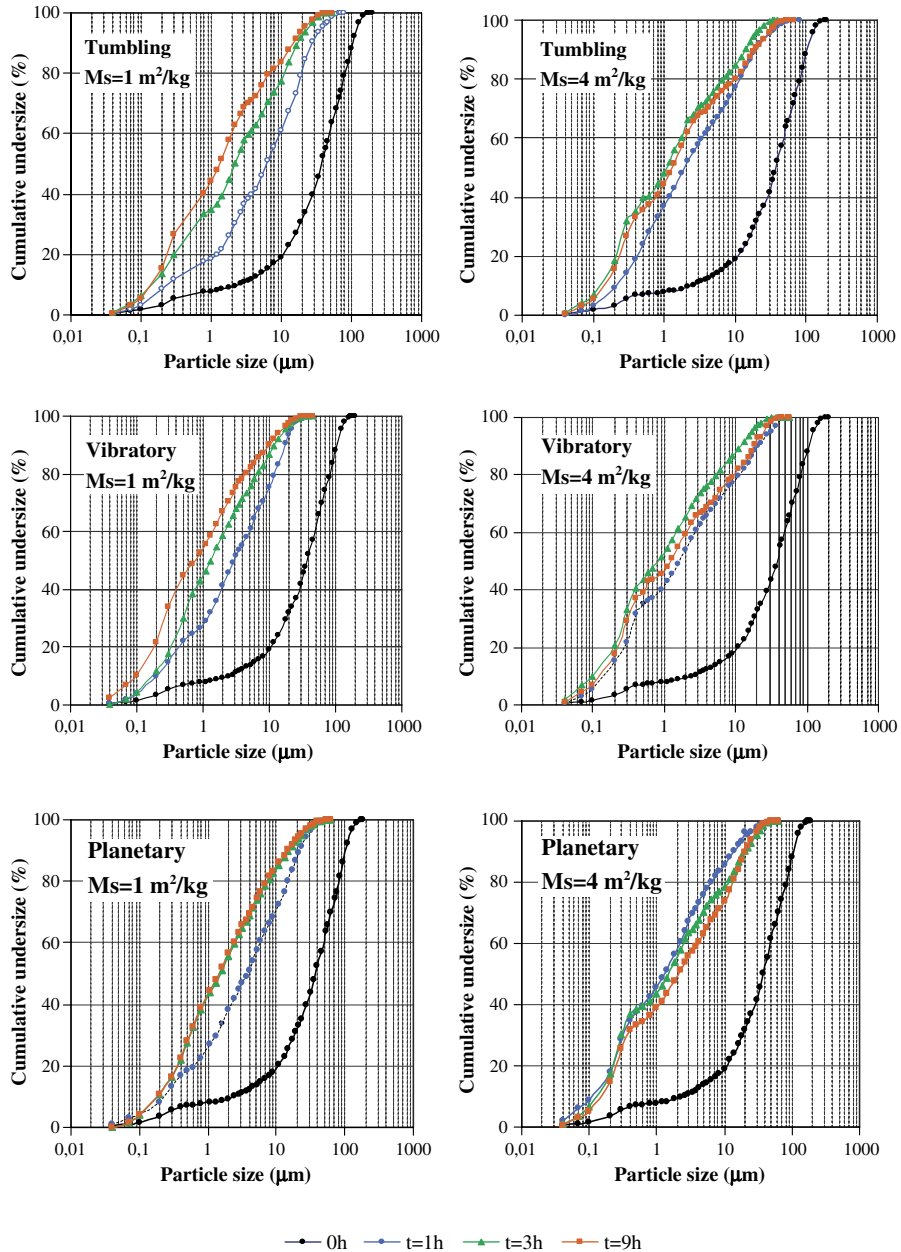


Fig. 4. Particle size distributions of activated Hematite concentrate using different milling devices and operational conditions along with the size distribution of initial Hematite.

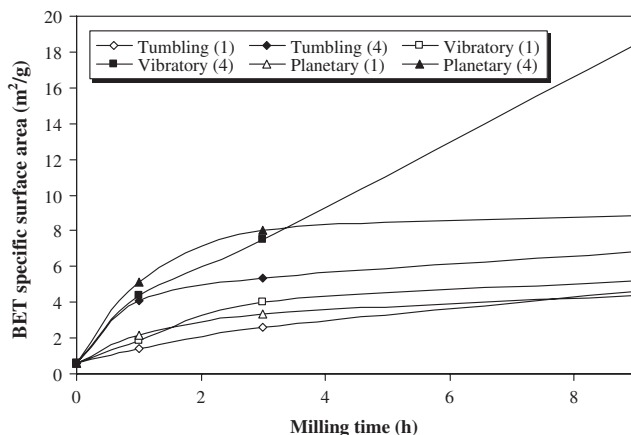


Fig. 5. The changes in the specific surface area of Hematite ground in three mills with two levels of media surface. The numbers in parentheses indicate the level of media surface in terms of m^2/kg .

displays higher BET specific surface area in spite of the agglomeration of particles but the granulometric surface values are markedly affected by the presence of the finest size fractions.

According to the obtained results, the higher media surface variable appears to be more effective in rapid production of smaller particles, increasing the BET surface area and the rate of agglomeration (a mean for reducing the specific surface energy of the particulate system). These could be related to the fact that the use of higher media surface accompanied with the higher impact force because of higher ball to powder weight ratio (see Table 1). Consequently, the number of collisions per unit time increases and more energy transfers to the particles being ground. Besides,

increasing of the milling time increases the number of pulses and subsequently more energy transfers to the particles being ground. Regarding milling types, although the planetary mill have large ability in the transferring energy to the particle, it seems that shear stressing mode and attrition of particles in the vibratory mill and generation of higher temperature up to 105°C assist the size reduction process and consequently the generation of large specific surface area.

4.2. X-ray diffraction analysis

4.2.1. XRD patterns

The collected XRD patterns of the hematite concentrate are summarized in Fig. 7 for 1 and 9 h grinding

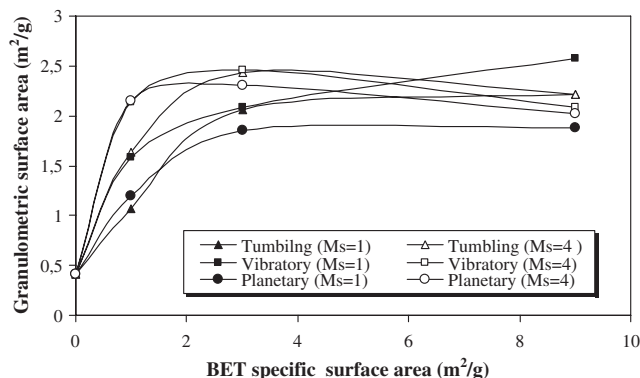


Fig. 6. The changes of granulometric surface area vs. grinding times for different mills.

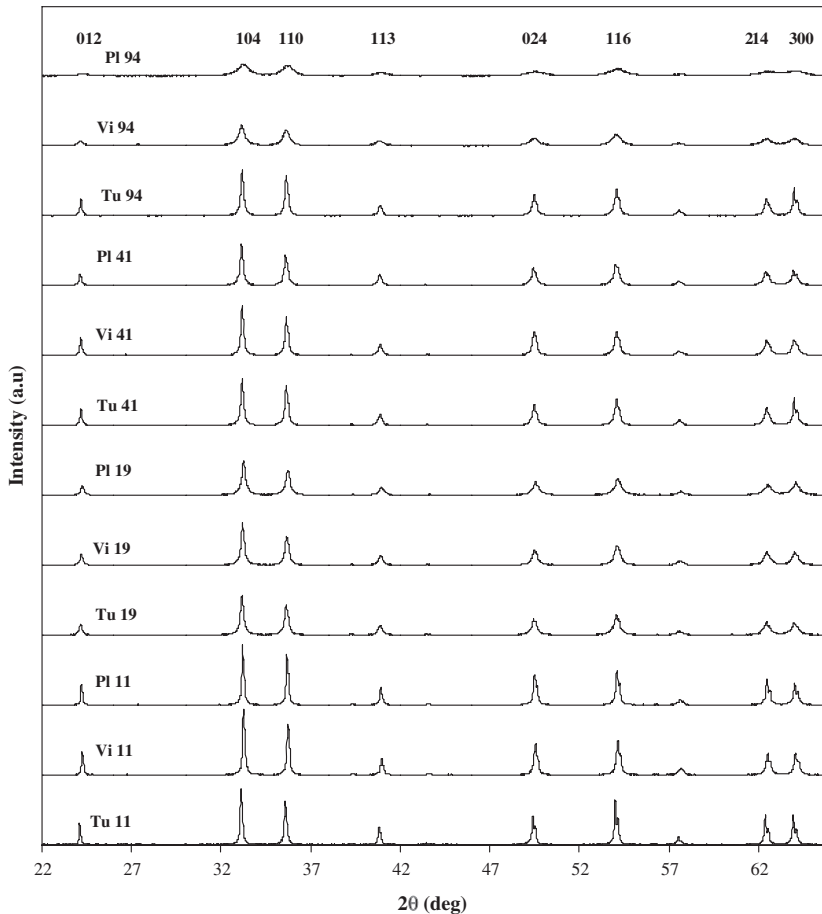


Fig. 7. The X-ray diffraction patterns of activated Hematite as function of the grinding time and media surface for mills. Tu, Vi and PI refer to tumbling, vibratory and planetary mills, respectively. The first and second numbers after the terms denote the media surface (m^2/kg) and grinding time (h), respectively.

times in mills. XRD patterns show only hematite reflection peaks, indicating that initial hematite did not undergo significant reactions during the milling. The XRD studies do not show phases below 2 wt.%. Our observations agree with the observations of Kaczmarek and Ninham (1994) and Stewart et al. (2003). However, our observation disagrees with the findings of Kosmac and Courtney (1992) and Zdujic et al. (1998). They reported the transformation of $\alpha\text{-Fe}_2\text{O}_3$ to Fe_3O_4 during ball milling in a planetary mill. Zdujic et al. made comprehensive studies to discuss the published results of the hematite transformation to Fe_3O_4 and subsequently to FeO. They stated that transferring of

sufficient energy to the particles is necessary to change the stability state of $\alpha\text{-Fe}_2\text{O}_3$ to Fe_3O_4 and subsequently to FeO thermodynamically. It is evident that our milling conditions could not change the stability of hematite.

According to Fig. 7, a continuous broadening of the diffraction peaks, due to disintegration and plastic deformation of particles, is evident with increasing milling time and media surface regardless of milling types. In addition, the structural disorder due to formation of the amorphous material is manifested by decreases in the integral intensity of diffraction lines. With increasing of the milling time and media surface the intensity of diffraction line decreased, suggesting the

production of more X-ray amorphous material. Rapid changes in line breadths and integral intensities for the samples milled in planetary mill were observed as the milling time increases.

For a quantitative comparison, the physical broadening (FWHM) for different grinding variables are depicted in Fig. 8. It can be observed that the planetary brings about the maximum broadening of reflection

peaks. The broadening for the samples milled with the tumbling mill and vibratory mill differs marginally; the vibratory mill products show slightly larger broadening than the products of tumbling mill. For example, after 9 h of milling with the lower media surface for the reflection (014), $\text{FWHM}=0.229^\circ$ with planetary mill, $\text{FWHM}=0.179^\circ$ with vibratory mill and $\text{FWHM}=0.162^\circ$ with tumbling mill were obtained.

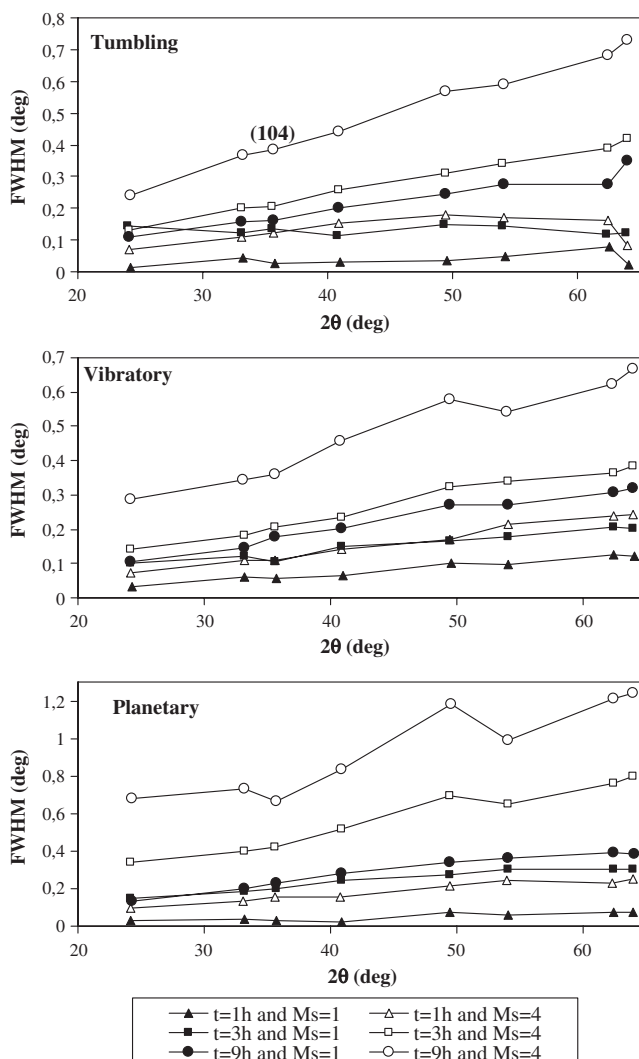


Fig. 8. The changes of physical FWHM for activated samples in different grinding times and media surface for three mills. Depending on the milling, the pronounced broadening occurs as a result of crystallite size reduction and increase of lattice strain.

4.2.2. The amorphization degree

The content of X-ray amorphous phase was determined by equation proposed by Ohlberg and Strickler (1962). In our calculations, the eight most intensive reflection peaks were used. It is assumed that the amorphous phase in the initial powder is negligible. The portion of X-ray amorphous phase on average is shown in Fig. 9. It is clear that the amorphization increases with increasing of the milling time and media surface. The amorphization climbs rapidly at the initial stages of milling and continues to increase gradually with progress in milling regardless of milling types. The maximum and minimum fractions of amorphous phase in the case of lower media surface created during grinding in the planetary and tumbling mills, accounting for 71.7% and 58.3%, respectively. In the case of higher media surface, with a first approximation, the planetary mill produces more X-ray amorphous material, after 9 h of milling, 85% of the initial hematite was converted into amorphous phase. The values 81.7% and 80.3% in the same condition are estimated for vibratory and tumbling mills, respectively.

4.2.3. The changes in lattice characters

The lattice parameters were refined in Hexagonal system by regression diagnostics method and using Unitcell software (Holland and Redfern, 1997). The regression diagnostics are numbers, calculated during the regression, which supply valuable information on the influence of each observation on the least squares result and on the estimated parameters. The initial hematite yields the value of lattice parameters ($a=5.0312$ Å, $c=13.7414$ Å and $V=301.2291$ Å³) displaying very slight variations to the values given in

the mineralogy database (Mineral database, 2005) ($a=5.0317$ Å, $c=13.737$ Å and $V=301.20$ Å³). The calculated lattice parameters a and c and unit cell volume for the activated samples as a function of milling time for different activation mills in the case of higher media surface level are shown in Fig. 10. It is seen that both unit cell parameters increased drastically at short time of activation and continue to increase gradually. This implies an expansion of hematite cell with an elongation of both a and c axis length during activation. The changes of unit cell volume in tumbling mill have a significant difference with vibratory and planetary mills in the grinding up to 1 h of milling. This also holds marginally for the planetary mill for 3 h of milling. Similar plots were constructed for the lower media surface but they did not carry more information and they have not been reported in the present paper.

4.3. Microstructural analysis

To obtain the microstructural characteristics, two methods including the simplified integral breadth and Warren–Averbach approach were used. The obtained results are discussed in the next sections.

4.3.1. Integral breadth method

The first step in analyzing line broadening is to ascertain the nature of any structural imperfections present. This can be achieved from the Williamson–Hall plots. The Williamson–Hall plots are illustrated in Figs. 11 and 12 for all activated samples using different mill types. The correlation coefficients were estimated between 0.8 and 0.97 depending on the sample. This indicates relatively a strong relationship between β_t^{*2} and d^{*2} .

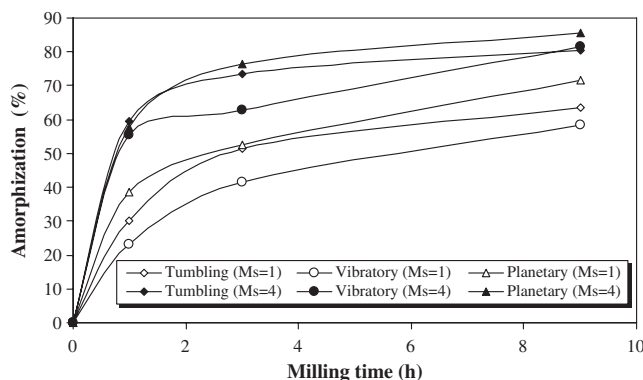


Fig. 9. Variation of amorphization with the time of mechanical activation and media surface in different milling devices. The values in parentheses refer to the level of media surface in terms of m²/kg of material.

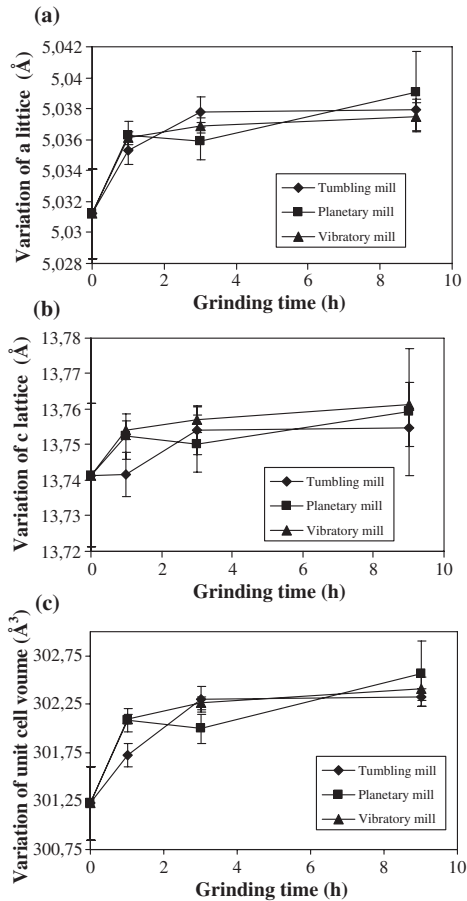


Fig. 10. The variation of lattice parameters with grinding time: (a) variation of a lattice parameter; (b) c lattice parameter; (c) the unit cell volume for higher media surface level ($M_s = 4 \text{ m}^2/\text{kg}$).

From the Williamson–Hall plots, lines for all intensive reflections and [012] direction have non-zero and different slopes and intercepts. This suggests that the strain and size contributions exist simultaneously in the milled samples. The increase of physical broadening vs. grinding time and media surface indicates that intensive milling extends great defects and deformations in materials. The scatter of the β_r^{*2} values indicates that the crystallite shape differs from a spherical one. Besides, the (024) reflection shows higher deviation than other reflections and its broadening enlarged as the intensity of milling increased. There is also a systematic deviation between the line connecting the two orders of (012) and (024) reflections and the line connecting all

intensive reflections, the line concerning to the [012] direction lie above it. This may be understood by considering the anisotropy in the elastic properties of the single-crystal hematite, indicating that hematite crystal is ‘soft’ between the (024) and the others crystallographic directions. The similar results have been observed for Fe powder (Bomer and Eckert, 1997; Vives et al., 2004) and ball-milled molybdenum powder (Lucks et al., 2004). This anisotropy character of line broadening attributed to the dislocation strain field anisotropy (Ungar and Borbely, 1996). It is beyond the scope of this paper to examine these anisotropic effects.

According to Figs. 11 and 12 for the same milling time and media surface, it can be further observed that the broadening for the samples milled with planetary mill is much larger than the broadening for the samples milled with vibratory and tumbling mills except the sample milled for 1 h. For evaluation, the strain and crystallite size of the samples were estimated from the slope and intercept of plots (Pourghahramani and Forssberg, 2006). The concerning results are summarized in Table 3. Regarding the Williamson–Hall data as a sort of quantitative analysis, the values of strain and size make sense. With more damage, the particles receive more strain and reduction of the size of the defect-free subcrystals. The products of planetary mill, with a first approximation, yield smaller crystallite size and higher strain than other mill products. Prolonged grinding with higher media surface favors the generation of small crystallites and the induction of higher strain in hematite.

4.3.2. Size-strain in the [012] direction

As discussed, the Warren–Averbach analysis based on Fourier analysis provides detailed information regarding the crystallite size, lattice strain and their distributions. The results are discussed in next sections.

4.3.2.1. The microstrain distributions. The strain distributions for samples ground in different mills and operational conditions are given in Fig. 13. A plot of $\langle \epsilon_L^2 \rangle^{1/2}$ as a function of crystallite length, L , shows a decreasing curve for increasing L values. From this kind of plot, it is possible to appreciate the degree of disorder in samples from the observed trend in the $\langle \epsilon_L^2 \rangle^{1/2}$ vs. L plot. The lattice disorder can be attributed to (1) paracrystalline distortions, which arise due to fluctuations in the interplanar distance due to inhomogeneities in samples, and to (2) the presence of dislocations, which results in a Gaussian distribution of the microstrain (Jyung and Jenq, 1997). The high efficiency of the ball milling process on the domain size reduction and

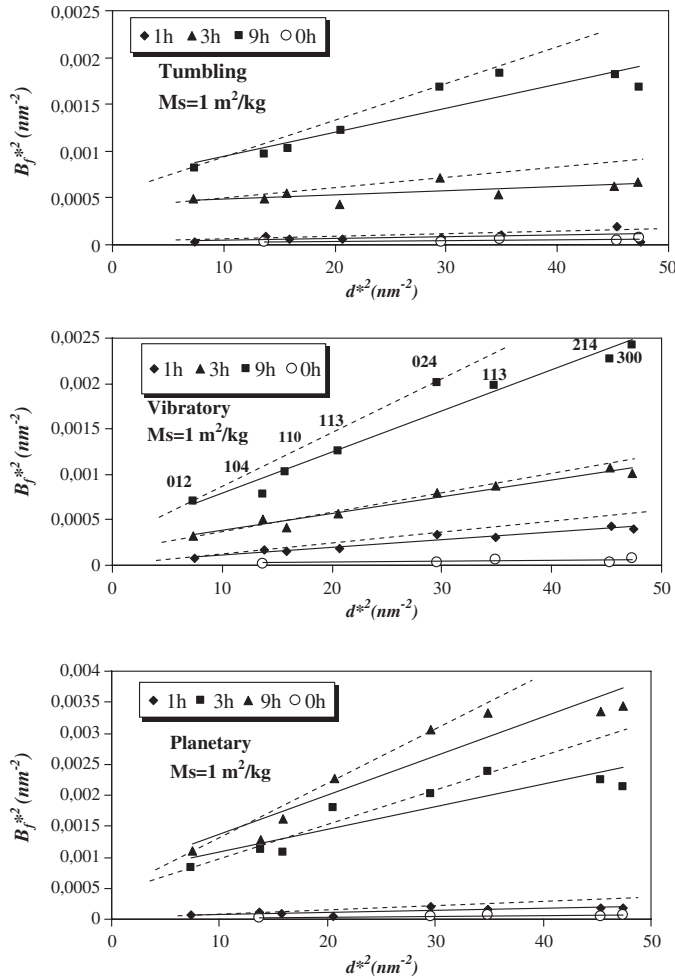


Fig. 11. Williamson–Hall plots, B_f^2 vs. d^{*2} , for samples milled in the tumbling, vibratory and planetary mills with lower media surface. The solid and dashed line refers to all intensive reflection peaks and direction [012], respectively.

strain increasing has been noticed whatever milling methods employed. The use of planetary mill brought about more reduction of domain size than vibratory and tumbling mills in the intensive grinding conditions.

4.3.2.2. The variations in the crystallite size and lattice strain. The crystallite size quantity and the root mean square strain $\langle \epsilon_{L=10 \text{ nm}}^2 \rangle^{1/2}$ are given in Table 4. The results depict the nature of progressive evolution of the microstructure of the milling products vs. grinding conditions. Generally, the surface-weighted crystallite size shows decreasing and root mean square strain

($\langle \epsilon_{L=10 \text{ nm}}^2 \rangle^{1/2}$) increasing trend as both grinding time and media surface increase whatever mill used. In the earlier stages of milling, the crystallite size decreases rapidly to the nanometer range. Further refinement proceeds slowly and the final average grain size is in the order of 5–27 nm. Comparing the strain ($\langle \epsilon_{L=10 \text{ nm}}^2 \rangle^{1/2}$) and crystallite size values for grinding up to 1 h indicates no clear pattern among the products of different mills. As the intensity of milling increases, the ground hematite in planetary mill yields more strain and smaller crystallites than that of ground in vibratory and tumbling mills. The planetary mill decreases the

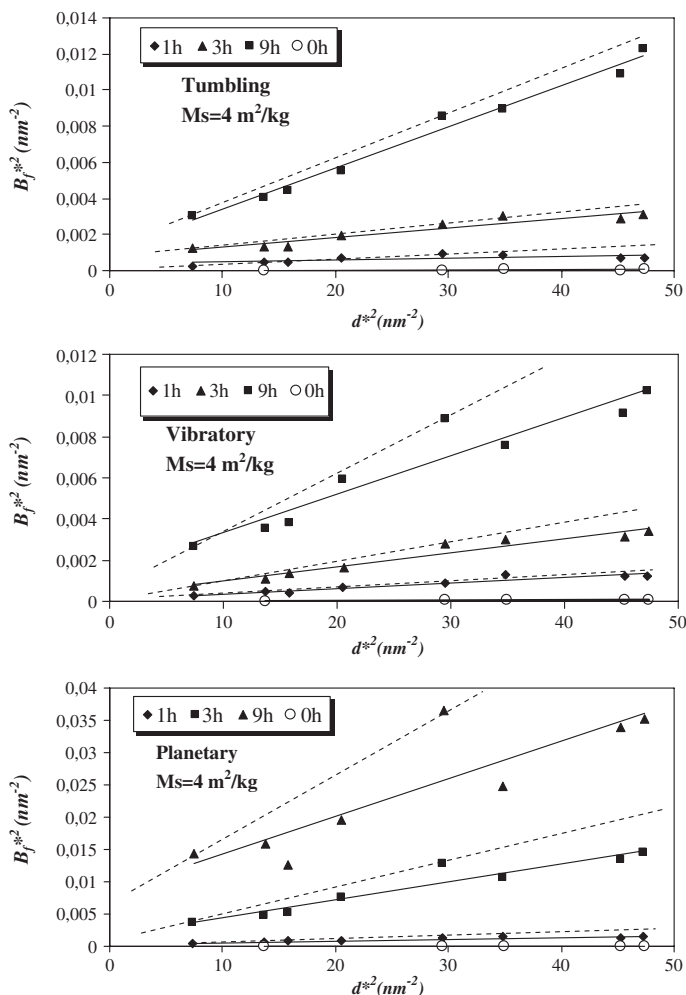


Fig. 12. Williamson–Hall plots, B_f^{*2} vs. d^{*2} , for samples milled in the tumbling, vibratory and planetary mills with higher media surface. The solid and dashed line refers to all intensive reflection peaks and direction [012], respectively.

crystallite size to a value of lower than 6 nm and increases strain to a value of higher than 5.3×10^{-3} by using higher media surface after 9 h of milling. This may be also attributed to the use of higher ball to powder weight ratio for milling in planetary mill (Table 1). The steady state was not observed for grinding conditions, suggesting that the production of small crystallites is possible with increasing the grinding intensity. Obviously, variations in the ball media surface have a more influence on the crystallite refinement.

The results concerning to tumbling and vibratory mills' products indicate some differences between size and strain components when the media surface changes in milling process. Obviously, grinding of hematite with lower media surface in vibratory mill resulted larger crystallite and higher strain than grinding in tumbling mill marginally as opposed with higher media surface case. This may be related to the changes in stressing manner of particles in milling process especially in vibratory mill. In non-rotary ball mills, the material is under the action of a combined stress and the

Table 3

Crystallite size (D_V) and lattice strain (ϵ) obtained using integral breadth method for different mills

Parameters		Ms=1 m ² /kg		Ms=4 m ² /kg	
Milling type	Time (h)	D_V (nm)	ϵ ($\times 10^{-3}$)	D_V (nm)	ϵ ($\times 10^{-3}$)
Tumbling mill	1	158.1 \pm 86 (223.6)	0.77 \pm 0.13 (0.7)	50 \pm 17.6 (–)	1.58 \pm 0.7 (2.73)
	3	50 \pm 16.3 (50)	1.12 \pm 0.4 (1.6)	35.3 \pm 10.6 (35.4)	3.54 \pm 0.6 (3.87)
	9	37.8 \pm 9.09 (44.7)	2.7 \pm 0.3 (3.2)	30.2 \pm 10.1 (28.9)	7.07 \pm 0.4 (7.1)
Vibratory mill	1	182.6 \pm 80 (–)	1.50 \pm 0.2 (1.6)	105.4 \pm 50 (141.4)	2.74 \pm 0.2 (2.7)
	3	70.7 \pm 22 (70.7)	2.2 \pm 0.3 (2.2)	57.7 \pm 27 (111.8)	4.18 \pm 0.5 (4.7)
	9	57.7 \pm 23 (57.7)	3.5 \pm 0.2 (3.9)	25.8 \pm 10.8 (40.8)	7.00 \pm 0.8 (8.7)
Planetary mill	1	141.4 \pm 55 (182.5)	0.89 \pm 0.2 (1.2)	57.7 \pm 19.8 (100)	2.73 \pm 0.3 (3.2)
	3	37.8 \pm 13 (50)	3.2 \pm 0.7 (3.5)	24.3 \pm 8.8 (37.8)	8.6 \pm 0.4 (10)
	9	37.8 \pm 14.1 (44.7)	3.9 \pm 0.4 (4.74)	10.9 \pm 4.5 (12.1)	12.2 \pm 0.4 (15.8)
Initial Hematite ^a	0	316.2 \pm 180 (–)	0.5 \pm 0.4 (–)	–	–

Confidence levels of data are given at 95%. The values corresponding to [012] direction are given in parentheses.

^a Calculated using five reflection peaks.

predominant mode of stress varies depending upon the mode of mill performance (Tkacova, 1989). In our opinion, the use of low media surface supplies much material around grinding media and material stressing proceeds dominantly in compressive and impact mode. Consequently, this condition induces high strain in material being ground. Applying large media surface changes the dominant type of stress from compressive and impact to shear and/or attrition. These changes facilitate the size reduction and breakage in fine and ultrafine range.

4.3.2.3. The relative frequency of crystallite length distribution. The relative frequency, a number which describes the proportion of observations (crystallite length) falling in a given category, of crystallite length as a function of milling operation is given in Fig. 14. At first glance, in the earlier stages of milling (low milling intensity), the two main crystallite groups were observed. With progress in milling in particular increasing the grinding periods, the size distribution curve represented mainly single crystallite group. Besides, the maximum relative frequency values for the crystallite length at the initial stages of milling are less than that of intensive milling. Approximately, the crystallites size (length) distributions at intensive milling follow the lognormal distribution behavior. This was reported previously for several minerals and materials; ball-milled molybdenum (Lucks et al., 2004) and milled iron powders (Vives et al., 2004).

Regarding the milling devices, the existence of the two main crystallite groups was extended for milling up to 3 h with low media surface in vibratory and tumbling mills. This stands only for grinding within 1 h with low media surface in planetary mill. In addition, the maximum relative frequency of the planetary mill's

products is greater than other mill products for the same milling condition. There is no clear difference between the products of vibratory and tumbling mills. We can draw the conclusion that fragmentation of coarser particles results in the establishment of more uniform contact between the grinding media and particles being ground. The intensive grinding leads to uniform activation of hematite. In earlier stages of grinding especially with lower media surface, the coarse particles prevent the media from coming into contact with finer particles. Hence, hematite is activated non-uniformly. Having this in mind, the existence of two main crystallite size groups can be attributed either to the new phase formation or to the changes of the materials being ground. However, in our investigation we did not observe any phase transformation or new phase formation according to the XRD patterns. In our opinion, the non-uniform stressing of powders resulted in a non-uniform crystallite length distribution.

4.3.3. The variations in dislocation density

To estimate the dislocation density, ρ_D , ρ_ϵ and ρ , of the ball-milled hematite powders, the simple approach of Williamson and Smallman (1956) was followed, relating ρ to crystallite size D and strain $\langle \epsilon_L^2 \rangle^{1/2}$:

$$\rho_D = \frac{3}{D^2}; \quad \rho_\epsilon = \frac{k \langle \epsilon_L^2 \rangle}{b^2}; \quad \rho = (\rho_D \rho_\epsilon)^{1/2} \quad (1)$$

where ρ_D , ρ_ϵ and ρ correspond to the dislocation due to domain size, dislocation due to microstrain and real dislocation density respectively. The coefficient k depends on the mechanical properties of the crystal, its microstructure and on the type of distribution of displacement in it (its value are usually between 2 and 25) and b is the Burger's vector, which determines the

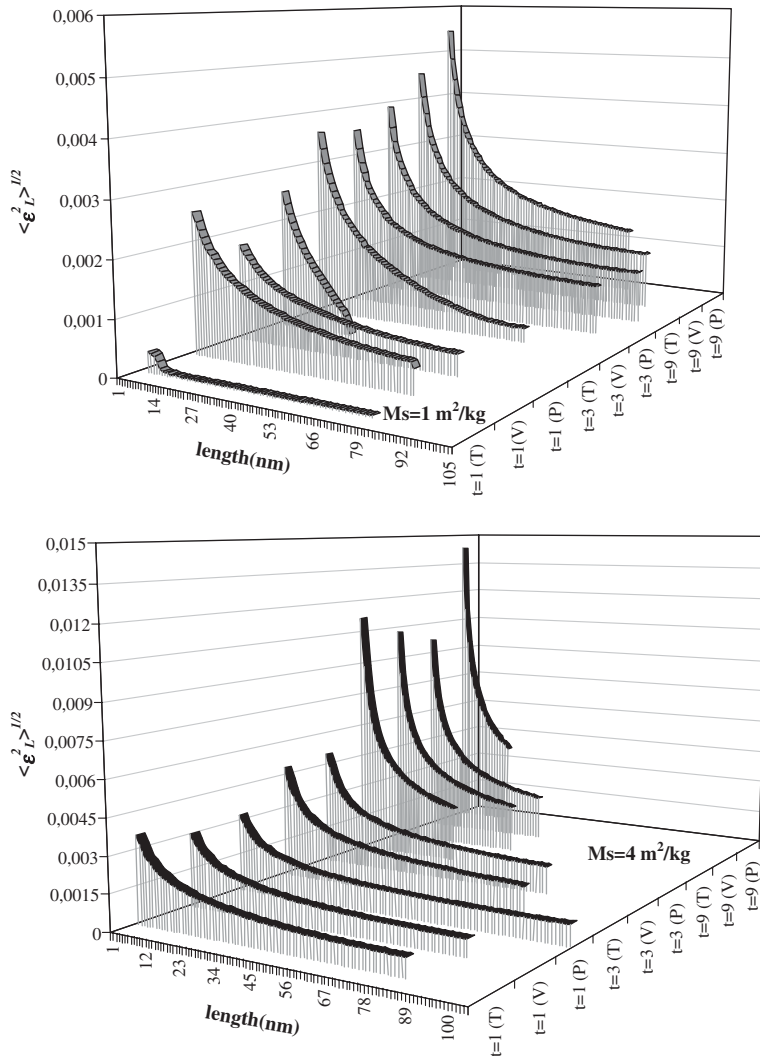


Fig. 13. The RMSS strain distribution as function of crystallite length with milling types and operational conditions. t refers to the activation time in h. V, T and P in parentheses correspond to the vibratory, tumbling and planetary mills, respectively.

distance and direction of displacement. We assumed that the Burger's vector direction of hematite is the same as for Corundum, in the [100] direction. Thus, the value of Burger vector for hematite in direction [100] was found about $5.03 \times 10^{-10} \text{ m}$. Since the value of k for hematite was not found through literature; we assumed $k=2$. The results obtained by taking D_S and $\langle \epsilon_{L=10 \text{ nm}}^2 \rangle^{1/2}$ from the Warren–Averbach analysis are given in Table 5. The dislocation density increases to a value of $\approx 46 \times 10^{14}$

after 9 h of milling with media surface of $4 \text{ m}^2/\text{kg}$ in the planetary mill. Regardless of milling machines, as hematite is imposed to intensive grinding, the dislocation density increases. The ground hematite in vibratory mill showed slightly higher dislocation than tumbling mill's products. The planetary mill induced much more dislocation in hematite, with the exception of the sample ground for 1 h with lower media surface. It seems that the hindering of grinding media because of a higher

Table 4

The microstructural characteristics in [012] direction using the Warren–Averbach method for activated Hematite in different environments

Parameters		Ms=1 m ² /kg		Ms=4 m ² /kg	
Milling type	Time (h)	D _S (nm)	$\langle \epsilon_{L=10\text{ nm}}^2 \rangle^{1/2} \times (10^{-3})$	D _S (nm)	$\langle \epsilon_{L=10\text{ nm}}^2 \rangle^{1/2} \times (10^{-3})$
Tumbling mill	1	54.16	0.062	44.4	2.236
	3	42.6	1.52	25.0	2.84
	9	27.3	2.25	17.3	4.44
Vibratory mill	1	73.5	1.75	36.4	1.84
	3	43.5	2.08	23.7	2.79
	9	29.6	2.58	12.2	3.95
Planetary mill	1	66.7	1.25	28.1	1.94
	3	20.5	2.03	11.6	4.44
	9	16.5	3.011	5.6	5.32
Initial Hematite ^a	0	199.1	n.d.(0)		

D_S and $\langle \epsilon_{L=10\text{ nm}}^2 \rangle^{1/2}$ indicate the surface weighted crystallite size and root mean square strain (RMSS) at L=10 nm, respectively.^a Calculated using single peak method.

powder to ball weight ratio prevented the refinement of microstructure characters in the sample ground for 1 h with lower media surface in the planetary mill.

5. The contribution of long-lived defects to the energy state of activated hematite

For the interpretation of the mechanical activation process, the context between structures and energy content of the mechanically activated solids and consumed mechanical energy are of important and interest. As a result of previous investigations (Heegn, 1979; Heegn et al., 2003; Tkacova et al., 1993), the following defect structures of essential meaning for the energetic condition of the solids are: (1) dislocation concentration with the specific energy, (2) energy contributions of new surface formation, and (3) content of newly formed phases and amorphous fraction. The quantitative estimate of the increase in molar chemical free energy (increase in stored energy) due to dislocation concentration has been calculated by expression proposed by Tromans and Meech (2001). Besides, the energy fraction of amorphous phase and surface area are estimated using equations proposed by Heegn (1979). The estimation have been calculated with the material data for hematite of $\sigma_S=1769\text{ erg/cm}^3$ (specific interfacial energy) and $E_A=90.99\text{ kJ/mol}$ (molar amortization energy) (Heegn, 1987). Table 6 contains calculations of the energy parts and the sum of excess energy for activated hematite in different conditions and mills. From the data presented in Table 6, it follows that the contribution of amorphization energy to the energy change at activation amounted to 93–98.5%. Similar energy distributions were found for Quartz, Calcite, Magnesite, Kaolinite and Iron (Heegn, 1986a,b) and periclase (Tkacova et al., 1993). From Table 6, it is

apparent that energy contribution of new surface formation of activated hematite in vibratory mill accounted for the maximum values comparing to other mill products. Besides, the planetary mill products amounted to the greatest energy contribution of amorphization. These also include the largest part of energy due to dislocation density with exception of activation within 1 h.

6. The relationship between excess energy and grinding work

To compare the stored energy due to defect structures with grinding energy, the specific grinding work (stress energy) were calculated by expressions proposed by Heegn (1986b, 2000). The specific grinding work vs. stored energy is depicted in Fig. 15. It can be seen that the excess enthalpy content (stored energy) increases with growing the amount of grinding work. For a given stress energy, a higher stored energy was observed for tumbling mill products. For example, to achieve an excess energy in hematite by mechanical treatment about 60 kJ/mol, the required stress energy in tumbling, planetary vibratory milling is around 1300, 2800, 17,000 kJ/kg, respectively. In agreement with studies by Miyasaka and Senna (1985) and Tkacova et al. (1987) the excess enthalpy (ΔH) can be related to stress energy or grinding work (W) by the equation, where b and c are the constant values.

$$\Delta H_T = b \log_{10} W - c.$$

7. Conclusion

- The use of higher media surface and prolonged grinding lead to higher specific surface area, X-ray

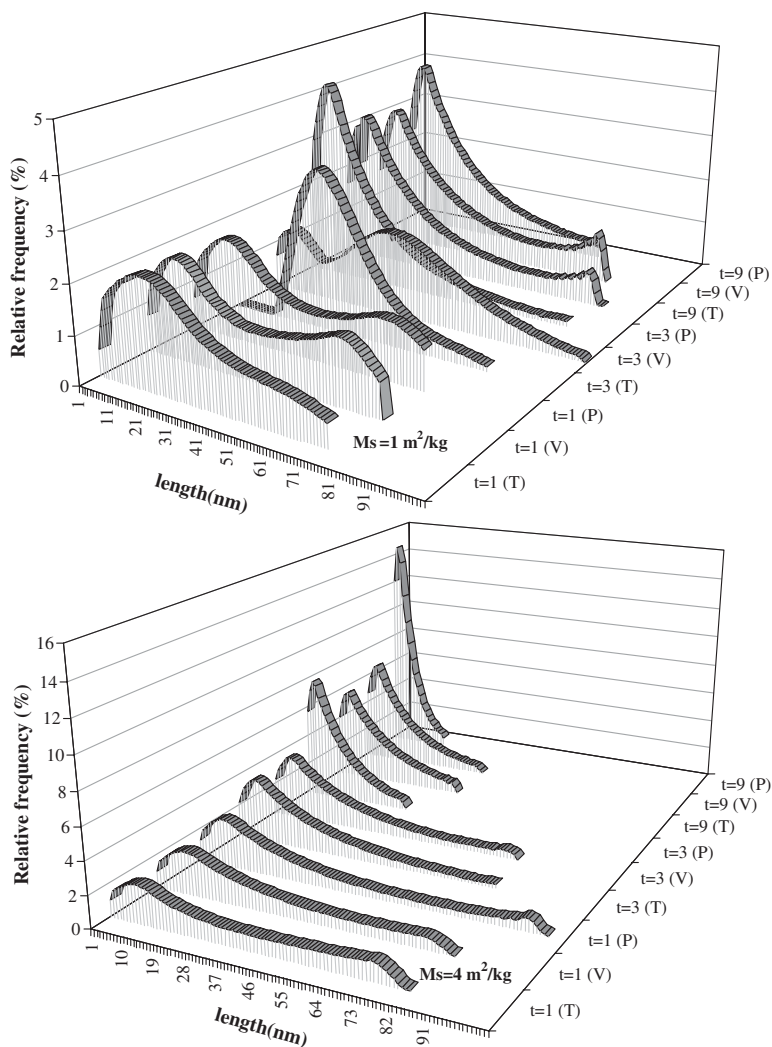


Fig. 14. The relative frequency of column length as a function of milling conditions. t indicates the activation time in h. V, T and P in parentheses correspond to the vibratory, tumbling and planetary mills, respectively.

amorphous material, physical broadening, micro-strain, dislocation density, stored energy and smaller crystallites whatever milling types were applied.

- The samples activated in the tumbling mill resulted the lowest specific surface area among the mills used, being between $1.41 \text{ m}^2/\text{g}$ and $6.83 \text{ m}^2/\text{g}$ depending on the grinding variables. The maximum specific surface area, $18.42 \text{ m}^2/\text{g}$, and amorphization degree, 85%, were achieved from the milling in the vibratory and planetary mills, respectively, with higher media

surface after 9 h of milling. The vibratory mill produced approximately the minimum X-ray amorphization material compared to the other milling devices. Generally, the maximum and minimum line breadths of XRD diffraction were observed for the products of the planetary and tumbling mills respectively.

- From the Williamson–Hall plots, it was concluded that the hematite crystal is ‘soft’ between (024) direction and other crystallographic directions. The

Table 5

The dislocation density, $\rho \times 10^{14}$ (m/m³), for activated Hematite in different grinding mills and operational conditions

Grinding variables		Mill types		
Grinding time (h)	Media surface (m ² /kg)	Tumbling mill	Vibratory mill	Planetary mill
1	1	0.6	1.2	0.9
3	1	1.7	2.3	4.8
9	1	4.0	4.2	8.9
1	4	2.4	2.5	3.4
3	4	5.5	5.7	18.6
9	4	12.5	15.8	46.3

Warren–Averbach method suggested that the planetary mill products have smaller crystallites and higher microstrain than the products of tumbling and vibratory mills with the exception for the samples activated for 1 h with low media surface. The final products contain crystallites between 73.5 and 5.6 nm and the lattice strain (RMSS) at $L=10$ nm, $\langle \epsilon_{L=10}^2 \rangle^{1/2}$, varies from 0.06×10^{-3} up to 5.32×10^{-3} depending on the milling performance.

- The energy contribution of amorphization is much more than the energy contribution of dislocation density and surface area changes, accounting for 93–98.5% of overall enthalpy or stored energy. The enthalpy contents in the activated material increased to the values between 21.5 and 81.32 kJ/mol of hematite. The planetary and vibratory mills need

much more energy to reach the same effect as tumbling mill.

- The results suggest that the precise characterization of microstructures, make possible to distinguish differences among the used mills. The results indicated that for a given stress energy the products of tumbling mill have higher reactivity potential. However, experimental reactivity tests are needed to explore the real effect and availability of structural changes. Therefore, further study is needed to answer the remaining question.

Nomenclature

A	Peak area
b	Burger's vector
D_S	Surface-weighted crystallite size
D_V	Volume-weighted crystallite size
d	Interplanar spacing
FWHM	Full width at half-maximum of profile
(hkl)	Miller indices
I_{\max}	Maximum intensity
RMSS	Root mean square strain
β	Integral breadth
β_r	The integral breadth of the physically broadened profile
β^*	$\beta \cos \theta / \lambda$, Integral breadth in the units of d^* (nm ⁻¹)
$\langle \epsilon_L^2 \rangle$	Mean square strain, orthogonal to diffracting planes, averaged over the distance L

Table 6

Energy contributions of new surface formation, ΔH_S , dislocation density, ΔH_d , and amorphization, ΔH_A , to the overall change in enthalpy, $\Sigma \Delta H$, of Hematite with three types of mills in different condition

Mill types	Ms (m ² /kg)	Time (h)	ΔH_S		ΔH_d		ΔH_A		$\Sigma \Delta H$
			kJ/mol	%	kJ/mol	%	kJ/mol	%	
Tumbling mill	1	1	0.40	1.44	0.019	0.07	27.3	98.49	27.72
	1	3	0.73	1.53	0.054	0.11	46.9	98.36	47.68
	1	9	1.30	2.20	0.115	0.19	57.8	97.61	59.22
	4	1	1.17	2.11	0.074	0.13	54.1	97.75	55.34
	4	3	1.51	2.20	0.154	0.22	66.9	97.57	68.56
	4	9	1.93	2.56	0.320	0.42	73.1	97.01	75.35
Vibratory mill	1	1	0.53	2.46	0.037	0.17	21.0	97.37	21.57
	1	3	1.13	2.90	0.070	0.18	37.7	96.92	38.90
	1	9	1.47	2.69	0.121	0.22	53.0	97.09	54.59
	4	1	1.24	2.39	0.074	0.14	50.6	97.46	51.91
	4	3	2.13	3.57	0.159	0.27	57.3	96.16	59.59
	4	9	5.21	6.51	0.394	0.49	74.4	93.00	80.00
Planetary mill	1	1	0.6	1.68	0.03	0.08	35.1	98.24	35.73
	1	3	0.95	1.95	0.136	0.28	47.7	97.77	48.79
	1	9	1.25	1.87	0.236	0.35	65.2	97.77	66.72
	4	1	1.45	2.69	0.098	0.13	52.4	97.13	53.95
	4	3	2.26	3.13	0.456	0.63	69.5	96.24	72.22
	4	9	2.50	3.07	1.020	1.25	77.8	95.67	81.32
Initial Hematite	—	—	0.17	—	—	—	—	—	—

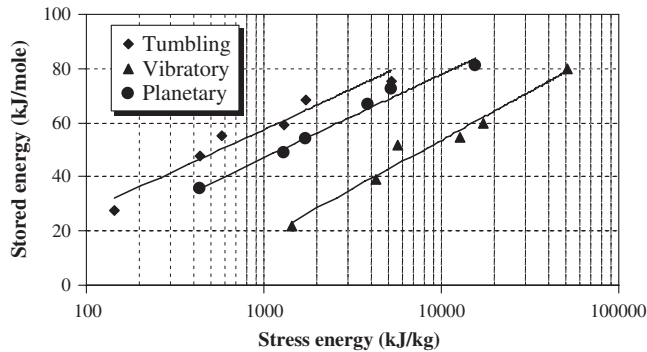


Fig. 15. The comparison of relationship between the specific grinding work (stress energy) and stored energy in activated Hematite with various mills.

θ	Bragg angle
λ	X-ray wavelength
ρ	The real dislocation density
ρ_D	the dislocation due to domain size
ρ_e	dislocation due to microstrain
\AA	Angstrom unit (10^{-11} m)
LPA	Line profile analysis
Ms	Grinding media surface level (m^2/kg) of milled sample)
W	Specific grinding work (kJ/kg)

Acknowledgments

The authors would like to thank Prof. Claes I Helgesson for his valuable comments on this paper.

References

- Balaz, P., 2000. Extractive Metallurgy of Activated Minerals, first ed. Elsevier, Amsterdam.
- Balaz, P., Huhn, H.J., Tkacova, K., Heegn, H., 1988. Laugungsverhalten und physico-chemische Eigenschaften von in unterschiedlichen Mullen vorbehandeltem Chalkopyrit. *Erzmetall* 41, 325–331.
- Balaz, P., Ficeriova, J., Sepelak, V., Kammel, R., 1996. Thiourea leaching of silver from mechanically activated tetrahedrite. *Hydrometallurgy* 43, 367–377.
- Bernhardt, C., Heegn, H., 1978. Mechanische Aktivierung von Ton in einer diskontinuierlich und kontinuierlich arbeitenden Schwingmühle. *Silikattechnik*, Berlin 29 (12), 373–376.
- Boldyrev, V.V., Pavlov, S.V., Goldberg, E.L., 1996. Interrelation between fine grinding and mechanical activation. *Int. J. Miner. Process.* 44–45, 181–185.
- Borner, I., Eckert, J., 1997. Nanostructure formation and steady-state grain size of ball-milled iron powders. *Mater. Sci. Eng., A Struct. Mater.: Prop. Microstruct. Process.* 226–228, 541–545.
- Cruz Sanchez, E., Torres, M.E., Diaz, C., Saito, F., 2004. Effects of grinding of the feldspar in the sintering using a planetary ball mill. *J. Mater. Process. Technol.* 152, 284–290.
- Halder, N.C., Wagner, C.N.J., 1966. Separation of particle size and lattice strain in integral breadth measurements. *Acta Cryst.* 20, 312–313.
- Heegn, H., 1979. Effect of fine grinding on structure and energy content of solids. *Proc. of 6th POWTECH*, Birmingham, pp. 61–69.
- Heegn, H., 1986a. Changes in the properties of solids during mechanical activation and fine grinding. Sc.D. Thesis, Research Institute of Mineral Processing of the Academy of the GDR, Freiberg (in German).
- Heegn, H., 1986b. Concerning some fundamentals of fine grinding. In: Leschonski, K. (Ed.), *Proc. 1st World Congress on Particle Technology: Part II. Comminution*. Nürnberg Messe und Ausstellungsgesellschaft, Nürnberg, pp. 63–67.
- Heegn, H., 1987. Model describing the resistance against structural changes and the hardness of crystalline solids. *Cryst. Res. Technol.* 22 (9), 1193–1203.
- Heegn, H., 2000. Mechanical induced changes in structure and properties of solids. *Proceedings of the XXI International Mineral Processing Congress: Part A4. Comminution, Classification and agglomeration*, Rome, Italy, pp. 52–59.
- Heegn, H., Birkeneder, F., Kampfner, A., 2003. Mechanical activation of precursors for nanocrystalline materials. *Cryst. Res. Technol.* 38 (1), 7–20.
- Holland, T.J.B., Redfern, S.A.T., 1997. Unit cell refinement from powder diffraction data; the use of regression diagnostics. *Mineral. Mag.* 61, 65–77.
- Jyung, D.L., Jenq, G.D., 1997. The use of X-ray line profile analysis to investigate crystallite size and microstrain for zirconia powders. *J. Mater. Sci.* 32, 5779–5790.
- Kaczmarek, W.A., Ninham, B.W., 1994. Preparation of Fe_2O_4 and $\gamma\text{-Fe}_2\text{O}_3$ powders by magnetomechanical activation of hematite. *IEEE Trans. Magn.* 30 (2), 732–734.
- Karagedov, G.R., Lyakhov, N.Z., 2003. Mechanochemical grinding of inorganic oxides. *Kona* 21, 76–86.
- Kosmac, T., Courtney, T.H., 1992. Milling and mechanical alloying of inorganic nonmetallics. *J. Mater. Res.* 17 (6), 1519–1525.
- Lucks, I., Lamparter, P., Mittemeijer, E.J., 2004. An evaluation of methods of diffraction-line broadening analysis applied to ball-milled molybdenum. *J. App. Cryst.* 37, 300–311.
- Mineral database, 2005. <http://webmineral.com/data/Hematite.shtml>.
- Miyasaka, K., Senna, M., 1985. Calorimetric and thermoanalytical assessment of mechanically activated PbCO_3 . *Thermochim. Acta* 83 (2), 225–233.

- Ohlberg, S.M., Strickler, D.W., 1962. Determination of percent crystallinity of partly devitrified glass by X-ray diffraction. *J. Am. Ceram. Soc.* 45, 170–171.
- Pourghahramani, P., Forssberg, E., 2006. Microstructure characterization of mechanically activated hematite concentrate using XRD line broadening analysis. *Int. J. Miner. Process* 79, 106–119.
- Senna, M., 1983. Criteria of activation of powdery materials by a preliminary mechanical treatment. *Kona* 1, 48–52.
- Stewart, S.J., Borzi, R.A., Cabanillas, E.D., Punte, G., Mercader, R.C., 2003. Effects of milling-induced disorder on the lattice parameters and magnetic properties of hematite. *J. Magn. Magn. Mater.* 260, 447–454.
- Tkacova, K., 1989. *Mechanical Activation of Minerals*, first ed. Elsevier, Amsterdam.
- Tkacova, K., Balaz, P., 1996. Reactivity of mechanically activated chalcopyrite. *Int. J. Miner. Process.* 44–45, 197–208.
- Tkacova, K., Heegn, H., Stevulova, N., 1987. Changes in structure and enthalpy of carbonates and quartz accompanying grinding in air and aqueous environments. *Powder Technol.* 52, 161–166.
- Tkacova, K., Heegn, H., Stevulova, N., 1993. Energy transfer and conversation during comminution and mechanical activation. *Int. J. Miner. Process.* 40, 17–31.
- Tromans, D., Meech, J.A., 2001. Enhanced dissolution of minerals: stored energy, amorphism and mechanical activation. *Miner. Eng.* 14 (11), 1359–1377.
- Ungar, T., Borbely, A., 1996. The effect of dislocation contrast on X-ray line broadening: a new approach to the line profile analysis. *Appl. Phys. Lett.* 69, 3173–3175.
- Vives, S., Gaffet, E., Meunier, C., 2004. X-ray diffraction line profile analysis of iron ball milled powders. *Mater. Sci. Eng., A Struct. Mater.: Prop. Microstruct. Process.* 366, 229–238.
- Welham, N.J., 2001. Enhanced dissolution of tantalite/columbite following milling. *Int. J. Miner. Process.* 61 (3), 145–154.
- Welham, N.J., Llewellyn, D.J., 1998. Mechanical enhancement of the dissolution of ilmenite. *Miner. Eng.* 11 (9), 827–841.
- Williamson, G.K., Smallman, R.E., 1956. Dislocation densities in some annealed and cold-worked metals from measurements on the X-ray Debye–Scherrer spectrum. *Philos. Mag.* 1, 34–45.
- Zdujic, M., Jovalekic, C., Karanovic, Lj., Mitric, M., Poleti, D., Skala, D., 1998. Mechanochemical treatment of α -Fe₂O₃ powder in air and atmosphere. *Mater. Sci. Eng., A Struct. Mater.: Prop. Microstruct. Process.* 245, 109–117.
- Zhang, Q., Kasai, E., Saito, F., 1996. Mechanochemical changes in gypsum when dry ground with hydrated minerals. *Powder Technol.* 87, 67–71.
- Zoltan Juhasz, A., 1998. Aspects of mechanochemical activation in terms of comminution theory. *Colloids Surf., A Physicochem. Eng. Asp.* 141, 449–462.

Paper III

Changes in the Structure of Hematite by Extended Dry Grinding in Relation to Imposed Stress Energy

Parviz Pourghahramani & Eric Forssberg, Submitted for publication in Powder Technology

Changes in the structure of hematite by extended dry grinding in relation to imposed stress energy

Parviz Pourghahramani* and Eric Forssberg

Division of Mineral Processing, Luleå University of Technology, Luleå, Sweden

Abstract

The effect of extended dry milling in different mills on the structural changes of hematite concentrate has been investigated using a combination analysis of XRD line broadening, BET and particle size measurements. Structural changes were followed by XRD line broadening analysis using integral breadth method and Warren-Averbach approach. For analysis, the stress energy was estimated by considering different grinding variables in different mills and changes in the structure discussed in terms of stress energy.

Within comparable range of stress energy, lower BET surface area was produced by grinding in the vibratory mill. The maximum surface area increased to $18.4 \text{ m}^2/\text{g}$ in the vibratory mill after releasing 51300 kJ/kg energy. The conversion of the 80% of initial hematite to amorphous phase during extended dry grinding by tumbling, planetary and vibratory mills, needs 4000, 8500 and 50000 kJ/kg energy respectively. It was understood that vibratory mill introduces the minimum lattice strain and gives the largest crystallites when applying the same level of stress energy. The smallest crystallites with grinding in tumbling, vibratory and planetary mills were obtained about 17.3, 13.5 and 5.6 nm after releasing 5230, 51300 and 15600 kJ/kg respectively. For these levels of stress energy, in turn, the microstrain $\langle \varepsilon_{L=10\text{nm}}^2 \rangle^{1/2}$ exceeds 4.4×10^{-3} , 3.9×10^{-3} and 5.3×10^{-3} .

It was further revealed that higher concentrations of defects (Amorphization and excess energy) per unit surface area were induced by grinding in the planetary and tumbling mills. A theoretical calculation of the energy contribution to the long-lived defects indicated that products from tumbling and planetary mills have higher excess energy compared to the products from vibratory mill for the same stress energy. The maximum theoretical excess energy was estimated about 75.4, 80.0 and 81.3 kJ per mole of the ground hematite with tumbling, vibratory and planetary mills after releasing 5230, 51300 and 15600 kJ/kg of stress energy respectively. Grinding in vibratory mill needs much more energy to reach the same effect as the other used mills. A comparison of specific energy input and stress energy among the used mills points out that for generation of the same levels of stress energy, the planetary mill consumes more energy than the other used mills.

Keywords: Dry grinding, Stress Energy, Structural Changes, Mechanical Activation, Hematite, Grinding Methods

1. Introduction

The production and properties of ultrafine iron oxides continue to attract considerable interest and attention because of their importance in various technologies. Part of this interest arises

* Corresponding author: Tel:+46 920 491313; fax:+46 92097364
E-mail address: Parviz.Pourghahramani@ltu.se

from the fact that ball milling is a novel technique for the preparation of new materials and phases and it can be used successfully for changing structures and improving properties of materials.

The application of high energy mills (such as planetary mill, vibratory mill, and tumbling mill or jet mill) allows a dramatic change of the structure and surface properties of solids to be induced [1,2]. Mechanical treatment in a high energy mill generates a stress field within solids. Stress relaxation can occur via several channels: (1) heat release, (2) development of surface area as a result of brittle fracture of the particles, (3) generation of various sorts of structural defects and (4) stimulation of chemical reaction within solids. All relaxation channels cause changes in the reactivity of the solid substance under treatment, which is why the resulting action is called mechanical activation [3]. The concentration of the mechanically induced defects and their spatial distribution depend upon the condition of the energy transfer in the mill. The concentration and distribution of the mechanically induced defects can be also influenced by varying the external conditions of stress. The creation of defects enhances the stored energy (enthalpy) in the solids and consequently causes a decrease of activation barrier for the process and/or subsequent processes [4].

A large number of studies have been devoted to the understanding of the influence of the grinding variables and conditions on the structural changes of mechanically-activated material. Structural changes of inorganic oxides have been shown to be intensified with increasing grinding media density, acceleration and duration of milling in a planetary mill [5]. It has been further reported that the crystallite size decreased exponentially with increasing milling time and the strain increased by extending activation time during mechanical activation of ilmenite [6]. A comparative study of the influence of Attritor, Ball and vibratory mills on the reactivity of sulphide minerals was carried out by Balaz et al. [7]. $\gamma - Fe_2O_3$ samples ground with smaller amplitude in a vibratory mill showed higher reactivity [8]. Among the various factors controlling defect development, the mill power and the efficiency of the energy transfer in the mill are the most important. On the other hand, grinding variables and conditions diverge widely through literatures; and therefore the direct comparison of mills and their efficiency are complicated tasks. Even comparing structural changes data on the same material obtained using different equipment or mill parameters is difficult. For example, the production of BET surface area around $3 \text{ m}^2/\text{g}$ took about three hours using a planetary mill and less than one hour with a vibratory mill [9]. The question is how to compare the different mill effects on structure changes and at the same time consider most of the grinding variables. Direct comparison of mills will be possible, if the efficiency and ability of mills in transferring energy to the particles being ground are known.

However, the measurement of the efficiency of mills in energy transfer is really a complicated task; because the energy transfer in the course of grinding of particulate system takes place in three stages:

(1) The conversion of kinetic energy of drive to the grinding medium characterized by the effectiveness of a mill itself as the energy transformer.

(2) Transferring of the mechanical action to the particles being ground and the effect of grinding intensity on the efficiency of energy transferring from grinding medium to treated solids. If the energy input is too high, the energy utilization decreases with increasing of grinding intensity.

(3) Transferring of energy taken up by a treated substance into the actual result of treatment [2, 10].

On the other hand, the efficiency of mills in energy transferring and evaluation of grinding intensity have not been adequately established as far as we know. In this case, some generalized factors are proposed by Heegn [11, 12] to characterize kinetic energy of grinding as a method for comparison of different mills. Although these considerations are based on a very simple model, they will be helpful for a better understanding of the influence of different mills and operating parameters on mechanical activation results and we used those generalized factors in this paper for comparison of mills.

The aim of this study is to investigate mechanically-induced changes in the hematite structure during extended dry milling using different mills. This is another way of comparing of different mills with respect to stress energy in various mills. Several microstructural characteristics like lattice strain, amorphization, crystallite size and integral breadths of XRD diffraction lines etc obtained using line profile analysis (LPA). The obtained parameters are correlated with stress energy to distinguish and interpret the differences among the used mills with considering grinding variables simultaneously instead of individual variables to gain insight into mill efficiency.

2. Experimental

In this section, the grinding condition and characterization methods are described.

2.1. Grinding

Dry grinding tests were carried out using three mills, vibratory, tumbling and planetary mills, in air atmosphere. Steel media was used as grinding bodies with dimensions between 22.2 mm and 6 mm with bulk density of 4.875 g/cm^3 . The grinding tests were performed in closed condition, i.e., the lids of the mills were kept bolted during the grinding. The media surface was determined from the number and dimension of the grinding media. The media surface levels were set to 1 and 4 m^2 per kg of hematite and the related ball to powder weight ratio was recorded. The grinding tests were extended up to 9 hours. Among the used mills, only the vibratory mill had plastic liner. The grinding experimental conditions are given in Table 1.

Table 1. Experimental milling conditions and mill types.

Milling conditions	Tumbling	Vibratory	Planetary
Media filling (%)	38.9	70	23.4
Weight of grinding bodies (kg)	24.375	33.160	1.031
Ball to powder weight ratio	16.77:1 67:1	16.92:1 67.68:1	19.1:1 76.34:1
Media surface (m^2 / kg)	1, 4	1, 4	1, 4
Milling time (h)	1, 3, 9	1, 3, 9	1, 3, 9
Number of revolutions (min^{-1})	60	1000	100 (axle) 200 (drum)
Amplitude (mm)	--	8	--
$L \times D$ (mm \times mm)	275 \times 245	320 \times 185	87 \times 115
Stress rate (m / s)	2.2	1.67	1.95
Material temperature ($^{\circ}\text{C}$)	24-38	48-105	39-68

The specific energy input consumed by the mills was measured after finishing each run of grinding tests by an electrical meter called Micro VIP (Elcontrol Co., Italy). The frequency and amplitude in vibratory grinding and the drum and axle (sun wheel) speed in planetary mill were maintained constant during the experiments. The temperature of the activated hematite in the mill chamber was measured immediately after stopping mill by a thermometer. Each grinding test was performed continuously and independently. To obtain an impression about the intensity of the mechanical stress and to correlate the changes in structure with mechanical stress, the stress energy was calculated using expressions, proposed by Heegn [12], on the basis of the energy or intensity of single impact stressing factor and stressing energy for the sum of impacts:

$$E_{th} = \frac{1}{2} \left(\frac{m_1}{m_2} \right) n t V^2 \quad (1)$$

where m_1 , m_2 , n , t and V refer to mass of grinding media, mass of material charge, speed, grinding time and stress rate in the mills respectively. The rate of stress was estimated for planetary and tumbling milling from the gravitational acceleration (tumbling mill $b/g=1$; planetary mill $b/g=1.67$) and mill diameter. The rate of stress for vibratory mill determined from the frequency and amplitude (Table 1). The terms b and g denote the acceleration and gravitational acceleration respectively.

2.2. Characterization

Size distributions of the samples were obtained from Laser diffraction analysis using a *CILAS 1064* particle size analyser in liquid mode. From the Laser diffraction measurements, the granulometric surface area was calculated. The BET specific surface area was measured using the N_2 -adsorption technique and a *Flow Sorb II2300* (Micromeretics Co. Ltd., USA) volumetric gas adsorption analyser.

The activated and non-activated hematite was also characterized using X-ray powder diffraction (XRD). The XRD analysis was performed using a *Siemens D5000* powder diffractometer with Bragg-Brentano geometry equipped with a curved graphite monochromator in the diffracted beam arm and using $Cu K\alpha$ ($\lambda = 0.1546 nm$) radiation (Siemens, Germany). The XRD patterns of samples were recorded in the range $2\theta = 10 - 90^\circ$ using a step size of 0.02° and a counting time of 5 s per step. The same procedure was made for standard reference sample LaB_6 , a standard proposed by the National Institute of Standards and Technology of USA (NIST), to remove the instrumental effect from the observed profile broadening.

The eight most intensive reflection peaks of hematite were considered for further characterization using the line profile analysis (LPA), known as line broadening technique. The Profile software [13] was used in profile fitting procedure to extract the line broadening characteristics. For this purpose, the Pseudo-Voigt line shape function, a linear combination of Cauchy and Gaussian line shape function, was fitted to the resulted XRD diffraction patterns. For each adjusted line profile, the following parameters were obtained:

- (1) The maximum height of the peak (I_{max})

- (2) The integral breadth of line profile ($\beta = A/I_0$ where A is the peak area)
- (3) The full-width at half of maximum (FWHM)
- (4) The mixing factor (η) of Lorentzian and Gaussian functions in the adjusted Pseudo-Voigt function for measured XRD patterns.
- (5) The peaks position (2θ)

An example of profile fitting is given in Fig. 1.

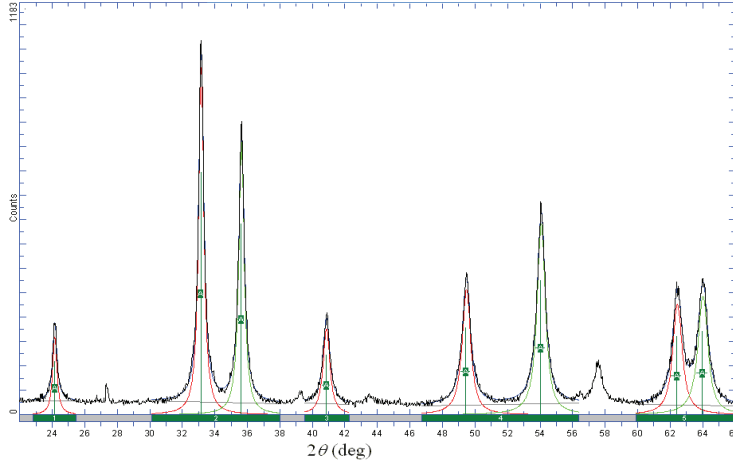


Fig. 1. An example of profile fitting in which the Pseudo-Voigt function fitted to the XRD pattern of hematite ground after releasing 51300 kJ/kg stress energy in the vibratory mill.

The physically-broadened lines and integral breadths of the XRD diffraction patterns were obtained after removing the instrumental broadening from XRD line breadths by the standard sample, LaB_6 , according to the Halder-Wagner [14] approximation. The degree of amorphization of the samples was determined from X-ray diffraction patterns. For this proposes, the degree of crystallinity was defined as:

$$X = \frac{U_0}{I_0} \times \frac{I_x}{U_x} \times 100 \quad (2)$$

where U_0 and U_x refer to the background of non-activated sample and activated sample, while I_0 and I_x are integral intensities of diffraction lines of non-activated sample and activated sample. The degree of amorphization (content of X-ray amorphous phase) is defined by equation [15]:

$$A = 100 - X \quad (3)$$

For the deconvolution of the strain and crystallite contributions, the Warren-Averbach approach [16] was used in the [012] direction. Consequently, the lattice stain and crystallite size (surface weighted) were calculated. The total stored energy (enthalpy) in mechanically-activated hematite concentrate was obtained by adding up the three sources of energy contributing to defect structures. The expressions and more information regarding the line broadening analysis were given in previous works [17].

3. Material

High purity of natural hematite concentrate from LKAB (Luossavaara Kiirunavaara Aktiebolag) company in Sweden was used in this study. The particle size analysis of hematite concentrate indicated a particle size distribution of 90% <110 μm , 50 %< 46 μm and a 10% <2.5 μm . The chemical analysis showed that initial hematite powder contained 97.91% Fe_2O_3 , 0.73% Al_2O_3 , 0.73% SiO_2 , 0.26% TiO_2 , 0.20% MgO , 0.022% MnO , and 0.088% P_2O_5 . The BET measurements gave a specific surface area of $0.59 \text{ m}^2 / \text{g}$. The density of the starting material was calculated about $5240 \text{ kg} / \text{m}^3$ using a Pycnometer (Micromeritics Co. Ltd., USA). The XRD patterns showed only the hematite reflections.

4. Results and discussion

4.1. Surface area changes by milling

The mechanical activation of materials is accompanied by disintegration and generation of fresh previously-unexposed surfaces. The size distribution and the specific surface area also depend on the secondary processes like aggregation and agglomeration [18]. Fig. 2 shows how the BET surface area and granulometric surface area change with stress energy in different mills.

It is obvious that the rate of new surface formation depends on both applied stress energy and the types of mills. The BET surface area shows an increasing trend, especially at lower levels of stress energy. The BET surface area continues to increase during the intensive grinding stages when hematite is subjected to the milling in tumbling and vibratory mills. On the other hand, the BET surface area of the ground samples in the vibratory mill increases sharply at higher level of stress energy. With growing stress energy, the products of planetary mill produce marginally higher specific surface area than the products of tumbling mill as opposed to the initial stage of milling bearing lower intensity. However, the specific surface area in planetary doesn't follow a clear trend with stress energy. As discussed in previous work [9], the agglomeration of particles in planetary mill occurred in two stages including under lower media surface and higher media surface after three and one hours of milling respectively. Thus, the agglomeration at different stages disturbs the trend of BET surface area changes in terms of stress energy. It can be also concluded from the changes in the granulometric surface area as shown in Fig. 2b. The granulometric surface area increases at lower levels of stress energy in tumbling and vibratory milling operations. As the grinding progresses, the granulometric surface area tends to decrease, indicating the formation of agglomerates among particles. The agglomerates productions take place after releasing energy of 1740 and 12800 kJ/kg in the tumbling and vibratory mills respectively. It can be further concluded that the BET surface area increases in spite of the agglomeration of particles. Therefore, the agglomeration with available pores (soft agglomerates) occurred in tumbling and vibratory mill at intensive grinding condition. The agglomeration of the particles during extended dry

grinding was reported for sulphide minerals [1], oxide minerals [2], and olivine [19]. This behavior is common for dry grinding and is usually explained by agglomeration of the structurally modified particles following the initial reduction of particle size. This is because of the tendency of the activated material to reduce their surface free energy.

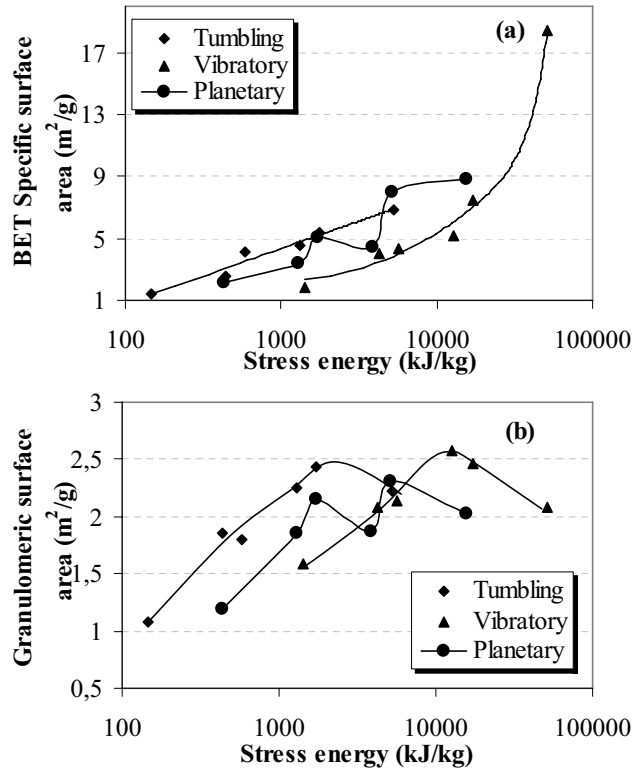


Fig. 2. Change in specific surface area (a) and granulometric surface area (b) in different mills as a function of stress energy.

In addition, the vibratory mill products that obtained at certain stress energy produce smaller specific surface area than the other mills. As a result, the tumbling and planetary mills show roughly higher efficiency in the production of a specific surface area than vibratory mill at certain stress energy levels. The maximum specific surface area was attained about 18.4 m^2/g for the ground sample in the vibratory mill after energy releasing around 51,300 kJ/kg . The maximum BET surface area in the products of the planetary and tumbling mills were ranged with the values of 8.8 and 6.8 m^2/g after releasing 15,600 and 5,230 kJ/kg energy respectively. It can be further understood that that the production of unit surface area in the vibratory mill needs to release more energy than other mills.

4.2. XRD diffraction

The structural changes and the characterization of the microstructure characters were investigated using XRD analysis. The X-ray diffraction patterns were collected for all activated and non-activated samples. An example of the XRD patterns is given in Fig. 3 for comparison.

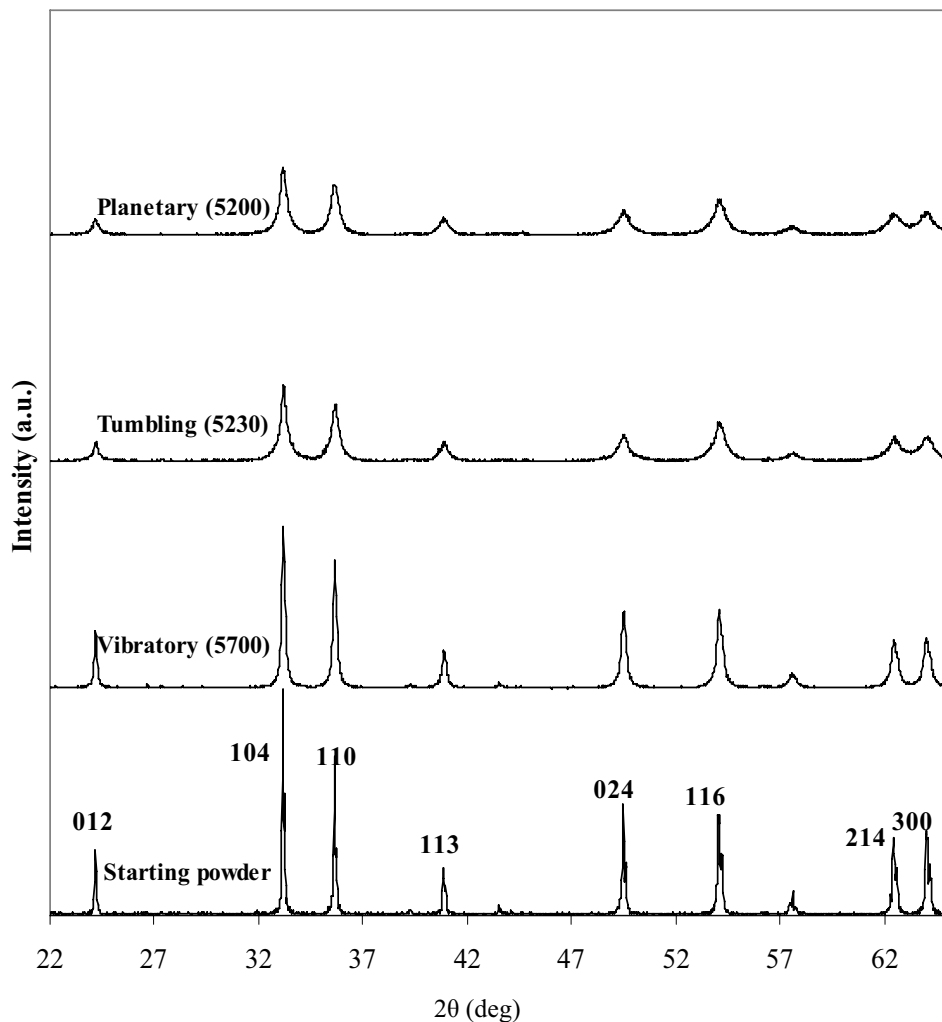


Fig. 3. The XRD patterns of the starting and milled samples in different grinding devices. The values in parentheses correspond to the stress energy.

The diffraction peaks for mechanically-activated samples are lower and broader than of those for non-activated samples, mainly due to a disordering process of hematite crystal structure by intensive grinding. The reduction of diffraction peaks intensities implies the formation of amorphous material. The decrease of X-ray diffraction intensities is accompanied by a general broadening of the XRD patterns. The increase of the XRD line breadths is due to the plastic deformation and disintegration of hematite. The XRD patterns showed only the

hematite reflections, indicating that hematite did not undergo significant reaction and phase changes. The presence of small, but remarkable, reflection peaks after intensive grinding in the grinding mills can be taken as a further indication of the high milling resistance and mechanical strength of the submicron hematite crystallites. Regarding the effect of different mills, it can be observed that planetary and tumbling mills bring about weaker and broader peaks than vibratory mill despite the release of larger stress energy in the vibratory mill.

4.3. The effect of grinding on the physical XRD line breadths

For quantitative comparison of the influence of the grinding mills on the alteration of the hematite structure, further investigations were followed by profile fitting technique. After adjusting a proper line shape (Pseudo-Voigt) for XRD diffraction profiles, the physical integral breadths of the reflection peaks were calculated. The physical integral breadth for (104) reflection and the average physical line breadths obtained from the eight most intensive reflection peaks of hematite were considered for comparison. The obtained results are exemplified in Fig. 4 in relation to applied stress energy.

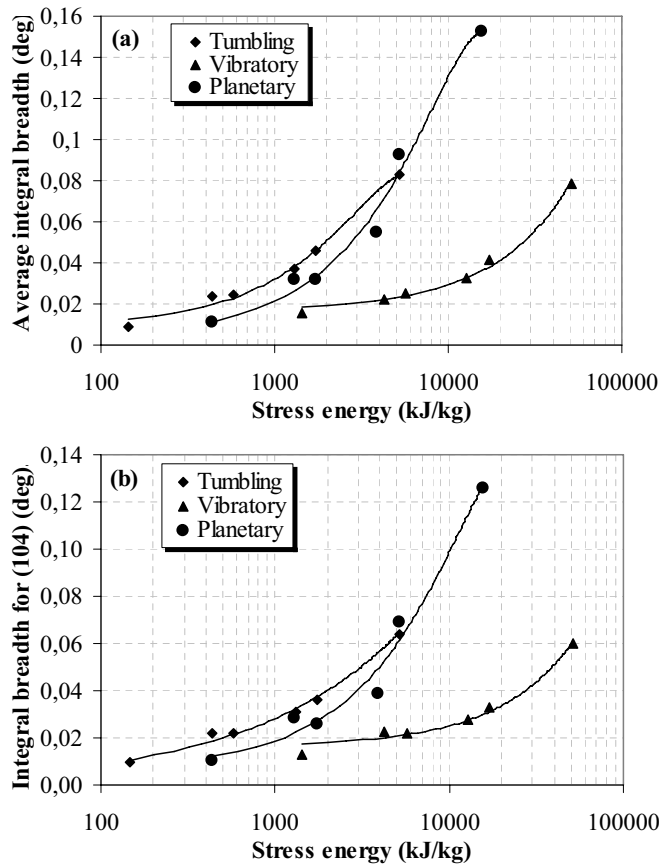


Fig. 4. The comparison of the physical integral breadth for the ground hematite in different mills for the (104) reflection (a) and the average integral breadth (b).

It should be reminded that both lattice strain and crystallites size components are contributing to the line breadths which will be resolved later for obtaining the microstructure characters. The plots for the reflection (014) and average physical integral breadths displayed similar trends. This also stands for other reflections, implying that all eight studied lattice faces are disordered during mechanical stressing of hematite. After releasing 5230, 51300 and 15600 kJ/kg energy in the tumbling, vibratory and planetary mills, the broadening of the (014) reflection increased to 0.0639, 0.0598 and 0.1260 degree respectively.

The development of the integral breadth vs. stress energy in various milling methods can be observed in Fig. 4. The broadening of the diffraction lines at lower levels of the stress energy develops steadily and continues to increase sharply with growing stress energy whatever milling machines used. The curve trends give evidence to more plastic deformation and disordering of the hematite lattice in the intensive grinding conditions. The influence of the mills is also reflected on the plots as well. The tumbling mill brings about approximately more plastic deformation and/or structural changes at the initial stages of milling. As the milling intensity increases, the broadening resulted from the planetary milling exceeds the broadening obtained from the tumbling milling. For a given stress energy, the vibratory mill caused far less broadening in the XRD diffraction patterns. The difference of both tumbling and planetary mills with the vibratory mill becomes more distinguished as the stress energy increases. This may be related to the fact that most of grinding energy in intensive grinding stages are used for establishment and development of plastic deformation rather than grinding energy in the initial stages of milling in which a part of energy is consumed for size reduction process. In other words, when grinding proceeds into ultrafine grinding range at intensive grinding, the stress energy is used mainly for creating structure defects not size reduction. The reduction of XRD diffraction intensities and the broadening of different peaks appear to be the common X-ray diffraction characteristics of the dry milled hematite. The minimum average broadening about 0.0087 was attained in the tumbling mill with 145 kJ/kg stress energy. The maximum average broadening was obtained from planetary milling around 0.1522 degree applying 15600 kJ/kg energy.

4.4. The degree of amorphization

In this section, the average relative intensity of the reflection peaks obtained from the eight most intensive reflection peaks of the ground hematite and the amorphization degree of hematite are studied. As discussed, the intensity of XRD patterns reduces during mechanical treatment of hematite because of the formation of the amorphous material. The obtained results are depicted in Fig. 5. The diffraction peaks show a progressive reduction in intensity when comparing with the starting powder diffractions. The tumbling and planetary mills bring about much more reduction in the intensity of the X-ray diffraction peaks than the vibratory mill with certain stress energy. The reduction of XRD diffraction intensities is intensified with increasing of the grinding intensity.

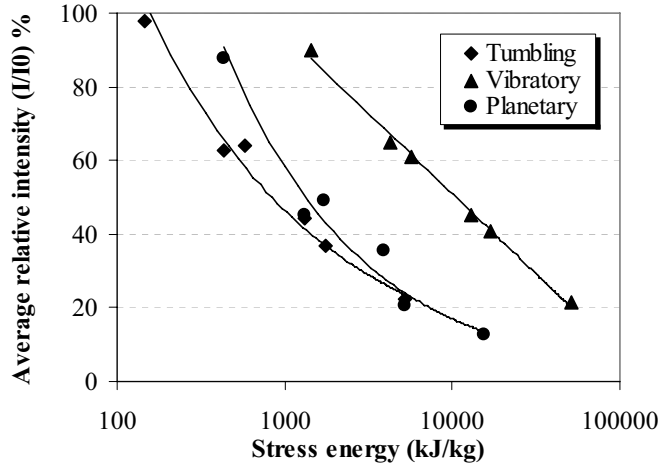


Fig. 5. The effect of grinding mills on the intensity reduction of the reflection peaks. Terms I and I_0 refer to the peak intensity of the milled and starting samples respectively.

From the intensity of the reflection peaks and their background, the degree of X-ray amorphization is estimated according to equation (3) and the results are depicted in Fig. 6.

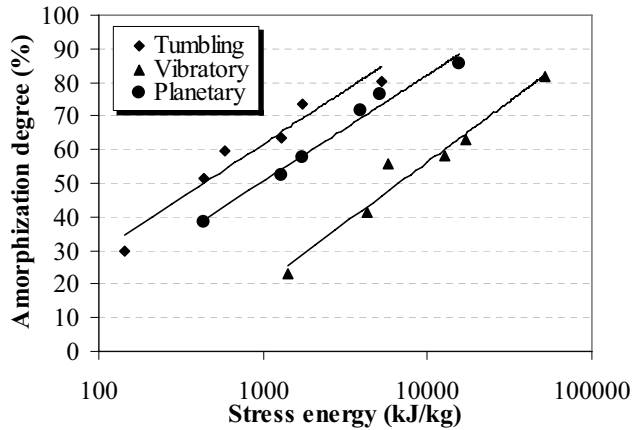


Fig. 6. The content of X-ray amorphous phase in different milling environment as a function of stress energy.

The content of X-ray amorphous phase in hematite depends on both grinding mill and stress energy field. The portion of X-ray amorphous phase in the ground hematite with tumbling mill is even higher than that of ground hematite in the planetary mill for a given stress energy. The fraction of the X-ray amorphization increases steadily with growing amount of grinding work despite the particle size reduction in mills and the BET surface area values during the grinding in the planetary mill. These results are in line with relative intensity reduction as well. The amorphization degree increased to 80, 82 and 86% by grinding in the tumbling, vibratory and planetary mills respectively, after releasing 5230, 51300 and 15600 kJ/kg of energy. These results show that more energy is needed in the vibratory and planetary mills

than tumbling mill to produce the same amorphization degree. The increase of X-ray amorphous phase due to intensive milling was reported for calcite, quartz and magnesite [20, 21] and sulphide minerals [2]. The amorphization is in fact a highly distorted periodicity of lattice elements, and it is often characterized as a short range order in contrast to the long order of a fully crystalline structure.

4.5. Microstructural characteristics

To obtain the microstructural characteristics, the Warren-Averbach method based on Fourier analysis, which can precisely determine microstructure characters [22], was used for direction [012]. In this method, the experimentally observed broadening of the line profile was corrected for instrumental effects using Stokes deconvolution [23] and Warren-Averbach method. From the Warren-Averbach method, We calculated the root mean square strain (RMSS), $\langle \varepsilon_L^2 \rangle^{1/2}$, and surface weighted crystallite. The surface weighted crystallite size of the ground samples in the mills are compared in Fig. 7.

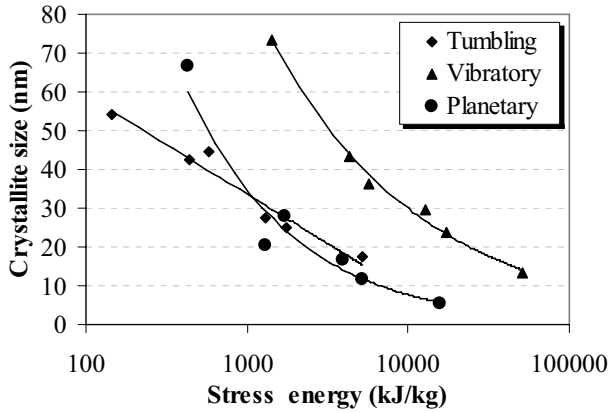


Fig. 7. Variations of the surface weighted crystallite size in [012] direction with milling in different mills as a function of stress energy.

A large difference exists between the obtained crystallite sizes from vibratory mill and other mills used. It is evident that the ground samples in the vibratory mill have larger crystallites than the ground samples both in the tumbling and planetary mills within comparable range of stress energy. It can be observed from Fig.7 that the planetary mill products yield marginally smaller crystallite than tumbling mill when hematite is subjected to intensive grinding in contrary to less intensive milling stage. The planetary mill gives larger crystallites than tumbling mill in the initial stages of milling. It seems that the hindering of grinding media because of higher powder to ball weight ratio prevent the refinement of microstructure characters in the sample ground in the initial stages of milling in the planetary mill. We can draw a conclusion that the largest crystallites are resulted from the milling in the vibratory mill at the same stress energy level. With the planetary, tumbling and vibratory mills, the hematite crystallites refined up to the values of 5.6, 17.3 and 13.5 nm, respectively; after receiving the stress energy levels to the values of 15600, 5230 and 51300 kJ/kg during grinding in mills.

The root mean square strain values $\langle \varepsilon_{L=10nm}^2 \rangle^{1/2}$ for activated hematite in mills are displayed in Fig. 8.

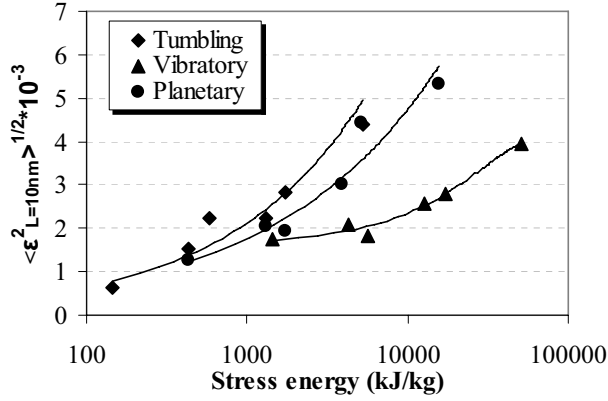


Fig. 8. Variations of the lattice strain ($\langle \varepsilon_{L=10nm}^2 \rangle^{1/2}$) values in different grinding machines vs. stress energy.

At lower levels of stress energy, there is minor difference among the mills in deformation of hematite lattice; while with growing the grinding intensity the difference becomes greater. With a first approximation, distinguished difference among mills starts above 1700 kJ/kg of energy and the magnitude of differences maintains to increase as the stress energy intensifies. Changes in the microstructural characteristics, integral breadth, microstrain and crystallite size reveals that in the initial stages of milling, the particles tend to grind easily. With the progress of milling, the particle size falls into the ductile range and they undergo mainly plastic deformation and consequently the long-lived defects accumulate in the particles being ground. Interestingly, the trend of crystallite size and strain components contributed to the line breadth appears to change in the tumbling and planetary mills as a function of grinding intensity.

The dislocation lines, as line defects, inducted in the case of mechanically-activated material, is another energy carrier in the stressed materials [24, 25] in addition to the generation of fresh new surfaces and phase transformation. The dislocation density summarizes the effects of microstructure characters (crystallite size and strain) of mechanically-stressed material altogether. The minimum dislocation density was determined according to Williamson and Smallman expression [26]. Our results are presented in Fig. 9 as a function of stress energy for ground hematite in various milling devices. Since the dislocation density includes both characters of the lattice strain and crystallite size, the difference among the mills can be easily detected. The lower efficiency of the vibratory mill is pronounced here once again. In other words, to achieve the same effect in vibratory mill, much more energy is needed. These results confirm the previous results. The tumbling mill induced marginally more damage and dislocation defects to hematite lattice than planetary mill at lower levels of stress energy.

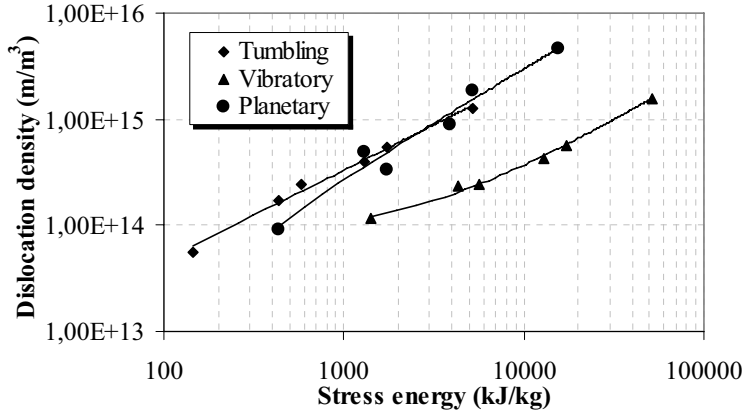


Fig. 9. Change in dislocation density with the stress energy for mechanically stressed hematite by various mills.

4.6. The relationship between defect characteristics

Figure 10 shows the variation of amorphization degree and excess energy versus the BET specific surface area in different mills. Generally, a distinguished difference can be observed between tumbling and vibratory mills. According to Fig. 10, it can be seen that the formation of unit surface area in tumbling is associated slightly with a sharper increase in the amorphization degree. The difference between tumbling and planetary mills is negligible. The concentration of defects in the ground hematite with vibratory mill appears to be slightly less than of those in tumbling and planetary mills. Besides, with regard to the rate of stress in mills, structural defects that are vital for mechanical activation are accumulated in the near surface layer for ground hematite in mills.

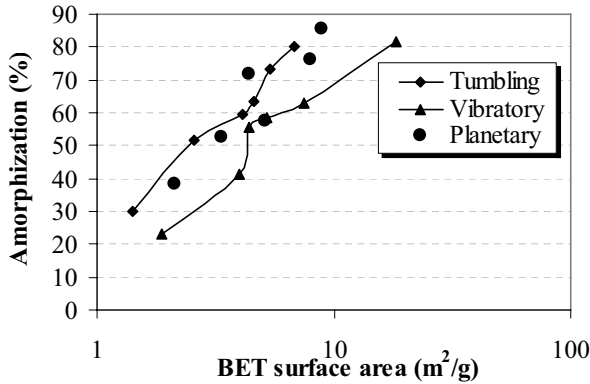


Fig. 10. X-ray amorphous phase versus specific surface area of hematite samples ground in various mills.

According to Tkacova [2], the long-lived defects are being equally distributed throughout the bulk of particles when the material is subjected to grinding in mills bearing higher stress rate such as jet mills and high-speed disintegrator. If the material is subjected to the grinding in mills producing lower rate of stress like tumbling and planetary mills, the long-lived defects accumulate preferentially in the near surface layer. This can be assumed as a consequence of

a quasiadiabatic energy accumulation at the mechanical action of shorter duration than the time required for the formation of the critical crack ($t < t_{crit}$). At higher number of loading cycles and substantially slower rates of stress in the three used mills, the defects are accumulated near the surface layer due to the mechanism of cyclic micro plastic deformation. This agrees with the rate of stress in different mills in which the rate of stress set to a comparable range during experiments, varying between 1.7 and 2.2 m/s (table.1). Their differences are at of least important.

4.7. The stored energy contributions to the long-lived defects

For the interpretation of the mechanical activation process, the context between structures and energy–content of the mechanically activated solids and consumed mechanical energy are of important and interest.

Real solids and in particular, nanodisperse or mechanically activated solids, must be calculated with different types and concentrations of defects in meta-stable condition. As a result of previous investigations [24, 25], the defect structures of essential meaning for the energetic condition of the solids are dislocation concentrations with the specific energy ΔH_d , energy contributions of new surface formation ΔH_s and content of newly-formed phases and amorphous fraction ΔH_A . The quantitative estimate of the increase in molar chemical free energy (increase in stored energy or enthalpy) due to dislocation defects has been calculated by expression proposed by Tromans and Meech [27]. Energy fraction of newly-formed phases (our experiments suggested only amorphization, not the formation of other new phases) and specific surface area as a measure for the grain boundary to the surrounding medium were evaluated by equations expressed by Heegn [24]. The stored energy (excess enthalpy) on basis of long-lived defects is compared for various mills as a function of stress energy in Fig.11.

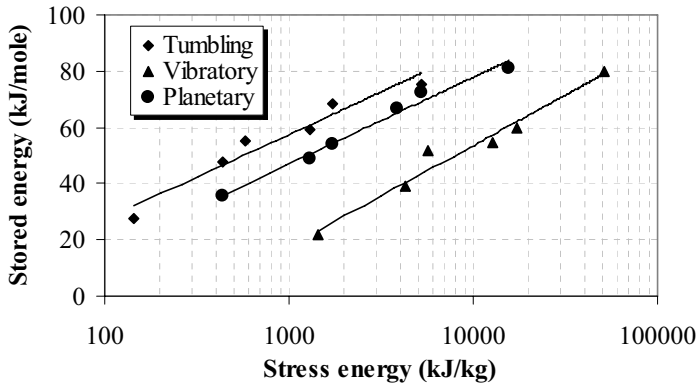


Fig. 11. The relationship between the stress energy and excess energy of the mechanically activated hematite by different mills.

Obviously, there is a direct relationship between excess energy and stress energy, i.e. the higher grinding work (stress energy), the more excess energy is stored in hematite. According to Fig. 11, distinguished differences can be observed between vibratory mill and the other two used mills. In other words, for a given stress energy, the activated hematite in the tumbling mill contains higher excess enthalpy (stored energy) and in the vibratory mill has lower

excess energy. For example, to achieve an excess energy in hematite by mechanical treatment of about 60 kJ/mole, the required stress energy in tumbling, planetary and vibratory milling is around 1300, 2800 and 17000 kJ/kg respectively. It is worthwhile to mention that the energy contribution from amorphization or quasi-amorphization to the energy changes at activation amounted to 92-98 % of overall stored energy [9] and subsequently these curves have similar trend as of Fig. 6. These results are in line with the results obtained for quartz, calcite, magnesite, kaolinite and iron [20, 21] and periclase [25]. In agreement with the study by Miyasaka and Senna [28] and Tkacova et al. [29], the excess enthalpy (ΔH_T) can be related to stress energy (W) by the equation:

$$\Delta H_T = b \ln W - c \quad (4)$$

where b and c are the constant values. The corresponding equations for different mills are:

$$\Delta H_T = 13.15 \ln W - 33.38 \quad \text{Tumbling mill} \quad (5)$$

$$\Delta H_T = 13.37 \ln W - 45.38 \quad \text{Planetary mill} \quad (6)$$

$$\Delta H_T = 15.58 \ln W - 89.95 \quad \text{Vibratory mill} \quad (7)$$

The correlation coefficients exceed 0.96, suggesting excellent model.

A comparison of mills based on input and stress energy can be seen in Fig. 12. There is a direct relationship between stress energy and specific energy input for mills. This suggests that only a part of specific energy input affects the particles being ground. The planetary mill needs more specific energy input than the other mills to achieve identical stress energy. In this sense, the vibratory mill consumes minimum specific energy input to release the same stress energy as the vibratory and planetary mills.

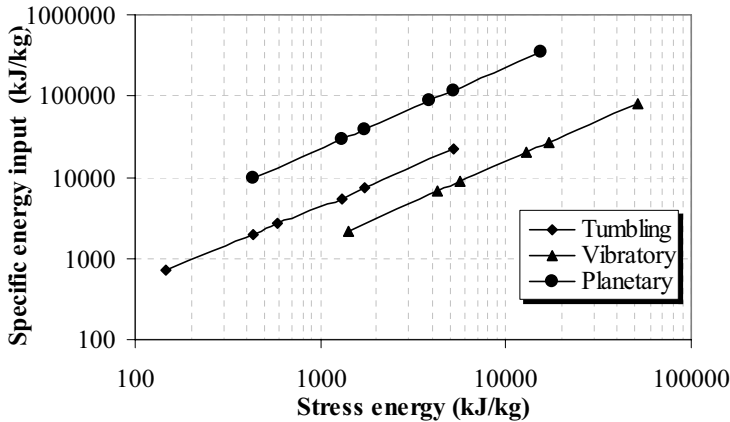


Fig. 12. The comparison of the specific energy input and stress energy for mills.

Although these considerations are based on a very simple model, they will be useful for a better understanding of the influence of different mills and operating parameters on grinding results, mechanical activation and induction of microstructure characters in hematite crystal. Another aspect that should be also kept in mind is the potentiality of upscaling of the milling process for application and commercialization. The results suggest that the mechanically-

activated hematite in tumbling mill and planetary mill have theoretically higher reactivity than the activated hematite in the vibratory mill. The further study is needed to study the availability of the stored energy in an actual reaction which is addressed by many authors [30-33].

5. Conclusions

It is shown that structural changes characters in different mills can be correlated with stress energy (grinding work), which addresses roughly the grinding intensity. This correlation enables a general understanding of the extended dry grinding behavior of different mills on the induction of structural changes. The grinding in vibratory mill needs much more stress energy to reach the same effect as both tumbling and planetary mills. It was revealed that the planetary mill consumes more specific energy input to reach the same level of stress energy as vibratory and/or tumbling mills. This is related to the scale and capacity of the used mills and is of another aspect that has to be considered in practical applications. The obtained results show that tumbling and planetary mills favor the induction of structural changes and subsequently the enhancement of reactivity irrespective to capacity and specific energy input and stress energy. Comparing the tumbling and planetary mills in terms of specific energy input and capacity, the tumbling mill seems promising device for activation. In other words, tumbling mill shows higher efficiency than the other used mills with regard to grinding intensity. It should be noted that the planetary mill used in this study had less intensity than the others often used in the literature.

Experiments for measuring the actual reactivity of the mechanically-activated hematite in mills are recommended for verifying and correlating with structural changes as the parameters studied so far. Feasibility studies after actual reactivity tests are essential to evaluate accurately their applicability.

Acknowledgments

The authors would like to thank professor Claes I Helgesson for his valuable discussions on this paper. The financial support for the project by Agricola Research Centre (ARC) is gratefully acknowledged

References

- [1] P. Balaz, Extractive Metallurgy of Activated minerals, Elsevier (2000), Amsterdam.
- [2] K. Tkacova, Mechanical Activation of Minerals, Elsevier (1989), Amsterdam.
- [3] V.V. Boldyrev, K. Tkacova, Mechanochemistry of solids: Past, Present, and Prospects, Journal of Material synthesis and Processing 8 (Nos.3/4) (2000) 121-132.
- [4] U. Steinike, K. Tkacova, Mechanochemistry of solids-Real structure and Reactivity, Journal of Material synthesis and Processing 8 (Nos.3/4) (2000) 197-203.
- [5] G.R. Karagedov, N.Z. Lyakhov, Mechanochemical grinding of inorganic oxides, Kona 21 (2003) 76-86.
- [6] N.J. Welham, D.J. Llewellyn, Mechanical enhancement of the dissolution of ilmenite, Mineral Engineering 11 (9) (1998) 827-841.
- [7] P. Balaz, H.J. Huhn, K. Tkacova, H. Heegn, Laugungsverhalten und physico-chemische Eigenschaften von in unterschiedlichen Mullen vorbehandeltem chalkopyrite, Erzmetall 41(1988) 325-331.

- [8] M. Senna., Criteria of activation of powdery materials by a Preliminary mechanical treatment, *Kona* 1(1983) 48-52.
- [9] P. Pourghahramani, E. Forssberg, Comparative Study of Microstructural Characteristics and Stored Energy of Mechanically Activated Hematite in Different Grinding Environments, *International Journal of Mineral Processing*, in press.
- [10] A.S. Kheifets, I.J. Lin, Energy transformations in a planetary grinding mill Part1; General treatment and model design, *International Journal of Mineral Processing* 47(1996) 1-19.
- [11] H. Heegn, Stressing of Solids by Fine Grinding and Mechanical Activation, *Proceedings of 1st International Conference on Mechanochemistry*, Kosice, Slovakia (1993), pp. 127-133.
- [12] H. Heegn, Mechanical induced changes in structure and properties of solids, *Proceedings of the XXI International Mineral Processing Congress, Part A4, Comminution , Classification and Agglomeration*, Rome, Italy (2000), pp.52-59.
- [13] Siemens AG, *Diffac plus profile fitting manual program* (1996), pp. 23-26.
- [14] N.C. Halder, C.N.J. Wagner, Separation of particle size and lattice strain in integral breadth measurements, *Acta Crystallography* 20 (1966) 312-313.
- [15] S.M. Ohlberg, D.W. Strickler, Determination of Percent Crystallinity of Partly Devitrified Glass by X-Ray Diffraction, *Journal of the American Ceramic Society* 45 (1962) 170-171.
- [16] B.E. Warren, *X-ray diffraction*, Addison-Wesley (1969), New York
- [17] P. Pourghahramani, E. Forssberg, Microstructure Characterization of Mechanically Activated Hematite using XRD Line Broadening, *International Journal of Mineral Processing*, in press.
- [18] A.Z. Juhasz, Mechanochemical activation of silicate minerals by dry fine grinding, *Aufbereitungs-Technik* 10 (1974) 558–562.
- [19] R.A. Kleiv, M. Thornhill, Mechanical activation of olivine, *Minerals Engineering*, 2005, forthcoming
- [20] H. Heegn, Changes in the properties of solids during mechanical activation and fine grinding. In: Sc.D. Thesis, Research Institute of Mineral Processing of the Academy of the GDR, Freiberg (in German) (1986).
- [21] H. Heegn, Concerning some fundamentals of fine grinding. In: Leschonski, K., Editor, 1986. *Proc. 1st World Congress on Particle Technology, Part II. Comminution*, Nürnberger Messe und Ausstellungsgesellschaft, Nürnberg (1986), pp. 63–67.
- [22] D. Balzar, Voigt-Function Model in Diffraction Line-Broadening Analysis, in *Defect and Microstructure Analysis from Diffraction*, edited by R.L. Snyder, H.J., Oxford university (1999), New York, pp. 94-126.
- [23] A.R. Stokes, A numerical Fourier-analysis method for the correction of widths and shapes of lines on X-ray powder photographs, *Proceedings of the physical society* 61 (1948), London, pp. 382-391.
- [24] H. Heegn, Effect of fine grinding on structure and energy content of solids, in: *Proc.of 6th POWRECH* (1979), Birmingham, pp. 61-69.
- [25] K. Tkacova, H. Heegn, N. Stevulova., Energy transfer and conversation during comminution and mechanical activation, *International journal of mineral processing* 40 (1993) 17-31.
- [26] G.K. Williamson, R.E. Smallman, Dislocation densities in some annealed and cold-worked metals from measurements on the X-ray Debye-Scherrer spectrum, *Philosophical Magazine* 1 (1956) 34-45.
- [27] D. Tromans, J.A. Meech, Enhanced dissolution of minerals: stored energy, amorphism and mechanical activation, *Mineral Engineering* 14(11) (2001) 1359-1377.

- [28] K. Miyasaka, M. Senna, Calorimetric and thermoanalytical assessment of mechanically activated PbCO_3 , *Thermochemica Acta* 83 (1985) 225-233.
- [29] K. Tkacova, H. Heegn. N. Stevulova., Changes in structure and enthalpy of Carbonates and Quartz accompanying grinding in air and aqueous Environments, *Powder Technology* 52 (1987) 161-166.
- [30] M. Senna, The evaluation of activity and reactivity of mechanically treated fine powdered materials, *Kona* 5 (1987) 76-81.
- [31] M. Senna, Determination of effective surface area for the chemical reaction of fine particulate materials, *Particle and Particle Systems Characterization* 6(1989) 163-167.
- [32] K. Tkacova, P. Balaz, Structural and temperature sensitivity of leaching of chalcopyrite with Iron (III) sulphate, *Hydrometallurgy* 21 (1988) 103-112.
- [33] P. Balaz, A. Alacova, M. Achimovicova, J. Ficeriova, E. Godocikova, Mechanochemistry in hydrometallurgy of sulphide minerals *Hydrometallurgy* 77 (1-2) (2005) 9-17.

Paper IV

Statistical Interpreting and Modeling of Microstructural Characteristics of Mechanically Activated Hematite in Different Grinding Environments

Parviz Pourghahramani, Bertil Pålsson & Eric Forssberg, Submitted for publication in International Journal of Mineral Processing

Statistical interpreting and modeling of microstructural characteristics of mechanically activated hematite in different grinding environments

Parviz Pourghahramani^{*}, Bertil Pålsson and Eric Forssberg

Division of Mineral Processing, Luleå University of Technology, Luleå, Sweden

Abstract

A statistical analysis was done to investigate the relationship between grinding variables and structural changes during mechanical activation of hematite concentrate. Experiments were carried out according to a statistical design by varying the grinding time, media surface and mill type.

The variance analysis revealed that the media surface and grinding time significantly influence the five main response variables at 95% confidence level. An overview principle component analysis (PCA) on 27 variables yielded a three component model explaining 89% and predicting 76 % of the total variance. It was found that the observations belonging to low and high levels of media surface fall into two groups regardless of grinding mills. Most of the microstructural characteristics such as microstrain, dislocation and amorphization and granulometric surface area, BET specific surface area, specific energy input, stored energy, portion of smaller particles and stress energy coincide with high level of media surface group. The variables crystallite size, peak intensity and mean particle size appear with lower media surface. The PLS-DA (partial least squares discrimination analysis) made it possible to discriminate the three types of mills. From the projection of dummy variables, it was concluded that the vibratory mill caused comparatively less structural changes in hematite than the other mills in spite of releasing higher stress energy. The planetary mill introduced relatively higher dislocation defects and generated higher lattice strain. The hematite ground in tumbling and planetary mills had comparatively higher X-ray amorphization degree and subsequently higher excess energy than hematite ground in the vibratory mill. The tumbling mill produced relatively lower specific surface than the others. It was concluded that the products of tumbling mill represented higher defect concentration (amorphization) per unit surface area despite releasing lower stress energy level by the mill.

The PLS modeling of five main response variables gave one statistically significant component model with $R^2X = 0.52$, $R^2Y = 0.78$ and $Q^2 = 0.74$. The X variables specific energy input and stress energy were found as the most influencing factors.

Keywords: Iron ore, Mechanical activation, Statistical analysis, Structural changes, Modeling

1. Introduction

In recent years, mechanical activation of minerals is attracting a lot of interest from both technological and scientific point of view since structural changes affect strongly the properties of mechanically activated materials. Mechanical activation by grinding is a complex process involving alteration of structure, chemical composition, phase transformation and solid reactivity. According to Huttig (1943), the reactivity of a solid

^{*} Corresponding author: Tel:+46 920 491313; fax:+46 92097364
E-mail address: Parviz.Pourghahramani@ltu.se

system is the difference in free enthalpies between the activated and non-activated states. During mechanical activation the free energy of particulate material increases by addition of both surface free energy and volumetric strain energy. Consequently, the gained free energy can be relaxed through different available modes of energy relaxation as a formation of defect structure, agglomeration, amorphization and polymorphic transformation (Lin, 1998). Such structure defects determine the reactivity of materials (Boldyrev et al., 1996). As a result of previous investigations (Heegn, 1979; Tkáčová et al., 1993; Tromans and Meech, 2001) the defect structures of essential meaning for the energetic condition of the solids are: (1) dislocation concentration, (2) new surface formation, and (3) content of newly-formed phases and amorphous phases. In the case of negligible entropy (crystal structure disordering is slight), the difference of free energy between the activated and non-activated states can be predominantly determined by changes of enthalpy (stored energy relating to long-lived defects).

The requirements for finer powders having specific microstructure characteristics have been arisen as results of the development of new processes and products in chemical, minerals and ceramics industries. The detailed explanation of the correlation between grinding variables and structure defects to control their properties is of major significance for mechanically activated materials. The nature and the rate of structural and chemical transformations depend on both the powder properties and the ultimate limit of structural and thermodynamic stability reached during the mechanical activation. The latest, in turn, should be related to the severity of mechanical deformation at impact and then to the force acting on, or to the energy transfer to the powder trapped during a collision. Several attempts have been made to understand the relationships between grinding factors and changes in structure during mechanical activation. Karagedov and Lyakhov (2003) investigated the influence of the density of milling media in mechanical activation of inorganic oxides. Dry grinding was found to be more effective than wet milling in the dissolution of tantalite despite the generation of large specific surface in wet milling (Welham, 2001). Welham and Llewellyn (1998) reported that the crystallite size decreased exponentially and strain increased by extending of milling periods during the mechanical activation of ilmenite. Baláž et al. (1988) carried out a comparative study to investigate mainly the influence of mill types (attritor, ball and vibratory) on the reactivity of sulphide minerals. Baláž (2000) described the process of new surface formation in terms of milling time and the relationship between the deformation and surface area for sulphide minerals.

It was also stated that the kinetics of the microstructure evolution during the extended milling depends on the characterizing treatment in a milling device and mechanical properties of the material. For activation to take place, intensive grinding is needed to transfer sufficient energy to the particles being ground. In this area, a variety of milling equipment such as attritor, vibratory, planetary and tumbling mills have been used for mechanical activation in which the repetitive loading of particles takes place and consequently the plastic deformation induces in material network.

The objective of this study is to investigate the effects of grinding variables of mill type, grinding time, media surface the microstructure evolution during mechanical activation of hematite concentrate from a statistical view point. In addition to significance level and importance of the grinding variables, attempts were made to find how microstructure characteristics differ vs. grinding variables and what grinding conditions are appropriate for inducing large structural changes. In addition, the study put forward a key for prediction of structural changes considering several grinding variables simultaneously in stead of a single

variable. In the present work, variance and multivariate analysis are applied. Five models are proposed to describe different microstructure characters in terms of the five grinding variables. Warren-Averbach method and line profile analysis (LPA) of X-ray data are used as the main characterization tools. Data have been collected according to an experimental design.

2. Experimental

2.1. Grinding

Three types of mills with loose media, tumbling, vibratory and planetary mills are applied in this study. To increase grinding intensity, grinding time and media surface were extended up to 9 h and 4 m^2 per kg of hematite respectively. The structural changes in hematite concentrate during mechanical activation were investigated. For data collection, a full factorial design with one qualitative and two quantitative factors was constructed. The qualitative factor, grinding mill, was set at three levels; tumbling, vibratory and planetary mills. The quantitative grinding time factor was leveled at 1, 3 and 9 hours. The two levels 1 and 4 m^2 per kg of material were chosen for media surface variable.

Dry grinding experiments were conducted according to the design in air atmosphere. The grinding tests were made in closed condition, i.e., the lids of the mills were kept bolted during the grinding. Steel media between 22.2 and 6 mm with bulk density (apparent density) of 4875 kg/m^3 was applied as grinding media. The media surfaces were calculated from number of grinding bodies and their dimensions. The material temperature was measured by a thermometer immediately after stopping the mill. The active energy consumed by the mills was measured by an electrical meter Micro VIP (Elcontrol Co., Italy). The obtained samples were sealed into plastic tubes and kept in a freezer for further analysis. Among the mills used, only the vibratory mill had plastic liner. The stress energy (specific grinding work) was calculated by an expression proposed by Heegn (1986, 2000):

$$SE = \frac{1}{2} \left(\frac{m_1}{m_2} nt \right) v^2 \quad (1)$$

where m_1 , m_2 , n , t , v correspond to mass of grinding media, mass of material charge, mill speed, grinding time and stress rate in different mills respectively. Although the rate of stress has a distribution in grinding mills, the maximum stress rate is determined by the specification of mills to give an insight into grinding intensity. The stress energy takes into account several grinding variables simultaneously. The rate of stress was estimated for planetary and tumbling milling operations from the gravitational acceleration (tumbling mill $b/g=1$ planetary mill $b/g=1.67$) and mill diameter and for vibration mill from the frequency and amplitude. The experimental milling conditions are given in Table 1.

Table 1. Experimental milling conditions and mill types.

Milling conditions	Tumbling mill	Vibratory mill	Planetary mill
Media filling (%)	38.9	70	23.4
Ball to powder weight ratio	16.77:1, 67:1	16.92:1, 67.68:1	19.1:1, 76.34:1
Speed (RPM)	60	1000	100 (axle), 200 (drum)
Amplitude (mm)	--	8	--
$L \times D$ (mm \times mm)	275 \times 245	320 \times 185	87 \times 115
Stress rate (m/s)	2.2	1.67	1.95

2.2. Characterization

The particle size distribution of samples was measured by method of laser diffraction (CILAS 1064) in the liquid mode. The mean particle size and granulometric surface area were calculated based on the particle size distribution assuming spherical shapes for particles. The specific surface area was determined using the nitrogen adsorption method (BET) with Flow Sorb II 2300 (Micromeritics Co. Ltd., USA), from which another mean particle size was estimated. Both calculated mean particle sizes were inserted in the dataset. The density of samples was measured by a Pycnometer (Micromeritics Co. Ltd., USA).

The X-ray diffraction (XRD) patterns were collected using a Siemens D5000 powder diffractometer with Bragg-Brentano geometry equipped with a curved graphite monochromator in a diffracted beam arm and using Cu K α ($\lambda = 0.154nm$) radiation. The XRD patterns of samples were recorded in the range of $2\theta = 10^\circ - 90^\circ$ using a step size of 0.02° and a counting time of 5 seconds per step. The eight most intensive reflection peaks of hematite were considered for further characterization and line profile analysis (LPA), known as line broadening technique, was applied. The Profile software (Siemens AG, 1996) was used in profile fitting procedure to extract the line broadening characters. For this purpose, the Pseudo-Voigt line shape function (a linear combination of Cauchy and Gaussian line shape functions) was fitted to the recorded XRD diffraction patterns. For each adjusted line profile, the following parameters were obtained: (1) the maximum height of the peak (I_{max}), (2) the integral breadth of line profile ($\beta = A/I_0$ where A is the peak area), (3) the full-width at half of maximum (FWHM), (4) the mixing factor (η) of Lorentzian and Gaussian functions and (5) peaks position (2θ).

For the deconvolution of strain and crystallite contributions, Williamson-Hall (1953) and Warren-Averbach (Warren, 1969) approaches were used. The Warren-Averbach method was applied in [012] direction. In the Williamson and Hall method, the physical line broadening was obtained after excluding the instrumental broadening to XRD line breadth using a standard sample, LaB₆, according to the Halder-Wagner (1966) approximation. Consequently, the lattice stain and crystallite size were calculated. The definition of expressions and detail information regarding to line profile analysis (LPA) and extracting the physical line broadening can be found in previous work (Pourghahramani and Forssberg, 2006a).

The dislocation density was estimated according to the Williamson and Smallman (1956) formula. The quantitative estimate of the increase in molar chemical free energy (increase in stored energy or enthalpy) due to dislocation defects was calculated by expression proposed by Tromans and Meech (2001):

$$\Delta H_d \approx (\rho M_v) \frac{b^2 \mu_s}{4\pi} \ln \left(\frac{2(\rho)^{-1/2}}{b} \right) \quad (4)$$

where M_v , b , μ_s and ρ correspond to the molar volume of mineral, Burgers vector, elastic shear modulus and dislocation density respectively.

Energy fractions of newly-formed phases (our investigations suggested only amorphization not the formation of other new phases) and the BET specific surface area as a measure for the

grain boundary to the surrounding medium were evaluated by equations expressed by Baláz et al. (2005) and Heegn (1979) respectively:

$$\Delta H_A = C_A E_A \quad (5)$$

$$\Delta H_S = \sigma_S o_S \quad (6)$$

where C_A , E_A , σ_S and o_S denote the concentration of amorphous phase, molar amorphization energy, specific interfacial energy and the BET specific surface area, respectively. The total stored energy (enthalpy) in the activated hematite concentrate was obtained by addition of the three sources of energy contributions to defect structures. Finally, data have been analyzed by commercial computer programs STATGRAPHICS PLUS 5.0 (Manugistics, 1999) and SIMCA-P10.0 (Umetrics, 2002).

3. Results

Based on a full factorial design, 18 experiments were conducted. At the first step, the five main response variables, which are thought to be of interest and importance in mechanical activation process, were considered. The design and response variables are given in Table 2. The response variables include the BET specific surface area, crystallite size and lattice strain obtained from the Warren-Averbach approach, amorphization degree and stored energy.

Table 2. Experimental worksheet and experimental results for five main response variables

Grinding variables			Response variables				
Grinding mill	Grinding time (h)	Media surface (m ² /kg)	X-ray amorphous (%)	Crystallite size (nm)	Lattice strain (%)	Specific surface area (m ² /kg)	Stored energy (kJ/mole)
Tumbling	1	1	30	54.16	0.062	1.41	27.72
Vibratory	3	1	41.4	43.5	0.208	3.98	38.9
Vibratory	1	1	23.04	73.5	0.175	1.88	21.57
Vibratory	9	4	81.73	13.5	0.395	18.42	80.00
Tumbling	3	4	73.5	25.0	0.284	5.34	68.59
Planetary	9	1	71.69	16.5	0.301	4.42	66.72
Vibratory	9	1	58.3	29.6	0.258	5.18	54.59
Planetary	1	4	57.58	28.1	0.194	5.12	53.95
Planetary	1	1	38.59	66.7	0.125	2.12	35.73
Tumbling	9	1	71.69	27.3	0.225	4.58	59.22
Tumbling	1	4	59.45	44.4	0.224	4.12	55.34
Vibratory	3	4	63.00	23.7	0.279	7.52	59.59
Planetary	3	4	76.34	11.6	0.444	8.00	72.22
Planetary	9	4	85.47	5.6	0.532	8.82	81.32
Planetary	3	1	52.43	20.5	0.203	3.37	48.79
Tumbling	3	1	51.5	42.6	0.152	2.58	47.68
Vibratory	1	4	55.57	36.4	0.184	4.37	51.91
Tumbling	9	4	80.319	17.3	0.44	6.83	75.35

3.1. Analysis of variance (ANOVA)

The analysis of variance (ANOVA) is used to check regression model significance. The initial analysis of the design suggested that the underlying assumptions were not valid for crystallite size response. Therefore, its natural logarithm was tested and considered in analysis. The significance levels (P-values) for grinding factors and their interaction are summarized in Table 3. If the significance level for a factor is less than 5%, the factor is statistically significant with 95% confidence.

Table 3. Significance levels (P-values) for main response variables

Source	Specific surface area	X-ray amorphous	Lattice strain	Ln(crystallite size)	Stored energy
Main effects					
A: Grinding mill	0.2573	0.0309	0.0666	0.0026	0.0251
B: Grinding time	0.0605	0.0005	0.0018	0.0003	0.0003
C: Media surface	0.0192	0.0004	0.0012	0.0004	0.0001
Interactions					
AB	0.4732	0.9044	0.3286	0.0721	0.5179
AC	0.4547	0.3768	0.1097	0.0911	0.3076
BC	0.4267	0.1509	0.1202	0.4025	0.3131

From Table 3, it is apparent that the significance levels of grinding variables differ for different response variables and a distinguished difference can be observed in P-values between the BET specific surface area and other response variables, i.e., the P-values for the BET specific surface area are larger than the other response variables. The comparison of the significance levels of the three main factors for response variables indicates that the grinding mill factor is the least influencing factor. Surprisingly, grinding mill factor does not have statistically significant effect in the production of the BET specific surface area even at 90% confidence level.

Surprisingly once more, none of interaction terms has a statistically significant effect on the response variables at 5 % significance level. i.e., the grinding variables influence independently most of the response variables. To assist the interpreting of the results, it is helpful to construct a graph of the average responses at each treatment combinations. The interaction plots AB are depicted in Fig. 1 as an example. It is clear that the use of higher media surface and prolonged grinding brings about more structural changes whatever milling devices are used. From the grinding mill and grinding time interaction plots (AB) it can be observed that the samples ground in vibratory mill have comparatively larger crystallites, higher BET specific surface area at prolonged milling, lower stored energy and amorphization degree than the products of the other used mills. i.e., the grinding time and media surface effects are the lowest when the vibratory mill used. The changes in the BET surface area between initial and prolonged stages of milling for hematite ground in the vibratory mill are conspicuous because of the generation of higher temperature (105 °C) and releasing of higher stress energy compared with the other used mills. The planetary mill products yielded more structural changes in hematite crystal.

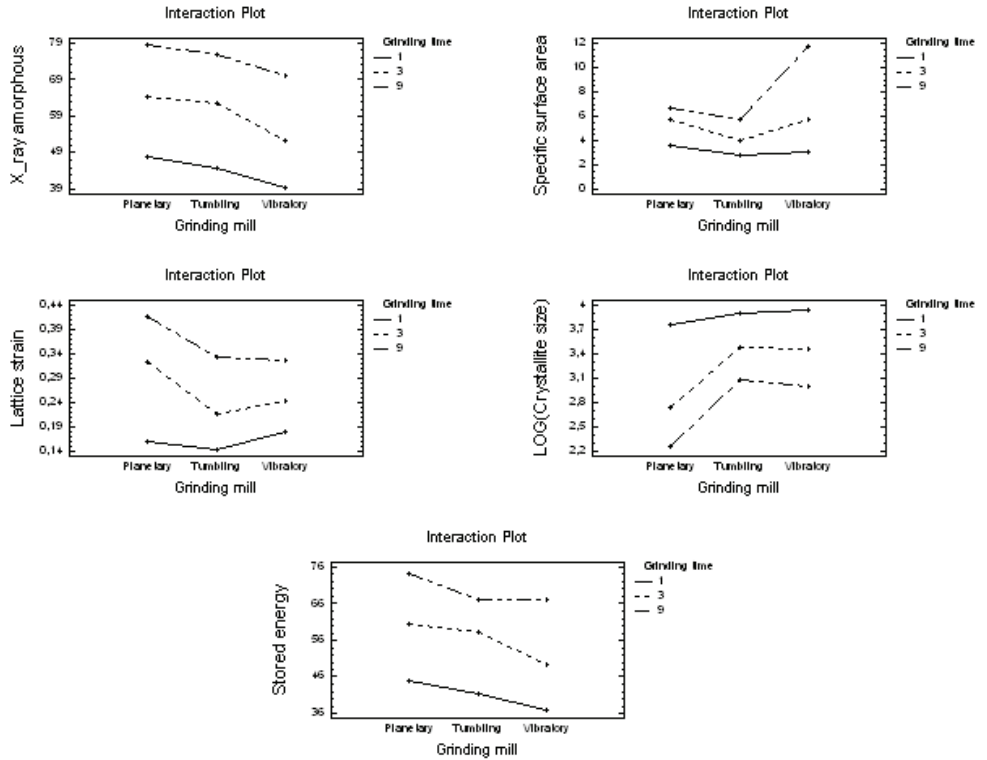


Fig. 1. Interaction plots for response variables.

3.2. Multivariate analysis

The most important feature of principle component analysis (PCA) method is its ability to project mathematically high dimensional process and quality data into smaller dimensional summary data set (Jackson, 1991). The most important advantages of PCA analysis are provision of data dimension reduction and robustness to highly correlated, noisy and missing data. In other words, if there are many variables and several factors, the multivariate analysis is better suited to analyze such problems compared to classical methods of statistics.

3.2.1. An overview PCA analysis

In our case study, the grinding tests were considered as objects. The microstructure characters and grinding factors were regarded as variables. In addition to the five main response variables (Table 1), the particle size data, line profile analysis (LPA) of XRD diffraction peaks, stress energy, ball to powder weight ratio and specific energy input were measured and inserted in data set. The complete data set is given in Appendix 1 and Table 1. The identification codes for the objects and variables are also given in Appendix 1 and Table 2. Thus, a data set is created with 18 objects and 27 variables.

An important step in principle component analysis (PCA) is pre-processing of measured data to adjust it to facilitate data analysis and model interpretation. The investigation of data set revealed that twelve variables have deviation from a normal distribution with large skewness

and low minimum to maximum ratio. Consequently, logarithmic transformation was carried out for 12 variables. Running the SIMCA software produced a PCA model having three statistically significant components. The cumulative explained variation is 89% and the cumulative predicted variation is 76% of the total variance. These goodness values imply a fairly good PC model.

Fig. 2 makes it possible to follow how the individual variables are modeled by the different principle components. The majority of microstructure variables are accounted for in the first component. The variables Gs, Sz and $fr < 10 \mu m$ and $fr < 1 \mu m$ are rather well captured by the second components and the grinding factors, material temperature (MT) and density (De) by the third components.

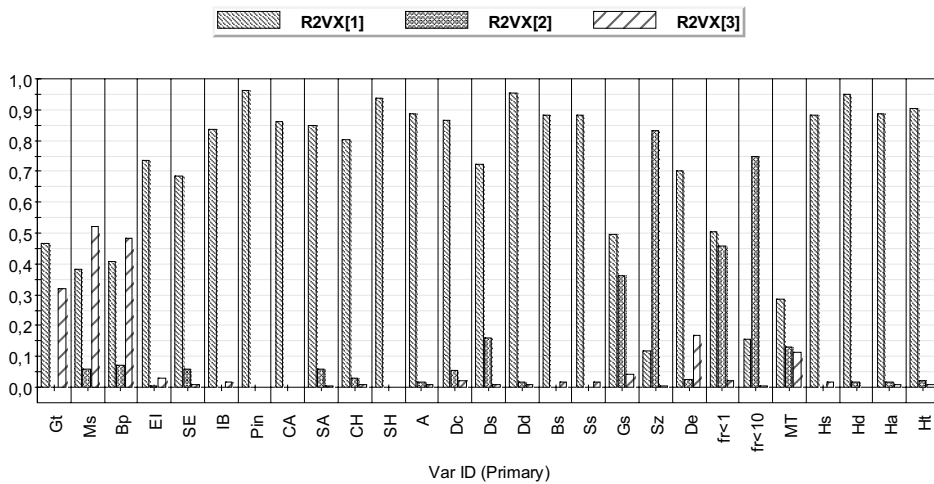


Fig. 2. Explained variation of the 27 variables by different PCA components

Studying of the score and loading plots of PCA model is a powerful presentation to have an overview of the model. The score plot shows how the observations are projected in two dimensions. The loading plot displays the relationship among the variables. This study presents only the score plot (t1/t3) and loading plot (p1/p3) because PC2 component does not give any clear grouping among the observation.

From the score plot (t1/t3) in Fig. 3, it is clear that the observations obtained from higher and lower media surfaces are fully separated from each other in Y-direction. In addition, a clear trend in each group can be observed. As the intensity of milling (grinding time) increases, the observations shift from the left to the right side of the plot. The observations that contain similar characteristics are projected closely to each other. However, grouping in terms of mill types can not be observed in the score plots. Following the trends in the projected observations within each group reveals that the array of the projected observations is regular for an identical grinding time, i.e., the projected order with increasing grinding time in both groups are: tumbling, vibratory and planetary identically.

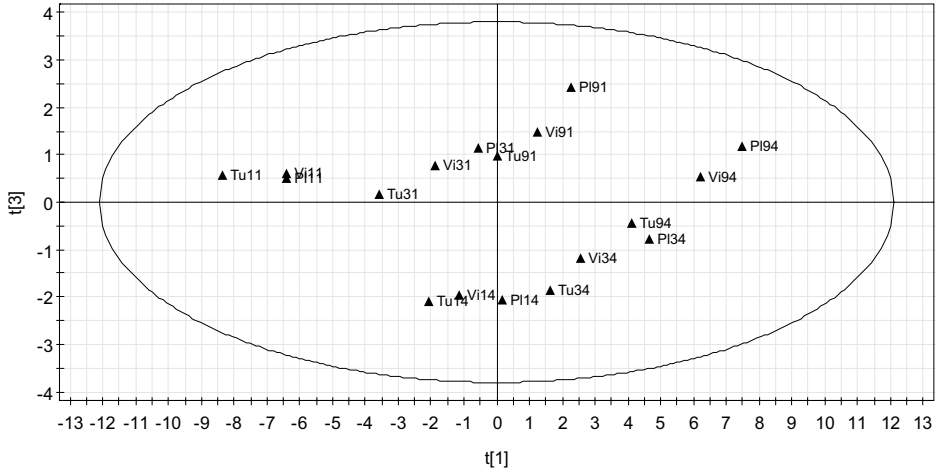


Fig. 3. PCA score plot (t_1/t_3) of data set. Terms PI, Tu and Vi denote planetary, tumbling and vibratory mills respectively. Hereafter, the first and second number after each abbreviation refer to the grinding time level (h) and media surface (m^2/kg) respectively.

According to the loading plot (p_1/p_3) in Fig. 4, it can be seen that two main groups of variables are fairly correlated in the left and right sides of X-direction: the variables CH, CA, Bs, Pin in left and the variables IE, SE, Dc, Ds, Dd, IB, SA, SH, A, Ht, Ha, Hs, Hd in the right part of the plot. The variables within both groups are far from the origin and subsequently have high influence on the model. The variables within each main group are correlated positively as well. Further, two main groups of correlated variables in the left and right sides of the plot are negatively correlated. This means that the reduction in the peak intensity (Pin), BET size (Bs) and crystallite size (CA and/or CH) with extending the milling intensity, correlates with an increase of the variables in the right hand of plot (IE, SE, Dc, Ds, Dd, IB, SA, SH, A, Ht, Ha, Hs, Hd). This is a basic concept in the characterization of microstructure characters based on the line profile analysis (LPA) of XRD diffraction (Pourghahramani and Forssberg, 2006a, b). These correlations show that with increasing grinding intensity more defects are induced in the hematite structure. As the grinding time goes up, the broadening of the diffraction peaks increases and the intensity of diffraction peaks decreases. This indicates that the degree of lattice disorder increases, the crystallite size decreases and the symmetry of the unit cell reduces until some fraction of the material becomes amorphous.

In addition, the variable media surface has a strong and positive correlation with ball to powder weight ratio. Interestingly, the portion of particles smaller than $1\ \mu m$ is positively correlated with granulometric specific surface area. This suggests the role and importance of such fraction of particles in dry grinding in the agglomeration of particles. As the agglomeration takes place, the BET surface area and the portion of particles $fr < 1\ \mu m$ decline. Moreover, the crystallite size displays a positive and strong correlation with the mean particle size that obtained from the BET specific surface area but not to that measured by laser diffraction method. This is because of the estimation of particle size of activated material in dry and prolonged milling is not reliable due to agglomeration of particles and only gives the

apparent particle size despite the BET method. The difference between crystallite size and strain obtained from the Williamson-Hall method (CH, SH) and Warren-Averbach approach (CA and SA) is related to the reliability of the Williamson-Hall method (Pourghahramani and Forssberg, 2006a).

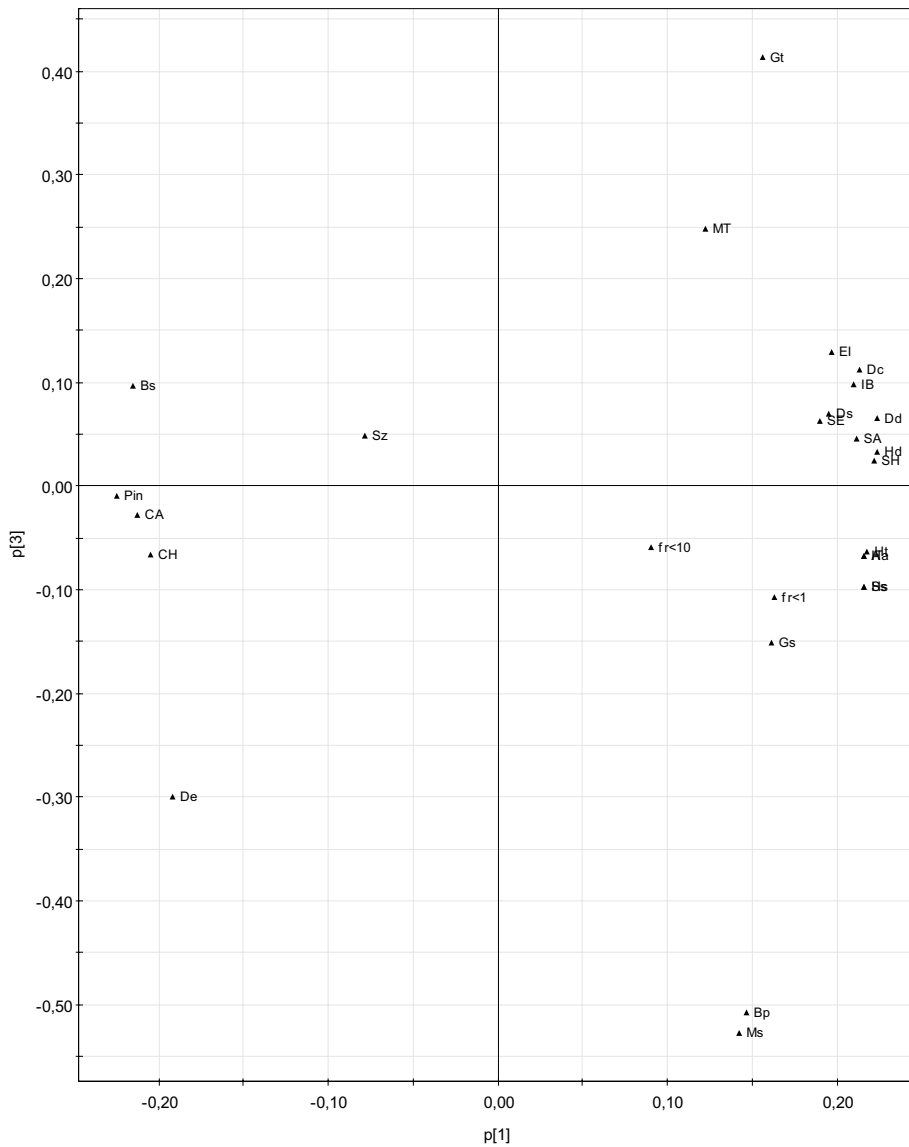


Fig. 4. Loading plot ($p1/p3$) of data set

The comparison of the loading and score plots (Figs. 3 and 4) reveals that the objects concerning low intensity of milling (short milling time and lower media surface) display large crystallites, BET size and higher peak intensity. As the milling time increases, objects shift to the right side of X-direction. The test samples of Tu11 and P194 yield the weakest and strongest structural changes during mechanical activation of hematite respectively. Other observations lead to the structural changes in magnitude spreads between those two limits. We can draw a conclusion that the variables of Sz, CA, CH and Pin correlate to low level of media surface, i.e., the observations obtained while grinding by applying low media surface ($Ms=1\text{ m}^2/\text{kg}$) have comparatively high level of such parameters. The variables of material temperature (MT) and grinding time belongs to both groups with a first approximation. Most of microstructure characters (IE, SE, Dc, Ds, Dd, IB, SA, SH, A, Ht, Ha, Hs, Hd), $fr<1\text{ }\mu\text{m}$, $fr<10\text{ }\mu\text{m}$ and Gs, are responsible for observations obtained from the grinding with higher media surface.

3.2.2. Class analogy recognition

It is desirable to analyze the similarities in the observations in terms of grinding variables. The question is, can the observations be separated and, if so, how do they differ with respect to each other and grinding variables.

To find how the observations belonging to the levels of media surfaces are differentiated, the SIMCA (soft independent modeling of class analogy) method (Wold, et al., 1984) was used. This method comprises the establishment of a work set with two classes, one for each media surface level. The aim was to investigate whether it would be possible to use the local PCA-models for classification. Therefore, PCA was used to model separately each class. Cross validation was used to determine the optimal complexity of each class model. Class 1 and class 2 correspond to low ($Ms=1\text{ m}^2/\text{kg}$) and high ($Ms=4\text{ m}^2/\text{kg}$) levels of media surface respectively. PCA analysis on each class indicated that one significant component is necessary to model adequately the class1 and class2 sample sets, respectively. The model of class 1 is characterized with $R^2X=0.78$ and $Q^2=0.70$ and the class two with $R^2X=0.67$ and $Q^2=0.55$. Fig. 5 shows DModx (class distance) for the class of higher media surface. The displayed critical distance D-Crit corresponds to 5% level, and defines a 95% tolerance interval. We find that all observations belonging to higher media surface class are within the critical distance. Moreover, it is obvious that lower media surface observations are outside of the tolerance interval of higher media surface DModx model, indicating that the observations belonging to higher media surface do not fit the observations of low media surface (class1). Consequently, they are different from each other. These results are in correspondence with the score plot (t1/t3) in Fig. 3. As a result, the similarities among the observations obtained using the same media surface exists in spite of applying different mills and grinding times in experiments. We can say that changing of media surface leads to drastic structural changes in hematite and media surface appear as an important factor in the grinding process. We can say if the similar structural changes are desirable, it is better to make grinding experiments for the same media surface level.

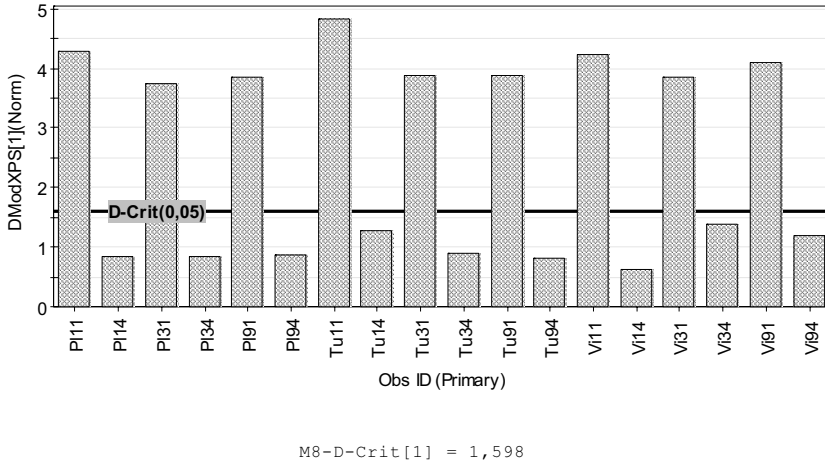


Fig. 5. DModx plot for high level of media surface ($M_s=4 \text{ m}^2 / \text{kg}$)

As discussed earlier, the classification of mill types has not been identified using score plots. In order to understand whether further separations are possible and which variables contribute to the separation, PLS-DA (partial least squares discrimination analysis) method (Sjöström et al., 1989) was used. PLS-DA analysis makes it possible to achieve a rotation of the projection to give latent variables that focus on class separation. PLS-DA encodes a class identity in the form of dummy variables, which is an artificial variable that assumes a discrete numerical value in the class definition. A dummy matrix of three Y-variables expressing class identity (mill type) of the samples was constructed using SIMCA software. PLS-DA analysis using SIMCA software yielded a four component model with $R^2X=0.90$, $R^2Y=0.87$ and $Q^2=0.62$. It should be noted that the Eigen value for the forth component is close to unity and making it weak. The forth component captures mainly the size characters obtained using laser diffraction method. Without the forth components, the model characterizes with $R^2X=0.85$, $R^2Y=0.70$, and $Q^2=0.421$. PLS score plot for the model with four components is given in Fig. 6. From the investigations of the score plots, it was found that the components t1 and t2 (t1/t2) displayed separation better than other components. As seen, the different mills are fairly separated from each other in the second direction, Y, in a way that the observations of tumbling, planetary and vibratory mills are placed in upper, middle, and lower parts of the plot, respectively. This implies that three mills might be different from each other based on data set variables.

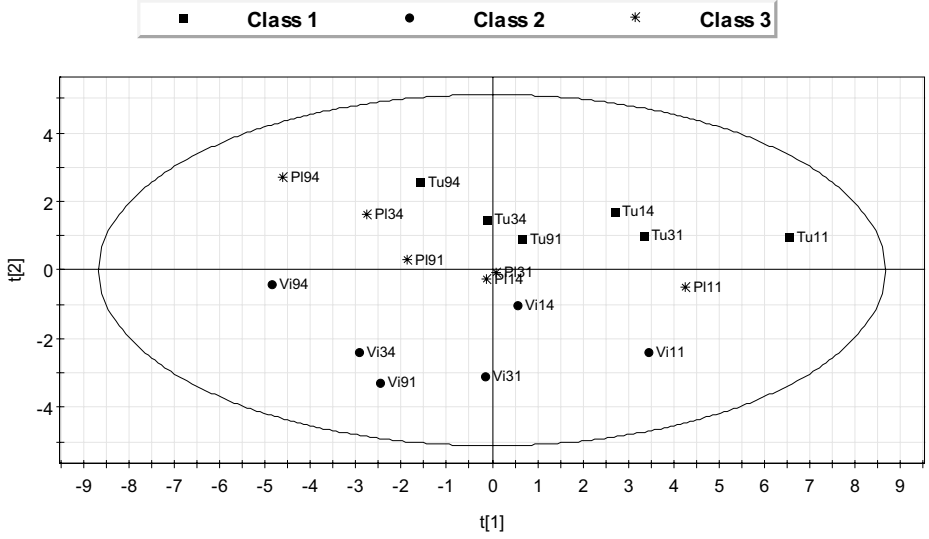


Fig. 6. PLS score plot and distributions of three dummy variables

The analysis of dummy variables is valuable. The three dummy variables are named by \$DA1 (tumbling mill), \$DA2 (vibratory mill) and \$DA3 (planetary mill) (Fig. 7). The variables close to a dummy variable contribute strongly to the separation of the class. The planetary mills observations have comparatively higher dislocation density, its energy contribution, lattice strain and integral breadth in spite of releasing lower stress energy. These variables are grouped with Bp, Gt and Ms as grinding variables, i.e., higher ball to powder weight ratio, media surface and grinding time favor the induction of higher lattice strain and dislocation defects in planetary mill compared to the other mills used. The observations of tumbling mill have relatively larger particle (S_z), higher material density, lower stress energy and lower specific energy input. The products of tumbling and planetary mills yield higher amorphization degree amorphization energy and subsequently higher total stored energy (excess enthalpy) than the products of the vibratory mill. The vibratory mill observations have comparatively high material temperature, stress energy, large crystallites and roughly higher portion of smaller particles than $1\ \mu m$ and $10\ \mu m$. This implies that the grinding in vibratory mill brings about less plastic deformation and changes in the structure of hematite despite releasing higher stress energy, suggesting lower efficiency of vibratory mill than other mills used.

On the other hand, some discrepancies can be observed between tumbling and planetary mills. In addition to the production of larger particles in grinding with tumbling mill, it has been granted approximately the same level of amorphization, amorphization energy and total stored energy in planetary mill. The observations of tumbling mill have relatively lower BET surface area; therefore, it can be concluded that the amorphization degree per unit surface area in tumbling mill is slightly higher than planetary and vibratory mills. Comparing the stress energy and specific energy input shows that vibratory mill needs more stress energy to

reach the same effect as tumbling and planetary mills. In addition, the vibratory grinding device produces relatively smaller particles but does not lead to smaller crystallite size in spite of the planetary mill, i.e. the crystallite size depends not only on particle size reduction, but also on defect concentration in hematite.

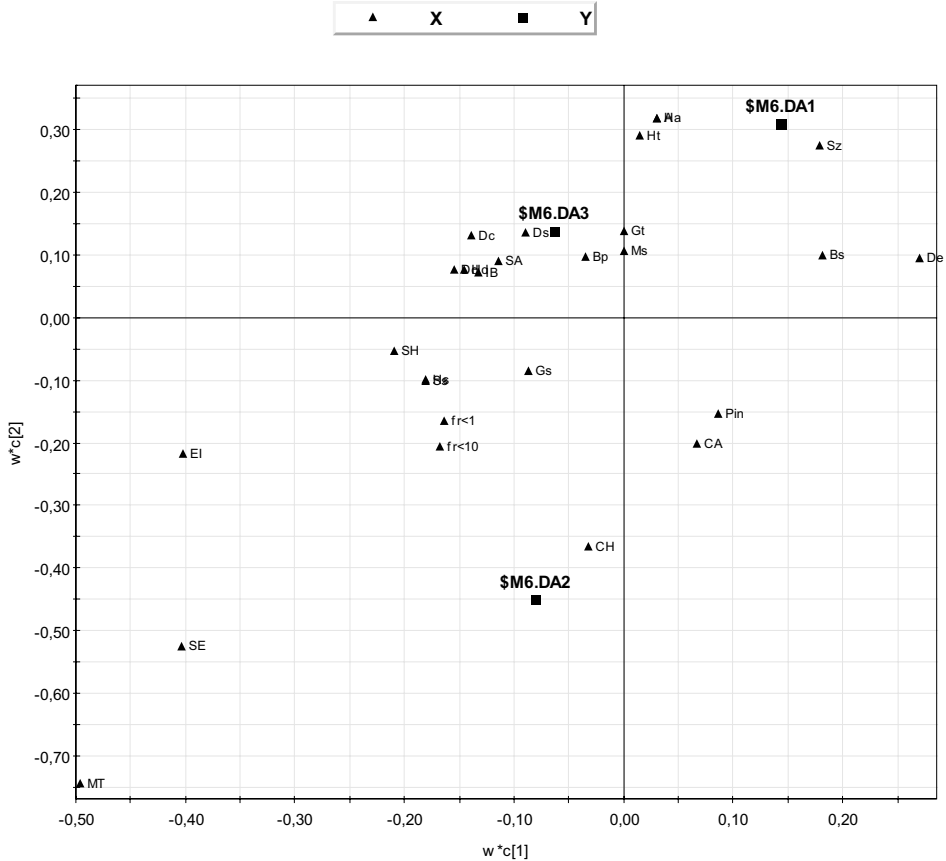


Fig. 7. PLS weight plot and distributions of three dummy variables

To investigate the discriminatory power of each variable, the variable importance plot (VIP) was constructed, which is an overall assessment of the variable importance. Fig. 8 displays the VIP plot for the PLS-DA model. The two strongest variables are energy input (EI) and Material temperature (Mt). This is mainly because only the vibratory mill had plastic linear among the used mills and it resulted in higher material temperature. The Energy input (EI) strongly depends on the mill geometry and manufactured characteristics. It is clear that several microstructure characters such as CH, CA, Ds, Ht, Ha, A and particle size accounted for a strong discriminatory power, which have higher VIP than 1. This reveals that not only the structural changes are contributed fairly to the classification of mills but also the mills

characteristics also have strong effect on the classification of the mills. The variables with smaller VIP than 1 have relatively less influence on the classification than of those having higher VIP.

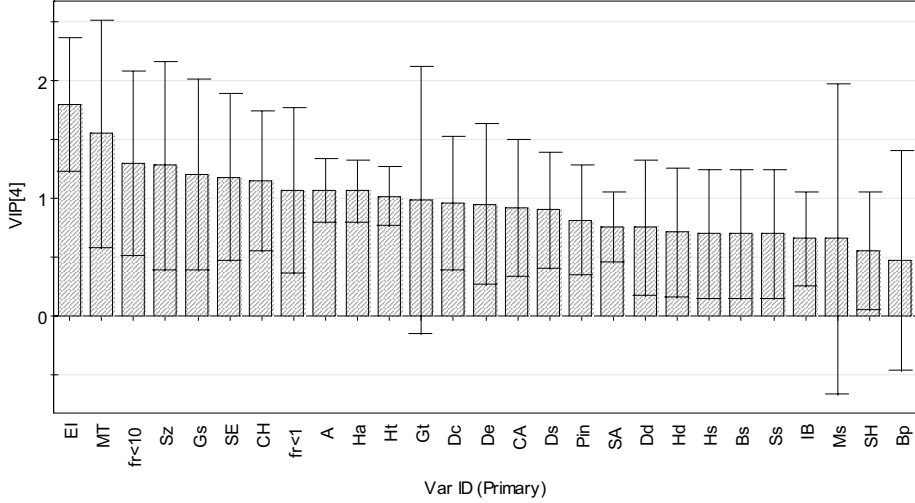


Fig. 8. VIP plot of the PLS-DA model

3.2.3. PLS analysis

PLS is used to connect the information in two blocks of variables X and Y to each other. The objective of PLS analysis in our case is to investigate the influence of five main X variables on the five response variables Y. The X-variables are media surface, grinding time, ball to powder weight ratio, specific energy input and stress energy. A detail analysis was performed for the most important microstructure characters to predict the effects of X-variables on the generation of microstructure characters in mechanically-activated hematite concentrate. A PLS model was constructed with the five X variables and five response variables simultaneously to find the prediction equations. The X matrix was expanded with cross and quadratic terms since the experiments were conducted according to a full factorial design. It was further refined with regard to VIP plot, which summarizes the importance of X-variables, for both the X and Y models (Eriksson et al., 2000). Consequently, the final PLS modeling yielded one significant component model with $R^2 X = 0.52$, $R^2 Y = 0.78$, and $Q^2 = 0.74$. This is a fairly acceptable model. The PLS weight plot does not carry more information and has not been reported here. The VIP plot for final PLS model is presented in Fig.9. Two predictors of specific energy input and stress energy with large VIP (larger than 1) are the most influential factors in the model. Since the stress energy takes into account the number of impulses, the rate of stress and ball to powder weight ratio is better suited to explain the response variables rather than individual variables such as grinding time, media surface and ball to powder weight ratio. As the energy input depends on the geometry of mills and their scales, we can conclude that the stress energy appears as a promising factor to explain better grinding

processes. It should be noted that the square term of grinding time also contributed to the model.

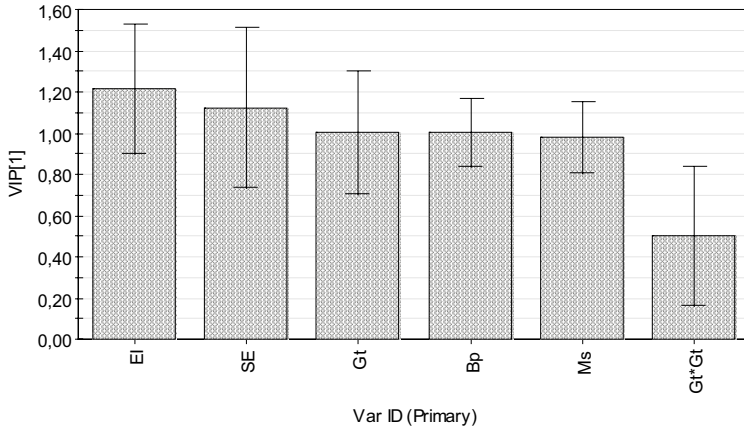


Fig. 9. VIP plot of PLS model on the five main response variables.

For validation of the model, the goodness factors R^2 and Q^2 , correlation coefficients for their normal probability plots (R^2_{n-p}) and predicted vs. observed values (R^2_{ob-pr}) are given in Table 4. The value of R^2_{n-p} is a measure of the mismatch between the observed and modeled values. If the residuals are normally distributed, the points on the probability plot follow close to a straight line and R^2_{n-p} becomes close to unit. The R^2_{ob-pr} shows the squared-correlation between observed and the fitted or predicted values. The results imply relatively good prediction and modeling of response variables by predictors (X variables). The BET specific surface area is well explained and predicted by model rather than other responses. The unscaled regression coefficients are given in Table 5. Variables with the same sign affect the response variables at the same direction.

Table 4. The model goodness and validation characteristics of response variables

Response variables	$R^2_{VY(1)}$	$Q^2_{Y(1)}$	R^2_{n-p}	R^2_{ob-pr}
Crystallite size (CA)	0.67	0.62	0.95	0.67
Lattice strain (SA)	0.79	0.76	0.97	0.80
Amorphization (A)	0.77	0.73	0.95	0.77
BET surface area (Ss)	0.87	0.84	0.78	0.73
Excess energy (Ht)	0.8	0.76	0.96	0.80

Table 5. The unscaled regression coefficients of variables.

Variable identity	CA	SA	A	Ss	Ht
Constant	93.5	-0.174	-3.02	-0.33	-5.25
Gt	0.82	-0.006	-0.83	-0.013	-0.82
Ms	-2.28	0.016	2.31	0.037	2.26
Bp	-0.13	0.0009	0.13	0.002	0.13
EI	-6.2	0.04	6.29	0.099	6.15
SE	-6.14	0.04	6.22	0.099	6.09
Gt*Gt	-0.21	0.0015	0.22	0.003	0.21

From the PLS modeling, it is clear that the input energy (EI) and stress energy (SE) have strong impact on the responses. In order to increase the structural changes in hematite, one should focus on running on a high level of stress energy and energy input and media surface. The response variables X-ray amorphization (A) and overall stored energy (Ht) exhibit similar regression coefficient profiles which suggest that the energy contribution from the amorphization component is dominant. Finally the possibility of the modeling of the microstructure characters vs. several grinding variables is promising because the modeling vs. single variable, e.g. grinding time, does not give appropriate prediction equations, i.e. the evaluated model deviates from one to another mill because of the variation of stress energy, media surface and ...and subsequently their influences on the microstructure characters.

4. Discussions

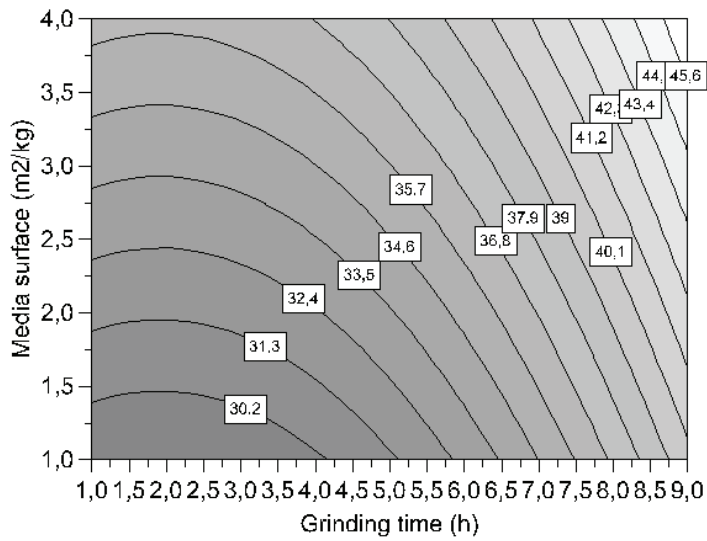
According to the PCA analysis, the mechanical stress of the studied hematite in the course of energy-intensive grinding brings about size reduction and accumulation of defects in the hematite network. The structural distortion reflected on XRD pattern data with increasing the line breadths (integral breadth) and reflection intensity reduction. The energetic excitation of the hematite structure is manifested by an increase in the excess enthalpy content in the ground hematite. The changes in the dislocation density, BET surface area and the formation of the amorphous material are the energy contributions to the excess enthalpy. The strongest correlation of amorphization (A) with excess enthalpy (Ht) indicates that the energy contribution from amorphization to the excess enthalpy (stored energy) is decisive. This is on line with our previous study (Pourghahramani and Forssberg, 2006b) and the observations of Tkáčová and Stevulová (1987) wherein it was found that the amorphization contribution to the total enthalpy (stored energy) exceeds 93%. Besides, the PCA plots assist to predict easily which grinding conditions lead to the induction of similar microstructure in different grinding conditions; for instance, the grinding in tumbling and planetary mills with low media surface for 9 and 3 hours of milling (Vi11 and PI11), respectively, causes similar microstructure characteristics with a first approximation. Particularly, this advantage will be promising when investigations are carried out under the circumstances comprising many variables.

The effects of three different mills with loose media on microstructural evolution have studied from a statistical view point. According to Tkáčová (1979, 1989), there is no significant difference between loose media mills on structural changes and thus those classified as a single group, while our studies reveals some differences among the used mills. In our opinion this is due to the characterization methods. Line broadening analysis of XRD patterns result in reliable and precise microstructure data and subsequently distinguishable differences between the mills. As discussed, the difference between the mills can be investigated from the PLS weight plot (Fig. 7). It was found that the vibratory milling

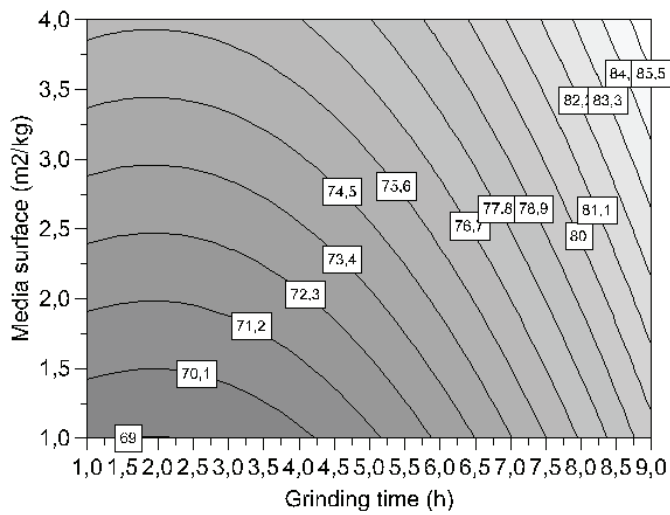
develops less structural changes and produce smaller particles compared with planetary and tumbling mill in spite of releasing higher stress energy for a given energy input. In our opinion, despite of the calculation of higher stress energy for the vibratory mill based on the grinding parameters at the given condition; it seems that the efficiency of energy transfer to the particles during vibratory milling worsened comparing with the other used mills. This is most likely due to the following reasons. (1) The existence of the plastic liner in vibratory mill which can diminish the impact force acting on the powder bed. (2) The generation of higher temperature because of plastic liner and attrition of particles can facilitate size reduction and consequently the increase of the number of layers in the material bed. Increasing the number of layer influence the spatial conditions of energy transfer in a mill (Tkáčová, 1989).

From PCA (Fig. 3) and SIMCA (Fig. 5) analysis, it is reveled that the observations belonging to media surface levels can be fairly distinguished from each other whatever millings machines are employed. This is in a good agreement with process knowledge. Grinding media was chosen between 6 and 22 mm and for increasing the media surface the different fractions of media are increased proportionally. As would be expected, the use of higher media surface and/or ball to powder weight ratio accompanied with higher contact points, impact force and stress. Increasing the powder charge causes a reduction in the impact forces. This behavior results from powder acting as a viscoelastic layer between colliding surfaces. Increasing the powder charge resulted in the amount of powder trapped in a collision, thus increasing the amount of viscoelastic damping of the collision and causing the impact force to be reduced. With increasing the ball to powder weight ratio the number of collisions per unit time increases and more energy transfers to the particles being ground. Thus, the use of higher media surface level facilitates the generation of long-lived defects and increases their energy fractions. The media surface becomes the most dominant factor in grouping of the observations. Besides, with extending the grinding time, more energy transfer to the particles and consequently leads to more structural distortion in hematite according to the PCA plot. With increasing either grinding time or media surface the particles are stressed intensively and undergo a great structural distortion. In addition, it seems that higher stress rate in tumbling and planetary mills leads to higher plastic deformation; while larger number of impulses in the vibratory mill leads to the production of finer particles and higher stress energy. Finally, the predominant stress modes in the planetary and tumbling mills (compact and compressive) seem to assist the production of amorphous phase compared to the vibratory mill; while the existence of shear and attrition modes of stress in vibratory mill and generation of higher temperature during milling appear to facilitate size reduction process relatively in vibratory mill.

The contour plots for the stored energy response, as an example, are depicted in Fig.11 in terms of grinding time vs. media surface and specific energy input against stress energy. The curvature arises from the importance of quadratic term of the grinding time factor. This type of plots makes it possible to predict the effect of single or multi-variables on the response variables. The contour plots in Fig. 10 reveals that the rate of changes in the stored energy are more sensitive to media surface variable than grinding time at earlier stages of milling. To enhance the stored energy in material during mechanical activation, both grinding time and media surface can be increased. When other X-variables are adjusted at their low levels, the stored energy goes up from 29 to 46 kJ per mole of hematite with increasing both grinding time and media surface. If the other X-variables are adjusted at their maximum levels, the stored energy increases from 69 to 86 kJ per mole of hematite. The maximum stored energy is attainable at higher media surface and grinding time.



(a)



(b)

Fig. 10. Response contour plots of total stored energy (Enthalpy), when the other X-variables are adjusted at their low levels (a) and high levels (b).

Fig. 11 shows the surface plot for the stored energy response. The stored energy increases sharply as the specific energy input and stress energy goes up. With intensive grinding, the rate of changes in the stored energy continues to increase gradually. It is revealed that the initial state changes to steady state (intensive grinding) when the excess energy reaches approximately 55 kJ/kg. If the other X-variables are adjusted at their low and high levels, the transition from initial to steady state takes place needs about 45 and 70 kJ/mole respectively.

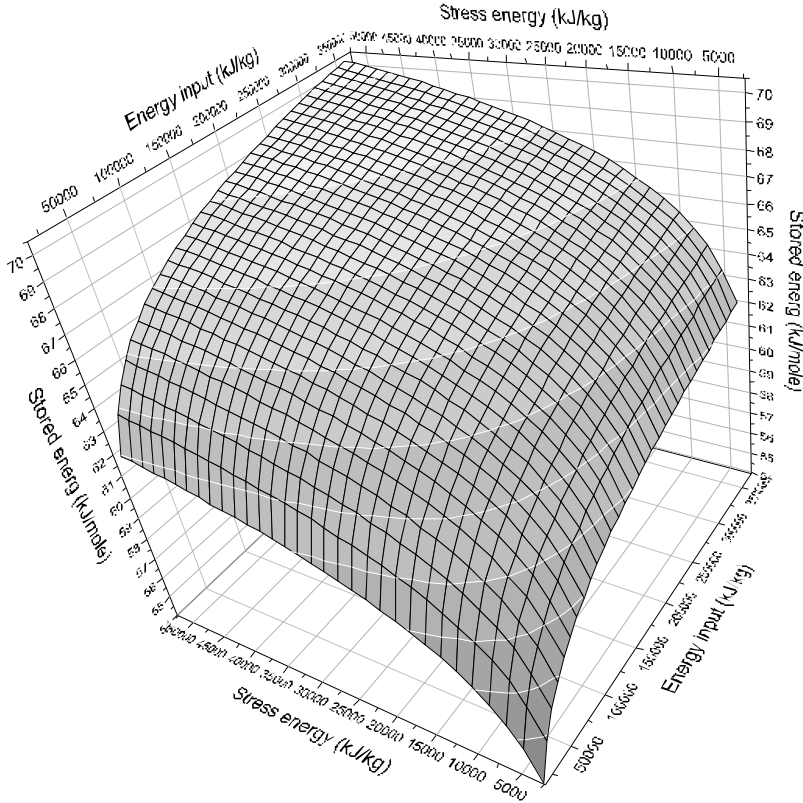


Fig. 11. 3D response surface plot for the stored energy in activated material vs. specific energy input and stress energy. Other X variables adjusted at their center levels.

5. Conclusions

Statistical analyses reveal some distinguished features in data analysis and facilitate the interpretation of data by considering all variables in a data set simultaneously. Since PCA analysis uncovers sudden shifts and softens the trends in data set, it gains the understanding of the relationship among the variables. From the statistical analysis, the following conclusions can be made:

1) ANOVA analysis revealed that two design factors of milling time and media surface have statistically significant effect on the five main response variables at 95% confidence. Grinding mill has not statistically significant effect at 95% confidence on the production of the BET surface area. Besides, no interaction terms have statistically significant effect on any responses at 95% confidence.

2) PCA analysis revealed that with increasing the grinding intensity, which can be attained by increasing the duration of grinding, media surface, specific energy input, stress energy, and /or ball to powder weight ratio individually or simultaneously, the structural damages are also enlarged. PCA makes it possible to predict which condition (observations) leads to production of similar properties or microstructure characters easily (e.g. Vi11 and P111).

3) Milling with higher media surface favors the production of more defects and plastic deformation of hematite and increasing stored energy (enthalpy) in activated hematite. This was also confirmed by soft independent modeling of class analogy (SIMCA).

4) PLS-DA analysis suggested that mills could be separated and differentiated from each other, i.e., the mills are different at 95% confidence level. The tumbling mill results in higher amorphization concentration per unit surface area in spite of lower stress energy and less specific energy input.

5) From the PLS analysis, in addition to the main X-variables, the quadratic term of grinding time variable influences the response variables. It was found that the specific energy input and stress energy influence the response variables more than the other X-variables. Those variables also explain the grinding process better than other grinding variables and accounting for the largest VIP value. This puts forward a key for further investigations. To achieve maximum stored energy in the activated material, one should focus on increasing grinding time, media surface, ball to powder weight ratio, specific energy input and stress energy. However, the use of stress energy explains better grinding process than individual variables. Probably, this will be useful for obtaining an identical stored energy and structural changes by altering other grinding variables in different milling devices, i.e., whether the same structural changes can be achieved by receiving the same level of stress energy through changing the other grinding variables such as amplitude, frequency and etc. But this needs further studies by considering other grinding variables.

6) The obtained results show that the tumbling and planetary mills favor the induction of structural changes and subsequently higher reactivity potential irrespective to capacity and specific energy input and stress energy.

Acknowledgement

The financial support for the project by Agricola Research Centre (ARC) is gratefully acknowledged.

APPENDIX1

Table 1. Complementary data set

G_Mill*	Bp	IE (kJ / kg)	SE (kJ / kg)	Pin (%)	IB (deg)	CH (nm)	SH (%)	DC (m / m ³)	DS (m / m ³)	DD (m / m ³)
PI11	19.1	9684.6	433.5891	100.4846	1.395842	141.42	0.0886	6.74E+14	1.23E+13	9.10E+13
PI14	76.34	38666.67	1732.99	53.0421	6.027176	57.73	0.273	3.80E+15	2.97E+13	3.36E+14
PI31	19.1	29220.7	1300.77	48.98395	5.105365	37.79	0.316	7.14E+15	3.25E+13	4.82E+14
PI34	76.34	116666.7	5198.983	21.6889	3.971345	24.25	0.86	2.23E+16	1.56E+14	1.86E+15
PI91	19.1	87996.3	3902.3	38.51925	11.69234	37.79	0.387	1.10E+16	7.16E+13	8.88E+14
PI94	76.34	351333.3	15596.94	13.40522	19.16162	10.91	1.22	9.57E+16	2.23E+14	4.63E+15
Tu11	16.77	718.56	145.098	110.6078	1.115058	158	0.077	1.02E+15	3.00E+10	5.57E+13
Tu14	67.08	2675.52	580.448	71.99436	2.905243	50	0.158	1.52E+15	3.95E+13	2.45E+14
Tu31	16.77	1933.2	435.302	68.68639	2.719867	50	0.118	1.65E+15	1.83E+13	1.73E+14
Tu34	67.08	7524	1741.21	39.45772	5.888669	35.3	0.354	4.80E+15	6.37E+13	5.53E+14
Tu91	16.77	5450.4	1305.91	47.57126	4.710672	37.79	0.274	4.03E+15	4.00E+13	4.01E+14
Tu94	67.08	22395.6	5223.64	23.75424	10.27267	30.15	0.707	1.00E+16	1.56E+14	1.25E+15
Vi11	16.92	2160	1425.013	99.65451	1.964863	182.57	0.15	5.55E+14	2.42E+13	1.16E+14
Vi14	67.68	9108	5700.05	67.26776	3.543592	105.41	0.274	2.26E+15	2.67E+13	2.46E+14
Vi31	16.92	6804	4275	70.47722	3.258239	70.71	0.224	1.59E+15	3.42E+13	2.33E+14
Vi34	67.68	26820	17100.15	44.09942	5.690993	57.73	0.418	5.34E+15	6.15E+13	5.73E+14
Vi91	16.92	20052	12825.1	49.43176	4.786944	57.73	0.353	3.42E+15	5.26E+13	4.24E+14
Vi94	67.68	78912	51300.47	22.8479	9.887232	25.82	0.7	2.02E+16	1.23E+14	1.58E+15

Table 1. Continued

G_Mill*	BS (nm)	Gs (m ² / gr)	Sz (μ)	De (gr / cm ³)	fr<1 (μ)	fr<10 (μ)	MT (C°)	Hs (kJ / mole)	Hd (kJ / mole)	Ha (kJ / mole)	Ht (kJ / mole)
PI11	540	1.1933	7.92	5.25	23.5	69.66	39	0.6	0.03	35.1	35.73
PI14	224	2.151	4.42	5.215	45.71	85.85	42	1.45	0.098	52.4	53.95
PI31	339	1.8525	4.98	5.1	42.17	84.04	47	0.95	0.136	47.7	48.79
PI34	143	2.31	6.03	5.001	44.39	78.58	51	2.26	0.456	69.5	72.22
PI91	259	1.8754	4.85	4.95	42.84	84.69	61	1.25	0.154	65.2	66.6
PI94	130	2.02451	6.71	4.9	38.78	74.03	68	2.5	1.02	77.8	81.32
Tu11	821	1.07437	10.96	5.25	19.28	61.76	24	0.4	0.019	27.3	27.72
Tu14	278	1.639985	6.74	5.25	36.97	77.2	27	1.17	0.074	54.1	55.34
Tu31	440	2.062835	5.87	5.25	34.83	77.35	30	0.73	0.054	46.9	47.68
Tu34	214	2.429984	4.08	5.163	46.99	85.11	33	1.51	0.154	66.9	68.59
Tu91	250	2.213913	4.5	5.157	44.34	83.91	35	1.3	0.115	57.8	59.22
Tu94	167	2.220059	5.68	5.126	44.51	79.88	38	1.93	0.32	73.1	75.35
Vi11	608	1.582895	6.21	5.25	27.96	75.36	48	0.53	0.037	21	21.57
Vi14	261	2.133958	5.37	5.25	41.61	79.75	51	1.24	0.074	50.6	51.91
Vi31	287	2.07946	3.89	5.153	45.57	86.67	74	1.13	0.07	37.7	38.9
Vi34	153	2.460841	3.44	5.075	53.04	88.05	81	2.13	0.159	57.3	59.59
Vi91	221	2.576072	3.22	5.146	54.26	89.99	98	1.47	0.121	53	54.59
Vi94	62	2.0808	7.17	4.96	42.88	73.59	105	5.21	0.394	74.4	80

*The term PI, Tu and Vi refer to the planetary, tumbling and vibratory mill respectively. The first and second number after each abbreviation refer to the grinding time (h) and media surface levels (m² / kg) respectively. For example, the term PI11 refers to the grinding test made in planetary mill with media surface 1 m² / kg and for 1 hour of milling. Integral breadth and peak intensity are the average ratio of physical integral breadth in activated material to non-activated material considering the eight most intensive reflection peaks.

Table 2. The abbreviation of variables

Abbreviation	Variable definition
A	X-ray amorphous portion
Bp	Ball to powder weight ratio
Bs	Mean particle size obtained using the BET method
CH	Crystallite size obtained from the Williamson-Hall plots
CA	Crystallite size obtained from the Warren-Averbach method
Dc	Dislocation due to crystallite size
Dd	Dislocation density
De	Bulk density of activated material
Ds	Dislocation due to strain
fr<1	Faction of particles smaller than 1 micron
fr<10	Fraction of particle smaller than 10 micron
Gs	Granulometric specific surface area
Gt	Grinding time
Ha	Excess energy due to amorphization
Hd	Excess energy due to dislocation density
Hs	Excess energy(enthalpy) due to the BET surface area
Ht	Total excess energy during mechanical activation process
IB	Average physical integral breadth ratio
EI	Specific energy input
Ms	Media surface variable
MT	Material temperature
Pin	Average peak intensity reduction ratio
Pl	Planetary mill
SH	Microstrain obtained from Williamson-Hall
SE	Stress energy
SA	The BET specific surface area
Ss	Microstrain obtained from Warren-Averbach
Sz	Mean size of particle resulted from laser diffraction
Tu	Tumbling mill
Vi	Vibratory mill
W-A	Warren- Averbach approach
W-H	Williamson-Hall approach

REFERENCES

- Baláz, P., *Extractive Metallurgy of Activated minerals*. 2000, Elsevier, Amsterdam
- Baláz, P., Huhn, H.J., Tkáčová, K., Heegn .H., *Laugungsverhalten und physico-chemische Eigenschaften von in unterschiedlichen Mullen vorbehandeltem chalkopyrite*. *Erzmetall*, 1988, 41, 325-331
- Baláz, P., Alacová, A., Briancin, J., Sensitivity of Freundlich equation constant $1/n$ for zinc sorption on changes induced in calcite by mechanical activation. *Chemical Engineering Journal*, 2005, 114(1-3), 115-121.
- Boldyrev, V.V., Pavlov, S.V., Goldberg, E.L., Interrelation between fine grinding and mechanical activation. *International journal of mineral processing*, 1996, 44-45, 181-185.
- Eriksson, L., Johansson. E., Kettaneh-Wold, N., and Wold, S., *Multi-and Megavariate Data Analysis; Principles and Applications*, 2000, Umetrics AB, Umeå, Sweden.
- Halder, N.C., Wagner, C.N.J., Separation of particle size and lattice strain in integral breadth measurements. *Acta crystallography*, 1966, 20, 312-313.
- Heegn, H., Effect of fine grinding on structure and energy content of solids. in: *Proc.of 6th POWTECH*, Birmingham, 1979, pp. 61-69.
- Heegn, H., Concerning some fundamentals of fine grinding. In: Leschonski, K., Editor, 1986. *Proc. 1st World Congress on Particle Technology, Part II: Comminution*, Nürnberger Messe und Ausstellungsgesellschaft, Nürnberg, 1986, pp. 63–67
- Heegn, H., Mechanical induced changes in structure and properties of solids. *Proceedings of the XXI International Mineral Processing Congress*, part A4. Comminution, Classification and Agglomeration. Rome, Italy, 2000, pp.52-59.
- Huttig, G.F., Zwischenzustand bei reaktionen im festen zustand und ihre bedeutung fur die katalyse. In: *Handbuch der katalyse IV*, Spring Verlag, WIEN, 1943, pp. 318-331.
- Jackson, J.E., *A user's guide to principal components*, 1991, John Wiley, New York.
- Karagedov, G.R., Lyakhov, N.Z., Mechanochemical grinding of inorganic oxides. *Kona*, 21, 2003, 76-86.
- Lin, J.I., Implications of fine grinding in mineral processing; mechanochemical approach. *Journal of thermal analysis and Calorimetry* 1998, 52, 453-361.
- Manugistics., *Tutorials for Statgraphics Plus for Windows*. Manugistics, Inc., 2115 East Jefferson Street Rockville, Maryland 20852, 1999, USA.
- Montgomery, D.C., *Design and Analysis of Experiments*, 1997, John Willey and Sons, New York.
- Pourghahramani, P., and Forssberg, E., Microstructure characterization of mechanically activated hematite using XRD line broadening. *International Journal of Mineral Processing*, 2006a, 79, 106-119
- Pourghahramani, P., Forssberg, E., Comparative study of microstructural characteristics and stored energy of mechanically activated hematite in different grinding environments. *International Journal of Mineral Processing*, 2006b, 79, 120-139
- Siemens AG, *Diffra Plus Profile Fitting Manual Program*, 1996, pp. 23-26.
- Sjöström, M., Eriksson, L., Hellberg, S., Johansson, J., Skagerberg, B., and Wold, S., Peptide QSARs: PLS Modelling and Design in Principle Properties. In: J. L. Fauchere (ed.) *QSAR-Quantitative Structure-Activity Relationship in Drug Design*. *Proc.7th European Symposium on QSAR*, Sept.1988, Interlaken, Switzerland. Alan R. Liss, Inc., New York, 1989, pp. 131-134.
- Tkáčová, K., *Mechanical Activation of Minerals*, 1989, Elsevier, Amsterdam.
- Tkáčová, K., Heegn, H., Stevulová, N., Energy transfer and conversation during comminution and mechanical activation. *International journal of mineral processing*, 1993, 40, 17-31

- Tromans, D., Meech, J.A., Enhanced dissolution of minerals: stored energy, amorphism and mechanical activation. *Mineral Engineering*, 2001, 14(11), 1359-1377.
- Umetrics, Tutorial to SIMCA-P, SIMCA-P⁺. Multivariate Modelling, Data analysis and Design of Experiments group, 2002, S-90719 Umeå, Sweden.
- Warren, B.E., X-ray Diffraction, 1969, Addison-Wesley, New York.
- Welham, N.J., Enhanced dissolution of tantalite/columbite following milling. *International Journal of Mineral Processing*, 2001, 61, 145-154.
- Welham, N.J., Llewellyn, D.J., Mechanical enhancement of the dissolution of ilmenite. *Minerals Engineering*, 1998, 11(9), 827-841.
- Williamson, G.K., Hall, W.H., X-ray line broadening from field aluminum and wolfram. *Acta Metallurgy*, 1953, 1, 22-31.
- Williamson, G.K., Smallman, R.E., Dislocation densities in some annealed and cold-worked metals from measurements on the X-ray Debye-Scherrer spectrum. *Philosophical Magazine*, 1956, 1, 34-45.
- Wold, S., Albano, C., Dunn, W.J., Edlund, U., Esbensen, K., Geladi, P., Hellberg, S., Johansson, E., Lindberg, W., and Sjöström, M., Multivariate data analysis in chemistry. In: B.R. Kowalski, Editor, *Chemometrics: Mathematics and Statistics in Chemistry*, 1984, Reidel Publishing company, Dordrecht, Holland, pp.17-95.

Paper V

The Characterization of Structural Changes in Hematite Ground in a Confined Particle Bed Using Rietveld Analysis

Parviz Pourghahramani & Eric Forsberg, Submitted for publication in International Journal of Mineral Processing

The characterization of structural changes in hematite ground in a confined particle bed using Rietveld analysis

Parviz Pourghahramani* and Eric Forssberg

Division of Mineral Processing, Luleå University of Technology, SE-971 87, Luleå, Sweden

Abstract

The interparticle breakage of fine feed fraction of hematite concentrate was investigated by stressing two particle beds with a pressure between 255 and 1000 MPa. The experiments were conducted in such a way that the wall friction effects during compression were eliminated. The effects of interparticle breakage in a confined bed on the structural changes of hematite concentrate were studied using a combination analysis of XRD line broadening, BET and particle size measurements. The specific energy comminution was estimated using loading and de-loading hysteresis curves.

It was found that energy absorption by the particle bed varies between 6 and 31 J/g depending on the applied pressures and bed heights. The experiments indicated that energy absorption was a major factor for the interparticle breakage of hematite. In addition, it was revealed that an increasing bed height brought about a higher stiffness and hence reduced energy absorption and subsequently declined the surface area, solid content as well as structural changes. The linear energy-force relationship stands well even if the particle bed heights are changed. The maximum BET surface area was measured about $1.4 \text{ m}^2 / \text{g}$ after energy absorption of 31 J/g by the particle bed.

Structural changes were followed by XRD line broadening analysis using Rietveld refinement and Warren-Averbach approach. It was found that the intensity and the broadening of XRD diffraction patterns decreased and increased, respectively, by increasing energy absorption with a first approximation. With increasing absorbed energy by the bed up to 15 J/g the degree of amorphization increased sharply and afterwards continued to change slightly. The maximum X-ray amorphization was calculated at maximum energy absorption, accounting for 31%. The volume and surface weighted crystallite sizes reduced to about 108 and 53 nm, respectively, after releasing 31 J/g specific grinding energy. For the same energy, the root mean square strain (RMSS), $\langle \varepsilon_{L=10nm}^2 \rangle^{1/2}$, and maximum lattice strain, e , increased to 9.4×10^{-4} and 4.1×10^{-3} respectively. The comparison of bed grinding with tumbling milling revealed that the grinding in tumbling mill needs much more energy to induce the same structural changes as in bed grinding. The results obtained from the two methods are discussed and compared in details.

Keywords: high pressure comminution, structural changes, mechanical activation, interparticle breakage

1. Introduction

The term “interparticle breakage” is used for the grinding process in which a material bed is subjected to compression, a stressing mode as performed in roller-table and high pressure

* Corresponding author: Tel: +46 920 491313; fax: +46 92097364
E-mail address: Parviz.Pourghahramani@ltu.se

roller mills (Schönert, 1991; Reichardt & Schönert, 2003). In particle bed comminution energy is transferred directly to the charge mass in spite of conventional grinding mills; and breakage occurs by very high stresses generated locally at the contact points between the particles of the strongly compressed bed (Fuerstenau et al., 1991). The tendency of a particle to fracture when compressed in a confined bed of particles depends, not only on the material properties such as Young's modulus but also on the granular composition of the particle bed (Gutsche and Fuerstenau, 1999). If a single particle or rock is compressed, the initial fracture propagates along a line which is more or less parallel to the loading direction (Kou et al., 2001). If the force increases, secondary breakage of the ground particles in the initial state will occur depending on the position of the particles. The secondary breakage can be limited under a certain arrangement of particles in the bed. With the increase of force, the surrounding particles shield the products of fracture and the fine material is placed in the spaces. The particles are re-stressed if the force further increases (Viljoen et al., 2001). According to Gutsche and Fuerstenau (1999), the fracture strength of particles in confined particle bed exceeds their single-particle fracture strength because of the compaction of the particle bed and associated granulometric stabilization which assist the distribution of stress.

The investigation of this grinding mode in laboratory and the batch process in a piston-die press has several advantages over the continuous process in high pressure roll mills. They are as follows: (1) small amount of sample, (2) preloading of samples is possible, (3) establishment of a fully confined bed is easy, (4) higher pressure is attainable and (5) the die-press is a versatile tool and facilitates the study of energy absorption, utilization and dissipation (Fuerstenau et al., 1996). Several studies have been made on particle-bed comminution and undoubtedly the intensive and systematic works in this area is by Schönert and co-workers. According to Aziz and Schönert (1980), an ideal particle bed is characterized by: (1) homogenous structure of the bed (stochastic homogeneity), (2) homogeneous compaction of the bed, (3) known volume or mass of the stressed particles and (4) wall effects are negligible in respect to the overall size reduction effect. The effect of the container can be eliminated if the following inequalities are fulfilled (Aziz and Schönert, 1980):

$$h > 6 X_{\max} ; D > 3h ; D > 10 X_{\max} \quad (1)$$

where h , X_{\max} and D are the initial bed height, maximum particle size and die diameter respectively.

The influence of the particle bed configuration was studied by Schönert (1996). It was indicated that stressing single particles produce a steeper size distribution than stressing a particle bed. The transition from a close to a moderately wide confinement does not affect strongly the size reduction. The comminution in confined particle bed by using the additive caproic acid was investigated by Oettel et al. (2001). It was stated that the decrease of internal friction due to additives, exerts a small influence on the comminution system, while the material escape from the stressing zone is decisive. The caproic acid improves only the energy utilization in the case when the particle bed is not fully confined. The repetition of an uniaxial stressing with the same pressure does not in principle increase either the compaction of the bed or the size reduction. In this case, Schönert and Reichardt (1993) designed a 4 piston unit (cross piston press) for multiple compression of the particle bed. It was found that the achievement of the same fine particles under higher pressure with single compressive loading is also possible using multiple stressing with lower pressure.

Mechanical activation is another effect when the material is ground to the brittle-ductile transition range. Excess enthalpy increases due to structural distortions such as amorphization

of material, changes in surface area, crystallite size and strain and phase transformation. Such structural changes are essential factors in determining the reactivity of material (Boldyrev et al., 1996). Nowadays, loose media millings such as planetary milling are frequently employed for activation of materials. On the other hand, Fuerstenau and Kapur (1994) stated that the particle bed comminution has higher energy efficiency, lower metal wear and higher energy transfer to the particles being ground compared to the ball millings. Thus, the application potentiality of the bed comminution for activation of minerals comes into question and subsequently the structural changes during comminution in the confined particle bed have yet to be studied.

The goal of the paper is to study the comminution behaviors and structural changes of hematite ground in the confined particle bed by single compressive load. For microstructural characterization, two methods of Warren-Averbach analysis and Rietveld refinement are used.

2. Experimental

Experiments were designed to investigate the effects of bed pressure and bed height on compaction in compression-loaded particle beds, BET surface area and structural changes of hematite concentrate.

2.1. Material

High purity hematite concentrate was obtained from LKAB (Luossavaara Kiirunavaara Aktiebolag) in Sweden. The chemical composition of the starting samples is given in Table 1. A narrow size of hematite concentrate was obtained using a sieve of $62\ \mu\text{m}$. The surface area of the initial sample was measured about $0.72\ \text{m}^2 / \text{g}$.

Table 1. The chemical analysis of the initial hematite (%).

Fe_2O_3	Al_2O_3	SiO_2	TiO_2	MgO	MnO	P_2O_5	Other elements
97.91	0.73	0.73	0.27	0.20	0.022	0.088	0.051

2.2. Experimental apparatus

Grinding tests were carried out in a piston-die press which consists of a steel die and a piston of 50 mm diameters, which can be fairly considered as a fully confined system. The material was loaded with a high pressure rock testing load frame X-Z-450-enhanced. The unit consists of a rigid steel load frame capable of handling at least 5000kN. In the lower end of the load frame, there was a hydraulic actuator capable of 4500kN of static load. The actuator was controlled by a Dartec servo controller with ability to ramp and also to perform cyclic loading. Even though the load frame and actuator were capable of handling 4500kN, the load cell was restricted to 2250kN. The instrument was equipped with two external sensors, so called LDVTs, for measurement of the displacement and lateral expansion of the mould (Fig. 1). The use of LDVTs1 provided precise calculation of displacement in a range of $1 \times 10^{-6}\ \text{mm}$. Measured signals were collected with a HBM spider-8 data logger. Data was processed in a computer through HBM's program Catman professional 5.02. For each test the displacement and force were measured. The force-displacement data from press were logged digitally and numerically integrated to obtain the work of compression. It was observed that the lateral expansion of mould was negligible during loading tests. The mass of samples were

chosen 50 and 25 g yielding a bed height of 10.7 and 6 mm respectively after preloading with 0.16 kN. The loading and unloading rates were adjusted at 10 kN per second. A series of test was designed for single compression with forces of 500, 1000 and 2000 kN on the beds with 10.7 and 6 mm. After achieving the maximum load, the samples were maintained under load for 1 minute to establish the particle bed.

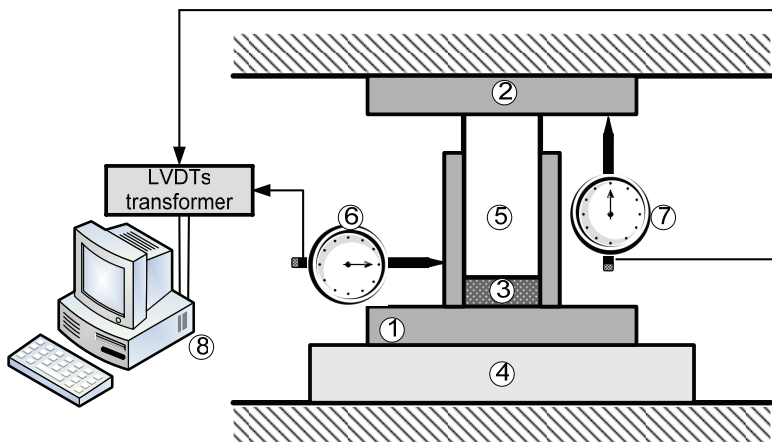


Fig. 1. Schematic of experimental apparatus: 1. piston-die press base; 2. upper part of piston-die press; 3. sample bed; 4. testing machine; 5. piston; 6. lateral LDVTs (LDVTs2); 7. displacemet LDVTs (LDVTs1); 8. computer.

2.3. Characterization

At the end of compaction, the compressed bed was broken manually and a part of the resulting aggregates were immersed in water and then subjected to an ultra-sonic treatment for de-agglomeration. For de-agglomeration, hexametaphosphate (1g/L) was added to the suspension and a 50W ultrasonic treatment was applied for 30 minutes for all of the samples. The de-agglomerated parts were used in the measurements of the particles size and surface area. The particle size distributions of the samples were measured by laser diffraction (CILAS 1064) in the liquid mode in the presence of hexametaphosphate (1g/L). The mean particle diameter and granulometric surface area were calculated based on the particle size distribution. The specific surface areas of the samples were determined by the BET method with the Flow Sorb II 2300 (Micromeretics; USA). Samples were degassed by heating at 200°C for 90 minutes immediately prior to measurements.

The XRD patterns were obtained by using a Siemens D5000 powder diffractometer with Bragg-Brentano geometry equipped with a curved graphite monochromator in the diffracted beam arm and using Cu K α radiation ($\lambda = 0.15406$). The XRD patterns of the samples were recorded using a step size of 0.02° and a counting time of 5s per step. Slit size of 0.1 mm was used. To characterize the microstructural characteristics encountered during the mechanical activation of specimens, two methods of Warren-Averbach and Rietveld analysis were applied.

2.4. Microstructure characterization (background)

2.4.1. Warren-Averbach analysis

Line broadening analysis of XRD patterns is the pre-processing in the Warren-Averbach approach (1952). The eight most intensive reflection peaks of the samples were used in the line broadening analysis. The Profile software supplied by Bruker/Socabin was used in the profile fitting procedures and in the extraction of the parameters. The obtained X-ray diffraction patterns were fitted to Pseudo-Voigt line shape function, which is a linear combination of Cauchy and Gaussian functions. For each adjusted line profile, the following parameters were obtained: (1) The maximum intensity of peaks (I_{\max}), (2) The full-width at half of its maximum intensity ($FWHM$), (3) the integral breadth (β), (4) the mixing factor (η), and (5) the peak position (2θ). An example of adjusted line function for the (104) and (110) reflections is given in Fig. 2. The same procedure was applied for the standard sample, LaB_6 (SRM660a), proposed by National Institute of Standards and Technology (NIST) of USA to obtain the instrumentally broadened profile. The goodness factors in this method have been refined to a value smaller than 7%. Once the line parameters were extracted, the Warren-Averbach method was used for resolving of size and strain contributions from XRD patterns. The profile fitting procedure and principles of the Warren-Averbach method were discussed in details in previous works (Pourghahramani and Forssberg, 2006a, b).

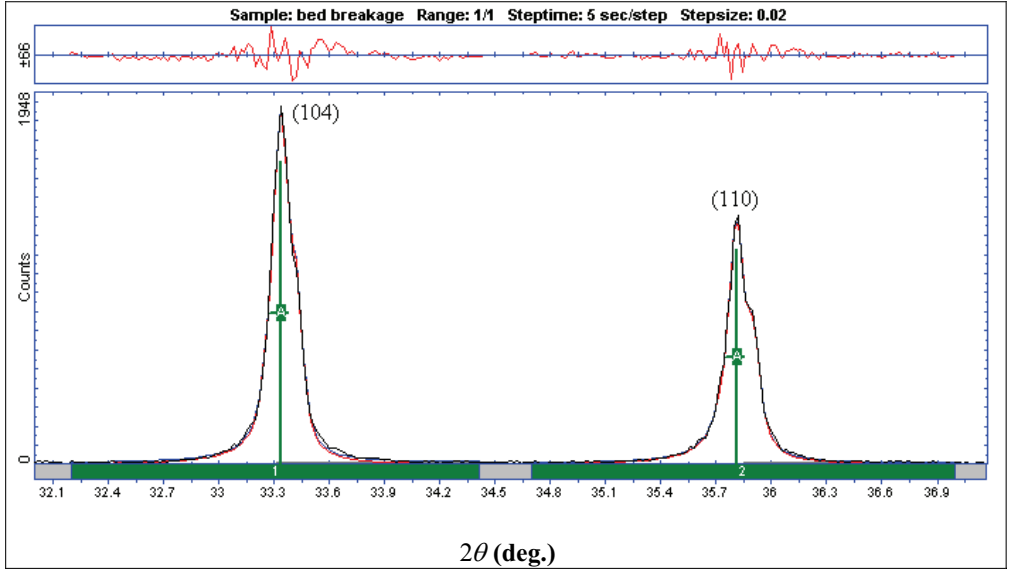


Fig. 2. A Pseudo- Voigt function fitted to the (104) and (110) reflections of the XRD pattern of the sample ground in the piston-die press with absorption energy of 31 J/g. The net difference between observed and calculated data are given at the top of the curve. The goodness factors for the peaks refined to a value smaller than 5%.

2.4.2. Rietveld analysis

Rietveld method is becoming progressively more popular for microstructure characterization of materials. It is common practice to estimate domain size and strain values from the refined profile width parameters. The method is a so- called “full pattern method”. In the Rietveld refinement, all the data points of a powder pattern were fitted to structure models, which depend on adjustable parameters. The fitting to the measured XRD pattern was performed by a least-square calculation. The calculated curve was based on the crystallographic structure models, which also takes into account samples and instrumental effect. The parameters of this model were refined simultaneously to achieve the best fit to the data by least square method. By least square refinement, a so-called figure of merit function R is defined, which describes the residual between calculated and measured data (Young, 1993):

$$R = \sum_i w_i [y_i(obs) - y_i(calc)]^2 \rightarrow \min \quad (2)$$

where R is the residual value of the figure-of-merit function, w_i is $1/y_i$, $y_i(calc)$ denotes the calculated density and $y_i(obs)$ is the measured intensity at the i^{th} step.

The software TOPAS 2.1 from Bruker AXS (2003) was used for refinement, in which it is possible to make all of the corrections and refinement processes. The software package TOPAS 2.1 uses the fundamental parameter approach (FPA), and is therefore capable of estimating the instrumental influence. In the TOPAS software, the Double-Voigt approach (Balzar, 1999) is used for resolving of size and strain components. Besides, the Double-Voigt approach can be applied with fundamental parameters approach (FPA) and measured instrument functions. As exclusively Lorentz (Cauchy) or Gauss functions can not satisfactorily model the specimen broadening, it is assumed that the both size and strain effects are approximated by Voigt function. According to Balzar (1999), integral breadths of the size and strain components of Cauchy and Gauss parts can be expressed:

$$\beta_C = \beta_{SC} + \beta_{DC} \quad \beta_G^2 = \beta_{SG}^2 + \beta_{DG}^2 \quad (3)$$

where β_C and β_G are the Cauchy and Gauss components of total integral breadth β respectively. The term β_{SC} and β_{DC} are the Cauchy components of size and strain integral breadth, respectively and β_{SG} and β_{DG} are the corresponding Gaussian components. Once the components are calculated, the maximum lattice strain, e , and volume weighted crystallite size, D_V , can be calculated (Balzar et al., 2004):

$$e = \beta_D / 4 \tan \theta \quad D_V = \lambda / \beta_S \cos \theta \quad (4)$$

where β_D and β_S are the integral breadth of a Voigt function comprising a Gaussian and a Lorentzian components respectively. λ is the wave length and θ is diffraction angle.

2.4.3. Refinement procedure

After inserting the instrumental parameters, Pseudo-Voigt line function was chosen for adjusting on the XRD patterns. The starting sample and ground hematite were indexed in a hexagonal (trigonal) symmetry (R-3c space group). All atoms positions of the ground samples were assumed to be in special positions like the initial sample. Therefore, the only structural parameters refined were the lattice parameters and microstructural characteristics such as crystallite size and strain components, crystal density. By an initial refinement, it was found that the Gaussian component of the crystallite size in most of the cases was negligible. Thus, for all data sets, Lorentzian size parameters refined to a non-zero value; however, both

Gaussian and Lorentzian strain components were refined to a non-zero value for the strain calculation. A preferred orientation-correction refinement was initially attempted, but did not yield significant improvement for any of the patterns and consequently it was excluded from the refinement process in the final refinement. The global factors included the scale factor, 2θ zero correction, specimen displacement, LP factor and background parameters (Chebychev polynomials function with five orders of the series) and crystal linear absorption coefficient were refined for all the data sets. Subsequently, the Bragg reflection profile can be calculated by convolution of mathematical functions of these parameters. Several criteria of fit (R factor) for judging the quality of a Rietveld refinement have been proposed. Those criteria show the deviation in accordance with the used model in percent. The most common R factors are the weighted profile R-factor (R_{wp}), the expected R factor (R_{exp}) and goodness of fit ($GOF = R_{wp} / R_{exp}$). The goodness factor for our experiments was attained between 0.95 and 1.35 which imply excellent fits to measured data. An example of whole pattern fitting using Rietveld refinement is shown in Fig. 3.

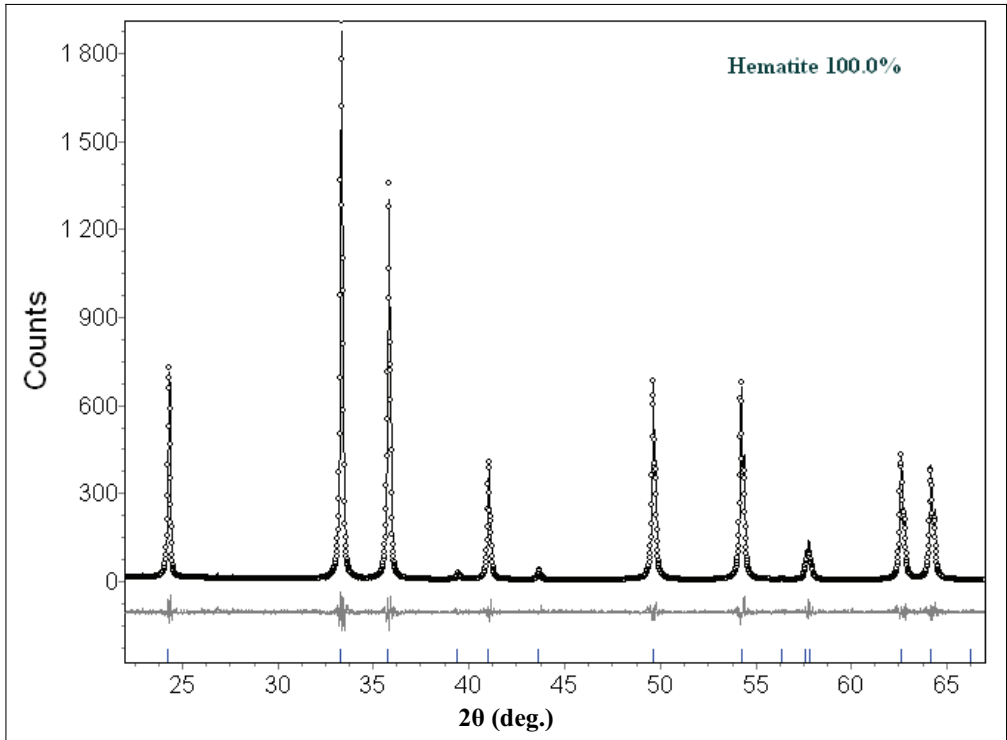


Fig. 3. A selected graphical representation of Rietveld analysis for X-ray powder diffraction of the sample ground in the confined die press with absorption energy of 31 J/g. Experimental data are shown as continuous solid line, simulated patterns are shown as dots. The difference between experimental data and simulated pattern is shown as continuous gray line under diffraction pattern.

3. Results and discussion

The obtained results will be discussed in the following sections.

3.1. Comminution behaviors

The comminution behaviors of hematite are discussed in the next section.

3.1.1. Force-displacement curves

Fig. 4 shows the compaction diagrams for different bed heights and pressures. In the diagrams, the pressure is plotted over the piston displacement related to the initial bed height, h . The features of the plots are the same as features previously reported in literatures (Reichardt and Schönert, 2003; and Oettel and Husemann, 2004). Diagrams contain the hysteresis of loading and de-loading curves. The arrangements of the particles take place during the loading process as well as the particle bed react with particles crushing. At lower forces, a rapid compaction in the material bed can be observed. With increasing force, the material bed undergoes smaller densification compared to the initial stages of the compaction. Generally, the use of higher forces brings about more compactions during loading and developments of the bed height at de-loading stages. The displacement is proportional to the volume of the stressing zone below the piston. For the fully confined particle bed, this means a mass-constant densification. As expected, the compaction diagram of the bed with larger height is steeper than that one of smaller height. This indicates that achieving the same compaction in terms of relative piston displacement with larger height needs more force. In the de-loading cycle, the smaller bed height expands more than the higher bed height. This is because the higher bed has higher stiffness. The de-loading trajectories at different forces remain approximately parallel.

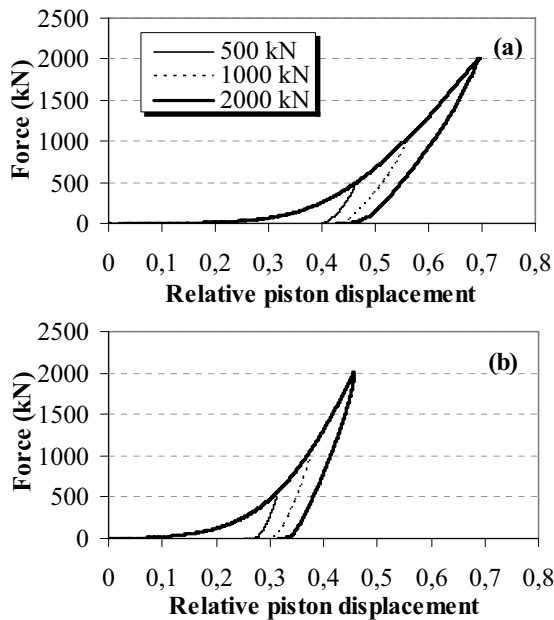


Fig. 4. Compaction curves of the hematite. (a) $h = 6$ mm, (b) $h = 10.7$ mm

Schönert (1996) also stated that the breakage data can be described uniformly by absorption energy rather than pressure. Absorption energy (E) gives an impression regarding the stress

intensity. Therefore, the absorption energy is defined as the consumed energy given by the hysteresis of the compression diagram and is related to the volume or the mass of the stressed particles. The force-displacement curves explain the ways of the piston into the particle bed due to an applied force and is approximately equated with the work of compression per unit feed mass (E_m):

$$E_m = \frac{A}{M} \int_0^{s_{\max}} p \, ds \quad (2)$$

where A is the die cross-section area, M is charge mass and s is the piston travel distance.

The energy absorption was calculated from Eq. 2 using the compaction diagrams. Fig. 5 shows typical curves of volume fraction of solid in the bed and absorbed energy as a function of pressure for hematite. The compressibility of the smaller bed height in terms of solid content of the compact is significantly greater than that of the larger bed height. At the pressure about 1000 MPa, the smaller bed height hematite can be compacted to about 98 percent solids content as against about 85 percent for larger bed height. Besides, the energy adsorption by the smaller bed height is considerably large. An increasing bed height causes a higher stiffness and hence the energy absorption reduces (Schönert, 1996). A definitive linear relationship can be observed between energy absorption and pressure. Nonlinear relationships have been previously reported in the comminution of coarser barite, galena, quartz and taconite (Fuerstenau et al., 1996) and quartz (Schönert, 1996) and linear relationship for finer limestone (Oettel et al., 2004) and finer quartz (Reichardt and Schönert, 2003). The feed particles size appears to be the most important factor influencing the required grinding energy; the same as conventional grinding methods in which is well established that the larger particles need less energy to grind than smaller ones.

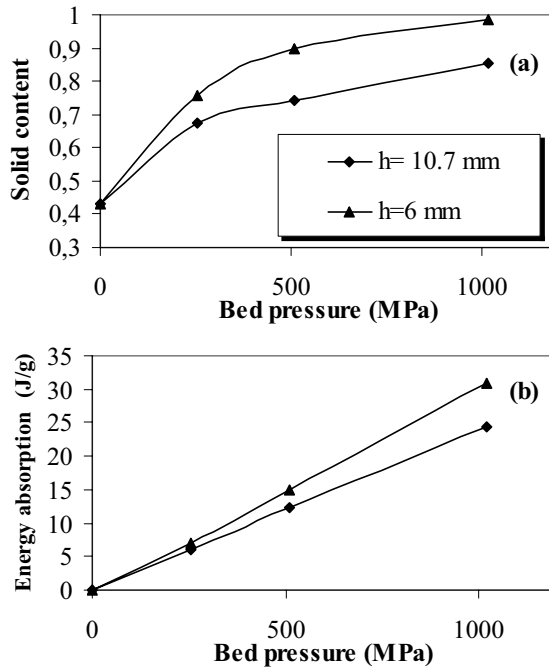


Fig. 5. Solid content (a) and energy absorption (b) as a function of applied pressure in particle bed comminution of hematite with various heights

3.1.2. Particle size distribution and surface area

The particle size distributions of the samples ground in the confined piston-die press with absorption energy up to 31 J/g are given in Fig. 6. The product fineness increases with increasing absorption energy whatever particle bed heights are applied. The dominant size reduction takes place at the initial stages of compression. As expected, with further increasing of the pressure and/or absorption energy, the rate of size reduction decreases. For a given pressure, the grinding in the thin bed produces slightly smaller particle because of slightly more absorbed energy by the bed. For the beds with $h=10.7$ and $h=6$ mm heights, the value of d_{50} from $13.3 \mu\text{m}$ in the initial sample decreased to around 7.33 and $5.3 \mu\text{m}$ respectively in the final products. The increase of the pressures neither in higher bed height nor in smaller bed height can break all coarse particles in the bed. This is a typical feature of interparticle breakage because the finer particles in the bed protect the coarser particles as they surround them. In this way, more contact points arise and the stress level in the contact region is reduced (Hoffmann and Schönert, 1971). The trend in the particle size distribution suggests that the further size reduction would be possible with increasing the absorption energy or pressure.

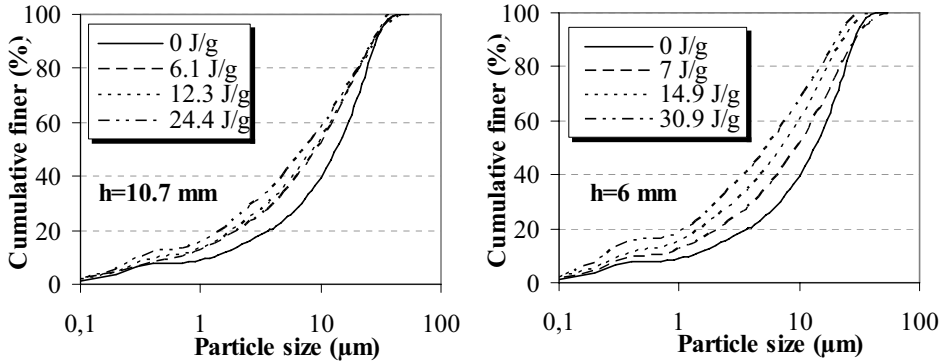


Fig. 6. Particle size distributions of the hematite products ground in piston-die press with initial heights of 10.7 and 6 mm.

As shown in Fig. 7, the size distribution curves of hematite particles generated in particle-bed comminution are self similar when plotted against a dimensionless size that has been scaled by the median size. It is clear that all data of Fig. 6 fall onto a single mastercurve. This means that a unique size distribution is associated with any given median size, and the size spectrum is driven forward on its trajectory by reduction in median size only. This characteristic of the size distribution is in fact a consequence of the geometrically similar crack patterns formed (Fuerstenau and Kapur, 1995). The initial sample ground in a ball mill in mineral processing plant previously, also follows the self-similar behavior which has been confirmed for the ground samples in the ball mill by Kapur (1972).

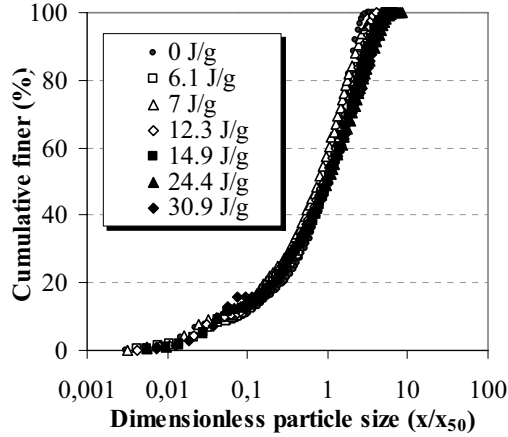


Fig. 7. Self-similar behavior of particle size distributions of the initial and ground hematite in piston-die press.

The changes in the BET and granulometric surface areas for the samples are shown in Fig. 8 over the energy absorption. Clearly, both surface areas develop linearly by increasing the energy absorption. This view is also supported by particle size distribution curves. The linear increase of the surface area during the comminution of corundum in a confined die press has been reported by Schönert and Reichardt (1993). The BET surface area is higher than the granulometric surface area which can be due to the presence of micro pores in the initial and ground samples. The BET surface area increased from $0.73 \text{ m}^2 / \text{g}$ in the initial sample to $1.38 \text{ m}^2 / \text{g}$ after energy absorption of 31 J/g . A higher growth rate of surface area at higher levels of energy absorption may be related to the weakening of the particles at higher levels of pressure and consequently to the grinding of weakened particles during ultrasonic treatment. The weakening of the particles in a particle bed breakage has been well established by Schönert (1991) and Tavares (2005).

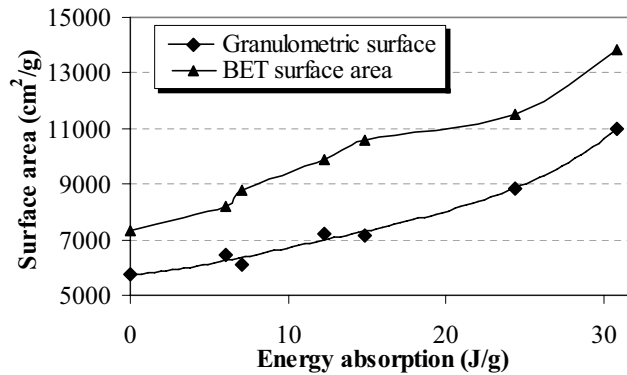


Fig. 8. Changes in the surface area of hematite ground in piston-die press as a function of energy absorption.

3.2. Structural changes

3.2.1. XRD pattern characteristics

The XRD patterns of the initial sample and ground samples in the piston die-press are given in Fig. 9 as a function of energy absorption. The XRD patterns represent only the hematite reflections. This could indicate no phase transition during compressive loading of hematite. The distortion of structure is reflected in the line broadening, the reduction of peak intensity and the sifting of reflections. The (104) and (110) reflections are initially very strong and decrease remarkably in intensity after comminution, compared with other indexed reflections. Their intensity decreases with increasing the energy absorption in the particle bed. The reduction of reflection intensity implies the formation of some amorphous materials. The amorphization is in fact a highly distorted periodicity of lattice elements, and it is often characterized as a short range order in contrast to the long order of a fully crystalline structure. With a first approximation, the intensity of the other reflections changes very slightly but the profile fitting data indicates a narrow broadening in all reflections, which reveals that the structural changes like lattice strain and crystallite size take place at all crystallographic planes.

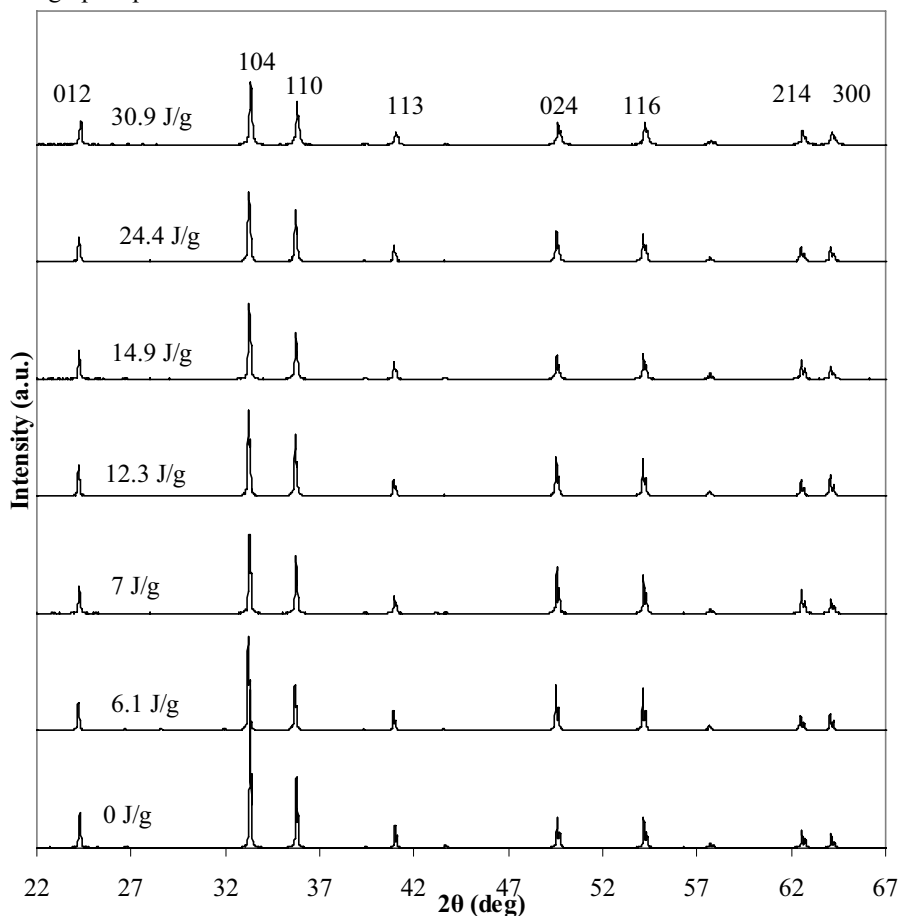


Fig. 9. XRD patterns of hematite ground in piston-die press as a function of energy absorption.

A quantitative comparison of integral breadths, β , of the samples is given in Fig. 10 as a function of absorption energy and diffraction angles. It can be observed that the increase of energy absorption brings about higher broadening of reflection peaks. The broadening of the samples ground at lower stress energy differs marginally. With increasing the absorption energy, the ground products give distinguished broadening which can be attributed to a great plastic deformation under higher pressures. For example, after absorption of 31 J/g energy by the particle bed, the integral breadths accounted for 0.1643, 0.1769 and 0.2077 degree for the reflections of (014), (110) and (300) respectively. A slight fluctuation in the values of the integral breadth in particular at lower energy absorption can be related to the heterogeneity of the particle beds where adequate numbers of larger particles still exist in the bed. The variation of the integral breadth vs. diffraction angle can be related to the Bragg's angle effect (line breadths increases normally with Bragg's angle) crystallite shape and microstructure characters or anisotropy which has been found in the previous work for hematite (Pourghahramani and Forssberg, 2006a, b).

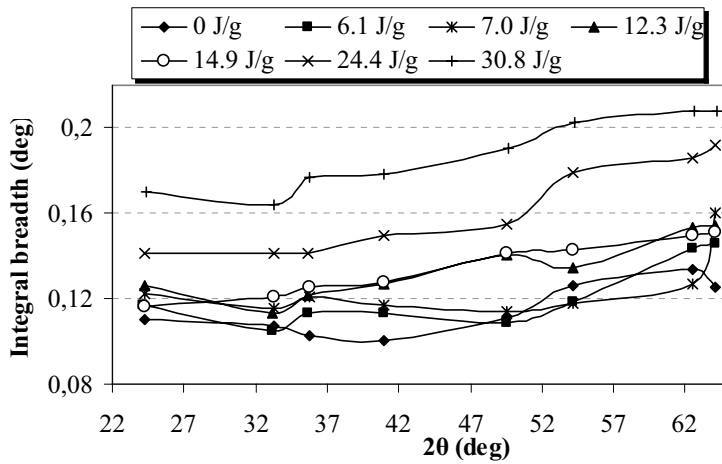


Fig. 10. Changes in the integral breadths of hematite ground in piston-die press as a function of energy absorption.

Balaz (2000) considered that the effect of comminution can be evaluated by the mass fraction of the crystalline phase in the comminuted solids compared to the unground samples, which is assumed to correspond to 100% crystallinity. The crystallinity index (X) and subsequently the X-ray amorphization degree (A) defined by Ohlberg and Strickler (1962), was used to quantify the progressive structural damage. This index comprises the background and peak intensities.

$$X = \frac{U_0}{I_0} \times \frac{I_x}{U_x} \times 100 \quad ; \quad A = 100 - X \quad (7)$$

where U_0 and U_x refer to the background of the initial and ground samples respectively, while I_0 and I_x are integral intensities of diffraction lines of the initial and ground samples. In our calculations, the two most intensive reflection peaks (014) and (110) were used. It is assumed that the amorphous phase in the initial powder is negligible. For calculation, equation 8 was applied on the data extracted from profile fitting. The average X-ray amorphization degrees for the ground samples are given in Fig. 11. Clearly, with increasing

absorbed energy by the bed up to 15 J/g the degree of amorphization goes up sharply and afterwards continues to change slightly. A rapid disintegration of the particles at lower levels of energy absorption facilitates the formation of the short range order structure (amorphous material) in the hematite bed. The maximum amorphization degree of about 31 % is obtained during the compaction of the bed in the piston-die press. The further increase of the absorption energy tends to increase the line broadening (see Fig. 10 compared to Fig. 11) rather than to decrease the reflection intensity and/or amorphization. It is expected that the ground samples under higher energy absorption give smaller crystallites and higher microstrain. To our knowledge, there is no data in literature yet in the bed comminution effects on structural changes to compare the obtained results.

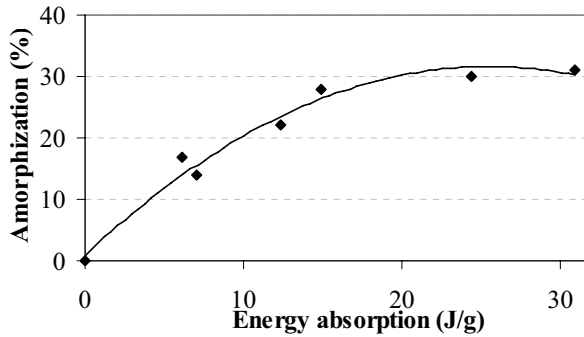


Fig. 11. Variations of the amorphization degree as a function of energy absorption. The amorphization degree was calculated considering (104) and (110) reflections.

3.2.2. Microstructural characteristics

The variation of crystallite size and lattice strain of hematite phase with energy absorption by the particle bed is given in Table 2. These values are calculated following (1) Warren-Averbach approach and (2) Rietveld analysis. For the Rietveld method, the results were averaged by considering all reflections in the whole profile, although the microstructure results of each reflection shows slight deviations from each other due to the anisotropy behaviors in the XRD patterns. The results of the Warren-Averbach method were calculated and given for direction [012] using the (012) and (024) reflections. The normally quoted values for strains are the local values, i.e., at $L=0$. However, the microstrain at $L=0$ can not be directly determined by using the Warren-Averbach method. The experimental A_L^D functions (Fourier coefficients of strain) are often affected by errors, in particular due to the truncation in the Fourier transformation of the diffraction lines (Lucks et al., 2004). Thus, we decided to calculate the strain at $L = 10 \text{ nm}$ ($< \varepsilon_{L=10\text{nm}}^2 >^{1/2}$). According to Table 2, both the values of crystallite size (D_s and D_v) decreases gradually with increasing absorbed energy by the particle bed. The values of the surface weighted crystallite size and volume weighted crystallite size from 186 and 205 nm in the initial sample reduces to about 53 and 108 nm respectively after energy absorption 31 J/g. The lattice strain also gives increasing trends with increasing the energy absorption whatever the methods are employed. The root mean square strain (RMSS), $< \varepsilon_{L=10\text{nm}}^2 >^{1/2}$, and maximum strain (ϵ) are increased to 9.4×10^{-4} and 4.1×10^{-3} after energy absorption of 31 J/g respectively. The detection of strain contribution

from XRD patterns at lower $L=10\text{ nm}$ using Warren-Averbach method is impossible up to energy absorption of 7 J/g by the bed due to very small strain contribution to XRD patterns.

Table. 2. Microstructure characters obtained using Warren-Averbach for [012] direction and Rietveld analysis for whole profile of the hematite ground in piston-die press

Absorption energy (J/g)	Warren-Averbach		Rietveld	
	$D_s\text{ (nm)}$	$\langle \varepsilon_{L=10nm}^2 \rangle^{1/2} (10^{-4})$	$D_v\text{ (nm)}$	$e(10^{-3})$
0	186.2	nd.	205.7	0.8
6.1	99.7	nd	182.7	1.6
7.0	77.9	nd	177.2	1.8
12.3	68.8	4.6	176.6	2.0
14.9	72.4	8.2	165	2.1
24.4	67.3	8.6	141.3	2.2
30.9	53.4	9.4	108	4.1

The quantitative analysis and comparison of size and strain without considering the underlying assumptions in each method is impossible. In the case of pure-gauss strain broadening, the RMSS is independent of L and the relationship between $\langle \varepsilon_L^2 \rangle^{1/2}$ and e , strain resulting from integral method, is given by Balzar (1999), Halder and Wagner (1966) and Keijsers et al. (1983) follows as:

$$\langle \varepsilon_0^2 \rangle^{1/2} = \langle \varepsilon_{L=0}^2 \rangle^{1/2} = (2/\pi)^{1/2} e \quad (8)$$

However, there is no clear connection between RMSS and e ; if the strain broadened pattern contains a Cauchy component. A rough estimate was given by Balzar (1999) when the Gauss and Cauchy extremes of the strain broadened Voigt profile exist:

$$0.5 \leq e / \langle \varepsilon_L^2 \rangle^{1/2} \leq 2 \quad (9)$$

If D_v and D_s denote the volume weighted and the surface weighted crystallite sizes respectively, the relationship between D_v and D_s has been given by Balzar (1999) and Lucks et al. (2004):

$$1.31 \leq \frac{D_v}{D_s} \leq 2 \quad \text{for a Voigt size-broadened profile} \quad (10)$$

$$\frac{D_v}{D_s} \geq r \quad \text{otherwise (Alternative methods)} \quad (11)$$

r ranges typically between 1 and 3.

Our findings from the Rietveld analysis agree with the ones from the Warren-Averbach analysis. An existing slight higher value in the strain (e) when compared with regard to the above mentioned expressions can be related to the fact that for the crystallite size refinement only the Lorentz component is taken in calculation. As a result, a small Gaussian size broadening component in XRD pattern may be accounted for strain calculations.

The changes in the lattice parameters are evaluated using Rietveld refinement. The results associated with standard deviations as error bars, are given in Fig. 12a. The length of a axes

decreases slightly with increasing energy absorption while the length of c axes increases initially and decrease at higher energy absorption. The comparison of these results with changes in the density of material (Fig. 12b) confirms the compaction of hematite lattice over the compressive load in a confined particle bed. Comparison of these results with loose media millings in previous work (Pourghahramani and Forssberg, 2006b), where we observed the expansion of hematite lattice, reveals that the changes in the lattice depends on the stressing manner.

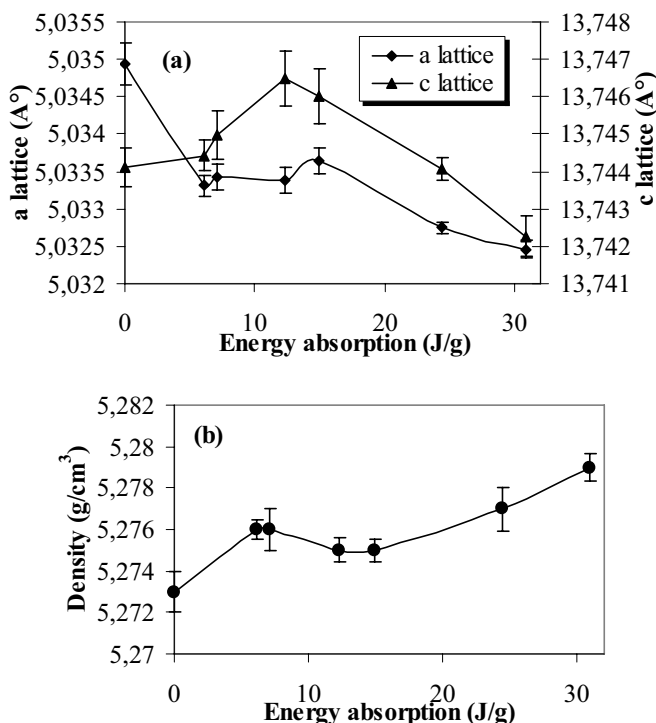


Fig. 12. (a) Variation of hematite lattice parameters and (b) density as a function of energy absorption using Rietveld analysis. The standard deviations are given as error bars.

4. Comparison with loose media milling

For comparison, hematite was ground in a tumbling mill (Mergan) and the same methods were employed for characterization of structural changes in the ground hematite. The experimental procedures and characterization are given in details elsewhere (Pourghahramani et al., 2006). The tumbling mill has been calibrated in such a way to obtain the net grinding energy. The obtained results are compared with the results of the confined bed grinding as a function of energy terms. The X-ray amorphous phase content, surface weighted crystallite size from Warren-Averbach method and maximum microstrain obtained from Rietveld analysis are considered in comparison. The results are displayed in Figs, 13, 14 and 15. It is evident that tumbling milling needs much more energy to cause the same structural changes as particle bed grinding. For achieving the X-ray amorphous phase about 30%, the tumbling milling needs 88 J/g net grinding energy while the particle bed grinding needs 31 J/g. For the same levels of the energy in the two grinding regimes, the surface weighted crystallite size

reaches about 54 nm. After releasing of 1000 J/g net grinding energy in tumbling mill, the lattice strain increases to about 3.6×10^{-3} . The same lattice strain achieved after energy absorption of 30 J/g by the particle bed. A close look on the results reveals that the structural defects are vital for mechanical activation are formed in bed grinding in coarse particles than in tumbling mill with loose media. As a result, the particle bed grinding shows higher efficiency in structural changes than tumbling milling with respect to grinding energy. This can be related to the fact that in tumbling mill considerable energy losses occur in overcoming friction and the wear of media and mill liners when energy transferred to particles by the grinding media. Furthermore, many collisions turn out to be largely ineffective simply because the entrapment of particles in the impact zone is a highly probabilistic hit-and-miss affair. On the other hand, no separate medium is required for transfer of energy when a confined bed of particles is loaded under compression. Thus, no withstanding energy losses exist due to interparticle friction (Fuerstenau and Kapur, 1995).

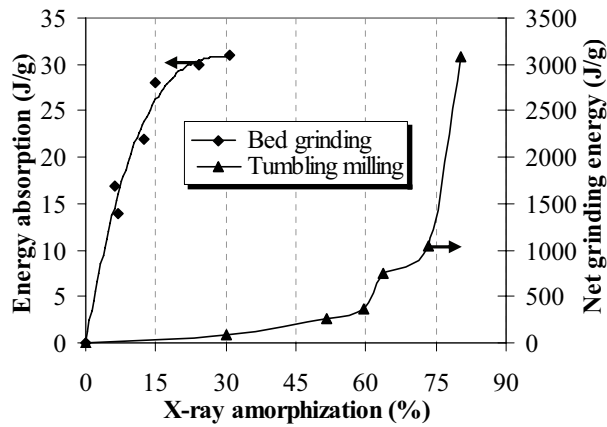


Fig. 13. Comparison of the X-ray amorphization degree of hematite ground in tumbling mill and confined particle bed.

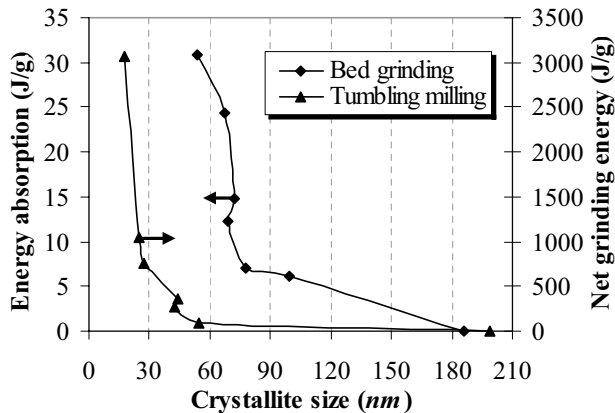


Fig. 14. Comparison of the crystallite size of hematite ground in tumbling mill and confined particle bed.

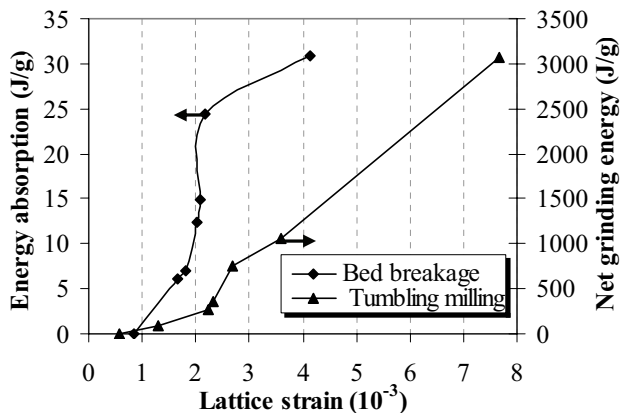


Fig. 15. Comparison of the lattice strain of hematite ground in tumbling mill and confined particle bed.

To summarize, it is interesting that all the results can be fairly described as a function of energy absorption. It was also found that the interparticle breakage causes plastic deformation in material and subsequently induces changes in the structure of the ground hematite. The trends in the results of structural changes indicate that further structural refinement would occur at higher energy absorption levels. Therefore, the structural changes in particle bed breakage make it possible to apply for mechanical activation of minerals. However, for severe structural changes and subsequently for higher reactivity, the particle bed must be subjected to higher pressure or to another system of piston-die press in which not only the cyclic loading can be made but also the particles can be re-arranged after the preceding compaction. More investigations are recommended to explore the influence of other variables like feed size fraction, cyclic loading, etc.

5. Conclusions

The following conclusions based on the experimental results presented in the article, have been made:

- The energy absorption results from the compaction diagram. The energy absorption is the dominating factor for the size reduction, surface area and induced structural changes in the particle bed comminution.
- The absorption is proportional to the applied force. The linear energy-force relationship stands well even if the particle bed heights are changed.
- For a given pressure, the higher particle bed height gives lower energy absorption by the bed, surface area, amorphization degree and microstrain and larger particles and crystallites size than the smaller particle bed height.
- The broadening and intensity reduction of the XRD patterns take place as hematite is subjected to compaction. Their magnitudes can be interrelated with energy absorption by the particle bed. The further increase of the absorption energy tends to increase the line broadening rather than to decrease the reflection intensity and/or amorphization.
- From the Warren-Averbach method and Rietveld analysis, the final product is characterized with a surface weighted crystallite size of 53 nm and a volume weighted

crystallite size of 108 nm. Similarly, the root mean square strain at $L=10$ nm, $\langle \varepsilon_{L=10nm}^2 \rangle^{1/2}$, is calculated about 9.4×10^{-4} and maximum strain about 4.1×10^{-3} .

- The Rietveld refinement of the lattice parameters confirms the compaction of the hematite lattice over the compressive load in a confined particle bed. It can be concluded that the changes in the lattice depends on the stressing manner.
- It was revealed that bed comminution has higher efficiency in energy transfer to the particles and subsequently structural changes compared to the tumbling mill. More investigations are recommended to explore the influence of other variables like feed size fraction, cyclic loading etc.

Acknowledgments

The authors would like to thank professor Claes I Helgesson for his valuable comments on this paper. The financial support for the project by Agricola Research Centre (ARC) is gratefully acknowledged.

References

- Aziz, A., Schönert, K., 1980. Einzelkomzerkleinerung und Gutbettbeanspruchung von Zementklinkerfraktionen. Zement-Kalk-Clips, 5, 213-218.
- Balaz, P., 2000. Extractive Metallurgy of Activated minerals, Elsevier, Amsterdam.
- Balzar, D., 1999. Voigt-function model in diffraction line-broadening analysis. Microstructure Analysis from Diffraction, edited by R. L. Snyder, H. J. Bunge, and J. Fiala, International Union of Crystallography.
- Balzar, D., Audebrand, N., Daymond, M. R., Fitch, A., Hewat, A., Langford, J. I., Bail, A. Le., Louër, D., Masson, O., McCowan, C. N., Popa, N. C., Stephens, P.W., Toby, B.H., 2004, Size-strain line-broadening analysis of the ceria round-robin sample, J. Appl.crys.37, 911-924.
- Boldyrev, V.V., Pavlov, S.V., Goldberg, E.L., 1996. Interrelation between fine grinding and mechanical activation. Int. J. Miner. Process. 44-45, 181-185.
- Bruker AXS, 2003. DIFFRACplus TOPAS/TOPAS R/TOPAS P Version 2.1 Technical Reference, printed in Germany.
- Fuerstenau, D.W., Gutsche, O., Kapur, P.C., 1996. Confined particle bed comminution under compressive loads, Int. J. Miner. Process.44-45, 521-537
- Fuerstenau, D.W., Kapur, P.C., 1995. Newer energy approach to particle production by comminution, Powder Technol. 82, 51-57
- Fuerstenau, D.W., Shukla, A., Kapur, P.C., 1991. Energy consumption and product size distributions in choke-fed, high-compression roll mills. Int. J. Miner. Process., 59-79.
- Gutsche, O., Fuerstenau, D.W., 1999. Fracture kinetics of particle bed comminution-ramifications for fines production and mill optimisation, Powder Technol. 105, 113-118
- Halder, N.C., Wagner, C.N.J., 1966. Separation of particle size and lattice strain in integral breadth measurements. Acta Cryst. 20, 312-313.
- Hoffmann, N. and Schönert, K., 1971. Bruchanteil von Glaskugeln in Packungen von Fraktionen und binären Mischungen. Aufbereitungs-Technik 12, 513-518.
- Kapur, P.C., 1972. Self-preserving size spectra of comminuted particles. Chem. Eng. Sci. 27, 425-431.
- Keijser, TH. H. DE., Mittemeijer, E.J., Rozendaal, C.F., 1983. The determination of crystallite –size and lattice –strain parameters in conjunction with the profile –refinement method for determination of crystal structures. J. Appl. Cryst. 16, 309-316.

- Kou. S. Q., Liu. H. Y., Lindqvist. P.A., Tang. C. A., Xu. X. H., 2001. Numerical investigation of particle breakage as applied to mechanical crushing- Part II: Interparticle breakage, Int. J. Rock Mech. Min. Sci. 38, 1163-1172
- Lucks, I., Lamparter, P., Mittemeijer, E.J., 2004. An evaluation of methods of diffraction-line broadening analysis applied to ball-milled molybdenum. J. Appl. Cryst. 37, 300-311.
- Oettel, W., Husemann, K., 2004, The effects of a grinding aid on comminution of fine limestone particle beds with single compressive load, Int. J. Miner. Process. S74S, S239-S248
- Oettel, W., Nguyen, A.-QU., Husemann, K., Bernhardt, C., 2001. Comminution in confined particle beds by single compressive load, Int. J. Miner. Process. 63, 1-16
- Pourghahramani. P., Forssberg, E., 2006a. Microstructure characterization of mechanically activated hematite using XRD line broadening. Int. J. Miner. Process. 79, 106-119.
- Pourghahramani, P., Forssberg, E., 2006b. Comparative study of microstructural characteristics and stored energy of mechanically activated hematite in different grinding environments, Int. J. Miner. Process. 79, 120-139.
- Reichardt, Y., Schönert, K., 2003. Interparticle breakage of fine hard materials by single and multiple compression. Chem. Eng. Technol. 26, 191 - 197
- Reichardt, Y., Schönert, K., 2004. Cross piston press for high pressure comminution of fine brittle materials, Int. J. Miner. Process. 74S, S249-S254
- Ohlberg, S. M., Strickler, D.W., 1962. Determination of percent crystallinity of partly devitrified glass by X-Ray diffraction, J. Am. Ceram. Soc., 45, 170-171.
- Schönert, K. and Mueller, F., 1990. Representation of breakage fraction and breakage function of inter-particle stressing, Aufbereitungs-Technik, 3 1: 248-256.
- Schönert, K., 1991. Advances in comminution fundamental, and impacts on technology. XVII Inter. Nat. Miner. Process. Cong., Dresden, Vol 1, Sept., pp 1-21.
- Schönert, K., 1996. The influence of particle bed configurations and confinements on particle breakage, Int. J. Miner. Process. 44-45, 1-16
- Schönert, K., Reichardt, Y., 1993. Interparticle breakage of very fine materials by alternating crosswise stressing with a high pressure. XVIII international mineral processing congress, Sydney, 23-28 May, pp 213-217.
- Tavares. L. M., 2005. Particle weakening in high-pressure roll grinding, Minerals Engineering 18, 651-657
- Viljoen, R. M., Smit, J. T., Du Plessis, I., SER, V., 2001. The development and application of in-bed compression breakage principles, Minerals Engineering 14, 465-471
- Warren, B. E., Averbach, BL., 1950. The Effect of Cold-Work Distortion on X-Ray Patterns, J. Appl. Phys. 21, 595-599.
- Young, R. A., 1993. Introduction to the Rietveld method.- The Rietveld Method, edited by R.A. Young, IUCr Book Series, Oxford University Press.

Paper VI

Microstructural Characterization of Hematite during Wet and Dry Millings Using Rietveld and XRD Line Profile Analyses

*Parviz Pourghahramani, Erguen Altin, Wolfgang Peukert, & Eric Forssberg, Submitted for
publication in Powder Technology*

Microstructural characterization of hematite during wet and dry millings using Rietveld and XRD line profile analyses

Parviz Pourghahramani^a, Erguen Altin^b, Wolfgang Peukert^c, and Eric Forssberg^d

^{a, d} *Division of Mineral Processing, Luleå University of Technology, SE-971 87, Luleå, Sweden*
^{b, c} *Institute of Particle Technology, Friedrich-Alexander University, Cauerstr. 4, 91058 Erlangen, Germany*

Abstract

The effects of extended milling in a stirred media mill and a tumbling mill on the structural changes in hematite concentrate have been examined using a combination analyses of particle size, BET surface areas, X-ray diffraction (XRD), thermal (TG and DSC) and FTIR measurements. Rietveld's whole profile fitting based on crystal structure refinement is applied to monitor the microstructural evolution of hematite phase. Warren-Averbach's method of X-ray line profile analysis is also made to compare the obtained results.

It is found that the BET surface area, X-ray amorphization phase content and XRD line breadths increase with progress in milling. The use of stirred media mill exhibits larger surface areas, smaller particle sizes, more XRD line broadening and subsequently greater structural distortions compared to the tumbling mill for a given energy input; although the X-ray amorphous phase content remains unaffected by the grinding environments. The maximum X-ray amorphization degree are calculated about 80 and 95 % after releasing of 22400 and 82000 kJ/kg energy in the tumbling and stirred media mills respectively. The maximum specific BET surface area in the stirred media and tumbling milling increases to about 72.5 and 6.8 m^2 / g after 82000 and 22400 kJ/kg energy consumption respectively. As a result of structural refinement during milling, the surface weighted crystallite size in ground hematite are 17 and 4 nm after consuming 22400 and 82000 kJ/kg in the tumbling and stirred media mills respectively, corresponding to the volume weighted crystallite size of 17 and 11 nm. For the same energy consumption in the mills, in turn, the root mean square strain, $\langle \varepsilon_{L=10nm}^2 \rangle^{1/2}$, increases to about 4.4×10^{-3} and 4.9×10^{-3} . The results of the two applied methods are compared and discussed in details.

In addition, thermogravimetric analysis of the wet ground samples reveals that the TG curves represent two weight loss steps. A weight loss is observed around 100 °C in the sample which is attributed to the removal of adsorbed water due to the wet milling operations. A strong weight loss step starting from 100 to 400 °C is attributed to surface/ bulk dehydroxilation of iron hydroxides. The weight loss increases with extending of the milling. In contrast, the dry milled samples yield negligible weight losses comparing with the wet ground samples.

Keywords: Structural Changes, Iron Oxide, Mechanical Activation, Wet and Dry Milling

1. Introduction

If the material is subjected to intensive grinding and ground to ductile-brittle transition rang, the plastic deformation occurs in the materials being ground and a variety of structural

^a Corresponding author: Tel:+46 920 491313; fax:+46 92097364
E-mail address: Parviz.Pourghahramani@ltu.se

changes are formed in the materials. These structural changes and mechanochemical transformations include formation of amorphous phases, surface activation, polymorphic transformation, chemical reaction, structural refinement etc. The formation of highly-active surface areas as well as changes in the physical behavior of solids can be directly attributed to permanent rearrangement of the crystal lattice, and structural alteration of the grains during grinding [1, 2]. Mechanical induced structural changes and reactions play an important role in the processing of solids. It has been reported that mechanical activation substantially accelerates the leaching kinetics of several sulphide and oxide minerals, even at ambient pressure. The enhanced effect is attributed to the increase of specific surface area and structural disorder [3], enhanced strain [4], amorphization of mineral particles [5], preferential dissolution of select crystal faces [6], microtopography [7], and formation of new phases more amenable to leaching [8]. Thus, the ground samples under higher intensive milling can not be characterized by a particle size distribution alone and the characterization of structural changes have to be considered.

Two grinding modes including dry and wet modes are applied in the grinding processes such as ceramic, pharmaceutical, paint, mechanical activation of material and/or minerals, mechanochemistry and many other industries to improve the martial properties. The comparison of the wet and dry grinding effects on the structural changes usually was made at the same grinding mill. For example, the effect of dry and wet milling in a vibratory mill for carbonates and quartz in air and aqueous environments was investigated by Tkáčová and Stevulová [9]. It was indicated that the use of an aqueous environment resulted only in enlarged specific surface area of the ground products. Baláž et al. [4] concluded that during wet milling in either an attritor or a vibration mill yield the least structural changes compared with their dry milling modes. According to Tkáčová [10], wet grinding proceeds with the preferential formation of new surfaces and little bulk deformation in the particles. Since the contribution of the non-equilibrium defects to the integral excess enthalpy content is considerably higher than the contribution resulting from the surface energy, the expected magnitude of excess enthalpy in wet grinding is lower than that one in dry grinding.

The goal of this paper is to investigate the structural changes in hematite concentrate during wet stirred media and dry tumbling millings using Rietveld and Warren-Averbach analyses. Several structural characteristics like BET surface area, amorphization, crystallite size, lattice strain, surface properties and thermal behaviors of the ground samples in the mills are studied and discussed in details.

2. Experimental

2.1. Material

The high purity hematite concentrate containing about 97.91% Fe_2O_3 was supplied by the LKAB (Luossavaara Kiirunavaara Aktiebolag) Company in Sweden. The XRD pattern of hematite concentrate (hereafter referred to as initial hematite) only showed the hematite reflection peaks. The chemical analysis of initial hematite is also given in Table 1. From the BET measurement, the specific surface area was estimated about $0.59 \text{ m}^2 / \text{g}$. The mean diameter, F_{80} and density of starting hematite were calculated to around 46, $80 \mu\text{m}$ and $5240 \text{ kg} / \text{m}^3$ respectively.

Table 1. The chemical analysis of the initial hematite (%).

Fe_2O_3	Al_2O_3	SiO_2	TiO_2	MgO	MnO	P_2O_5	Other elements
97.91	0.73	0.73	0.27	0.20	0.022	0.088	0.051

2. 2. Pre-treatment

Since the initial particles were large, a pre-grinding test was made to achieve a proper particle size for measuring ζ potential of the particles. A laboratory stirred media mill PE075 from Netzsch (Germany) has been used for comminution experiments. This media mill has a chamber volume of 0.6 liter. The stirrer is equipped with 3 perforated discs. In order to reduce the amount of wear from materials of the mill, the grinding chamber is made of ceramic (Al_2O_3) and the stirrer is equipped with discs from SiC. The experimental set-up provides a batch mode comminution of the product. Y_2O_3 -stabilized ZrO_2 grinding beads were used for milling. 1405 g of grinding media with density of 6065 kg/m^3 is introduced into the grinding chamber which completely covers the three discs of the stirrer. 225 g of a suspension was introduced into the grinding chamber. The number of revolutions of stirrer per time can be adjusted by a rotary speed controller. The rotary speed was chosen 1300 RPM. The grinding time was 3 hours. The solid content of the pulp was adjusted at 20%. Milling media was separated from the product by sieving and samples were collected for potential measurements. The final product was used to measure the zeta potential as a function of the pH (see Fig. 1). To avoid the agglomeration of the particle during milling in the stirred media mill, a hematite suspension at pH=3 was adjusted where the highest absolute value for the potential were obtained; thus, the best conditions provided for electrostatic stabilization of the particles.

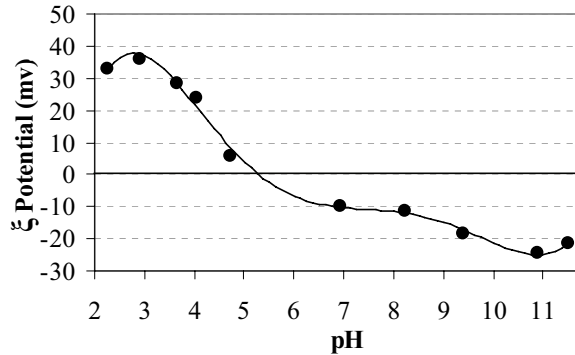


Fig.1. pH-dependency of the zeta-potential of the final hematite product in the batch mill

2.3. Milling

Dry and wet grinding tests were carried out using a tumbling mill and a stirred media mill respectively. For tumbling milling, a mixture of ball steel media with dimensions between 6 and 22.2 mm and with apparent density of 4875 kg/m^3 was used as grinding media. The grinding tests were performed in closed condition, i.e., the lids of the mills were kept bolted during the grinding. The grinding tests were extended up to 9 hours. The energy input was recorded during milling using an energy meter. The grinding experimental conditions are given in Table 2.

A stirred media mill which was operated in a re-circulated mode at a fixed flow rate was used for grinding. It consists of a 200 mm×90 mm stainless steel cylinder chamber (0.95 l of net grinding chamber volume) and an agitator with six perforated discs installed on a horizontal driven shaft. For cooling purpose, the grinding chamber is equipped with a water jacket. The feed material is pre-dispersed by a disperser. The suspension is pumped from the grinding chamber into a stirred vessel and from there back into the grinding chamber through the

ultrasonic spectrometer (dispersion technology). Torque and number of revolutions are measured by a torque sensor shaft which is installed in the stirred media mill. The grinding chamber is lined with ceramic walls (SiSiC) and the stirrer is equipped with discs of polyurethane (PU). The ground suspension is discharged from the mill chamber through a sieve cartridge which permits passing the particles smaller than 0.05 mm. Yttrium-stabilized zirconia beads of 0.5 mm diameter with density of $6065 \text{ m}^3/\text{kg}$ were used. The filling ratio of the mill chambers by grinding beads was around 46.2% in the mill. Besides, the mill is equipped with different sensors to measure simultaneously the temperature, the pH value and conductivity as well as zeta potential. The solid content was set at 20%. The pH value of the pulp was adjusted at 3 using commercially available nitric acid (HNO_3).

Table 2. Experimental milling conditions and mill types.

Milling conditions	Tumbling milling	Stirred milling
Specific input energy (kJ/kg)	720-22400	410-82000
Media filling (%)	38.9	46.2
Maximum milling time (h)	9	24
Ball to powder weight ratio	16.77:1, 67:1	7
Speed (RPM)	60	2220
Media apparent density (gr/cm^3)	4.875	6.065
Solid content (%)	100	20
Media diameter (mm)	6-22	0.5
$L \times \phi$ mm	275×245	200×90

2. 3. Characterization

The XRD patterns were obtained using a Siemens D5000 powder diffractometer with Bragg-Brentano geometry equipped with a curved graphite monochromator in the diffracted beam arm and using Cu $K\alpha$ radiation ($\lambda = 0.15406$). The XRD patterns of the samples were recorded using a step size of 0.02° and a counting time of 5s per step. Slit size of 0.1 mm was used. To characterize the microstructural characteristics encountered during the mechanical activation of specimens, Warren-Averbach and Rietveld analyses were applied.

The particle size distribution of the samples ground in the tumbling mill (dry mode) was measured by laser diffraction (CILAS 1064) in the liquid mode in the presence of hexametaphosphate (1g/L). The mean particle diameter and granulometric surface area were calculated based on particle size distributions. Samples ground in the stirred mill were diluted with distilled water and the pH was adjusted to 3 (1 M HNO_3) before sonication for 3 min with ultrasonic probe to ensure a homogeneous mixing. The particle size measurement was performed by means of a dynamic light scattering technique in an Ultra particle analyzer (UPA, Microtrak), from which the volume and surface median particle diameter were obtained.

The specific surface areas of the samples were determined by the BET method with the Flow Sorb II 2300 (Micromeritics). Samples were degassed by heating at 200°C for 90 min immediately prior to measurements, from which the equivalent particle diameter assuming spherical shape for particles was determined.

Thermogravimetric analyses (TG) were conducted using a TA instrument at a heating rate of $10^\circ\text{C min}^{-1}$ to 800°C . The high temperature furnace was protected by injection of inert nitrogen gas. The heating was performed under highly pure nitrogen with a rate of flow of 40 ml min^{-1} . The mass of samples was almost 50-60 mg.

Infrared spectra were measured using an evacuable Bruker IFS 66v FTIR spectrometer (DRIFT measurements), which features excellent noise and stability performance. The spectra of the samples were recorded in the range of 400-4000 cm^{-1} .

2.4. Microstructural characterization (background)

2.4.1. Warren-Averbach analysis

Line broadening analysis of XRD patterns is the pre-processing step in the Warren-Averbach approach [11]. The eight most intensive reflection peaks of the samples were used in the line broadening analysis. The Profile software supplied by Bruker/Socabin was used in the profile fitting procedures and in the extraction of the parameters. The obtained X-ray diffraction patterns were fitted with Pseudo-Voigt line shape function, which is a linear combination of Cauchy and Gaussian functions. For each adjusted line profile, the following parameters were obtained: (1) The maximum intensity of peaks (I_{\max}), (2) The full-width at half of its maximum intensity ($FWHM$), (3) Integral breadth (β), (4) the mixing factor (η), and (5) peak position (2θ). The same procedure was applied for the standard sample, LaB_6 (SRM660a), proposed by National Institute of Standards and Technology (NIST) of USA to obtain the instrumental profile. Values of the goodness factors with this refinement method are smaller than 7%. Once the line parameters were extracted, the Warren-Averbach method was used for resolving of domain size and strain contributions on XRD patterns. An example of profile fitting is shown in Fig.2. The profile fitting procedure and principles of the Warren-Averbach method were discussed in details in previous works [12, 13].

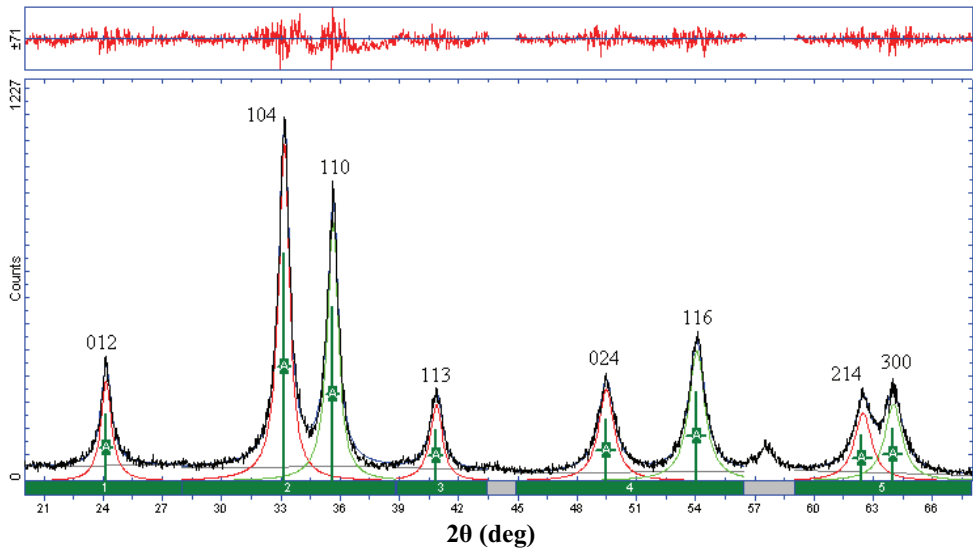


Fig. 2. An example of profile fitting in which the Pseudo-Voigt function is fitted to the hematite sample ground for 5 hours in the stirred media mill. The net difference between the observed and measured profile is given on top of plot.

2.4.2. Rietveld analysis

Rietveld method is becoming progressively popular for microstructural characterization of material. It is common practice to estimate domain size and strain values from the refined

profile width parameters. The method is a so- called “full pattern method”. In the Rietveld refinement, all of data points of a powder pattern are fitted to structure models, which depend on adjustable parameters. The fitting to the measured XRD pattern is performed by a least-square calculation. The calculated curve is based on the crystallographic structure models, which also take into account samples and instrumental effect. The parameters of this model are refined simultaneously to achieve the best fit to the data by least square method. By least square refinement, a so-called figure of merit function R is defined, which describes the residual between calculated and measured data [14]:

$$R = \sum_i w_i [y_i(obs) - y_i(calc)]^2 \rightarrow \min \quad (1)$$

where R is the residual value of the figure-of-merit function, w_i is $1/y_i$, $y_i(calc)$ denotes the calculated density and $y_i(obs)$ is the measured intensity at the i^{th} step.

The intensity of a Bragg reflection is influenced by the structure factor, the absorption and polarization correction, the Lorentz factor, grain size effect and preferred orientations (texture). Besides, the profile of Bragg reflection is affected by different factors such as emission profile of X-ray source, the crystallinity, deviations of lattice parameters, the geometry of diffractometer and the size of slits. The software TOPAS 2.1 from Bruker AXS [15] was used for Rietveld refinement in this work, in which it is possible to make all of the corrections and refinement processes. The software package TOPAS 2.1 uses the fundamental parameter approach (FPA), and is therefore capable of estimating the instrumental influence. In the TOPAS software, the Double-Voigt approach [16] is used for resolving of size and strain components. In addition, the Double-Voigt approach can be applied with fundamental parameters approach (FPA) and measured instrument functions. As Lorentz (Cauchy) or Gauss functions can not satisfactorily model the specimen broadening, it is assumed that the both size and strain effects are approximated by Voigt function. According to Balzar [16], a convolution of two Voigt functions is also a Voigt function and the size and strain integral breadths of Cauchy and Gauss parts can be combined:

$$\beta_C = \beta_{SC} + \beta_{DC} \quad \beta_G^2 = \beta_{SG}^2 + \beta_{DG}^2 \quad (2)$$

where β_C and β_G are the Cauchy and Gauss components of total integral breadth β respectively. The term β_{SC} and β_{DC} are the Cauchy components of size and strain integral breadth, respectively and β_{SG} and β_{DG} are the corresponding Gaussian components. Once the components are calculated, the maximum lattice strain, e , and volume weighted crystallite size, D_v , can be calculated [17]:

$$e = \beta_D / 4 \tan \theta \quad D_v = \lambda / \beta_S \cos \theta \quad (3)$$

where β_D and β_S are the integral breadth of a Voigt function comprising a Gaussian and a Lorentzian components respectively. λ is the wavelength of the X-ray source and θ is diffraction angle.

After inserting the instrumental parameters, Pseudo-Voigt line function were adjusted on the XRD patterns. The starting sample and ground hematite are indexed in a hexagonal (trigonal) symmetry (R-3c space group). All atoms positions of the ground samples were assumed to be in special positions like the initial sample. Therefore, the only structural parameters refined were the lattice parameters and microstructural characteristics such as crystallite size, strain components and crystal density. It was found that the Gaussian component of the crystallite size in the most cases is negligible by an initial refinement attempt. Thus, for all data sets, Lorentzian size parameters refined to a non-zero value. However, for the strain both Gaussian and Lorentzian strain components refined to non-zero values and average value of strain from

all reflections (e) are reported in the paper. A preferred orientation-correction refinement initially was attempted, but did not yield significant improvement for any of the patterns and consequently it was excluded from the final refinement process. The global factors included the scale factor, 2θ zero correction, specimen displacement, LP factor and background parameters (chebychev polynomials function with five orders the series) and crystal linear adsorption coefficient were refined for all data sets. Subsequently, the Bragg reflection profile can be calculated by convolution of mathematical functions of these parameters. Several criteria of fit (R factor) for judging the quality of a Rietveld refinement have been proposed [9]. They show the deviation in accordance with the used model in percent. The most common R factors are the weighted profile R-factor (R_{wp}), the expected R factor (R_{exp}) and goodness of fit ($GOF = R_{wp} / R_{exp}$). The goodness factor for our experiments was attained between 0.95 and 1.4 which implies satisfactory fit to the measured data. An example of whole pattern fitting using Rietveld refinement is shown in Fig. 3.

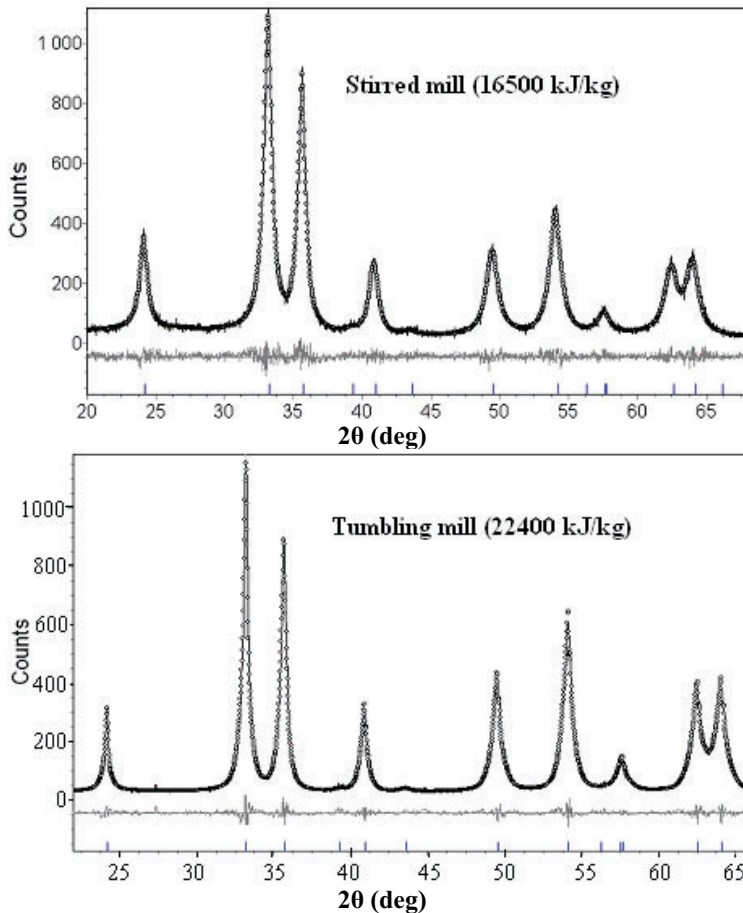


Fig. 3. Some selected graphical representation of Rietveld analysis for X-ray powder diffraction patterns of the milled samples. Experimental data are shown as continuous solid line, refined simulated patterns are shown as dots. The difference between experimental data and fitted simulated pattern is shown as continuous gray line under each diffraction pattern.

3. Results and discussion

3.1. Granulometrical changes

The mean diameter of the ground samples, as shown in Fig. 4, decreases rapidly during the initial stages of milling and then levels off or increases slightly depending on milling operation. The granulometrical changes are mainly observed in the initial stages of milling. In the case of tumbling milling, the particle size reduction is completed after consuming about 5500 kJ/kg energy, indicating that further size reduction is impossible. The products of the stirred media mill are smaller than the products of the tumbling mill over the grinding energy. When grinding with stirred media mill, further particle size reduction is possible even at higher levels of energy, although the rate of size reduction decreases drastically with progress in milling. The final particle size in the stirred media mill is obtained around 200 nm. The increase in mean particle size that occurs after intensive grinding in the products of the tumbling mill is an indication of re-agglomeration, which is inevitable in the dry fine grinding regimes. As the grinding prolonged, the agglomeration is more pronounced. The agglomeration of particles during extended milling was reported for various minerals by Balaz [4], Welham [8], Welham and Llewellyn [18] and Zhang et al. [19]. These results suggest that agglomeration phenomena may be a feature of extended dry milling.

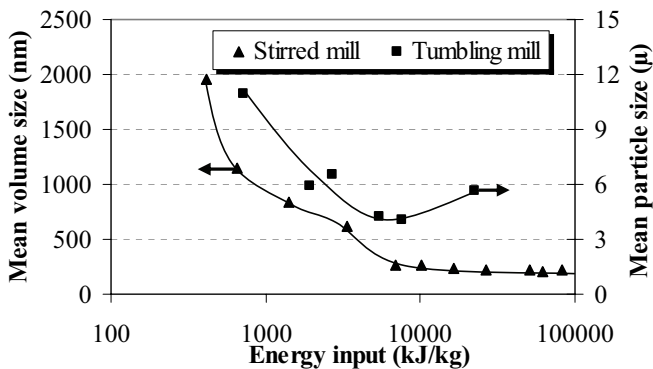


Fig. 4. Variations of mean particle size as a function of energy input in the mills

In addition, the calculation of the particle size based on the BET surface area, as shown in Fig. 5, reveals that the nanometer particles produced during grinding in both mills. However, the stirred media mill produced finer particles than the tumbling mill and the particle size decreases continuously with extending of milling. Comparing these results with the results in Fig. 4 shows that the calculated values from the BET method is smaller than the mean values in the same figure (Fig. 4). This is because nitrogen gas can penetrate the pores among the attached particles and consequently results in smaller values. The formation of pores may be related to the removal of the hydroxide during pre-treatment prior to the BET measurements. The formation of hydroxide is proved during wet milling (see section 3.3).

The decreasing trends in the particles size are supported as well by the BET surface area measurements as shown in Fig. 6. i.e., the BET surface area increases steadily over the grinding processes. The samples ground in the stirred media mill represents higher BET surface area compared with the samples milled in the tumbling mill. The BET surface area in the final products of the tumbling mill and stirred media mill are calculated about 6.5 and 72 m^2/g respectively. It is note worthy to mention that the BET surface areas in the products of

the mills increase sharply in the initial stages of the milling (the x-axis is scaled in logarithm). With progress in the milling, the production of the BET surface area in the stirred media continues to increase gradually while in the tumbling mill increases very slightly. The granulometry and BET surface area changes indicate higher ability of the stirred media mill in the production of nanometer-particles compared with the tumbling mill. This could be related to the effect of dispersions role (particle stability) and higher stress intensity in the stirred media mill. Consequently, severe structural changes in the stirred media milling are expected.

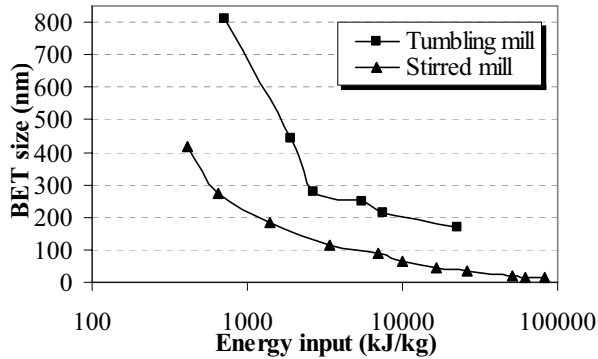


Fig. 5. Variations of mean BET particle size as a function of the energy input in the mills

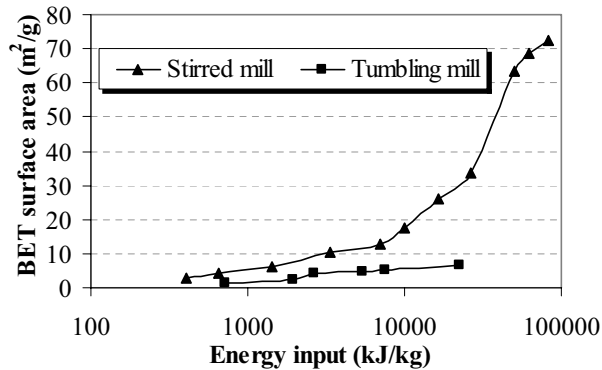


Fig. 6. Changes in the BET surface area as a function of energy input in the mills

3.2. Structural changes

3.2.1. XRD Pattern characteristics

The structural changes and the characterization of the microstructure characters were investigated using XRD analysis. The XRD patterns of the samples are given in Figs. 7 and 8 as function of energy input in the mills. The distortion of structure is reflected in the line broadening, the reduction of peak intensity and the shifting of reflections. The diffraction peaks for mechanically-treated samples are lower and broader than of those for initial sample whatever milling methods were applied, mainly due to disordering process of hematite crystal structure by intensive grinding. The reduction of diffraction peaks intensities implies the formation of amorphous material. The decrease of X-ray diffraction intensities is

accompanied by a general broadening of the XRD patterns. The increase of the XRD line breadths is due to the plastic deformation and disintegration of hematite. The XRD patterns showed only the hematite reflections, indicating that hematite did not undergo significant reaction and phase changes. The presence of small but remarkable reflection peaks after intensive grinding can be taken as a further indication of high milling resistance and mechanical strength of the submicron hematite crystallites. Regarding the effect of different mills, it can be observed that the stirred media mill brings about weaker and broader peaks than tumbling mill for a given energy input. The effects of dry and wet milling at the same mill are investigated for tantalite (columbite) by Welham [8] and for chalcopyrite by Baláz et al. [20]. It was found that the peaks present in the wet milled sample remained narrower and more intense, indicating that there was less crystalline damage occurring in the presence of water as against to our results. This is because our grinding tests were made in different mills and stirred media mill is more intensive than tumbling mill.

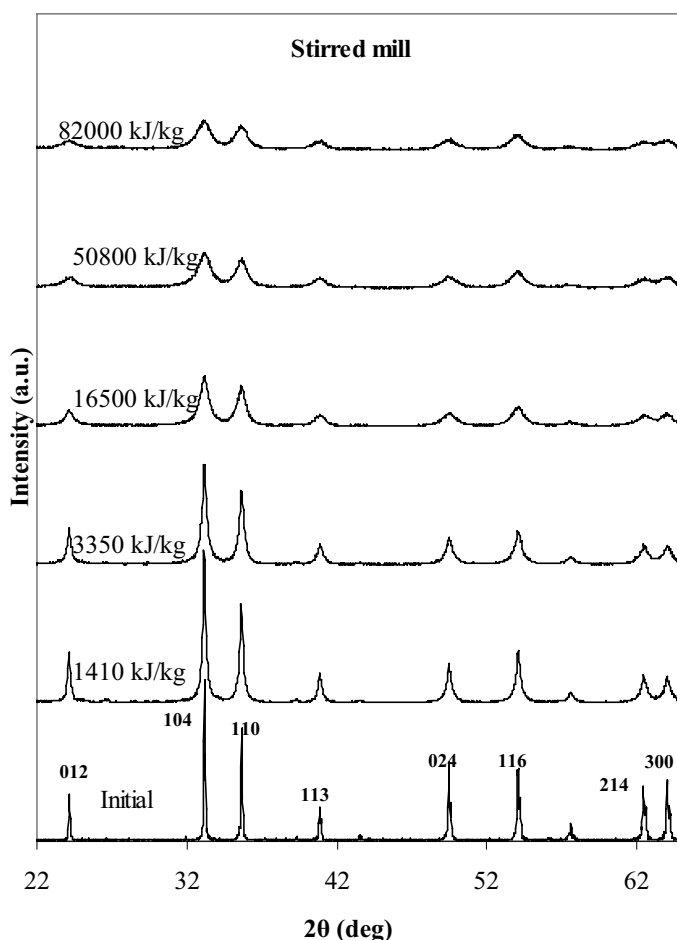


Fig. 7. XRD patterns of the initial and ground samples as a function of energy input in the stirred media mill

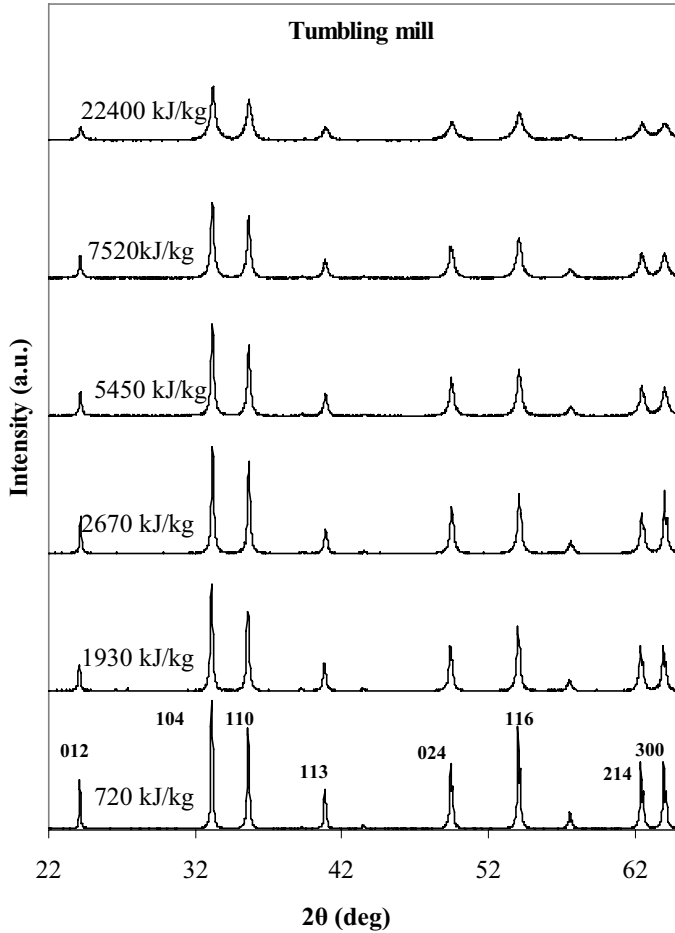


Fig. 8. XRD patterns of the ground samples as a function of energy input in the tumbling mill

For a quantitative comparison, the physical broadenings for the ground samples in the mills are depicted in Fig. 9. The integral breadths of the XRD line are determined from Profile fitting. It can be observed that the increase of energy input brings about higher broadening of reflection peaks in the ground samples. It can be further observed that the stirred media mill causes the maximum broadening of reflection peaks. Clearly, for a given energy input, the stirred media mill leads to higher XRD line broadening compared with tumbling mill. For example, the integral breadths for the reflection (104) in the sample ground with 22400 kJ/kg in the tumbling mill is 0.58821 degrees and for the sample milled in the stirred media by 16500 kJ/kg exceeds 1.046 degrees. The variation of the integral breadth vs. diffraction angle can be related to the Bragg's angle effect (line breadths increases normally with Bragg's angle) crystallite shape and microstructure characters or anisotropy which has been reported in the previous works on hematite [12, 13].

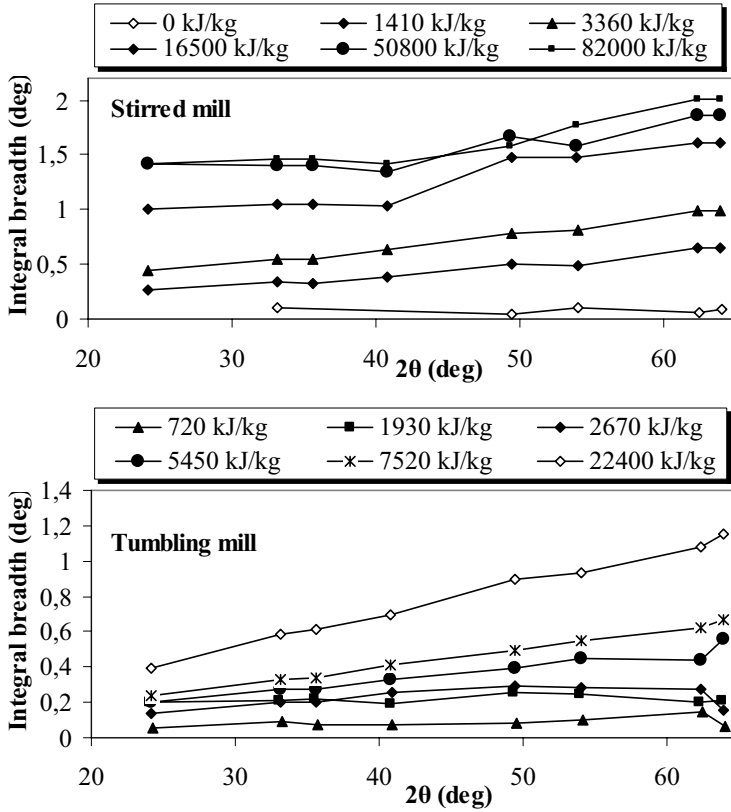


Fig. 9. Changes in the physical integral breadth of the ground samples in the mills as a function of energy input in terms of diffraction angle.

3.2.2. Amorphization degree

Baláz [4] considered that the effect of comminution can be evaluated by the mass fraction of the crystalline phase in the comminuted solids, compared to the unground samples, which is assumed to correspond to 100% crystallinity. The crystallinity index (X) and subsequently the X-ray amorphization degree (A) defined by Ohlberg and Strickler [21], was used to quantify the progressive structural damage. This index comprises the background and peak intensities.

$$X = \frac{U_0}{I_0} \times \frac{I_x}{U_x} \times 100 \quad ; \quad A = 100 - X \quad (7)$$

where U_0 and U_x refer to the background of the initial and ground samples respectively, while I_0 and I_x are integral intensities of diffraction lines of the initial and ground samples.

The X-ray amorphization degrees are calculated based on the Profile fitting data and the obtained results (on average) are displayed in Fig. 10 as a function of energy input. It is evident that X-ray amorphous material content in the ground material develops with increasing the grinding energy input. The X-ray amorphization degree increases rapidly in the earlier stages of milling. The amorphization degrees reached almost 80 and 95% after consuming the energy of 22400 and 82000 kJ/kg by the tumbling and stirred media mills respectively. The trends in the curves indicate that the long-range ordering of hematite was

lost rapidly at the early stages of grinding. It is of interest that the degrees of amorphization in the samples ground by the mills differ marginally for a given energy input. With a first approximation, the content of X-ray amorphous phase in hematite is independent of the grinding environment. This is in a good agreement with previously reported results for carbonates and quartz by Tkáčová and Stevulová [9]. The amorphization is in fact a highly distorted periodicity of lattice elements, and it is often characterized as a short range order in contrast to the long range order of a fully crystalline structure. This may be interpreted as the formation of a metastable “amorphous phase”, because line broadening and the reduction of diffraction peaks intensity take place on X-ray pattern after prolonged milling.

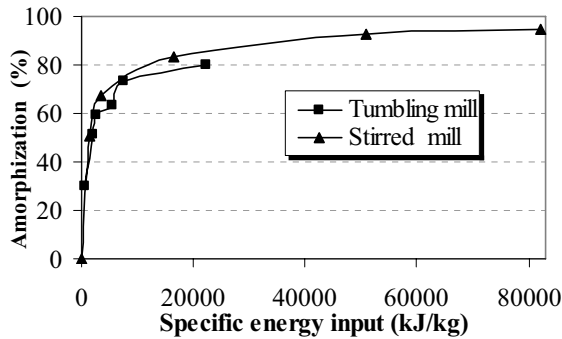


Fig. 10. The degree of amorphization for the products of the ground samples in the mills

The amount of amorphous phase is plotted vs. changes in the BET surface area for the products of the mills in Fig. 11. Generally, a distinguished difference can be observed between tumbling and stirred media mills. According to Fig. 11, it can be seen that the formation of unit surface area in tumbling mill is associated with a sharper increase in the amorphization degree compared with the stirred media mill. According to Tkáčová [10], the long-lived defects are being equally distributed throughout the bulk of particles when the material is subjected to grinding in mills bearing higher stress rate such as jet mills and high-speed disintegrator. If the material is subjected to the grinding in mills producing lower rate of stress like tumbling and planetary mills, the long-lived defects accumulate preferentially in the near surface layer. This can be assumed as a consequence of a quasiadiabatic energy accumulation at the mechanical action of shorter duration than the time required for the formation of the critical crack ($t < t_{crit}$).

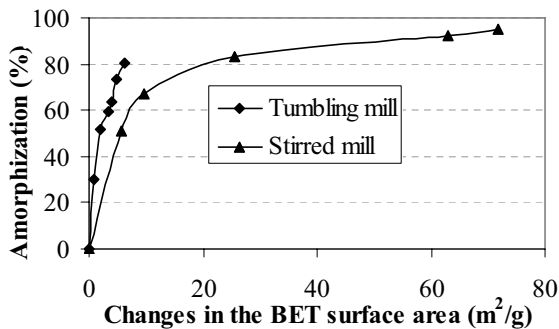


Fig. 11. Changes in BET surface area vs. amorphization degree in the mills

3.2.3. Changes in lattice parameters

The lattice parameters were refined in hexagonal system by Rietveld analysis using TOPAS software. The initial hematite yields the value of lattice parameters ($a=5.03086$ Å, $c=13.74508$ Å) displaying very slight variations from the values given in the mineralogy database [22] ($a=5.0317$ Å and $c=13.737$ Å). The changes in the lattice parameters, a -parameter and c -parameter, for samples were calculated and displayed in Fig. 12. Generally, we observed a unit cell expansion and an increase of the lattice parameters in comparison to the starting material. The comparison of these results with our previous work [13, 23] indicates that the expansion and shrinkage of lattice parameters depend on stressing manner of the particles during comminution. i.e., in the milling with loose media and grinding with compressive load in a confined bed, the lattice parameters undergo an expansion and shrinkage respectively.

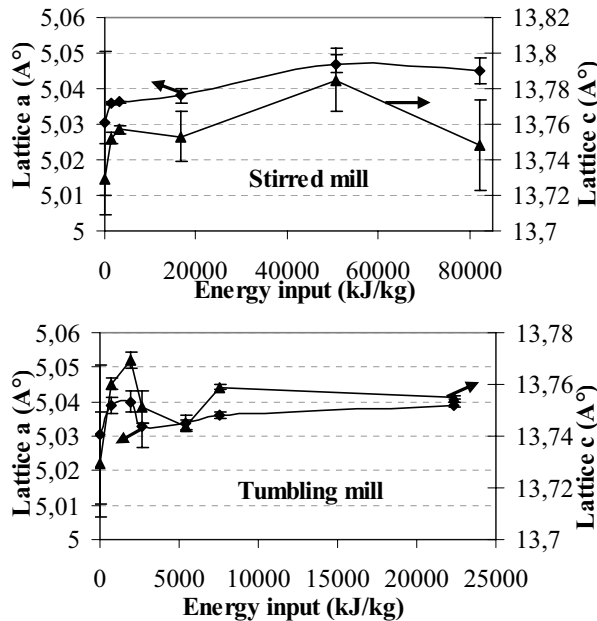
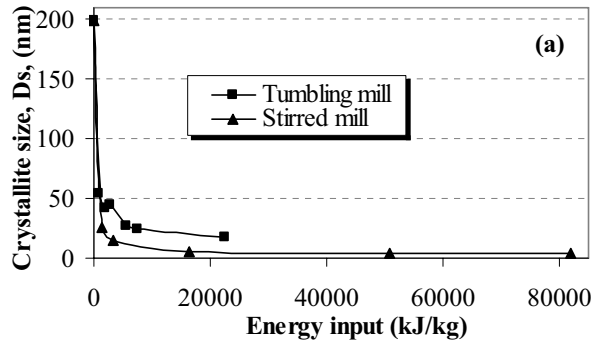


Fig. 12. Variation of lattice parameters vs. energy input in the mills using Rietveld analysis. The standard deviations are shown as error bars.

3.2.4. Size and strain analyses

The values of size and strain are calculated following (1) Warren-Averbach approach and (2) Rietveld analysis. For the Rietveld method, the results are averaged by considering all reflections in whole profile, although the microstructure results show slight deviations from one to another reflection due to the anisotropy behaviors in the XRD patterns. The results of the Warren-Averbach method are calculated and given for direction [012] using the (012) and (024) reflections. The normally quoted values for strains are the local values, i.e., at $L=0$. However, the microstrain at $L=0$ can not be directly determined by using the Warren-Averbach method. The experimental A_L^D functions (Fourier coefficients of strain) are often affected by errors, in particular due to the truncation in the Fourier transformation of the diffraction lines [24]. Thus, the root mean square strain at $L=10\text{nm}$, $\langle \varepsilon_{L=10\text{nm}}^2 \rangle^{1/2}$, are calculated.

The crystallite size quantity and the root mean square strain $\langle \varepsilon_{L=10nm}^2 \rangle^{1/2}$ are presented in Fig. 13 and are also compared with Rietveld analysis in Table. 3. The results depict the nature of progressive evolution of the microstructure in the milling products vs. grinding energy input. Obviously, the surface-weighted crystallite size shows decreasing trend and root mean square strain ($\langle \varepsilon_{L=10}^2 \rangle^{1/2}$) increasing trend as a function of energy input whatever mills used. In the earlier stages of milling, the crystallite size decreases rapidly to the nanometer range. As the intensity of milling increases, the ground hematite in stirred media mill yields more smaller crystallites than that of ground in tumbling mill. Further refinement proceeds slowly and the final surface weighted crystallite size is in the order of 4 and 17 nm in stirred media and tumbling mills, respectively, corresponding to the volume weighted crystallite sizes of 11 and 17 nm. The stirred media milling increased the root mean square strain to a value of higher than 4.9×10^{-3} with grinding by 82000 kJ/kg energy, corresponding to maximum strain (e) of 12.9×10^{-3} using Rietveld analysis. The maximum root mean square strain by the tumbling mill exceeds 4.4×10^{-3} corresponding with maximum strain of 7.7×10^{-3} after releasing of 22400 kJ/kg energy. The steady state was not observed for grinding in tumbling mill, suggesting that the production of smaller crystallites is still possible with increasing the grinding intensity, while the steady state can be observed with prolonged milling in the stirred media mill. No distinguished difference in the crystallite size and microstrain in the products of the stirred media mill after 16500 kJ/kg energy can be observed. This phenomenon is indicative of some kind of annealing effects during milling. As the crystallite size of hematite reached its saturation value (surface weighted crystallite size about 6 nm), the dissipation of impact-shock energy due to particle fracture stops and then the accumulated impact energy is chiefly utilized for annealing of highly stressed particles [25, 26]. As a result, the lattice strain of ground hematite in stirred media mill decreases or remains almost constant depending on the grinding condition. The lubrication action and enhanced heat conduction of a wet grinding environment are possibly responsible for the differences observed in the crystal structure refinement as compared to dry grinding environment [27].



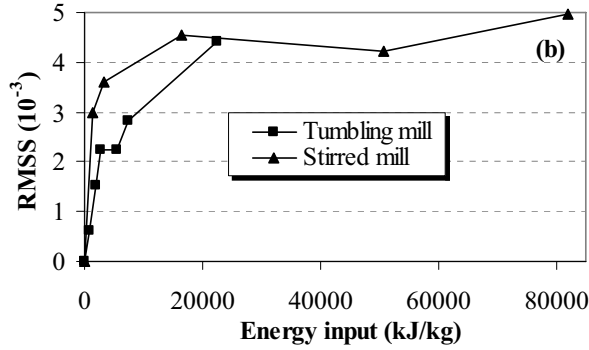


Fig. 13. The variation of the microstructure characters obtained from the Warren-Averbach method for the ground samples in the mills in terms of energy input.

Table 3. The summary of microstructure characters obtained using W-A and Rietveld analysis for the samples ground in the mills vs. energy input. D_s and D_v refer to the surface weighted and volume weighted crystallite sizes respectively. $<\epsilon_{L=10nm}^2>^{1/2}$ and e are the root mean square strain at $L = 10 \text{ nm}$ and maximum lattice strain obtained using Warren-Averbach and Rietveld methods respectively.

Mill type	Energy Input (kJ/kg)	Warren-Averbach methods		Rietveld analysis	
		$D_s (nm)$	$<\epsilon_{L=10nm}^2>^{1/2} (10^{-3})$	$D_v (nm)$	$e (10^{-3})$
Tumbling mill	720	54.2	0.62	61.7	1.30
	1930	42.6	1.52	48.4	2.2
	2670	44.4	2.24	32	2.3
	5450	27.3	2.25	27.9	2.7
	7520	25.0	2.84	26.8	3.6
	22400	17.3	4.4	17.4	7.7
Stirred mill	1410	25.5	2.9	26	2.4
	3350	14.9	3.6	19.6	6.7
	16500	5.8	4.5	12.7	11.4
	50800	3.8	4.2	11.9	12.8
	82000	3.6	4.9	10.9	12.9
Initial*	0	199	n.d. (0)	106	0.57

*In the warren-Averbach of the initial sample, the values calculated using single peak method.

The quantitative analysis and comparison of size and strain without considering the underlying assumptions in each method is impossible. Results obtained from model dependent (Double-Voigt) and independent (Warren-Averbach) approaches are usually not comparable due to different parameter definitions [16, 28] being an underlying source of disagreement between the results obtained from both methods. If the strain broadened pattern contains a Cauchy component, no clear connection exists between RMSS (root mean square strain) and maximum strain (e). When the Gauss and Cauchy extremes of the strain broadened Voigt profile exist, a rough estimate was given by Balzar [16]:

$$0.5 \leq e / <\epsilon_L^2>^{1/2} \leq 2 \quad (9)$$

The ratio of maximum strain to the RMSS can be increased to around 5 depending on the Voigt parameter [16].

If D_v and D_s denote the volume weighted and the surface weighted crystallite sizes respectively, the relationship between D_v and D_s has been given as [16, 24]:

$$1.31 \leq \frac{D_v}{D_s} \leq 2 \quad \text{for a Voigt size-broadened profile} \quad (10)$$

$$\frac{D_v}{D_s} \geq r \quad \text{otherwise (Alternative methods)} \quad (11)$$

with r in the range between 1 and 3.

Results from the Rietveld analysis agree with the ones from the Warren-Averbach analysis. An existing slight higher value in the strain (ϵ) when compared with the above mentioned expressions in the products of the stirred media mill can be related to the fact that only the Lorentzian component is considered in the crystallite size refinement. As a result, a small Gaussian size broadening component in XRD pattern may be accounted for strain calculations.

3.3. DRIFT and thermal analyses

Due to high surface sensitivity, DRIFTS measurements were conducted to monitor the changes of the surface properties of the ground particles in both mills (Fig. 14). The chemical characterization of surface bonds absorbing specific IR radiation allows access to possible structural changes of the hematite particles during the grinding experiments with increasing energy input and decreasing particle size and therefore increasing surface area.

A special emphasis is taken for observing new peaks in the spectra, which in turn is characteristic of mechanochemical changes of the particles due to the high energy impact. By comparison of the evolution of the spectra with the energy input, it is clearly observable that in the case of the tumbling mill experiments, no significant changes occur leading to the conclusion that no mechanochemical changes takes place in the dry mode. Contrarily, in the stirred media mill new peaks were observed at around 3600 cm^{-1} which are characteristics of the O-H vibration mode. The peak area of the hydroxyl group is increasing with the milling time, indicating that with the increase of the specific surface area, as shown before, an increase of the surface O-H groups takes place. Physical adsorbed water can be excluded due to the pre-treatment of the powders allowing the assumption that a new phase may be obtained due the high energy input. However, new phases could not be observed in the diffraction patterns, which is not surprising since the amount of possible new phases are significantly small compared to the bulk. Further surface sensitive measurements will be conducted in forthcoming works to gain a better insight about the mechanochemical characteristics in high energy grinding experiments.

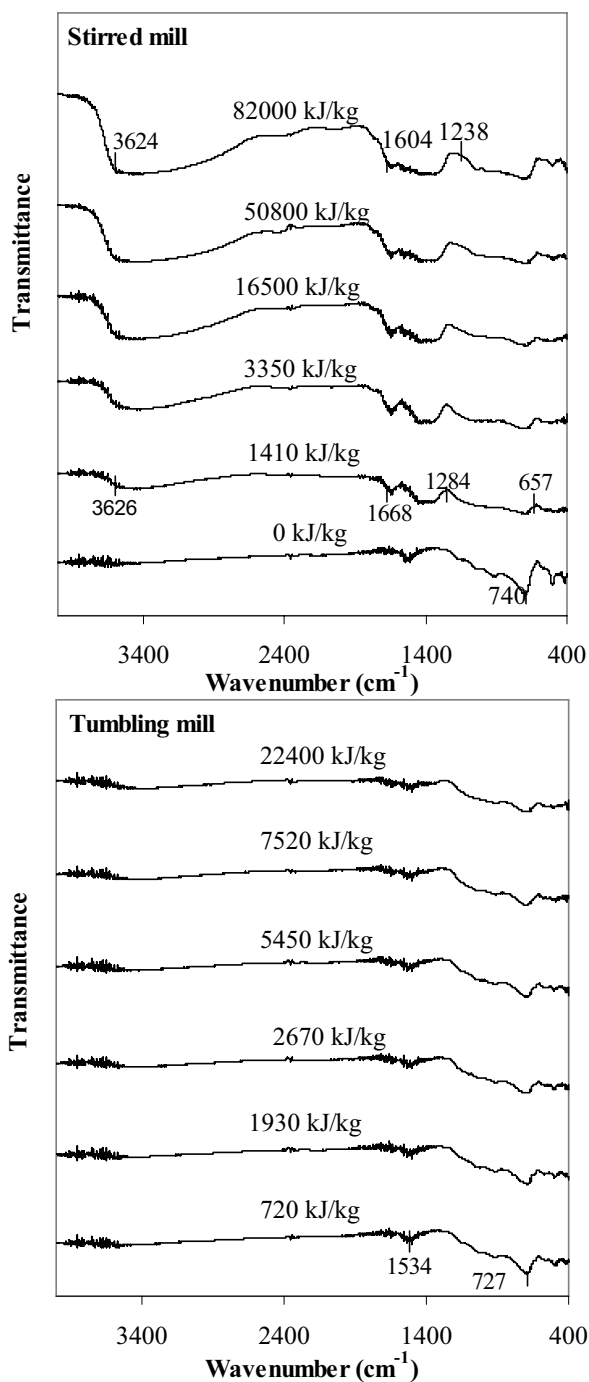


Fig. 14. DRIFTS measurements of ground hematite in stirred media and tumbling mills as a function of energy input.

This behavior is also reflected by the thermogravimetric measurements. Fig. 15 shows the thermal behavior of the ground powder with milling energy measured by the TG analysis. Typically, the curves represent two weight loss steps which can be identified by the changes in the slope of the curves. There is a weight loss around 100 °C in the sample which can be attributed to the removal of adsorbed water due to the wet milling operations. There is a strong weight loss starting from 100 to 400 °C, which can be attributed to surface/ bulk dehydroxilation of hydroxides [29, 30]. The weight loss process develops with increasing the milling energy. The similar experiments were performed for dry ground samples in the tumbling mill. It was found that the weight losses in dry ground samples are negligible compared with wet ground samples in the stirred media mill, being maximum 0.5%; while the wet ground samples yield weight losses up to 15% depending on the grinding energy input. The increasing weight loss as a function of grinding intensity may be related to the fact that the intensive milling brings about structural distortion and breaking the bonds of oxygen and iron in hematite phase and consequently more water and O-H groups adsorbed by the broken and unstable bonds.

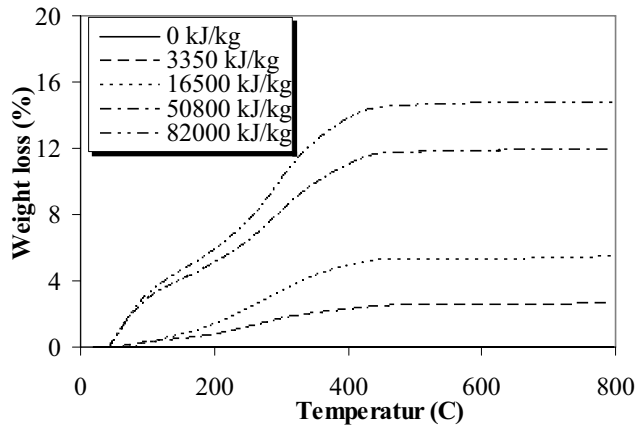


Fig. 15. The weight loss calculated using TG analysis for the samples ground in the stirred media mill at different grinding energies and initial sample as a function of temperature.

Conclusions

- With increasing energy input in the mills, higher specific surface area, X-ray amorphous material, physical broadening, microstrain, and smaller crystallites resulted whatever milling types were employed. Prolonged dry milling in the tumbling mill leads to the agglomeration of finely milled particles.
- The ground hematite in the stirred media mill displays higher specific BET surface area and XRD line broadening and lattice strain, smaller crystallite size and particle size compared with the hematite milled in the tumbling mill. The X-ray amorphous phase content remains unaffected by different grinding environments for a given energy input. The BET surface area in the final products of the tumbling and stirred media mills are calculated about 6.5 and 72 m^2/g respectively in correspondence with 80 and 95% X-ray amorphization degree.
- The smallest volume weighted crystallites with grinding in tumbling and stirred media mills were around 17 and 11 nm after consuming of 22400 and 82000 kJ/kg energy

respectively. For these energy levels in the mills, in turn, the maximum microstrain (ϵ) exceeds 7.7×10^{-3} and 12.9×10^{-3} .

- For the samples ground in the stirred media mill, DRIFT measurements revealed that new peaks appeared at around 3600 cm^{-1} which are characteristics of the O-H vibration mode. The peak area of the hydroxyl group increased with the milling time, indicating that with the enlargement of the specific surface area an increase in the surface O-H groups takes place. The results were also verified by the thermogravimetric analysis.

Acknowledgments

We would like to thank Madhusudhan Rao Mallembakam for his help during milling experiments with stirred media mill at Erlangen University and Christoph Hessel and Prof. Neubauer in the Institute of Mineralogy at the university of Erlangen-Nuremberg for kindly providing the commercial software TOPAS from Bruker. The financial support for the project by Agricola Research Centre (ARC) is gratefully acknowledged.

References

- [1] V.V. Boldyrev, E. G. Avvakumov, Mechanochemistry of inorganic solids. Russ. Chem. Rev. 40 10 (1971) 847–859.
- [2] P. Yu. Butyagin, Kinetics and nature of mechanochemical reactions. Russ. Chem. Rev. 40 (11) (1971) 901–915.
- [3] P. Baláž, Influence of solid state properties on ferric chloride leaching of mechanically activated galena, Hydrometallurgy 40 (1996) 359–368.
- [4] P. Baláž, Extractive Metallurgy of Activated minerals, Elsevier, Amsterdam, 2000.
- [5] K. Tkáčová, P. Baláž, B. Mišura, V. E. Vigdergauz, V. A. Chanturiya, Selective leaching of zinc from mechanically activated complex Cu---Pb---Zn concentrate, Hydrometallurgy 33 (1993) 291–300.
- [6] A. F. M. Barton, S. R. McConnel, Rotating disc dissolution rates of ionic solids: Part 3. Natural and synthetic ilmenite, J. Chem. Soc., Faraday Trans. I 75 (1979) 971–983.
- [7] D. Tromans, J. A. Meech, Enhanced dissolution of minerals: Microtopography and mechanical activation, Miner. Eng. 12(1999) 609–625.
- [8] N. J. Welham, Enhanced dissolution of tantalite/columbite following milling, Int. J. Miner. Process. 61 (2001) 145–154.
- [9] K. Tkáčová, N. Stevulová, Change in structure and enthalpy of carbonates and quartz accompanying grinding in air and aqueous environments, Powder Technol. (1987) 161–166.
- [10] K. Tkáčová, Mechanical activation of minerals. In: Fuerstenau, D.W., Editor, Developments in Mineral Processing 11, Elsevier, 1989, pp. 93–105.
- [11] B. E. Warren, B. L. Averbach, The Effect of Cold-Work Distortion on X-Ray Patterns, J. Appl. Phys. 21 (1950) 595–599.
- [12] P. Pourghahramani, E. Forssberg, Microstructure characterization of mechanically activated hematite using XRD line broadening. Int. J. Miner. Process. 79 (2006a) 106–119.
- [13] P. Pourghahramani, E. Forssberg, Comparative study of microstructural characteristics and stored energy of mechanically activated hematite in different grinding environments, Int. J. Miner. Process. 79 (2006b) 120–139.

- [14] R. A. Young, 1993. Introduction to the Rietveld method.- The Rietveld Method, edited by R. A. Young, IUCr Book Series, Oxford University Press, 1993.
- [15] DIFFRAC^{plus} TOPAS/ TOPAS R/ TOPAS P Version 2.1, Technical Reference, Bruker AXS GmbH, Karlsruhe, 2003 and www.bruker-axs.com.
- [16] D. Balzar, Voigt-Function Model in Diffraction Line-Broadening Analysis, in *Defect and Microstructure Analysis from Diffraction*, edited by R.L. Snyder, H.J. Bunge, and J. Fiala, International Union of Crystallography Monographs on Crystallography No. 10 (Oxford University Press, New York, 1999) pp. 94-126.
- [17] D. Balzar, N. Audebrand, M. Daymond, A. Fitch, A. Hewat, J.I. Langford, A. Le Bail, D. Louër, O. Masson, C.N. McCowan, N.C. Popa, P.W. Stephens, B. Toby, Size-Strain Line-Broadening Analysis of the Ceria Round-Robin Sample, *Journal of Applied Crystallography* 37 (2004) 911-924.
- [18] N. J. Welham, D. J. Llewellyn, Mechanical enhancement of the dissolution of ilmenite. *Miner. Eng.* 11 (9) (1998) 827-841.
- [19] Q. Zhang, E. Kasai, F. Saito, Mechanochemical changes in gypsum when dry ground with hydrated minerals. *Powder Technol.* 87 (1996) 67-71.
- [20] P. Baláž, H. Huhn, K. Tkáčová, H. Heegn, Laugungsverhalten und physiko - chemische Eigenschaften in unterschiedlichen Mühlen vorbehandeltem Chalkopyrit. *Erzmetall* 41 (1988) 325-331.
- [21] S.M. Ohlberg, D.W. Strickler, Determination of percent crystallinity of partly devitrified glass by X-Ray diffraction, *J. Am. Ceram. Soc.* 45 (1962) 170-171.
- [22] Mineral database, 2005. <http://webmineral.com/data/hematite.shtml>.
- [23] P. Pourghahramani, E. Forssberg, The characterization of structural changes in hematite ground in a confined particle bed using Rietveld analysis, *Int. J. Miner. Process* (2007) under review.
- [24] I. Lucks, P. Lamparter, E. J. Mittemeijer, An evaluation of methods of diffraction-line broadening analysis applied to ball-milled molybdenum. *J. Appl. Cryst.* 37 (2004) 300-311.
- [25] S. Begin-Colin, T. Girot, G. Le caer, A. A. Mocellin, Kinetics and mechanisms of phase transformations induced by ball milling in anatase TiO₂, *J. Solid State Chem.* 149 (2000) 41-48.
- [26] I. J. Lin, S. Nadiv, D. J. M, Grodzian Pavlyukhin, Changes in the state of solids and mechano-chemical reactions in prolonged comminution processes. *Miner. Sci. Eng.* 7 (1975) 313-336.
- [27] O. A. Orumwense, E. Forssberg, Surface and structural changes in wet ground minerals, *Powder Technol.* 68 (1991) 23-29.
- [28] H. P. Klug, L. E. Alexander, L. E., X-ray diffraction procedures. - 2nd Edition, Wiley and Sons Inc., New York, 1974, 996 pp.
- [29] E. Patterson and R. Swaffield, Influence of adsorbed anions on the dehydroxylation of synthetic goethite, *J. Therm. Anal.* 18 (1980) 161-167.
- [30] F. Stenger, M. Götzinger, P. Jakob and W. Peukert, Mechanochemical changes of nanosized α -Al₂O₃ during wet dispersing in stirred media mills, Part. Part. Syst. Charact. 21 (2004), pp. 31-38.

Paper VII

Effects of Mechanical Activation on the Reduction Behavior of Hematite Concentrate

Parviz Pourghahramani & Eric Forssberg, International Journal of Mineral Processing, 82 (2007), 96-105.

Effects of mechanical activation on the reduction behavior of hematite concentrate

Parviz Pourghahramani *, Eric Forssberg

Division of Mineral Processing, Luleå University of Technology, SE-971 87, Luleå, Sweden

Received 4 August 2006; received in revised form 13 October 2006; accepted 8 November 2006

Available online 28 December 2006

Abstract

The effect of mechanical activation on the reduction behavior of a hematite concentrate has been examined using a combination of simultaneous thermal analysis (STA), X-ray diffraction (XRD), scanning electron microscope (SEM) analysis, and laser diffraction. The samples were activated in vibratory and planetary mills.

Differential thermal analysis (DTA) and thermogravimetric (TG) analysis revealed that reduction of mechanically activated and initial hematite proceeds stepwise ($\text{Fe}_2\text{O}_3 \rightarrow \text{Fe}_3\text{O}_4 \rightarrow \text{Fe}$). The hydrogen reduction of mechanically activated samples initiates at low temperatures compared with the initial sample. The beginning temperature (onset) of the reduction decreases from 421 °C in the initial sample to 330 °C in the mechanically activated sample, depending on the grinding intensity. Further, the reduction of hematite to magnetite in the activated samples is more pronounced due to mechanical activation. At low temperatures, the activated samples give a higher degree of conversion than the initial samples regardless of which milling device is used. Hematite reduces completely to iron metal.

A comparison of mill-type effect based on stress energy (specific grinding work) suggests that the mill-type effect is confined by a stress energy of 4300 kJ/kg. After releasing 4300 kJ/kg energy, mechanical activation by the planetary mill brings about a larger decrease in onset temperature and a slightly higher degree of conversion at lower temperatures than does activation by the vibratory mill for a given stress energy. A direct relationship between the reaction characters at lower temperatures and structure sensitivity character (S/X) and stored energy can be identified after releasing 4300 kJ/kg energy. However, partial sintering of material at higher temperatures during the reduction of the mechanically activated hematite became active, and the effects of disordering of the hematite structure vanished and subsequently the reduction reaction was retarded.

© 2006 Elsevier B.V. All rights reserved.

Keywords: Mechanical activation; Hematite; Thermal analysis; Direct reduction; Structural changes

1. Introduction

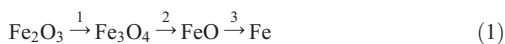
The increase of industrial interest in the direct reduction of hematite ores using gaseous reductants arises from the several technical advantages that this method

offers over the conventional blast furnace process (Pineau et al., 2006; Sastri et al., 1982). Although hydrogen reduction plays an important role in the preparation of magnetic recording materials (tapes) (Mendoza-Resendez et al., 2003), the use of H_2 doped with H_2S as a reducing atmosphere for the reduction of iron oxide causes residue sulfur problems, which have a detrimental effect on powder metallurgy applications. For this reason, many researchers have focused on

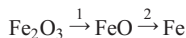
* Corresponding author. Tel.: +46 920 491313; fax: +46 92097364.
E-mail address: Parviz.Pourghahramani@ltu.se
(P. Pourghahramani).

activation of minerals using microwaves (Bradshaw, 1999) or on mechanical activation (Baláz, 2003; Tromans and Meech, 1999; Welham, 2001).

The reduction of iron oxide is a very complex process because it is a heterogeneous reaction in which several simultaneous reactions usually occur. Extensive studies were conducted by Bessieres et al. (1980) to explain the process mechanism. They deduced that the process could be described through three possible ways as follows:



a chain of single reactions



a combination of single and double reactions



The reduction rate of iron ore depends on numerous factors that vary from process to process. These factors include temperature, pressure, gas flow, mineralogical composition (including crystal size, porosity, and distribution within the ore) of the ore, and the interaction between the iron ore and the reducing atmosphere. In the reduction of iron ore with hydrogen, it was generally established that wüstite is unstable at temperatures lower than 570 °C under equilibrium condition, but it could be an intermediate product at temperatures below 570 °C under irreversible condition (Pineau et al., 2006; Sastri et al., 1982). Some investigations have experimentally shown that Fe_2O_3 reduces to Fe_3O_4 and that magnetite then reduces to metallic iron by hydrogen gas. FeO was not detected as an intermediate iron oxide (Munteanu et al., 1997). Several attempts were made to find a generalized kinetic equation for gaseous reduction of iron oxides (El-Rahaiby and Rao, 1979; Hayes, 1979; Tokuda et al., 1973). However, they were successful only in obtaining independent equations and modeling for different reaction conditions. It is also generally concluded that the gaseous reduction of iron oxides is a heterogeneous reaction whose rate is influenced by both a chemical-kinetics factor and a mass-transfer factor. Although excellent agreements have been achieved in the rate-controlling reactions, the kinetics of this reaction is still being debated and numerous disagreements in the reported kinetics data have been noted.

On the other hand, mechanical activation of solid substances is one component of modern scientific disciplines of mechanochemistry. At present, mechanical activation exhibits a wide range of potential applications. It has been reported that mechanical activation substantially accelerates the leaching kinetics of several sulfide and oxide minerals, even at ambient pressure. The enhanced effect is attributed to the increase of specific surface area and structural disorder (Baláz, 1996), enhanced strain (Baláz, 2000), amorphization of mineral particles (Tkáčová et al., 1993), preferential dissolution of select crystal faces (Barton and McConnel, 1979), microtopography (Tromans and Meech, 1999), and formation of new phases more amenable to leaching (Welham, 2001). Mechanical activation was also established to be successful for intensification of the thermal processes of sulfide minerals, such as oxidation, decomposition in inert atmosphere, and sublimation (Baláz and Ebert, 1991; Tkáčová et al., 1990). Hu et al. (2002, 2003) reported that mechanically activated pyrite and galena are more easily decomposed during thermal treatments than non-activated pyrite and galena. Mechanically activated sphalerite was found to oxidize more easily than non-activated sphalerite (Chen et al., 2002). Recently, the effect of extended milling on carbothermic reduction of ore manganese was investigated by Welham (2002). Milling of manganese ore with graphite led to enhanced reduction at decreased temperatures. The study of carbothermic reduction hematite (mixture of hematite and graphite) in air revealed that milling at ambient temperature increases the rate of reaction (Raygan et al., 2002). In this area, thermal properties of mechanically activated hematite concentrate using simultaneous thermal analysis have yet to be studied.

The goal of this paper is to describe the thermal behavior of mechanically activated hematite by applying high energy milling in the planetary and vibratory mills. The dependence of reduction behaviors of hematite on structural changes is also discussed.

2. Experimental

2.1. Material

The high-purity hematite concentrate used in this study was kindly supplied by the LKAB (Luossavaara Kiirunavaara Aktiebolag) company in Sweden. The chemical composition of the initial sample is given in Table 1. The XRD pattern of the initial hematite sample showed only hematite reflection peaks. The BET specific surface area of the starting hematite sample was 0.59 m²/g.

Table 1
The chemical composition of the initial sample (%)

Compounds	Fe ₂ O ₃	Al ₂ O ₃	SiO ₂	TiO ₂	MgO	MnO	P ₂ O ₅	Total
wt.%	97.91	0.73	0.73	0.27	0.20	0.02	0.09	99.95

2.2. Mechanical activation and characterization

Hematite concentrate was mechanically activated using a planetary mill (RETSCH) and a vibratory mill (HUMBOLDT; PALL 20 U). A mixture of ball steel media with dimensions between 6 mm and 22.2 mm and with apparent density of 4875 kg/m³ was used as grinding media. The milling experiments were performed continuously in air atmosphere. The media surfaces were calculated from the number of grinding bodies and their dimension. The experimental milling conditions are given in Table 2. The activated samples were sealed into plastic tubes and kept in a freezer.

The particle size distribution of the samples was measured by laser diffraction (CILAS 1064) in the liquid mode. The mean particle diameter was obtained from the particle size distribution.

Simultaneous thermal analyses (STA) were conducted using a NETZSCH STA 409C instrument at a heating rate of 10 °C min⁻¹ to 800 °C. The high temperature furnace was heated by graphite heating elements, which were protected by injection of inert argon gas. The temperature of furnace was controlled by a tungsten thermocouple. The heating was performed under highly pure hydrogen as reduction gas with a rate of flow of 100 ml min⁻¹. The mass of samples was almost 95 mg.

The XRD patterns were obtained using a Siemens D5000 powder diffractometer with Bragg–Brentano geometry equipped with a curved graphite monochromator in the diffracted beam arm and using Cu K α radiation ($\lambda=0.15406$). The XRD patterns of the

samples were recorded using a step size of 0.02° and a counting time of 1 s per step.

The morphological characterization of the samples was performed using a Philips XL 30 scanning electron microscope (SEM) equipped with a LaB₆ emission source and running at 20 kV. After drying, the samples were gold coated using gold sputtering prior to SEM investigation.

3. Results and discussion

3.1. Granulometrical changes

The mean diameter of the ground samples, as shown in Fig. 1, decreases rapidly during the initial stages of milling and then levels off or increases slightly depending on milling operation. The granulometrical changes are observed mainly in the initial stages of milling. In the case of lower media surface ($M_s=1$ m²/kg), the particle size reduction is completed within 3 h of milling, indicating that further size reduction is impossible. When lower media surface is used, the products of the vibratory mill yield smaller particles than the products of the planetary mill. When grinding with higher media surface, the particle size reduction is completed within 1 h of milling in the planetary mill and within 3 h of milling in the vibratory mill. The increase in mean particle size that occurs after prolonged grinding at higher media surface is an indication of re-agglomeration, which is inevitable in the fine grinding regimes. As the grinding period increases, the agglomeration is more pronounced.

This view is supported by the results of the SEM analysis (Fig. 2). The SEM micrographs show how prolonged milling results in an increasing degree of agglomeration and a reduced amount of fines. The analysis revealed that distinct agglomerates are present in the fine fractions of all ground samples. As the milling

Table 2
Experimental milling conditions

Milling conditions	Vibratory milling	Planetary milling
Media filling (%)	70	23.4
Media surface, M_s (m ² /kg)	1, 4	1, 4
Mass of media (kg)	33.16	1.031
Milling time (h)	1, 3, 9	1, 3, 9
Ball to powder weight ratio	16.92:1, 67.68:1	19.1:1, 76.34:1
Speed (RPM)	1000	100 (axle), 200 (drum)
Amplitude (mm)	8	—
L(mm) \times ϕ (mm)	320 \times 185	87 \times 115
Acceleration (m/s ²)	—	16.4

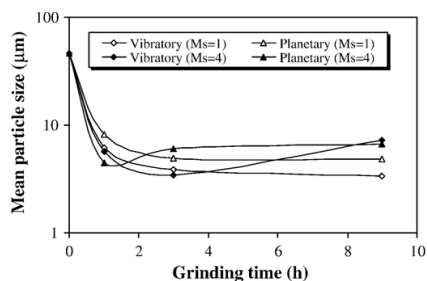


Fig. 1. Mean particle size of samples as a function of grinding variables. Hereafter, 0 h refers to the initial sample.

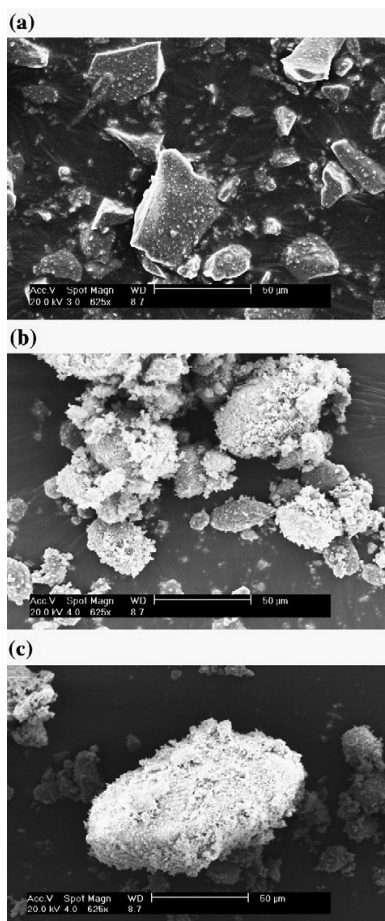


Fig. 2. Representative SEM micrographs of the initial sample (a) and ground sample in vibratory (b) and planetary (c) mills with higher media surface for 9 h.

intensity increases, the material consists entirely of agglomerates (Fig. 2b,c). The initial sample consists of angular particles having different sizes (Fig 2a). From Figs. 1 and 2, it can be concluded that massive and compact agglomerates form during intensive milling, especially in the planetary mill. The agglomeration of particles during extended dry grinding was reported for sulfide minerals (Baláz, 2000) and for oxide minerals (Tkáčová, 1989). This behavior is common during dry grinding and is usually explained by agglomeration of the structurally modified particles following the initial reduction of particle size. This occurs because of the tendency of the activated material to reduce its surface free energy. The microstructure

characterization of the samples was made using XRD line profile analysis and the Warren–Averbach method. Detailed information is given elsewhere (Pourghahramani and Forssberg, 2006a,b).

3.2. DTA and XRD results

Thermoanalytical methods provide a great deal of information about the structural changes of hematite that occur during mechanical treatment. The reduction behaviors of the initial and mechanically activated samples were studied between room temperature and 850 °C at non-isothermal condition with hydrogen gas. No remarkable change was observed below 200 °C. Fig. 3 shows DTA, DDTA (derivative differential thermal analysis) and DTG curves for the initial hematite between 200 °C and 850 °C. The investigation of DDTA and TG curves gives evidences for sequential reactions. A peak is centered at about 480 °C on the DDTA curve. The DTG curve displays a weight loss between 380 °C and 480 °C that is immediately continued by a second step of weight loss. The XRD pattern of the reduction product of the initial sample heated to 450 °C (Fig. 4) represents both magnetite and hematite phases. The weight loss was calculated at about 2.87% up to 450 °C, which is still lower than the weight loss value corresponding to the complete conversion of hematite to magnetite (3.33%). The reduction of the initial hematite to 500 °C produces reflection peaks of magnetite and iron phases in the XRD powder pattern. As a result, the reduction proceeds stepwise ($\text{Fe}_2\text{O}_3 \rightarrow \text{Fe}_3\text{O}_4 \rightarrow \text{Fe}$). However, the DTA peak corresponding to the first step of reduction is absent on DTA curve. Probably, the effect is weaker than and subsequently masked and/or overlapped by the strong endothermic effect of the second step.

Fig. 5 shows the DTA curves of the activated samples from the vibratory mill with higher media surface for different grinding periods. A broad and weak exothermic effect appeared at lower temperature after 3 h of milling. Developing and sharpening of the exoeffect can

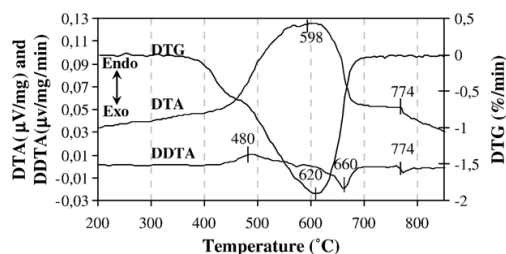


Fig. 3. DTA, DDTA and DTG curves of the initial sample.

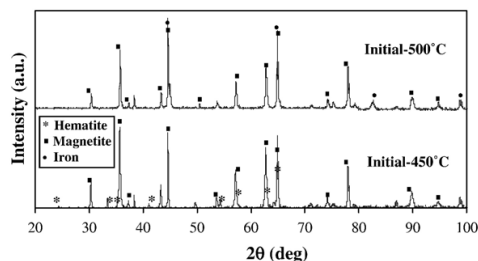


Fig. 4. XRD patterns of the reduction products of the initial sample.

be observed with increasing grinding time. This is a consequence of the reduction of the energy required to destroy the crystalline structure of hematite. The energy supplied by milling causes structural disorder through the distortion or breakage of the crystalline network. This was evident from the reduction of the intensities of XRD peaks reported in a previous work (Pourghahramani and Forssberg, 2006a). On the other hand, the appearance of the exoeffect may imply an increase of exothermic peak intensity. This also can be explained by the action of mechanical activation. The active mechanical energy partially transferred to the ground particles is stored in the form of lattice defects. In this way, the solid systems gain an activated state and energy (enthalpy) of ground hematite increases. Thus, the excess energy can be released when the activated material is heated. As a result, the exoeffect peak appears on the DTA curve. The exoeffect peak for the first step of reduction was previously reported by Sastri et al. (1982). The exothermic peak is followed by an important, broad and strong endothermic peak at higher temperature ranges. The maximum characteristic temperature of the endothermic peaks also shifts slightly to lower temperature with increasing grinding time. This peak is caused by the reduction of magnetite to iron metal. The reduction

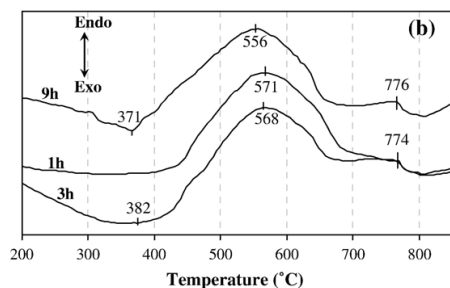


Fig. 5. DTA reduction curves of mechanically activated hematite in the vibratory mill with higher media surface.

of magnetite to wüstite as an intermediate reduction product was not observed, which agrees with previous observations (Munteanu et al., 1997; Sastri et al., 1982). The reduction product of the sample ground for 9 h with higher media surface in the vibratory mill after heating to 320 °C shows the reflection peaks of hematite and magnetite (Fig. 6). The calculated weight loss for the sample was 2.97%, which also confirmed that a small amount of hematite remained unchanged. The reduction product of the sample after heating to 450 °C shows both magnetite and iron phases. The final reduction products show only the reflection peaks of metallic iron, which suggests the complete conversion of hematite to iron. Similar plots were constructed (not reported) for the samples ground in the planetary mill, and the exothermic effect was observed after 1 h of milling with higher media surface. The plots corresponding to lower media surface do not contain further information and have not been reported in this paper.

A weak endoeffect at about 775 °C is due to the transition from the ferromagnetic state into the paramagnetic state and/or due to the transition of α -Fe to β -Fe. The Curie temperature of iron is around 1053 K (Murata and Morinaga, 2000). The latter transition is not detected by X-ray diffraction because X-ray diffraction runs are made at room temperature and the structural changes are reversible.

3.3. TG and DTG results

In order to obtain additional information about the weight loss of the sample obtained by milling, a TG analysis and a DTG analysis were performed. In these

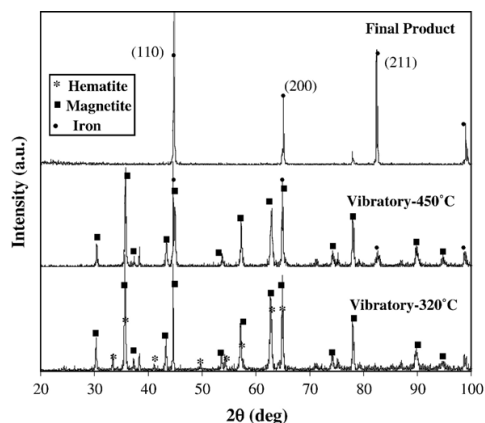


Fig. 6. XRD patterns of the reduction products of the sample ground in the vibratory mill for 9 h with higher media surface.

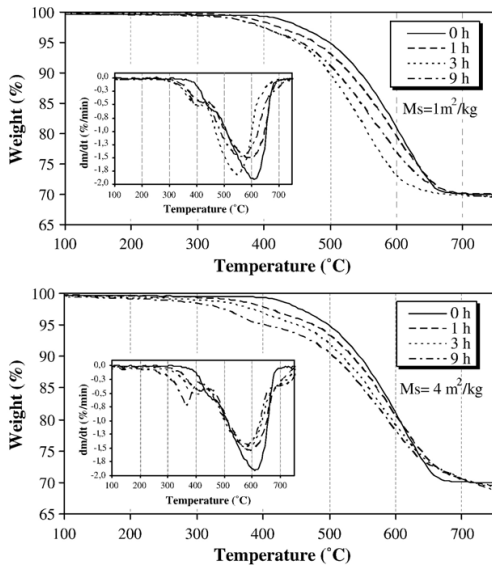


Fig. 7. TG and DTG curves (shown in the insets) for the initial sample and for samples ground in the vibratory mill as a function of temperature.

techniques, changes in the mass of a sample are studied while the sample is subjected to a controlled temperature program (Figs 7 and 8). Generally, the TG curves for the reduction of hematite exhibit a two-step weight loss that can be identified from changes in the slope of the curves. The total weight loss for all of the samples is 30%, which corresponds to the complete conversion of hematite to magnetite.

Fig. 7 shows mass changes in the initial sample and in samples ground in the vibratory mill as a function of temperature. For the hematite ground with lower media surface, the TG curves shift toward lower temperatures with increasing grinding time up to 3 h. However, the curve corresponding to prolonged milling for 9 h moves to higher temperatures compared with the sample ground for 3 h. This is especially true for the second step of the weight-loss process. The results are consistent with observations from thermal studies of ground pyrophyllite (Perez-Rodriguez and Sanchez-Soto, 1991; Temuujin et al., 2003). This effect is probably a result of the formation of agglomerates during extended dry milling, which overcomes the effect of structural changes. For the higher media surface case, the TG curve shifts to lower temperatures with increasing grinding time up to a temperature of about 640 °C. Gradual changes can be identified among the curves as a function of temperature.

At low temperatures, the grinding time variable has a large effect on the weight loss, but its effect is limited with progress of reaction. At temperatures beyond 640 °C, reduction in the ground samples is delayed and no significant difference exists among the activated samples. Contrary to the lower media surface case, prolonged milling with higher media surface does not affect the arrangement of the curves, especially in the initial stages of the reduction. Comparison of the lower media surface case with the higher media surface case indicates that the structural alterations associated with higher media surface milling dominate the agglomeration effect during the reduction process.

Similar plots were constructed for the samples ground in the planetary mill. The results are shown in Fig. 8. As the temperature increases to 500 °C, the weight loss curves corresponding to lower media surface milling shift slightly to lower temperatures with increasing grinding time. At temperatures beyond 500 °C, the order of the curves becomes inverted such that the TG curve moves to higher temperatures with increasing grinding time. The analogous behavior is apparent in the higher media surface case with the change occurring at a temperature of about 600 °C. Interestingly, the rate of reduction at low temperatures increases with grinding

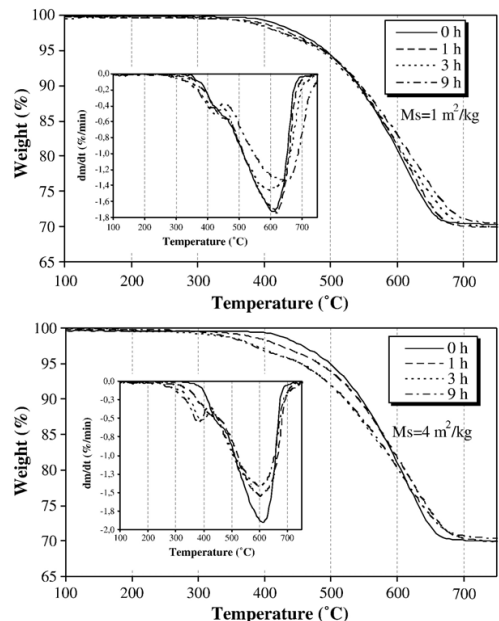


Fig. 8. TG and DTG curves (shown in the insets) for the initial sample and for samples ground in the planetary mill.

intensity for whichever mill was used. In contrast, the second step of reduction at higher temperatures was delayed depending on the milling intensity. It seems that as the agglomeration becomes stronger and more compact, the reduction is more retarded.

The above mentioned results are confirmed by the DTG curves shown in the insets of Figs. 7 and 8. The two weight loss steps are observed as minima in the DTG curves. Interestingly, the first step of weight loss for mechanically activated samples is more pronounced than for non-activated hematite. In addition, a plateau between two steps of reduction can be seen, in particular for the activated samples, which reveals that the mechanical activation discriminates two steps of reduction. Moreover, the area of peak in the second step of reduction decreases concomitantly as the area of peak in the first weight loss step centered approximately between 300 and 450 °C increases, depending upon grinding variables.

To understand why the reduction reaction retards at higher temperatures, especially in the mechanically activated samples, SEM investigation was employed on the reduction products. The SEM micrographs are presented in Fig. 9. Obviously, the SEM images of the mechanically activated samples show clusters of

rounded particles, whereas angular and detached particles are seen in the initial sample. This can be ascribed to the partial sintering of the ground samples at higher temperatures. With increasing grinding intensity, the sinter layer becomes extensive and a fully dense layer forms on the particle surface. This compact layer hinders the transport of hydrogen to material surface below, and the effects of disordering of the hematite structure are overlapped and/or removed by the formation of the dense layer. As the grinding intensity increases, it seems that the sintering of material intensifies. Thus, the reduction retards at higher temperature. Such observations have been reported by Pineau et al. (2006) for a commercial hematite powder.

4. The comparison of the mills

The differences between the effects of the two mills are studied with regard to their specific grinding work (stress energy). Direct comparison of mills will be possible if the efficiency and ability of the mills in transferring energy to the particles being ground are known. However, the measurement of the efficiency of energy transfer in mills is a complicated task, and, as far

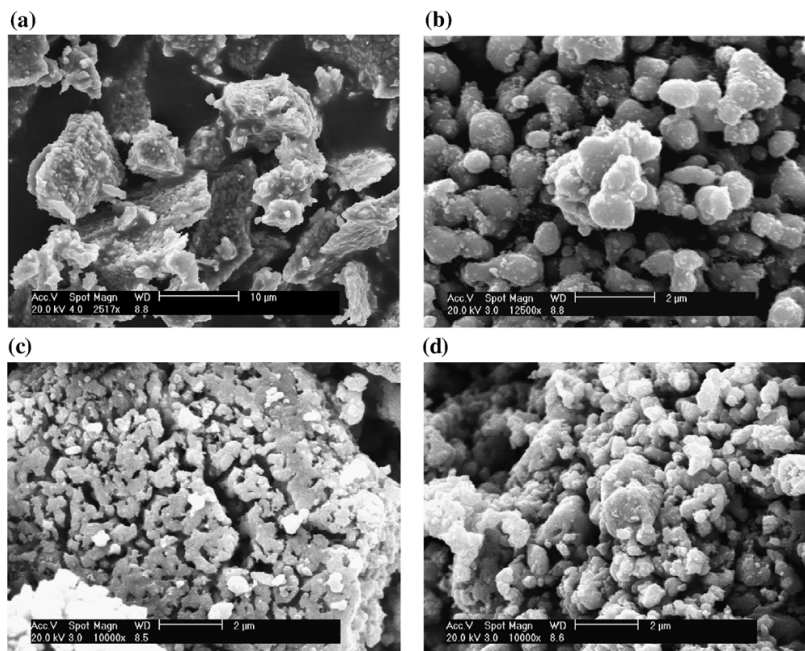


Fig. 9. SEM images of the reduction products; initial sample (a); sample ground in vibratory mill with higher media surface for 9 h (b); sample ground in vibratory mill with lower media surface for 9 h (c) and sample ground in planetary mill with lower media surface for 3 h (d).

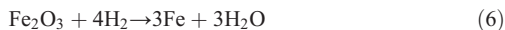
as we know, the evaluation of grinding intensity and mill efficiency has not been adequately established. In this study, the mills are compared using the specific grinding work (stress energy), SE, characters of the mills, which are proposed by Heegn (1986):

$$SE = \frac{m_B}{2m_S} n t_M (4\pi n a)^2 \quad \text{Vibratory mill} \quad (4)$$

$$SE = \frac{m_B}{m_S} b n t_M D \quad \text{Planetary mill} \quad (5)$$

where m_B , m_S , t_M , n , a , b and D refer to mass of grinding media, mass of material charge, grinding time, speed, amplitude in vibratory mill, acceleration in planetary mill, and mill diameter, respectively.

The two reduction parameters were considered in the comparison of the mills' effects. The beginning temperature (onset) of the reaction was derived from the curve of weight variation (TG) of the differential thermal analysis by the extrapolated peak onset method (Brown, 2001). Furthermore, it was determined that the total transformation of Fe_2O_3 into metallic iron corresponds to a 30% of total sample weight loss according to the stoichiometry of the following reaction:



Experimental data (decrease in sample weight) were then converted into degree of conversion at various temperatures and used in the comparison of the mills' effects. The obtained results are displayed in Fig. 10 as a

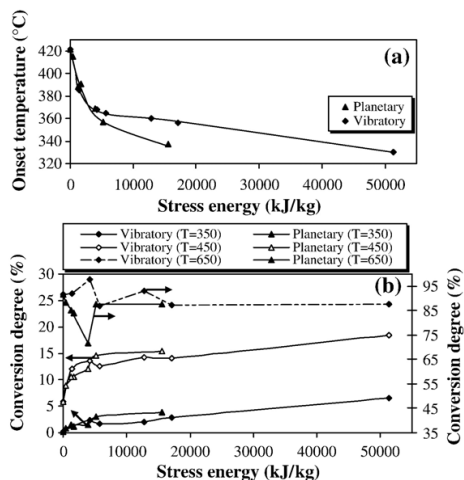


Fig. 10. Changes in onset temperatures (a) and degree of conversion at various temperatures (b) in terms of stress energy of the mills.

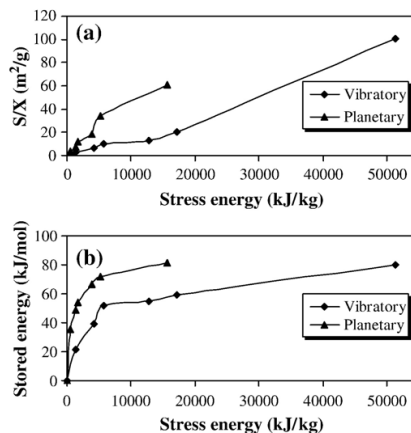


Fig. 11. The dependence of structure sensitivity character (S/X) and overall stored energy for mechanically activated samples in the mills with stress energy of the mills.

function of stress energy in the mills. As expected, mechanical activation decreased the ignition temperature of reaction for whichever milling method was employed. The mill-type effect is confined by the value of 4300 kJ/kg energy. With increasing stress energy, the effect of the planetary mill exceeds the effect of the vibratory mill. For a given stress energy, the onset temperatures of the samples ground in the planetary mill are lowered more than those of the samples ground in the vibratory mill at intensive grinding operation. The onset temperature of 421 °C in the initial sample decreased to about 337 °C and 330 °C after releasing 15,600 kJ/kg energy and 51,300 kJ/kg energy in the planetary and vibratory mills, respectively. As a consequence of mechanical activation, reactions that would normally require higher temperatures to begin start at lower temperatures because of the separation of reacting phases by the product phases and structural changes (Baláz, 2000).

The degree of conversion at three temperatures is displayed in Fig. 10b for the products of the mills. No distinguished difference between the mills is observed at stress energies up to 4300 kJ/kg at lower temperatures. The products of the planetary mill yield a slightly higher degree of conversion after 4300 kJ/kg energy is released when temperature reaches 450 °C. At a temperature of 650 °C, no clear trend can be seen in the changes of degree of conversion with stress energy. The products of the vibratory mill show a somewhat higher degree of conversion than those of the planetary mill, in particular before 4300 kJ/kg energy is released. It seems that the formation of massive and compact agglomerates at low

stress energy by grinding in the planetary mill intensifies the sintering process at higher temperatures compared with the vibratory mill.

To clarify, the structural changes and stored energy (enthalpy) in the hematite as a result of mechanical activation have to be investigated. Tkáčová and Baláz (1988) introduced a complex parameter that characterizes the overall disordering of solids by milling. This parameter, defined as S/X , describes the influence of surface area increase and crystallinity decrease on chemical processes. In addition, the partially transferred mechanical energy stored in the form of defects in the activated materials is of importance and interest. The energy contributions (excess enthalpy) of the long-lived defects were estimated based on changes in dislocation density, surface area, and extent of amorphization in the activated hematite. The detailed information is given in previous works (Pourghahramani and Forssberg, 2006b). The stored energy summarizes all effects of changes in BET surface area, extent of amorphization, crystallite size, and lattice strain in activated material.

According to Fig. 11, with increasing grinding intensity (stress energy), the values of S/X increase for whichever milling device is used. For a given stress energy, the products of the planetary mill have more structural changes and stored energy than the products of the vibratory mill. The difference between mills becomes notable with increasing intensity of grinding. The mill effects on structural changes and subsequently on stored energy (enthalpy) at low stress energy can be identified fairly, but mill effects on the reduction process are only manifested after 4300 kJ/kg of energy is released. This can be explained by the fact that the differences in structural changes at lower stress energy between the mills are not sufficient to distinguish the mill type effect on the reduction process. Probably, some structural changes and/or a part of some structural changes are not fully effective or available in the reduction process. This issue was noted by Senna (1989) and Tkáčová and Baláz (1988).

To summarize, it was observed that structural changes caused by mechanical treatments accelerate the reduction at lower temperatures and remarkably decrease the starting temperature of the reduction. The reduction at higher temperatures shows decreased effects of structural changes because of partial sintering of powders during reduction. The reduction of mechanically activated hematite would give better results at lower temperatures with low heating rate in non-isothermal conditions. More investigations are recommended to elucidate the relationship between structure characters and kinetics parameters of the hematite

reduction and to determine the effective structures in the reduction process.

5. Conclusions

The milling process has been shown to have a pronounced influence on the reduction (with the aid of hydrogen) of hematite:

- The mechanical activation of hematite by planetary mill and/or vibratory mill had a positive influence on the reduction of hematite with hydrogen gas at lower temperatures. At higher temperatures, the formation of a dense layer retarded the reduction.
- Mechanical activation of hematite concentrate led to the initiation of reduction at lower temperatures. The starting temperature of the reduction was decreased to about 90 °C. The activated samples had a higher degree of conversion at lower temperature ranges.
- The reduction of hematite to magnetite was pronounced in the activated samples compared to the initial sample, and the corresponding exoeffect was developed and sharpened after 1 and 3 h of milling with higher media surface in the planetary and vibratory mills, respectively.
- Planetary milling generated great structural changes compared to vibratory milling for a given stress energy over the grinding intensity. However, the mill-type effect on the reaction was confined by a stress energy of 4300 kJ/kg. After releasing 4300 kJ/kg energy, planetary milling decreased the onset temperature more than vibratory milling. More investigations are needed to explore the availability and influence of individual structure characters on the reaction.

Acknowledgments

The authors would like to thank Professor Claes I Helgesson for his valuable comments and discussions on this paper. We would like to express our gratitude to Dr. Nourreddine Menad for his assistance in the measurements of thermal analysis data.

References

- Baláz, P., 1996. Influence of solid state properties on ferric chloride leaching of mechanically activated galena. *Hydrometallurgy* 40, 359–368.
- Baláz, P., 2000. *Extractive Metallurgy of Activated Minerals*. Elsevier, Amsterdam.
- Baláz, P., 2003. Mechanical activation in hydrometallurgy. *Int. J. Miner. Process.* 72, 341–354.
- Baláz, P., Ebert, I., 1991. Thermal decomposition of mechanically activated sphalerite. *Thermochim. Acta* 180, 117–123.

- Barton, A.F.M., McConnel, S.R., 1979. Rotating disc dissolution rates of ionic solids: Part 3. Natural and synthetic ilmenite. *J. Chem. Soc., Faraday Trans. 1* 75, 971–983.
- Bessieres, J., Bessieres, A., Heizmann, I.J., 1980. Iron oxide reduction kinetics by hydrogen. *Int. J. Hydrogen Energy* 5, 585–595.
- Bradshaw, S.M., 1999. Applications of microwave heating in mineral processing. *South Afr. J. Sci.* 394–396.
- Brown, M-E., 2001. *Introduction to Thermal Analysis*. Second Edition. Techniques and Applications. Kluwer Academic Publishers, Secaucus, NJ, USA. <http://site.ebrary.com/lib/lulea>.
- Chen, Q., Hu, H., Yin, Z., Zhang, P., Ye, L., 2002. The oxidation behavior of unactivated and mechanically activated sphalerite. *Metall. Mater. Trans.* 33B, 897–900.
- El-Rahaiby, S.K., Rao, Y.K., 1979. The kinetics of reduction of iron oxides at moderate temperatures. *Metall. Trans.* 10B, 257–269.
- Hayes, P.C., 1979. The kinetics of formation of H_2O and CO_2 during iron oxide reduction. *Metall. Trans.* 10B, 211–217.
- Heegn, H., 1986. ScD. Theses, Research Institute of Mineral Processing of The Academy of Sciences of the GDR, Freiberg (in German).
- Hu, H., Chen, Q., Yin, Z., Zhang, P., Zou, J., Che, H., 2002. Study on the kinetics of thermal decomposition of mechanically activated pyrites. *Thermochim. Acta* 389, 79–83.
- Hu, H., Chen, Q., Yin, Z., Zhang, P., Ye, L., 2003. The thermal behavior of mechanically activated galena by thermogravimetry analysis. *Metall. Mater. Trans.* 34A, 793–797.
- Mendoza-Resedez, R., Morales, M.P., Serna, C.J., 2003. Reduction mechanism of uniform iron oxide nanoparticles to metal used as recording media. *Mater. Sci. Eng., C, Biomim. Mater., Sens. Syst.* C23, 1139–1142.
- Munteanu, G., Ilieva, L., Andreeva, D., 1997. Kinetic parameters obtained from TPR data for $\alpha-Fe_2O_3$ and $Au/\alpha-Fe_2O_3$ systems. *Thermochim. Acta* 291, 171–177.
- Murata, Y., Morinaga, M., 2000. Recrystallization behaviour of pure iron at Curie temperature. *Scr. Mater.* 43, 509–513.
- Perez-Rodriguez, L.J., Sanchez-Soto, P.J., 1991. The influence of the dry grinding on the thermal behaviour of pyrophyllite. *J. Therm. Anal.* 37, 1401–1413.
- Pineau, A., Kanari, N., Gaballah, I., 2006. Kinetics of reduction of iron ore oxides by H_2 ; part I: low temperature reduction of hematite. *Thermochim. Acta* 447, 89–100.
- Pourghahramani, P., Forssberg, E., 2006a. Microstructure characterization of mechanically activated hematite using XRD line broadening. *Int. J. Miner. Process.* 79, 106–119.
- Pourghahramani, P., Forssberg, E., 2006b. Comparative study of microstructural characteristics and stored energy of mechanically activated hematite in different grinding environments. *Int. J. Miner. Process.* 79, 120–139.
- Raygan, S., Khaki, J.V., Aboutalebi, M.R., 2002. Effect of mechanical activation on the packed-bed, high-temperature behavior of hematite and graphite mixture in air. *J. Mater. Synth. Process.* 10, 113–120.
- Sastri, M.V.C., Viswanath, R.P., Viswanathan, B., 1982. Studies on the reduction of iron oxide with hydrogen. *Int. J. Hydrogen Energy* 7, 951–955.
- Senna, M., 1989. Determination of effective surface area for the chemical reaction of fine particulate material. *Part. Part. Syst. Charact.* 6, 163–167.
- Temuujin, J., Okada, K., Jadambaa, T.S., MacKenzie, K.J.D., Amarsanaa, J., 2003. Effect of grinding on the leaching behaviour of pyrophyllite. *J. Eur. Ceram. Soc.* 23, 1277–1282.
- Tkáčová, K., 1989. *Mechanical Activation of Minerals*. Elsevier, Amsterdam.
- Tkáčová, K., Baláz, P., 1988. Structural and temperature sensitivity of leaching of chalcopyrite with iron (III) sulphate. *Hydrometallurgy* 21, 103–112.
- Tkáčová, K., Baláz, P., Bastl, Z., 1990. Thermal characterization of changes in structure and properties of chalcopyrite after mechanical activation. *Thermochim. Acta* 170, 277–287.
- Tkáčová, K., Baláz, P., Mišura, B., Vigdergauz, V.E., Chanturiya, V.A., 1993. Selective leaching of zinc from mechanically activated complex Cu–Pb–Zn concentrate. *Hydrometallurgy* 33, 291–300.
- Tokuda, M., Yoshikoshi, H., Ohtani, M., 1973. Kinetics of the reduction of iron ore. *Trans. Iron Steel Inst. Jpn. Trans. ISIJ* 13, 350–363.
- Tromans, D., Meech, J.A., 1999. Enhanced dissolution of minerals: microtopography and mechanical activation. *Miner. Eng.* 12, 609–625.
- Welham, N.J., 2001. Enhanced dissolution of tantalite/columbite following milling. *Int. J. Miner. Process.* 61, 145–154.
- Welham, N.J., 2002. Activation of the carbothermic reduction of manganese ore. *Int. J. Miner. Process.* 67, 187–198.

Paper VIII

Reduction Kinetics of Mechanically Activated Hematite Concentrate with Hydrogen Gas Using Non-Isothermal Methods

Parviz Pourghahramani & Eric Forssberg, Thermochimica Acta 454 (2007), 69-77

Reduction kinetics of mechanically activated hematite concentrate with hydrogen gas using nonisothermal methods

Parviz Pourghahramani*, Eric Forssberg

Division of Mineral Processing, Luleå University of Technology, SE-971 87 Luleå, Sweden

Received 10 August 2006; received in revised form 22 December 2006; accepted 22 December 2006

Available online 9 January 2007

Abstract

The reduction kinetics of both non-activated and mechanically activated hematite concentrate in a vibratory mill for different grinding periods have been studied using thermogravimetry (TG). Changes in the structure of hematite were studied using X-ray diffraction analysis. The isoconversional method of Kissinger–Akahira–Sunose (KAS) was used to determine the activation energy of the different reactions. The Vyazovkin model-free kinetic method was also used for prediction of kinetic behavior of the samples for a given temperature.

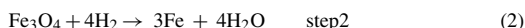
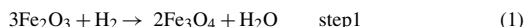
Fe₂O₃ was found to reduce to Fe in a two-step via Fe₃O₄. Intensive grinding resulted in improved resolution of overlapping reduction events. It was also established that the mechanical activation had a positive effect on the first step of reduction. With increasing the grinding time, the activation energy at lower extent of conversion ($\alpha \leq 0.11$) decreased from 166 to 106 kJ mol^{−1} range in the initial sample to about 102–70 kJ mol^{−1} in the sample ground for 9 h. The complexity of the reduction of hematite to magnetite and magnetite to iron was illustrated by the dependence of E on the extent of conversion, α ($0.02 \leq \alpha \leq 0.95$). The values of E decreased sharply with α for $0.02 \leq \alpha \leq 0.11$ range in the initial sample and mechanically activated samples, followed by a slight decrease in the values of E during further reduction by $\alpha \leq 0.85$ in the ground samples up to 3 h. A slight increasing dependence of E on α for mechanically activated sample within 9 h in the second step of reduction was observed due to the finely agglomerated particles during intensive milling and subsequently the formation of a dense layer during the reduction processes. In addition, the dependence of $\ln A_0$ on α was detected and it was found that the $\ln A_0$ shows the same dependence on α as the apparent activation energies.

© 2007 Elsevier B.V. All rights reserved.

Keywords: Mechanical activation; Iron oxide; Reduction kinetics; Thermogravimetry; Nonisothermal

1. Introduction

The reduction of iron oxides by hydrogen has been investigated extensively because of its relevance to iron production. The existence of a series of three successive reactions from hematite (Fe₂O₃) to iron through magnetite and wüstite (Fe_{1−x}O) is of interest from an academic point of view, regarding the possibility of coupling between two steps and the consequences of each step upon the following one. The literature [1,2] suggests that the reduction of Fe₂O₃ to iron metal, at lower temperature below 570 °C, proceeds in two steps via Fe₃O₄ intermediate as follows:



Step 1 is exothermic, whilst reduction to the metal in step 2 is endothermic [2]. Excellent agreements were achieved in the rate-controlling reactions. Kinetics data for the reduction of iron oxides are generally described in terms of nucleation/autocatalytic, diffusion and phase boundary models. However, discrepancies exist among the reported kinetics models for the reduction steps. Such inconsistencies may be attributed to the starting raw material characteristics, sample specimen used (powder, pellet, or ore), nature of reducing gas, temperature range, reduction step, presence of water, gas impurities, physical shape, etc. [3,4]. It is generally agreed that the rate of reduction by H₂ is significantly faster than that by CO [5]. However, during the final stage of reduction, the rate with hydrogen decreases compared with CO. In the reduction of iron ores with hydrogen, a dense iron shell forms around the particles (magnetite and/or wüstite grains) and subsequently inhibits gaseous transport during reaction [1,6,7]. Several investigations have been reported

* Corresponding author. Tel.: +46 920 491313; fax: +46 92097364.

E-mail address: Parviz.Pourghahramani@ltu.se (P. Pourghahramani).

that the reduction of Fe_2O_3 is catalyzed by metal additives in the presence of water vapor (2–7.5%, v/v in reducing mixture). This enhancement is ascribed to “hydrogen spill over” effect which provides the necessary active hydrogen at the reduction centers [2,8]. However, the addition of H_2O retards generally the reduction rate, especially for $\text{Fe}_3\text{O}_4 \rightarrow \text{Fe}$ step [3].

The concept of high-energy milling has attracted considerable scientific and technical interests in recent years as a consequence of higher reactivity and properties developed by this process. Mechanical activation has found a wide range of application potential such as the intensification of thermal reactivity of minerals [9]. Mechanical activation has usually a positive influence on the leaching reaction kinetics. In addition, the mechanical activation of minerals makes it possible to reduce their reaction temperature and/or their decomposition temperature or causes such a degree of disordering. Thermal behavior of mechanically activated galena and pyrite has been investigated by Hu et al. [10–12]. It has been found that mechanically activated pyrite and galena are more easily decomposed during thermal treatments than non-activated pyrite and galena. Moreover, the activation energy of the thermal decomposition of pyrite decreases as a consequence of mechanical activation. Mechanically activated sphalerite also oxidizes easily than non-activated sphalerite [13]. Milling of manganese ore with graphite led to enhanced reduction at decreased temperatures [14]. Mechanical activation of hematite concentrate can result in reduction of hematite to maghemite ($\gamma\text{-Fe}_2\text{O}_3$), magnetite and subsequently to FeO [15,16]. Since oxygen bonds on the hematite surface are broken, oxygen is released during high energy milling of hematite particles in air. However, the transformation of all hematite by milling process occurs after relatively long period of time. It is thought that the mechanical activation with a low temperature heat treatment can be successfully applied for reduction of hematite to magnetite.

The goal of this paper is to study the reduction kinetics of both non-activated hematite and mechanically activated hematite in a vibratory mill for various grinding times.

2. Experimental

2.1. Material

The high-purity hematite concentrate used in this study was kindly supplied by the LKAB (Luossavaara Kiirunavaara Aktiebolag) company in Sweden. The chemical analysis showed that the initial hematite powder contained about 97.91% Fe_2O_3 , 0.73% Al_2O_3 , 0.73% SiO_2 , 0.26% TiO_2 , 0.20% MgO , 0.022% MnO , and 0.088% P_2O_5 . Other components such as K_2O , CaO and Na_2O comprise 0.051%. The X-ray diffraction analysis represented only the hematite diffraction peaks.

2.2. Mechanical activation

The dry grinding tests were carried out using a vibratory ball mill with dimensions of $\text{L}320 \text{ mm} \times \text{Ø}185 \text{ mm}$. A mixture of ball steel media with dimensions between 6 and 22.2 mm and with apparent density of 4875 kg m^{-3} was used as grinding media.

Table 1
Milling conditions in the vibratory mill

Milling conditions	Vibratory milling
Media filling (%)	70
Mass of media (kg)	33.16
Milling time (h)	1, 3, 9
Ball to powder weight ratio	67.68:1
Speed (RPM)	1000
Amplitude (mm)	8

Milling experiments were made in air atmosphere under closed milling condition, i.e., the door of mill was kept closed during the whole milling process periods. The grinding conditions are summarized in Table 1. The samples were sealed into plastic tubes and kept in a freezer for further measurements.

2.3. Characterization

Thermogravimetric analyses (TG) were conducted with a NETZSCH STA 409C instrument at three heating rates of 10, 15 and $20^\circ\text{C min}^{-1}$ from room temperature to 850°C . The high temperature furnace was heated by graphite heating elements, which were protected by injection of inert argon gas. The temperature of furnace was controlled by a tungsten thermocouple. The heating was performed under highly pure hydrogen as reduction gas with a flow rate of 100 ml min^{-1} . The mass of samples was almost 95 mg.

The morphological characterization of the samples was performed using a Philips XL 30 scanning electron microscope (SEM) equipped with a LaB_6 emission source and running at 20 kV. After drying, the samples were gold coated using gold sputtering prior to SEM investigation.

The XRD patterns were obtained using a Siemens D5000 powder diffractometer with Bragg-Brentano geometry equipped with a curved graphite monochromator in the diffracted beam arm and using $\text{Cu K}\alpha$ radiation ($\lambda = 0.15406 \text{ nm}$). The XRD patterns of the samples were recorded using a step size of 0.02° and a counting time of 5 s per step.

3. Kinetic analysis

Several methods have been applied for kinetics studies of solid state reactions [17]. The methods of kinetics analysis can be classified based on experimental conditions selected and the mathematical analysis performed. The mathematical methods are divided into model fitting and isoconversional (model-free) methods. Modelistic methods have been criticized in nonisothermal studies because (1) they assume a constant kinetic triplet (A , E and model), (2) they involve fitting three parameters (A , E and model), which are simultaneously determined from a single curve, (3) they involve a single heating rate, which is not always sufficient to determine reaction kinetics and (4) the selection of the best model is a challenging task based on a statistical parameter (r^2) [18–22]. Model fitting methods were the most popular methods in the analysis of solid state kinetics. The popularities of these models have recently declined in favor of isoconversional methods which can compute kinetics parameters without

modelistic assumptions [22,23]. On the other hand, a successful kinetics analysis can be performed using several experiments at the same degree of conversion if careful experiments will be applied considering the suggestions by Ortega [24]. The basic assumption of isoconversional methods is that the reaction rate at a constant conversion is only a function of temperature, and the reaction model is independent of temperature of heating rate [25–28]. Thus, constant E values may be expected in the case of single-state decomposition, while a multi-step reaction E varies with conversion degree due to the variation in the relative contributions of the single step to the overall reaction rates. The goal of the model-free kinetics analysis is to use this variation, as an additional source of information on the reaction mechanism [29,30]. The main disadvantage of isoconversional approach is that they do not suggest direct evaluation of the pre-exponential factor without kinetic model. To use the isoconversional methods, a series of experiments has to be conducted at different heating rates [31].

In the kinetic analysis, a reaction progress expresses conventionally in terms of conversion fraction or extent of reaction as:

$$\alpha = \frac{w_i - w}{w_i - w_f} \quad (3)$$

where w_i , w and w_f are the initial, actual and final weight of the sample, respectively.

The rate of a solid state reaction can be described by:

$$\frac{d\alpha}{dt} = \beta \frac{d\alpha}{dT} = k(T)f(\alpha) = A \exp\left(\frac{-E}{RT}\right) f(\alpha) \quad (4)$$

where $k(T)$ is the rate constant at temperature T , $f(\alpha)$ is a function of α which represents the reaction mechanism, α the extent of reaction, t is the time and β is the heating rate. A and E correspond to the pre-exponential and activation energy, respectively. Eq. (4), can be expressed in the form of its integral, $g(\alpha)$, with Eq. (5).

$$g(\alpha) = \int_0^\alpha \frac{d(\alpha)}{f(\alpha)} = \frac{A}{\beta} \int_0^T \exp\left(\frac{-E}{RT}\right) dT; \quad (5)$$

If $\frac{E}{RT} = x \Rightarrow g(\alpha) = \frac{AE}{\beta R} \int_x^\infty \frac{e^{-x}}{x^2} dx = \frac{AE}{\beta R} \int_x^\infty p(x) dx$

where $p(x)$ is the temperature integral. The Eqs. (4) and (5) underlie most of the methods of kinetics processing. Several reaction models used in the analysis of solid state kinetics are listed in Appendix A in terms of $g(\alpha)$ and $f(\alpha)$. The $p(x)$ has no analytic solution, but several approximations have been made. One of the most widely used approximations has been given by Coats and Redfern [32,33] for exponential $p(x)$:

$$\ln \frac{g(\alpha)}{T^2} = \ln \left(\frac{AR}{\beta E} \left[1 - \left(\frac{2RT_{\text{exp}}}{E} \right) \right] \right) - \frac{E}{RT} \quad (6)$$

If: $\left(\frac{2RT}{E} \right) \ll 1 \Rightarrow \ln \frac{g(\alpha)}{T^2} = \ln \left(\frac{AR}{\beta E} \right) - \frac{E}{RT}$

where T_{exp} is the mean experimental temperature. A plot of $\ln g(\alpha)/T^2$ versus $1/T$ gives activation energy and pre-exponential

factor from the slope and intercept of the curve with a single heating rate, respectively. All integral functions in Appendix A can be tested and the best method can be selected with regard to a statistical parameter such as correlation coefficient (r).

On the other hand, the isoconversional methods calculate the kinetics parameters at a progressive degree of conversion (α) without the modelistic assumptions. Among the isoconversional methods, Kissinger–Akahira–Sunose (KAS) [34,35] method has been widely used to estimate activation energy regardless of the rate expressions of reactions as follows:

$$\ln \frac{\beta}{T^2} = \ln \left(\frac{AE}{g(\alpha)R} \right) - \frac{E}{RT} \quad (7)$$

For $\alpha = \text{const.}$, the plot $\ln \beta/T^2$ versus $1/T$ obtained from curves recorded at several heating rates, should be a straight line whose slope can be used to calculate the activation energy. In the present paper, the above mentioned methods were used for calculation of the kinetic parameters of the reduction of mechanically activated and non-activated hematite samples to iron.

The isoconversional method provides a model-free way of making kinetic predictions. Furthermore, model-free kinetics does not need the experimental values of A , and $g(\alpha)$ or $f(\alpha)$ for the practical purposes of kinetic predictions. The respective predictive equation [37,38] was given in the following form assuming the partial kinetic triplets remain the same over the temperature region related to a given conversion:

$$t_\alpha = \frac{\int_0^{T_\alpha} \exp(-E_\alpha/RT) dT}{\beta \exp(-E_\alpha/RT_0)} \quad (8)$$

This enables the time, t_α , at which a given conversion will be reached at an arbitrary temperature, T_0 , to be computed. T_α is an experimental value of the temperature corresponding to a given conversion at the heating rate β and E_α is the activation energy at a given conversion.

4. Results and discussion

4.1. X-ray diffraction analysis

The XRD patterns of non-activated and activated samples are given in Fig. 1. Considering the peaks of non-activated and activated hematite, the X-ray patterns of the milled samples only show the Bragg reflections of hematite, suggesting that the starting material did not undergo significant reactions either during milling or after prolonged milling. With the increased grinding time, a continuous broadening of the diffraction peaks and decreased intensity of diffraction peaks were observed. These indicate an increase in the degree of lattice disorder and a decrease in the crystallite size, thereby reducing the symmetry of the unit cell until some fraction of the material becomes amorphous. Comparing the XRD patterns indicates that the maximum line broadening and minimum intensity are obtained for hematite sample ground for longer time. In literature [9,11], it was reported that the mechanical activation resulted in the amorphization of minerals, development of large numbers of dislocation and their associated strain fields, decrease of crys-

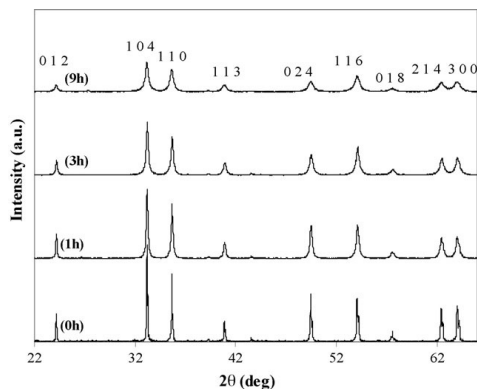


Fig. 1. X-ray diffraction patterns of non-activated and activated hematite. Hereafter, 0h refers to the initial sample or non-activated sample.

tallite size and change of the lattice parameters which might lead to an overall decrease in long range lattice periodicity. This may be interpreted as the formation of a metastable “amorphous phase”, because line broadening and the reduction of diffraction peaks intensity take place on X-ray pattern after prolonged milling.

4.2. Reduction behavior

Conventionally, reduction kinetics of iron oxides, such as hematite or magnetite, has been studied in terms of the extent of reaction (α). Fig. 2 shows changes in the degree of conversion with three different heating rates for the reduction of the initial sample by H_2 as a function of temperature. A close look on the curves indicates slight changes of slopes at different temperatures, the changes are more prominent at lower and higher temperature ranges. These are indicative of sequential reactions. The changes in the slope of the curves at $\alpha = 0.11$ correspond to the quantitative conversion of hematite to magnetite. The production of 89% H_2O associated with the subsequent reduction to Fe. The investigation of onset temperatures from the TG curves confirmed that the prerelution step to Fe_3O_4 is complete prior to the onset of the main reduction step to metal iron. This view is also supported by X-ray analysis of the reduction products

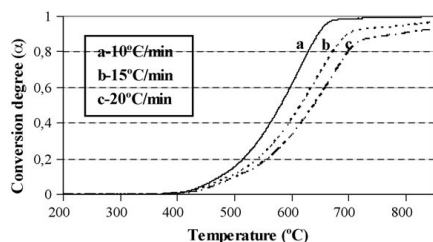


Fig. 2. Changes in the degree of conversion with three heating rates during the reduction of the initial sample as a function of temperature.

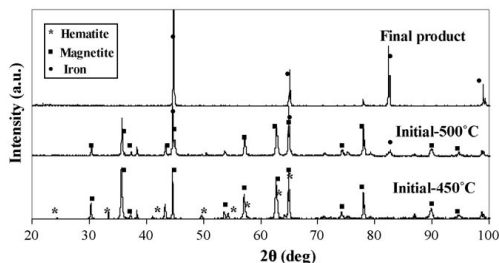


Fig. 3. XRD patterns of the reduction products of the initial sample. The products obtained under heating rate of $10^\circ C/min$.

(Fig. 3). The XRD pattern of the reduction product of the initial sample heated to $450^\circ C$ with heating rate of $10^\circ C min^{-1}$ represents both magnetite and hematite phases. The weight loss was calculated at about 2.87% up to $450^\circ C$, which is still lower than the weight loss value corresponding to the complete conversion of hematite to magnetite (3.33%). The reduction of the initial hematite to $500^\circ C$ produces reflection peaks of magnetite and iron phases in the XRD powder pattern. As a result, the reduction proceeds stepwise ($Fe_2O_3 \rightarrow Fe_3O_4 \rightarrow Fe$). This agrees with previous literature studies on powder Fe_2O_3 sample which generally report that the reduction proceeds in two consecutive steps [1,2]. Sastri et al. [2] reported that the findings from X-ray diffractometry, Mössbauer spectroscopy and photomicrography studies showed that the reduction precedes in a stepwise manner with only two phases, either Fe_2O_3 and Fe_3O_4 or Fe_3O_4 and Fe, existing at any stages throughout isothermal reduction below $570^\circ C$. It should be noted that the absence of wüstite in the XRD patterns of the reduction product does not mean that wüstite does not exist during the reduction because the dismutation reaction $Fe_{(1-x)}O$ can give Fe and magnetite.

According to Fig. 4, the slope of the curves corresponding to the activated samples changes when reaction progress reaches around 0.11. This indicates that the two steps of the reaction are resolved well as a result of mechanical activation. For non-activated hematite, the use of higher heating rates do not allow the complete conversion of hematite to iron metal at the same temperature ranges as it occurs for the samples ground by the mill. The maximum degree of conversion for all mechanically

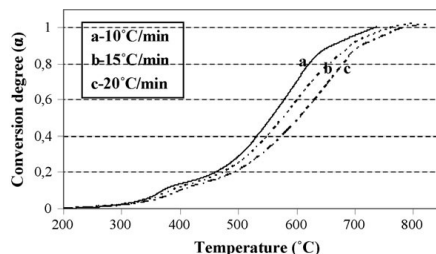


Fig. 4. Changes in the degree of conversion with three heating rates during the reduction of the sample ground for 9 h in the mill as a function of temperature.

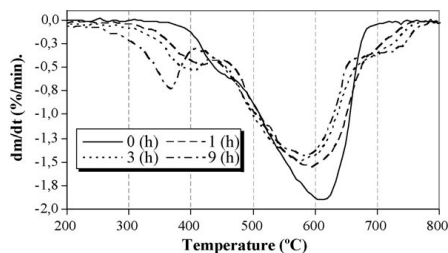


Fig. 5. TG curves of the initial sample and the samples ground for various grinding periods by the mill as a function of temperature.

activated samples is calculated close to unity, corresponding to the complete conversion of hematite to magnetite. It is clear that the reduction in the activated samples starts notably at lower temperatures (higher reactivity) than that in the initial sample. The beginning temperature of reaction decreases from 400 °C in the initial sample to about 250 °C in the sample ground for 9 h. Many workers have reported higher reaction rate at temperatures just below 600 °C than higher temperatures. Several reasons have been proposed for the occurrence of rate minimum [6,7]. These include sintering of the iron product which reduces diffusion of the reductant and the product gas to form the reaction interface. The rate minimum phenomenon is clear in the curve as shown in Fig. 4 at higher temperature for mechanically activated hematite.

The DTG curves corresponding to the heating rate of 10 °C min⁻¹ for the initial sample and the samples ground for different periods are shown in Fig. 5 as a function of temperature. The TG curves also represent a two-step weight loss which can be easily identified from the changes in the slope and the peaks of the curves. The first step of weight loss, corresponding to the reduction of hematite to magnetite, occurs at the lower temperatures. The second step (main step) of weight loss, the reduction of magnetite to iron, extends toward higher temperature sides up to 780 °C. Interestingly, the first step of weight loss is more pronounced for mechanically activated samples compared with the initial sample. In addition, a plateau between the two steps of reduction process can be observed. It is apparent that the resolution of the two events is greater for mechanically activated samples than for the initial sample. This is a consequence of the reduction of the energy required to reorganize the crystalline structure of hematite. The energy supplied by milling causes structural disorder through the distortion or breakage of the crystalline network. This was evident from the reduction of the intensities of XRD peaks reported in Fig. 1. Once more, this emphasizes that the mechanical activation results in improved resolution of overlapping reduction events. Moreover, the area of peak in the second step of reduction decreases concomitantly as the area of peak in the first weight loss step centered approximately between 300 and 450 °C increases, depending upon grinding time. For the non-activated hematite, the first step of reduction initiates and terminates at a certain temperature range. This is an expected property for crystalline hematite. However, activated hematite exhibits different starting and finishing tem-

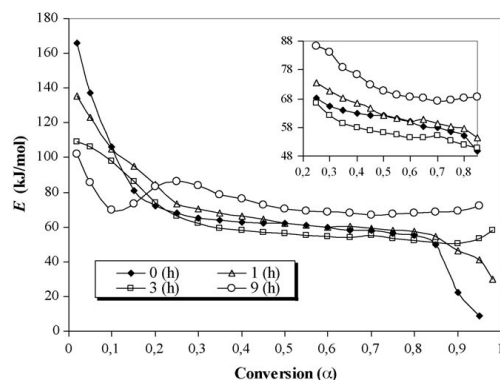


Fig. 6. Dependence of E on α characteristic of the reduction of non-activated hematite and mechanically activated hematite for various grinding times; a large scale of the curves for the range of $0.25 \leq \alpha \leq 0.85$ are shown in inset.

peratures of reduction in the first step of reduction, depending on grinding times and consequently the structural changes induced during milling.

4.3. Kinetic results

The application of the isoconversional methods requires the determination of the absolute temperature at which a fixed extent of reduction from the several TG curves recorded at different heating rates. The degree of conversion between 0.02 and 0.95 is investigated. The basic parameters such as conversion degree, heating rate and temperature were inserted into Eq. (7). The correlation coefficients for the linear regressions were higher than 0.94. The dependence of the activation energy E on α characteristic for hydrogen reduction of non-activated hematite and mechanically activated hematite for different periods is shown in Fig. 6.

The overall decreasing dependence of the activation energy on α indicates that the overall reaction contains at least two steps. A decrease in the activation energy is most likely caused by transition of the limiting step from the higher activation energy reaction to the lower activation energy reaction. The curves corresponding to the initial sample and the mechanically activated samples show that E decreases with extent of conversion (α) by $\alpha \leq 0.11$, corresponding the reduction of hematite to magnetite, with increasing the grinding time. After this range, the activation energy continues to decrease for the initial sample and mechanically activated samples up to 3 h as opposed with the activation energy for mechanically activated sample within 9 h in which the activation energy tends to increase slightly and then decreases by $\alpha \leq 0.85$. The activation energy of the initial sample and ground sample for 1 h decrease drastically when the conversion degree exceeds 0.85 as opposed with the reduction of the activated samples for more than 1 h. Since the reduction of the initial sample and activated sample for 1 h extends up to 900 °C at higher heating rates, the decreases of the activation energy can probably be due to the phase transition of α -Fe to γ -Fe (906 °C) [36].

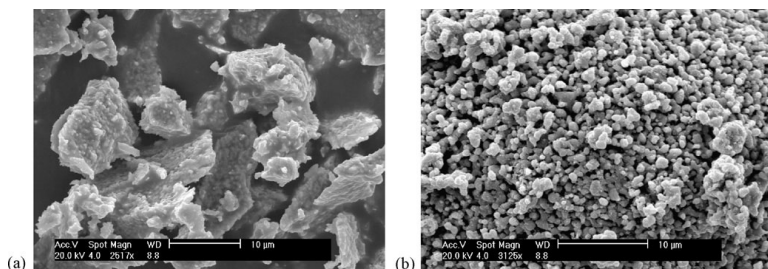


Fig. 7. SEM micrographs of the reduction products of the initial sample (a) and the sample ground for 9 h (b).

In the lower degree of conversion (lower temperature region), the reduction of non-activated hematite is much more sensitive to the extent of reaction. The first step of reduction, corresponding to $\alpha \leq 0.11$, in the initial sample describes with activation energy of about $166\text{--}106\text{ kJ mol}^{-1}$, while the calculated value for the second reduction step, corresponding to $0.11 \leq \alpha \leq 0.95$, is about $72\text{--}9\text{ kJ mol}^{-1}$. Comparison with literature data shows that discrepancies exist among the measured activation energies for the reduction of powdered iron oxides. Such variations may be associated with differences between the samples studied and or the conditions employed for sample reduction. For example, Munteanu et al. [39] reported the activation energies of 162 and 104 kJ mol^{-1} for the first and second steps of the reduction using temperature-programmed method between 450 and 700°C , where the precursor of Fe_2O_3 was ferrihydrite. Sastri et al. [2] reported that pretreatment at 850°C of $\alpha\text{-Fe}_2\text{O}_3$ resulted in an increase in activation energy to 73 kJ mol^{-1} relative to a value of 57 kJ mol^{-1} for a sample that had undergone no heat treatment. Thus, the activation energy is strongly sample dependent and conditions employed for the reduction. The decreasing trend of activation energy in the two steps of the reduction can be explained in the terms of a nucleation and growth the model of reduction in which the activation energy required during nucleation is higher than that needed in the growth stage (autocatalytic effects). Similar trends have been reported for the reduction of iron oxides where E has been found to decrease with extent of reduction using CR-TPR “rate Jump” technique [40].

For activated hematite, the activation energy for the range of $\alpha \leq 0.11$ decreases with increasing grinding time. The activation energy from 166 to 106 kJ mol^{-1} range in the initial sample

decreases to about $102\text{--}70\text{ kJ mol}^{-1}$ in the sample ground for 9 h. The disordering of structure in mechanically activated samples brings about an increase in the rate of reduction process and a decrease in the activation energy [9]. For the second step of reduction, the ground sample up to 1 h exhibits no significant difference in activation energy by conversion degree of 0.85. Grinding for 3 h result in a slightly smaller activation energy compared with the initial sample; while prolonged milling for 9 h leads to higher activation energy than the initial sample. This can be attributed to the agglomeration of finely ground particles during intensive milling and subsequently to the formation of a dense layer as a result of the partial sintering at higher temperatures. As a result, the effect of disordering of hematite structure overlapped by the formation of the dense layer. Therefore, the reduction is retarded [5]. It can be concluded that mechanical activation has a positive effect on the prereduction step in terms of activation energy and small positive effect on the second step of reduction in the samples ground up to 3 h.

Furthermore, the dependence of the apparent activation energy (E) on the extent of conversion (α) is a source of additional kinetic information of process [41]. The obtained results reveal that the dependence of the apparent activation energy (E) on the extent of conversion (α) helps not only to disclose the complexity of reduction processes, but also to identify its kinetic scheme. A decreasing dependence of E on α is often encountered in solid decompositions which follow: solid \rightarrow solid + gas [38]. The curves obtained for non-activated sample and mechanically activated samples up to 3 h reveal a typical reversible reaction according to Vyazovkin et al. [38,42–44]. Vyazovkin and Linert [42] have been shown that the decreasing dependence of E

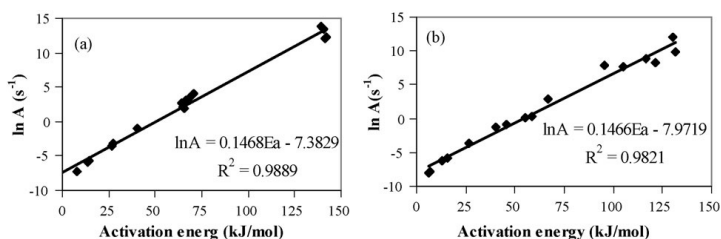


Fig. 8. The artificial isokinetic relationship ($\ln A$ vs. E) using Coats–Redfern method at heating rate of 10°C/min for the initial sample in the range of $0.02 \leq \alpha \leq 0.1$ (a), and $0.1 < \alpha < 0.95$ (b).

on α corresponds to the kinetic scheme of a reversible reaction followed by an irreversible one. For such process E is limited by the sum of the activation energy of the irreversible reaction and the enthalpy of the reversible reaction at low conversions. At high values of conversions, E is limited only by the activation energy of the irreversible reaction at high α [41]. In our case, the reduction of hematite to magnetite probably proceeds through the exothermic stage at low conversion degrees, which is characterized by a high value of the apparent activation energy between 166 and 70 kJ mol⁻¹ depending on the sample. The high values of the effective activation energy represent the sum of the enthalpy of the reversible process and of the apparent activation of the irreversible process. On the other hand, lower value of the activation energy at higher conversions is a characteristic of the process proceeding through a reversible endothermic process. For mechanically activated sample for 9 h, the decreasing dependence of the activation energy is followed by increasing and then decreasing the activation energy for $\alpha \geq 0.11$; indicating increasing difficulty in the progress of reaction. The second step is probably involving competing between the reduction of magnetite to iron and sintering process which may account for the increasing dependence of E on α .

Fig. 7 exhibits the morphological aspects of the reduction products using SEM studies at the initial and activated samples. Unlike the initial sample, the partial sintering can be clearly observed in the mechanically activated hematite. The partial sintering leads to the formation of rounded particles in the activated sample as a consequence of mass transport process by moving mass from particle surface and internal mass sources [45]. It seems that the agglomeration of the finely ground particles during extended dry milling facilitates the sintering process. The clusters of the partially sintered material can be further observed due to the formation of massive and compact agglomerates which was identified and reported during intensive dry grinding process elsewhere [46].

4.3.1. The evaluation of pre-exponential factor

The Coats–Redfern analysis of the thermogravimetric data recorded at a single heating rate has been carried out by inserting various $g(\alpha)$ in Appendix A into Eq. (6) that results in a set of Arrhenius parameters determined from the plot $\ln g(\alpha)/T^2$ versus $1/T$. Similar calculations were made for other heating rates

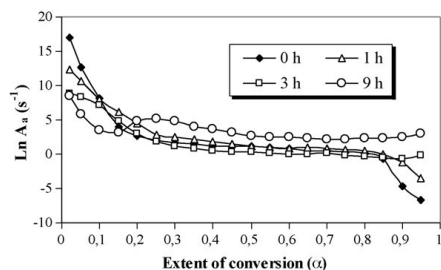


Fig. 9. Dependence of $\ln A_a$ on extent of conversion, α , estimated from Eq. (9) for different samples.

and samples. It was found that each TG curve could be equally well described by several kinetic models resulting in correlation coefficients close to unity. Therefore, the Arrhenius parameters derived were highly variable, exhibiting a strong dependence on the reaction function chosen and a weak dependence on the heating rate. This extra flexibility in the fitting procedure introduces errors in the functional form of the reaction model. This can be offset by making compensation errors in the Arrhenius parameters. Vyazovkin et al. [38,47,48] explored widely artificial isokinetic relationship (IKR) that occurs on fitting various reaction models to the same set of nonisothermal kinetic data. Originally, this procedure was suggested [48] for estimating the pre-exponential factor in the isoconversional method as applied to a single-step process. However, the procedure can be applied to isolate the $\ln A$ on α dependence for multi-step processes [38]. Use of the so-called artificial isokinetic relationship may be used to evaluate the pre-exponential factors for the model-free anal-

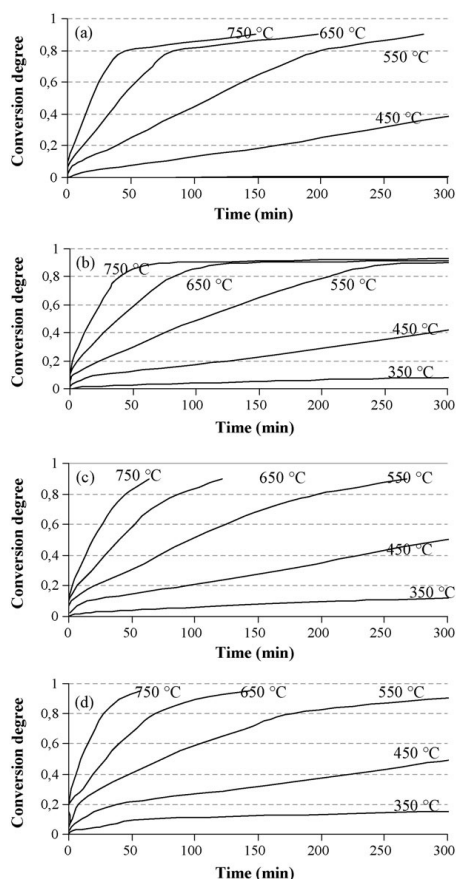


Fig. 10. Prediction at different temperatures using heating rate of 10 °C/min for the initial sample (a) and mechanically activated samples for 1 (b), 3 (c) and 9 (d) hours.

ysis. It is observed that the values of the activation energy and pre-exponential factor, obtained for different function of $g(\alpha)$, are correlated through the following relation of compensation:

$$\ln A_i = aE_i + b \quad (9)$$

where the subscript i refers to the one of the possible models considered ($g(\alpha)$ in Appendix A) to describe the process. This reveals that the rate of process can be fairly described by Eq. (6) with practically any model $g(\alpha)$ and fitting $k(T)$ which compensates the error of reaction model choice. An example of artificial isokinetic relationship for the initial sample is given in Fig. 8. All of the plots represent excellent fit where the correlation coefficient exceeds 0.97.

Once the correlation coefficients of the artificial isokinetic relationships have been evaluated, the E_a values from the iso-conversional methods are substituted for E_a in the compensation effect Eq. (9) [38] for the studied systems to estimate the corresponding $\ln A_a$ values and obtaining the dependence of $\ln A_a$ on α . The results are summarized in Fig. 9. Clearly, the $\ln A_a$ shows the same dependence on α as the apparent activation energies (E).

4.3.2. Predictions

Predictions are among the most important practical feature of kinetic analysis [42]. They are widely used to evaluate the kinetic behavior of materials beyond the temperature region of experimental measurements. By using Eq. (8), with nonisothermal kinetic data, the prediction of samples behavior in isothermal conditions is possible. Fig. 10 presents conversion curves of the reduction of the initial sample and ground samples in the mill as a function of time, for different temperatures. On the basis of the curves obtained for the samples, one may state that the conversion time decreases as a function of temperature. It is evident from the graph that the initial sample does not reduce at 350 °C as opposed with mechanically activated hematite. This agrees

with our nonisothermal experiments where the onset of reaction for the initial sample is calculated about 420 °C. It follows from the figure that a conversion of 0.1 is attainable for 70, 26, 14 and 10 min at $T=450$ °C in the initial sample and ground samples for 1, 3 and 9 h, respectively. With increasing temperature, the difference between the samples for achieving a given conversion at an identical temperature reduces. Achieving a conversion of 0.7 at $T=650$ in the initial sample and activated samples for 1, 3 and 9 h, respectively, takes about 67, 65, 65.2 and 58 min that samples are maintained under reducing program. The results reveal that the mechanical activation has large positive effect on the reduction of hematite at lower temperatures compared with reduction at higher temperatures.

5. Conclusion

The reduction of Fe_2O_3 to Fe was found to occur in a two step process via Fe_3O_4 . The TG and DTG analysis showed that the two reduction steps took place consecutively. The mechanical activation promoted partial amorphous solids along with some structural distortions in hematite. This pretreatment resulted in improved resolution of overlapping reduction events. The pre-reduction step in the activated samples initiated and completed at lower temperatures than that in non-activated samples. The activation energy of the first step of reduction decreased with increasing the grinding time. Intensive milling increased slightly the average activation energy of the second reduction step due to the present of finely agglomerated particles and intensive sintering of the particles in higher temperature ranges.

Our study shows that the activation energy of the two steps of the reduction depends greatly on the extent of conversion, implicating that the reduction of hematite to magnetite and magnetite to iron features multi-step characteristics. The decreasing trend of activation energy in the two steps of the reduction can be explained in the terms of a nucleation and growth the

Table A.1

Solid state rate expressions for different reaction models

Model	Differential form $f(\alpha) = \frac{1}{k} \frac{d\alpha}{dt}$	Integral form $g(\alpha) = kt$
Nucleation models		
Power law (P2)	$2\alpha^{(1/2)}$	$\alpha^{(1/2)}$
Power law (P3)	$3\alpha^{(2/3)}$	$\alpha^{(1/3)}$
Avrami-Erofe'ev (A1.5)	$3(1-\alpha)[- \ln(1-\alpha)]^{1/3}/2$	$[- \ln(1-\alpha)]^{2/3}$
Avrami-Erofe'ev (A2)	$2(1-\alpha)[- \ln(1-\alpha)]^{1/2}$	$[- \ln(1-\alpha)]^{1/2}$
Avrami-Erofe'ev (A3)	$3(1-\alpha)[- \ln(1-\alpha)]^{2/3}$	$[- \ln(1-\alpha)]^{1/3}$
Avrami-Erofe'ev (A4)	$4(1-\alpha)[- \ln(1-\alpha)]^{3/4}$	$[- \ln(1-\alpha)]^{1/4}$
Geometrical contraction models		
Contracting area (R2)	$2(1-\alpha)^{1/2}$	$[1 - (1-\alpha)^{1/2}]$
Contracting volume (R3)	$3(1-\alpha)^{2/3}$	$[1 - (1-\alpha)^{1/3}]$
Diffusion models		
1D Diffusion (D1)	$1/(2\alpha)$	α^2
2D Diffusion (D2)	$[- \ln(1-\alpha)]^{-1}$	$[(1-\alpha)\ln(1-\alpha)] + \alpha$
3D Diffusion–Jander Eq. (D3)	$(3/2)(1-\alpha)^{2/3}[1 - (1-\alpha)^{1/3}]^{-1}$	$[1 - (1-\alpha)^{1/3}]^2$
Ginstling–Brounshtein (D4)	$(3/2)(1-\alpha)^{-1/3} - 1)^{-1}$	$(1 - 2\alpha/3) - (1-\alpha)^{2/3}$
Reaction-order models		
Zero-order (F0/R1)	1	α
First-order (F1)	$(1-\alpha)$	$-\ln(1-\alpha)$
Second-order (F2)	$(1-\alpha)^2$	$(1-\alpha)^{-1} - 1$
Third-order (F3)	$(1-\alpha)^3$	$0.5[(1-\alpha)^{-2} - 1]$

model of reduction in which the activation energy required during nucleation is higher than that needed in the growth stage (autocatalytic effects). The prediction of reduction behavior of the samples revealed that with increasing temperature, the difference between the samples for achieving a given conversion reduces at an identical temperature.

Appendix A

See Table A.1 for solid state rate expressions for different reaction models.

References

- [1] A. Pineau, N. Kanari, I. Gaballah, *Thermochim. Acta* 447 (2006) 89.
- [2] M.V.C. Sastri, R.P. Viswanath, B. Viswanath, *Int. J. Hydrogen Energy* 7 (1982) 95.
- [3] O.J. Wimmers, P. Arnoldy, J.A. Moulijn, *J. Phys. Chem.* 90 (1986) 1331.
- [4] M. Shimokawabe, R. Furuichi, T. Ishii, *Thermochim. Acta* 28 (1979) 287.
- [5] T.L. Joseph, *Trans. AIME* 120 (1936) 72.
- [6] R.J. Fruehan, Y. Li, L. Brabie, E.J. Kim, *Scand. J. Metall.* 34 (2005) 205.
- [7] H.S. Ray, N. Kundu, *Thermochim. Acta* 101 (1986) 107.
- [8] R.P. Viswanath, B. Viswanath, M.V.C. Sastri, *React. Kinet. Catal. Lett.* 2 (1975) 51.
- [9] P. Bálaž, *Extractive Metallurgy of Activated Minerals*, first ed., Elsevier, Amsterdam, 2000.
- [10] H. Hu, Q. Chen, Z. Yin, P. Zhang, *Thermochim. Acta* 398 (2003) 233.
- [11] H. Hu, Q. Chen, Z. Yin, P. Zhang, J. Zou, H. Che, *Thermochim. Acta* 389 (2002) 79.
- [12] H. Hu, Q. Chen, Z. Yin, P. Zhang, L. Ye, *Metall. Mater. Trans.* 34A (2003) 793.
- [13] Q. Chen, H. Hu, Z. Yin, P. Zhang, L. Ye, *Metall. Mater. Trans.* 33B (2002) 897.
- [14] N.J. Welham, *Int. J. Miner. Process.* 67 (2002) 187.
- [15] M. Zdujic, C. Jovalekic, L.J. Karanovic, M. Mitric, D. Poleti, D. Skala, *Mater. Sci. Eng.* A245 (1998) 109.
- [16] T. Kosmac, T.H. Courtney, *J. Mater. Res.* 17 (1992) 1519.
- [17] S. Vyazovkin, *Int. Rev. Phys. Chem.* 17 (1998) 407.
- [18] M.E. Brown, M. Maciejewski, S. Vyazovkin, R. Nomen, J. Sempere, A. Burnham, J. Opfermann, R. Strej, H.L. Anderson, A. Kemmler, R. Keuleers, J. Janssens, H.O. Desseyen, C.R. Li, T.B. Tang, B. Roduit, J. Malek, T. Mitsuhashi, *Thermochim. Acta* 355 (2000) 125.
- [19] A.K. Burnham, *Thermochim. Acta* 355 (2000) 165.
- [20] M. Maciejewski, *Thermochim. Acta* 355 (2000) 145.
- [21] B. Roduit, *Thermochim. Acta* 355 (2000) 171.
- [22] S. Vyazovkin, *Thermochim. Acta* 355 (2000) 155.
- [23] A. Khawam, D.R. Flanagan, *Thermochim. Acta* 429 (2005) 93.
- [24] A. Ortega, *Thermochim. Acta* 284 (1996) 379.
- [25] J.H. Flynn, L.A. Wall, *J. Res. Natl. Bur. Stand. Sect. A* 70 (1966) 487.
- [26] S. Vyazovkin, D. Dollimore, *J. Chem. Inf. Comput. Sci.* 36 (1996) 42.
- [27] T. Ozawa, *Bull. Chem. Soc. Jpn.* 38 (1965) 1881.
- [28] H. Friedman, *J. Polym. Sci. C* 6 (1965) 195.
- [29] S. Vyazovkin, N. Sbirrazzuoli, *Macromol. Chem. Phys.* 200 (1999) 2294.
- [30] N. Sbirrazzuoli, Y. Girault, L. Elégant, *Thermochim. Acta* 293 (1997) 25.
- [31] S. Vyazovkin, *J. Comput. Chem.* 18 (1997) 393.
- [32] A.W. Coats, J.P. Redfern, *Nature* 201 (1964) 68.
- [33] A.W. Coats, J.P. Redfern, *J. Polym. Sci. B: Polym. Lett.* 3 (1965) 917.
- [34] H.E. Kissinger, *J. Anal. Chem.* 29 (1957) 1702.
- [35] T. Akahira, T. Sunose, *J. Res. Report Chiba Inst. Technol. (Sci. Technol.)* 16 (1971) 22.
- [36] A. Chakraborty, *J. Magn. Magn. Mater.* 204 (1999) 57.
- [37] S. Vyazovkin, C.A. Wight, *Thermochim. Acta* 340–341 (1999) 53.
- [38] S. Vyazovkin, *Int. J. Chem. Kinet.* 28 (1996) 95.
- [39] G. Munteanu, L. Ilieva, D. Andreeva, *Thermochim. Acta* 329 (1999) 157.
- [40] S. Vyazovkin, C.A. Wight, *Annu. Rev. Phys. Chem.* 48 (1997) 125.
- [41] M.J. Tiernan, P.A. Barnes, G.M.B. Parkes, *J. Phys. Chem.* 105 (2001) 220–228.
- [42] S. Vyazovkin, W. Linert, *Int. J. Chem. Kinet.* 27 (1995) 73.
- [43] S.V. Vyazovkin, A.I. Lesnikovich, V.A. Lyutsko, *Thermochim. Acta* 165 (1990) 17.
- [44] S.V. Vyazovkin, A.I. Lesnikovich, *Thermochim. Acta* 165 (1990) 273.
- [45] R.M. German, *Sintering theory and practice*, John Wiley and Sons, New York, USA, 1996.
- [46] P. Pourghahramani, E. Forsberg, *Int. J. Miner. Process.* 79 (2006) 120–139.
- [47] S. Vyazovkin, W. Linert, *Chem. Phys.* 193 (1995) 109.
- [48] S. Vyazovkin, A.I. Lesnikovich, *Thermochim. Acta* 128 (1988) 297.

